

Knowing Our Neighbors: Fundamental Properties of Nearby Stars

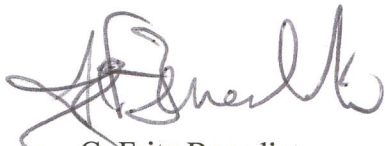
Jennifer Lynn Bartlett
Arlington, Virginia

Bachelor of Science, Rensselaer Polytechnic Institute, 1990
Master of Science, University of Virginia, 2001

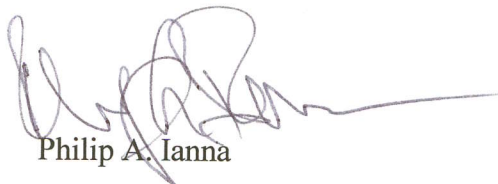
A Dissertation presented to the Graduate Faculty
of the University of Virginia in Candidacy for the Degree of
Doctor of Philosophy

Department of Astronomy

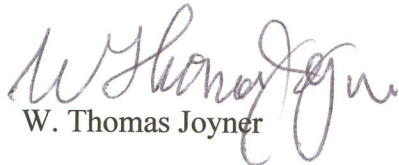
University of Virginia
January 2007



G. Fritz Benedict



Philip A. Ianna



W. Thomas Joyner



Robert T. Rood



D. Mark Whittle

©Copyright by
Jennifer Lynn Bartlett
All Rights Reserved
January 2007

Abstract

The stars within 25 parsecs (pc) of our Sun constitute the one stellar sample that we aspire to know thoroughly, but we still have not even identified all of the stars within 10 pc. We have still less knowledge of the nearby substellar population, especially the planets. The four studies described herein expand our knowledge of the solar neighborhood.

First, a re-analysis of the Leander McCormick Observatory photographic plates of Barnard's Star failed to detect any planets orbiting it, and this study would have detected planets with 2.2 Jupiter masses or greater. In addition, its parallax, proper motion, and secular acceleration were measured with results comparable with those from more modern equipment.

Second, increased information about nearby planets was sought through time series analyses of astrometric residuals to stars observed by the University of Virginia Southern Parallax Program. Of these, LHS 288 displays an intriguing signal, which might be caused by a very low mass companion. Twelve other stars demonstrate no astrometric perturbations.

While astrometry could reveal the presence of unseen companions, distances from trigonometric parallaxes define the solar neighborhood and identify its inhabitants. Preliminary parallaxes for 43 potential nearby stars being observed by the Cerro Tololo Inter-American Observatory Parallax Investigation (CTIOPI) confirmed 28 stars as being within 25 pc, including three stars—LP 991-84, LHS 6167, and LP 876-10—that

probably lie within 10 pc. Three more stars lie near the 25-pc boundary and their final parallaxes may qualify them as nearby. One recently established neighbor, LP 869-26, is a potential binary. For many stars in this third sample, preliminary photometry (V , R , and I bands), spectroscopy, and proper motions are also available.

Despite the continuing importance of ground-based parallax measurements, few active programs remain. The final project tested the recently installed infrared camera on the 31-inch (0.8-meter) telescope at Fan Mountain Observatory for astrometric stability. A parallax program would be feasible there and could provide much needed distances for brown dwarfs and very low mass stars.

Through this and similar efforts, we are establishing the foundations for understanding our Milky Way Galaxy, including its component stars and populations.

Table of Contents

ABSTRACT.....	I
TABLE OF CONTENTS	III
Chapter 1 The Solar Neighborhood: Still Under Development	1
1.1 INTRODUCTION	1
1.2 ROLE OF NEARBY STAR SAMPLES	3
1.3 DEFINING NEARBY STARS.....	7
1.4 DEVELOPMENT OF THE NEARBY STAR SAMPLES.....	12
1.4.1 Five-parsec Sample.....	13
1.4.2 Ten-parsec Sample.....	20
1.4.3 Twenty-parsec Sample.....	20
1.4.4 Twenty-five-parsec Sample.....	21
1.5 NEW AND COOL MEMBERS OF THE SOLAR NEIGHBORHOOD	22
1.5.1 M, L, and T Dwarfs.....	22
1.5.2 Low-mass Companions.....	24
1.6 FUTURE OF THE NEARBY STAR SAMPLE.....	26
Chapter 2 Barnard's Star: Parallax, Proper Motion, And Possible Planetary Perturbation	28
2.1 INTRODUCTION	28
2.2 HISTORY	30
2.2.1 Astrometric Studies	30
2.2.2 Radial-Velocity Studies.....	34
2.2.3 Direct Imaging Studies	35
2.2.4 Miscellaneous Studies.....	37
2.3 MEASUREMENT AND ANALYSIS.....	38
2.3.1 Relative Motions	39
2.3.2 Reduction to Absolute	43
2.3.3 Time-Series Analysis.....	62
2.3.4 Companion Mass Limits	76
2.4 DISCUSSION.....	85
Chapter 3 Planets In The South: Astrometric Search For Companions To Stars On The University Of Virginia Southern Parallax Program.....	87
3.1 INTRODUCTION	87
3.2 MEASUREMENT AND ANALYSIS.....	88
3.2.1 Concerns Regarding Time and Parallax Factor Calculations	98
3.2.2 Periodograms.....	102
3.2.2.1 LHS 34	103
3.2.2.2 LHS 271	108
3.2.2.3 LHS 288	112
3.2.2.4 LHS 337	125
3.2.2.5 LHS 532	129
3.2.2.6 LHS 1134	133
3.2.2.7 LHS 1565	137
3.2.2.8 LHS 2310	141
3.2.2.9 LHS 2739	145
3.2.2.10 LHS 2813	149

3.2.2.11	LHS 3064	154
3.2.2.12	LHS 3242	159
3.2.2.13	LHS 3418	163
3.2.3	<i>Companion Mass Limits</i>	167
3.2.3.1	Limits for the Sample Generally	172
3.2.3.2	Limits for LHS 288	174
3.3	DISCUSSION.....	177
Chapter 4 Solar Neighborhood Census: Identifying and Characterizing New Nearby Stars... 178		
4.1	INTRODUCTION	178
4.2	SELECTION.....	181
4.2.1	<i>Possible Nearby Stars</i>	181
4.2.2	<i>Probable Nearby Stars</i>	184
4.3	ASTROMETRY	206
4.3.1	<i>Stars with Preliminary Absolute Parallaxes</i>	217
4.3.1.1	2MA 0517-3349	222
4.3.1.2	LHS 6167	222
4.3.1.3	BD -10°3166.....	222
4.3.1.4	LHS 2880	223
4.3.1.5	2MA 1534-1418	223
4.3.1.6	LP 876-10.....	224
4.3.2	<i>Stars with Preliminary Relative Parallaxes</i>	224
4.3.2.1	LP 991-84.....	224
4.3.2.2	LHS 1363	225
4.3.2.3	2MA 0251-0352	225
4.3.2.4	2MA 0921-2104	225
4.3.2.5	LP 932-83	225
4.3.2.6	2MA 2306-0502	226
4.3.3	<i>Dropped Stars</i>	226
4.4	PHOTOMETRY	228
4.5	SPECTROSCOPY	239
4.5.1	<i>LP 655-43</i>	244
4.5.2	<i>LP 716-10</i>	244
4.5.3	<i>LHS 2024</i>	244
4.5.4	<i>LP 671-8</i>	245
4.5.5	<i>2MA 1155-3727</i>	245
4.5.6	<i>LP 734-34</i>	246
4.5.7	<i>LP 615-149</i>	246
4.5.8	<i>LHS 5226</i>	247
4.5.9	<i>CE 303</i>	247
4.5.10	<i>2MA 2351-2537</i>	247
4.5.11	<i>LP 704-15</i>	248
4.6	MULTIPLICITY	248
4.6.1	<i>2MA 0429-3123AB</i>	249
4.6.2	<i>LP 731-76 and BD -10°3166</i>	250
4.6.3	<i>LHS 2397aAB</i>	253
4.6.4	<i>LHS 2783AB</i>	254
4.6.5	<i>LP 869-26AB</i>	255
4.6.6	<i>LP 984-92 and LP 984-91</i>	257
4.6.7	<i>LP 932-83 and LTT 9210</i>	258
4.6.8	<i>LP 704-15 and LP 704-14</i>	259
4.6.9	<i>Distance Discrepancies</i>	260
4.7	DISCUSSION.....	261

Chapter 5	Continuing The Solar Neighborhood Census: Infrared Parallax Program At Fan Mountain Observatory	265
5.1	INTRODUCTION	265
5.2	FAN MOUNTAIN 31-INCH TELESCOPE	267
5.3	ASTROMETRIC CALIBRATION REGION	270
5.4	OBSERVATIONS AND ANALYSIS.....	278
5.5	DISCUSSION.....	286
Chapter 6	Further Development of the Solar Neighborhood.....	288
6.1	INTRODUCTION	288
6.2	BARNARD'S STAR	288
6.3	SOUTHERN PARALLAX PROGRAM	289
6.4	CTIOPI	290
6.5	FAN MOUNTAIN OBSERVATORY	291
6.6	DISCUSSION.....	292
	ACKNOWLEDGEMENTS	294
	REFERENCES	299
	APPENDIX A. FINDING CHARTS FOR POSSIBLE NEARBY STARS	316

יְהוָה אֲדַלְּמֵנוּ מִהָאֲדִיר שְׁמֶךָ בְּכָל־הָאָרֶץ אֲשֶׁר תִּנְהַ הַדּוֹרֶךְ עַל־הַשָּׁמַיִם:
 כִּי־אֲרָאָה שְׁמֶיךָ מַעֲשֵׂי אֲצַבְעֶיךָ יָרַח וְכּוֹכָבִים אֲשֶׁר כּוֹנְנָתָה
 מִהָאָנוּשׁ כִּי־תִזְכְּרֵנוּ וּבֶן־אָדָם כִּי תִפְקֹדֵנוּ:

O LORD our Lord,

how excellent *is* thy name in all the earth!

who hast set thy glory above the heavens.

When I consider thy heavens, the work of thy fingers,

the moon and the stars, which thou hast ordained;

what is man, that thou art mindful of him?

and the son of man, that thou visitest him?

Psalms 8: 1, 3–4 (*King James Version*)

Chapter 1 The Solar Neighborhood: Still Under Development

1.1 INTRODUCTION

Within human experience, knowing our neighbors provides a sense of community. Similarly, knowing more about the stars in the solar neighborhood gives us a sense of place within both our Milky Way Galaxy and the larger Universe. The stars within a limited distance of the Sun make up the one sample that we can hope to know thoroughly. Although a growing volume of observations and improved technology allows us to consider a current outer limit of 25 parsecs (pc) for the solar neighborhood, the 5-pc volume around the Sun first cataloged by Hertzsprung (1922) is still incomplete.

We can obtain more information observing nearby stars than observing similar stars that are more distant. For any intrinsic luminosity, the nearby stars are the brightest and easiest to examine from the Earth, so we can study their characteristics in detail and detect more subtle differences among similar stars. Using trigonometric parallax, we measure their distances directly; this measurement establishes whether they are truly nearby stars and improves our determinations of their luminosity and space velocity. Better knowledge of stars for which parallactic distances can be determined also enhances our techniques for estimating the distances and related properties for stars even farther away. Catalogs of stars within the solar neighborhood provide local examples of interesting categories for further study.

This dissertation is based on a study of historic photographic plates from Leander McCormick Observatory from 1969 through 1998, recent charge-coupled

device (CCD) observations from Siding Spring Observatory from 1991 through 2002, on-going CCD observations at Cerro Tololo Inter-American Observatory that began in 2003, and astrometric calibration regions observed at Fan Mountain Observatory in 2005. It expands our knowledge of fifty-eight nearby, or possibly nearby, stars:

- **Barnard's Star: Parallax, Proper Motion, and Possible Planetary Perturbation**—The second closest star to our Sun is Barnard's Star, which may be an old disk or halo star passing through the solar neighborhood. Analysis of its distance, proper motion, and secular acceleration fails to confirm earlier detections that planets orbit this star (van de Kamp 1963b, 1982).
- **Planets in the South: Astrometric Search for Companions to Stars on the Southern Parallax Program**—Using techniques similar to those used to evaluate the motion of Barnard's Star, preliminary parallaxes and proper motions of thirteen nearby stars in the southern hemisphere are investigated to detect possible planets. Although one star, LHS 288, exhibits signs of additional periodic motion, no star is clearly accompanied by a companion.
- **Solar Neighborhood Census: Identifying and Characterizing New Nearby Stars**—Preliminary parallaxes confirm that twenty-eight out of forty-three possible nearby stars do lie within 25 pc of the Sun. New photometry and spectroscopy is available for several of these helping to quantify their fundamental properties.

- Continuing the Solar Neighbor Census: Infrared Parallax Program at Fan Mountain Observatory—Preliminary study of the astrometric quality of the 31-inch (0.8-meter) reflector at Fan Mountain indicates an infrared parallax program would be feasible. Such a program would increase the number of parallactic distances available for very low mass stars and brown dwarfs, many of which should be members of the solar neighborhood.

1.2 ROLE OF NEARBY STAR SAMPLES

A well-understood, volume-limited sample of nearby stars is an essential input for the stellar luminosity function, the mass-luminosity relationship, stellar velocity distribution, and the stellar multiplicity fraction, including substellar companions. Such samples help us define stellar populations and estimate how much of the local mass is contributed by stars. In addition, the stars in this volume provide insight into stellar evolution and the history of star formation in the disk. These physical relationships and subsamples allow us to understand the make-up of our Milky Way Galaxy and by extension more distant galaxies (Kuiper 1942; Reid & Cruz 2002).

Stars definitely known to lie within the solar neighborhood have accurate distances measured with trigonometric parallaxes, which is the only direct method of measuring stellar distances. Stellar luminosity is determined from the apparent brightness of the star combined with its distance. Therefore, luminosities are also better determined when trigonometric parallaxes are used for distance determination.

The stellar luminosity function relates the number of stars with a given luminosity in a particular region, such as the solar neighborhood or a cluster, and the

mass-luminosity relationship estimates the mass of a star based on its luminosity. Together, these expressions reveal the initial mass function used to describe star formation. Structure and gradients in the stellar luminosity function can indicate historical star formation trends. The luminosity function provides a test of stellar evolutionary theories. An adequate luminosity function requires an accurate catalog of stars with well-determined luminosities (Bessell & Stringfellow 1993).

The mass of a star determines its development throughout its life. This defining quantity can only be measured directly for stars with companions, stellar or otherwise. The mass-luminosity relationship provides a mass estimate for single stars based on their luminosity, a more easily measured quantity and one that depends on distance. However, the relationship between mass and luminosity also depends on age and metallicity. Through the mass-luminosity relationship, the stellar luminosity function becomes a stellar mass function used in estimating the contribution of stars to the mass of the Galaxy. Small changes in the mass-luminosity relationship for the lowest mass stars, which are so populous, can have a significant effect on calculations of the Galactic mass (Henry 2004). Currently, the mass-luminosity relationship appears most likely to flatten for the lowest mass stars (Reid, Gizis, & Hawley 2002). The structure of this relationship could constrain theories about the formation of these cool objects. The mass-luminosity relationship used in this work to estimate the masses was determined by Delfosse *et al.* (2000), which expands on the work of Henry *et al.* (1999) though the inclusion of additional binary systems and consideration of infrared luminosities.

The stellar multiplicity fraction places constraints on theories of stellar formation, evolution of stellar systems, and history of the Galaxy. It also plays a significant role in the search for very low mass companions, including brown dwarfs and planets, and in the development of the mass-luminosity relationship. Approximately 67 percent (%) of systems with solar-type stars appear to contain multiple stellar members (Duquennoy & Mayor 1991). Worley (1977) found that 58% of nearby systems have at least two stellar members. However, the fraction appears smaller for lower mass stars. About 32–42% of M dwarfs are the primary star in a multiple configuration (Worley 1977; Henry & McCarthy 1990; Fischer & Marcy 1992). Furthermore, about 12% of solar-type stars appear to host planets (Marcy *et al.* 2005). Fewer planets have been detected orbiting M dwarfs than anticipated (Butler *et al.* 2004), but radial-velocity planet searches have studied only a handful of these cool stars because they are so faint. To increase the numbers of M dwarfs evaluated as planet hosts, Endl *et al.* (2003) have begun a radial velocity search program focused on these late types. These multiplicity estimates are lower limits of the incidence of such companions because the possibility of detecting additional companions always remains.

Baade (1944) first identified the bluer and more luminous stars of the Galactic disk as a separate stellar population from the redder and fainter stars found in globular clusters and elliptical galaxies, populations I and II respectively. Population I stars, which make up the bulk of the solar neighborhood, are younger and more metal-rich than population II stars, a small number of which may be found among the nearby stars. Population II stars may also be found in the Galactic bulge and halo indicating that

these regions formed before the disk where star formation is still continuing. The existence of an even older metal-free generation of stars, population III, has also been theorized but not detected; the most metal-poor star known, HE1327–2326, has about 250,000 times less iron than the Sun, or $[\text{Fe}/\text{H}]_{\text{non-LTE}} = -5.4 \pm 0.2$ (Frebel *et al.* 2005).

The Milky Way is not comprised of stars alone; it also contains gas, dust, and other dark matter. From its rotation curve, the mass contained within a particular radius can be measured. The dynamic mass is greater than the mass implied by the luminous matter. In order to determine the amount of missing mass, or dark matter, present, the stellar contribution to the local mass must be well-understood. The distribution of stellar types varies vertically through the disk. Counts of nearby stars along with models of the Galactic potential are used to estimate the stellar mass present.

The stellar velocity distribution is a measure of the gravitational potential of our Milky Way Galaxy. It also indicates the overall structure of our Galaxy and identifies subpopulations within it. Ideally, studies of stellar velocities should include both the radial and tangential velocities, which are obtained through spectroscopy and astrometry respectively. To obtain a tangential velocity, both a distance to the object and its angular motion across the sky must be measured. Although measuring tangential velocities is time-consuming, the resulting full three-dimensional space velocities map the Galactic potential in detail.

The traditional plotting of luminosities versus spectral types as was done by Hertzsprung (1911) and Russell (1913), the HR-diagram, or the more practical plotting of luminosities versus colors, the color-magnitude diagrams (CMD's), delineates the

stages through which stars evolve. With appropriate photometry, such diagrams can be prepared for nearby stars with known distances or for clusters with member stars all at the same age and distance. The illustrated relationships among luminosity, temperature, mass, and radius guided development of theories of stellar structure and atmospheres. Detailed observations of oscillations, spots, and other physical features of nearby stars continue to contribute to the development of these theories. In addition, comparisons of theoretical HR-diagrams or CMD's with observational ones test the plausibility of proposed star formation histories and Galactic evolution theories.

1.3 DEFINING NEARBY STARS

Astrometry is the precise measurement of the positions and motions of celestial bodies. It provides several fundamental measurements essential to the census of nearby stars: position on the sky, distance from Earth, and proper motion along the celestial sphere. Combining distance with proper motion produces tangential velocity. Of these measurements, distance from the Earth determined by trigonometric parallax is crucial because it determines whether a star lies within the solar neighborhood.

In addition to determining membership in the solar neighborhood, trigonometric parallaxes provide the second rung of the cosmic distance ladder, a highly stable rung. Trigonometric parallaxes depend on our knowledge of the distance between the Earth and Sun, the astronomical unit, which is established by radar ranging among Solar System bodies. In turn, trigonometric parallaxes are used to measure the distances to stars within 100 pc using ground-based telescopes, or farther with space-borne instruments. Nearby stars with parallaxes are plotted on HR-diagrams or CMD's to

produce the spectral type-absolute magnitude or color-absolute magnitude relationships used for spectroscopic and photometric distance estimates and for lower main-sequence fitting, which along with the moving cluster method, is used to estimate distances to stellar clusters. Trigonometric parallaxes measured by the Hubble Space Telescope (HST) Fine Guidance Sensors (FGS) appear to have established a distance to the Pleiades open cluster that is consistent with those by other techniques (Soderblom *et al.* 2005). Fewer discrepancies occurred among efforts to establish a trigonometric parallax for the Hyades open cluster (van Altena *et al.* 1997; Perryman *et al.* 1998; Narayanan & Gould 1999).

Classical astronomers and philosophers understood the significance of stellar parallaxes. In the fourth century BC, Aristotle argued that the lack of parallactic shift in the positions of stars was evidence of a stationary Earth. Brahe, arguably the greatest naked-eye astronomer, was unable to measure any stellar parallaxes leading him to develop a hybrid geocentric-heliocentric model of the Solar System in 1588. However, parallax angles are too small to be measured without the aid of a telescope. Bessel published the first trigonometric parallax of 61 Cygni in 1838. Parallaxes immediately followed for α Centauri by Henderson (1839), whose actual measurement was earlier but unpublished, and Vega by von Struve (1840). The first stars to be definitively identified as nearby were known.

At the beginning of the twentieth-century AD, parallaxes had been measured for fewer than one hundred stars (Newcomb 1904). Although the introduction of photography for measuring stellar parallaxes was initially controversial (Pritchard 1887,

1888; Ranyard 1887), it eventually improved the quality and quantity of parallax measurements (Hunter & Martin 1956). By 1924, Schlesinger, Palmer, and Pond listed 1,682 stars with parallaxes thought to be reliable. Progress continued steadily with measurements for stars within the solar neighborhood as well as many outside of it. The 1995 edition of *The General Catalogue of Trigonometric Stellar Parallaxes* contained parallaxes for 8,112 stars (Van Altena, Lee, & Hoffleit 1995; hereafter YPC). Shortly thereafter, the Hipparcos Space Astrometry Mission (ESA 1997, Hipparcos) made a tremendous contribution to the number of stars with parallaxes; and the associated Hipparcos catalog contains parallaxes for nearly 50,000 stars. However, Hipparcos observed for less than 3.5 years, which is a very short baseline for the measurement of proper motions (Perryman *et al.* 1997). For accurate proper motions, longer-lived ground-based programs or historical collections remain important.

The National Aeronautics and Space Administration (NASA) and Jet Propulsion Laboratory (JPL) expect the planned Space Interferometry Mission (SIM) to measure parallaxes with precisions better than 4 microseconds of arc (μas) and proper motions with precisions better than $3 \mu\text{as year}^{-1}$ for selected targets during an initial five-year mission (NASA & JPL 2005). As of 2006 November, SIM remains in the preliminary design stage with a target launch date to be determined by NASA.

The Leander McCormick Observatory (McCormick) published approximately a third of the trigonometric parallaxes measured before the Hipparcos mission. McCormick astrometrists measured proper motions and parallaxes from photographic plates taken between 1914 (Mitchell *et al.* 1921) and 1998 (Bartlett & Ianna 2001)

producing a collection of over 145,000 plates. McCormick holds over a thousand exposures of Barnard's Star starting in 1916. Chapter 2 describes the final measurement of its parallax and proper motion and an investigation of possible planetary perturbations. The results are comparable to those made with technology that is more modern (Benedict *et al.* 1999; YPC; Hipparcos).

In addition to the important and productive parallax program at McCormick Observatory, the University of Virginia (UVa) also operated programs at Fan Mountain Observatory outside of Charlottesville, Virginia, and at Mount Stromlo and Siding Spring Observatories in Australia. Chapter 3 presents preliminary parallaxes and proper motions for thirteen nearby stars from the CCD program at Siding Spring Observatory in order to search for companions. The deviations between measured and observed positions, or residuals, of those stars are investigated for possible perturbations that might be caused by planetary companions.

Spectroscopic and photometric distance estimates may provide strong indications that a star lies within the solar neighborhood. The possible nearby stars discussed in Chapter 4 were selected based on such estimates. However, without a direct distance measurement, provided by trigonometric parallax, such membership cannot be confirmed. By contrast, photometric and spectroscopic estimates of distance are indirect ones, the precision of which can be enhanced through additional trigonometric parallaxes. A spectroscopic distance is obtained by estimating absolute magnitude from spectral type. Because the mean relationships used to estimate absolute magnitudes do not address the actual scatter in the HR-diagram, an error of one

magnitude in estimating the absolute magnitude may produce distance errors of about 50%. Mean relationships may also fail to address the complications presented by possible multiplicity, various stellar populations, and different evolutionary stages. The HR-diagram and mean relationships, on which photometric and spectroscopic distances depend, will improve with better characterization of the solar neighborhood that in turn requires an increase in the number of stars with trigonometric parallaxes. Such improvements would be especially helpful for the cool, faint objects in the late M, L, and T classes because so few of these objects have trigonometric parallaxes.

Lutz and Kelker (1973) discuss a bias in individual absolute magnitudes calculated from parallaxes as a result of the observed parallaxes being too large on average. Because the volume represented by the upper limit of the error on the parallax measurement is larger than that represented by the lower limit, Lutz and Kelker argued that more stars will be scattered into the distance than out of it. The resulting distances and luminosities would, then, be systematically underestimated. However, individual parallaxes are not inherently or universally biased independent of the sample from which they are drawn (Smith 2003). The errors associated with the measurement of an individual parallax are those of position—for the star and its reference frame—and of modeling—plate constants and stellar motions—from which the parallax angle is determined; distance (d) is then calculated from the parallax angle (π)

$$d = \frac{1}{\pi} \tag{1.1}$$

where distance is in parsecs if the parallax is in seconds of arc. When absolute magnitudes are calibrated based on parallaxes, the appropriate truncation, modeling,

and transformation biases should be carefully considered and applicable modifications made (Smith 2003). This work deals with individual measurements of nearby stars; therefore, the Lutz-Kelker bias is not a concern. When additional stellar characteristics are calculated from the observed parallaxes as part of this work, no further refinements to those values are made.

For a star with a parallax that places it within the solar neighborhood, knowing its position, motion, spectral type including luminosity class, luminosity and variability, metallicity, and age are desirable. We also want to know whether it is truly a single star or if it has companions. For stars with companions, we want to identify whether these are stars, brown dwarfs, or planets. Completely characterizing nearby stars is a complex task, even for those known to lie within the solar neighborhood. This work concentrates on the distances (parallaxes), tangential velocities (proper motion plus distance), and the presence of astrometric companions (perturbation of proper motion) of stars in the solar neighborhood.

1.4 DEVELOPMENT OF THE NEARBY STAR SAMPLES

Historically, astronomers have defined the solar neighborhood to lie within volumes of radius 5–25 pc. The defining radius lengthens with time and as our understanding of the stars enclosed within grows. In 1907, Hertzsprung published a catalog of ninety-five stars within 10 pc, which he later refined to twenty-nine stars within 5 pc (Hertzsprung 1922). Van Maanen (1933) used his updated count of stars within 5 pc to estimate the expected number of stars within 10 and 20 pc; he noted that a substantial number of faint stars were not yet cataloged in these regions. In 1944,

Kuiper listed the data available for 254 stars within 10.5 pc in order to encourage other astronomers to make the observations necessary to complete the census. The Gliese catalogs attempted to describe even larger volumes, starting with a 20-pc sample in the 1957 edition and expanding to 25.6 pc in the 1991 edition (Gliese 1957; Gliese & Jahreiß 1991). Woolley *et al.* also produced a 25-pc catalog in 1970. For the purposes of this study, the solar neighborhood lies within 25 pc of the Sun, with particular attention to those stars within 10 pc. These distances were adopted in accordance with the arbitrary limits established by the NStars Database Project (Backman *et al.* 2000; Henry *et al.* 2000; hereafter NStars Database¹) and Research Consortium on Nearby Stars (RECONS), respectively.

1.4.1 Five-parsec Sample

The first sample of nearby stars included those known to be within 5 pc. It has grown from twenty-nine individual stars in twenty-one systems known in 1922 to sixty-five objects in forty-seven systems in 2001 (Hertzsprung 1922; NStars Database). Table 1.1 on the following page tracks its development during the intervening years. This small volume encompasses too few stars to address all the important astrophysical questions that are demanded of the nearby star sample. It also encloses few stars with early types or that have evolved off the main sequence. However, because of its manageable size, its census might be completed eventually. The number of

¹The NStars Database may be accessed at <http://nstars.arc.nasa.gov/index.cfm>

TABLE 1.1
HISTORICAL CATALOGS OF NEARBY STARS

Limit (pc)	Contents	Date	Compiler	Comment
10	95 stars	1907	Hertzsprung	
5	29 stars	1922	Hertzsprung	
5	37 stars	1930	van de Kamp	+8 borderline cases
5	47 stars	1940	van de Kamp	
10.5	255 stars	1942	Kuiper	
5	38 systems	1945	van de Kamp	+70 Ophiuchi AB
5.1	53 stars	1953	van de Kamp	+5 unseen companions
20	1,094 stars	1957	Gliese	combines parallaxes with spectroscopic estimates
5.2	59 stars	1969	van de Kamp	+6 unseen companions
22.2	1,328 stars	1969	Gliese	combines parallaxes with other distance estimates
25	2,150 objects	1970	Woolley <i>et al.</i>	includes some spectroscopic distances
25.6	3,803 stars	1991	Gliese & Jahreiß	substitutes other estimates when no or poor parallax
8	151 stars	1997	Reid & Gizis	only $\delta \geq -30^\circ$; includes spectroscopic distance estimates
8	150 objects	1999	Reid <i>et al.</i>	only $\delta \geq -30^\circ$; includes spectroscopic distance estimates
25	2,633 objects	2001	NStars Database	
8	151 objects	2002	Reid ^a	only $\delta \geq -30^\circ$; includes spectroscopic distance estimates
5	79 objects	2006	RECONS	extracted from 100 nearest systems; includes planets
6.7	156 objects	2006	RECONS	100 nearest systems; includes planets

NOTE—^aThe most recent 8-pc sample updated by I. N. Reid is available at <http://www-int.stsci.edu/~inr/8pc.html>

stars or systems known within 5 pc can be extrapolated to larger volumes and be used to estimate the completeness of larger samples of nearby stars (van Maanen 1933; Henry *et al.* 1997).

A current listing of stars within 5 pc can be extracted from the RECONS list of “The One Hundred Nearest Star Systems,”² as shown in Table 1.2 on the following pages. As of 2006 July 1, it included forty-nine stellar systems, including our own, with trigonometric parallaxes greater than 0.2 seconds of arc ("). These systems include sixty-seven individual stars or brown dwarfs plus four extrasolar planets. Three single stars lie on the boundary with errors that could remove two from the volume or bring one into it.

If the 5-pc sample is assumed to be complete, a density of 0.0936 ± 0.0057 systems pc^{-3} is implied. Then, a sphere with a 10-pc radius should enclose about 392 systems while one with a 25-pc radius should include approximately 6,130 systems. However, the NStars Database contains only 233 systems within 10 pc and 2,029 systems within 25-pc as of 2006 October 28. The RECONS census was 249 systems within 10 pc as of 2006 July 1. A substantial number of systems remain undetected or do not have distance measurements considered reliable enough for inclusion in these two tabulations. However, the 5-pc sample, itself, is still incomplete;

²“The One Hundred Nearest Star Systems” is available at <http://www.chara.gsu.edu/RECONS/TOP100.htm>

TABLE 1.2
STARS KNOWN TO BE WITHIN 5 PC

System	Star	Alternate Name	Position (2000.0)			Parallax (mas)	Proper Motion		Spectral Type	References
			α (hh mm ss.s)	δ (hh mm ss)			(mas yr ⁻¹)	(deg)		
	Sun ^a							G2V	1	
1	GJ 551	Proxima Centauri	14 29 43	-62 40 46	772.0 ^b ± 2.3	3853 ^c	281.5	M5.5V	2, 3 & 2, 2, 4	
	GJ 559A	α Centauri A	14 39 37	-60 50 02	747.2 ± 1.2	3710	277.5	G2V	2, 3 & 5, 2, 1	
	GJ 559B	α Centauri B	14 39 35	-60 50 14	747.2 ± 1.2	3724	284.8	K0V	2, 6, 2, 1	
2	GJ 699	Barnard's Star	17 57 49	+04 41 36	547.0 ^d ± 1.0	10358 ^e	355.6	M4.0V	2, 3 & 2, 2, 4	
3	GJ 406	Wolf 359	10 56 29	+07 00 53	419.1 ± 2.1	4696	234.6	M6.0V	1, 3, 1, 4	
4	GJ 411	Lalande 21185	11 03 20	+35 58 12	393.42 ± 0.70	4802	186.9	M2.0V	2, 3 & 2, 2, 4	
5	GJ 244A	Sirius	06 45 08.9	-16 42 58	380.0 ± 1.3	1339	204.1	A1V	2, 3 & 2, 2, 1	
	GJ 244B	Sirius B	06 45 08.9	-16 42 58	380.0 ± 1.3	1339	204.1	DA2	6, 6, 6, 1	
6	GJ 65A	UV Ceti	01 39 01.3	-17 57 01	373.7 ± 2.7	3368	80.4	M5.5V	1, 3, 1, 4	
	GJ 65B	BL Ceti	01 39 01.3	-17 57 01	373.7 ± 2.7	3368	80.4	M6.0V	6, 6, 6, 4	
7	GJ 729	Ross 154	18 49 49	-23 50 10	336.9 ± 1.8	666	106.8	M3.5V	2, 3 & 2, 2, 4	
8	GJ 905	Ross 248	23 41 55	+44 10 30	316.0 ± 1.1	1617	177.0	M5.5V	1, 3, 1, 4	
9	GJ 144	ϵ Eridani	03 32 56	-09 27 30	309.99 ± 0.79	977	271.1	K2V	2, 3 & 2, 2, 1	
	GJ 144b		03 32 56	-09 27 30	309.99 ± 0.79	977	271.1	Planet	6	
10	GJ 887	Lacaille 9352	23 05 52.0	-35 51 11	303.64 ± 0.87	6896	78.9	M1.5V	2, 3 & 2, 2, 4	
11	GJ 447	Ross 128	11 47 44	+00 48 16	298.7 ± 1.4	1361	153.6	M4.0V	2, 3 & 2, 2, 4	
12	GJ 866A	EZ Aquarii A	22 38 33	-15 18 07	289.5 ± 4.4	3254	46.6	M5.0V J	1, 3, 1, 4	
	GJ 866B	EZ Aquarii B	22 38 33	-15 18 07	289.5 ± 4.4	3254	46.6	...	6	
	GJ 866C	EZ Aquarii C	22 38 33	-15 18 07	289.5 ± 4.4	3254	46.6	...	6	
13	GJ 280A	Procyon	07 39 18	+05 13 30	286.05 ± 0.81	1259	214.7	F5IV-V	2, 3 & 2, 2, 1	
	GJ 280B	Procyon B	07 39 18	+05 13 30	286.05 ± 0.81	1259	214.7	DA	6, 6, 6, 1	
14	GJ 820A	61 Cygni A	21 06 54	+38 44 58	286.04 ± 0.56	5281	51.9	K5.0V	2, 3 & 2, 2, 4	
	GJ 820B	61 Cygni B	21 06 55	+38 44 31	286.04 ± 0.56	5172	52.6	K7.0V	2, 6, 2, 4	

TABLE 1.2 (CONTINUED)
STARS KNOWN TO BE WITHIN 5 PC

System	Star	Alternate Name	Position (2000.0)			Parallax (mas)	Proper Motion		Spectral Type	References
			α (hh mm ss.s)	δ (hh mm ss)			(mas yr ⁻¹)	(deg)		
15	GJ 725A		18 42 47	+59 37 49	283.0 \pm 1.7	2238	323.6	M3.0V	2, 3 & 2, 2, 4	
	GJ 725B		18 42 47	+59 37 37	283.0 \pm 1.7	2313	323.0	M3.5V	2, 6, 2, 4	
16	GJ 15A	GX Andromedae	00 18 23	+44 01 23	280.6 \pm 1.0	2918	81.9	M1.5V	2, 3 & 2, 2, 4	
	GJ 15B	GQ Andromedae	00 18 23	+44 01 23	280.6 \pm 1.0	2918	81.9	M3.5V	6, 6, 6, 4	
17	GJ 845A	ϵ Indi A	22 03 22	-56 47 10	275.84 \pm 0.69	4704	122.7	K5Ve	2, 3 & 2, 2, 1	
	GJ 845B	ϵ Indi B	22 04 11	-56 46 58	275.84 \pm 0.69	4823	121.1	T1.0	7, 6, 7, 8	
	GJ 845C	ϵ Indi C	22 04 11	-56 46 58	275.84 \pm 0.69	4823	121.1	T6.0	7, 6, 7, 8	
18	GJ 1111	DX Cancri	08 29 50	+26 46 37	275.8 \pm 3.0	1290	242.2	M6.5V	1, 3, 1, 4	
19	GJ 71	τ Ceti	01 44 04.1	-15 56 15	274.39 \pm 0.76	1922	296.4	G8Vp	2, 3 & 2, 2, 1	
20	GJ 1061		03 35 59.7	-44 30 45	272.0 \pm 1.3	826	117.7	M5.5V	4	
21	GJ 54.1	YZ Ceti	01 12 31	-16 59 57	268.8 \pm 3.0	1372	61.9	M4.5V	2, 3 & 2, 2, 4	
22	GJ 273	Luyten's Star	07 27 25	+05 13 33	263.8 \pm 1.3	3738	171.2	M3.5V	2, 3 & 2, 2, 4	
23	SO 0253-1652		02 53 00.9	+16 52 53	260.6 \pm 2.7	5106	138.2	M7.0V	4	
24	SCR 1845-6357A		18 45 05.3	-63 57 48	259.5 \pm 1.1	2664	76.6	M8.5V	4	
	SCR 1845-6357B		18 45 02.6	-63 57 52	259.5 \pm 1.1	2664	76.6	T	6	
25	GJ 191	Kapteyn's Star	05 11 41	-45 01 06	255.27 \pm 0.86	8670	131.4	M1.5V	2, 3 & 2, 2, 4	
26	GJ 825	AX Microscopii	21 17 15	-38 52 03	253.4 \pm 1.1	3455	250.6	M0.0V	2, 3 & 2, 2, 4	
27	GJ 860A	Kruger 60 A	22 27 60	+57 41 45	248.1 \pm 1.4	990	241.6	M3.0V	2, 3 & 5, 2, 4	
	GJ 860B	Kruger 60 B	22 27 60	+57 41 45	248.1 \pm 1.4	990	241.6	M4.0V	6, 6, 6, 4	
28	DEN 1048-3956		10 48 15	-39 56 06	247.7 \pm 1.6	1530	229.2	M8.5V	9, 4, 4, 4	
29	GJ 234A	Ross 614A	06 29 23	-02 48 50	244.3 \pm 2.0	930	131.7	M4.5V J	2, 3 & 5, 2, 4	
	GJ 234B	Ross 614B	06 29 23	-02 48 50	244.3 \pm 2.0	930	131.7	...	2, 6, 6	
30	GJ 628	Wolf 1061	16 30 18	-12 39 45	236.0 \pm 1.7	1189	184.5	M3.0V	2, 3 & 2, 2, 4	
31	GJ 35	WD 0046+051	00 49 09.9	+05 23 19	231.9 \pm 1.8	2978	155.5	DZ7	2, 3 & 2, 2, 1	

TABLE 1.2 (CONTINUED)
STARS KNOWN TO BE WITHIN 5 PC

System	Star	Alternate Name	Position (2000.0)			Parallax (mas)	Proper Motion		Spectral Type	References
			α (hh mm ss.s)	δ (hh mm ss)			(mas yr ⁻¹)	(deg)		
32	GJ 1		00 05 24	-37 21 27	229.2 ± 1.1	6100	112.5	M3.0V	2, 3 & 2, 2, 4	
33	GJ 473A	Wolf 424A	12 33 17	+09 01 15	227.9 ± 4.6	1811	277.4	M5.5V J	1, 3, 1, 4	
	GJ 473B	Wolf 424B	12 33 17	+09 01 15	227.9 ± 4.6	1811	277.4	...	6	
34	GJ 83.1	TZ Arietis	02 00 13	+13 03 08	224.8 ± 2.9	2097	147.8	M4.5V	1, 3, 1, 4	
35	GJ 687		17 36 26	+68 20 21	220.49 ± 0.82	1309	194.2	M3.0V	2, 3 & 2, 2, 4	
36	LHS 292		10 48 13	-11 20 14	220.3 ± 3.6	1644	158.5	M6.5V	1, 3, 1, 4	
37	GJ 674		17 28 40	-46 53 43	220.3 ± 1.6	1050	146.9	M3.0V	2, 3 & 2, 2, 4	
38	GJ 1245A	G 208-44A	19 53 54	+44 24 55	220.2 ± 1.0	731	143.1	M5.5V J	1, 3, 1, 4	
	GJ 1245B	G 208-45	19 53 55	+44 24 56	220.2 ± 1.0	731	143.1	M6.0V	1, 6, 6, 4	
	GJ 1245C	G 208-44B	19 53 54	+44 24 55	220.2 ± 1.0	731	143.1	...	6	
39	GJ 440	WD 1142-645	11 45 43	-64 50 29	216.6 ± 2.0	2688	097.4	DQ6	2, 3 & 2, 2, 1	
40	GJ 1002		00 06 44	-07 32 22	213.0 ± 3.6	2041	203.6	M5.5V	1, 3, 1, 4	
41	GJ 876A	Ross 780	22 53 17	-14 15 49	212.6 ^f ± 2.0	1174 ^g	125.1	M3.5V J	2, 3 & 2, 2, 4	
	GJ 876d		22 53 17	-14 15 49	212.6 ± 2.0	1174	125.1	Planet	6	
	GJ 876c		22 53 17	-14 15 49	212.6 ± 2.0	1174	125.1	Planet	6	
	GJ 876b		22 53 17	-14 15 49	212.6 ± 2.0	1174	125.1	Planet	6	
42	LHS 288		10 44 21.2	-61 12 36	209.0 ± 2.7	1643	347.7	M5.5V	4	
43	GJ 412A		11 05 29	+43 31 36	206.0 ± 1.1	4511	282.1	M1.0V	2, 3 & 2, 2, 4	
	GJ 412B	WX Ursae Majoris	11 05 30	+43 31 18	206.0 ± 1.1	4531	281.9	M5.5V	2, 6, 1, 4	
44	GJ 380		10 11 22	+49 27 15	205.81 ± 0.67	1452	249.7	K7.0V	2, 3 & 2, 2, 4	
45	GJ 388		10 19 36	+19 52 10	204.6 ± 2.8	506	264.0	M3.0V	1, 3, 1, 4	
46	GJ 832		21 33 34.0	-49 00 32	202.8 ± 1.3	819	183.2	M3.0V	2, 3 & 2, 2, 4	
47	LP 944-20 ^h		03 39 35	-35 25 41	201.4 ± 4.2	439	47.6	M9.0V	1, 10, 1, 4	
48	DEN 0255-4700 ^h		02 55 03.7	-47 00 52	201.4 ± 3.9	1149	119.5	L7.5V	4, 4, 4, 6	

TABLE 1.2 (CONTINUED)
STARS KNOWN TO BE WITHIN 5 PC

System	Star	Alternate Name	Position (2000.0)		Parallax (mas)	Proper Motion		Spectral Type	References
			α (hh mm ss.s)	δ (hh mm ss)		(mas yr ⁻¹)	(deg)		
49	GJ 682 ⁱ		17 37 03.7	-44 19 09	199.7 ± 2.3	1176	217.1	M4.5V	2, 3 & 2, 2, 4

NOTES.— ^aSun has at least eight planets, none of which are listed here.

^bAccording to Hubble Space Telescope results, Proxima Centauri has an absolute parallax of 768.7 ± 0.3 mas (11).

^cAccording to Hubble Space Telescope results, Proxima Centauri has a proper motion of $3.8517 \pm 0.0001''$ yr⁻¹ in $281.52 \pm 0.03^\circ$ (11).

^dAccording to Hubble Space Telescope results, Barnard's Star has an absolute parallax of 545.4 ± 0.3 mas (11). A value of 552 ± 7 mas is measured in Chapter 2.

^eAccording to Hubble Space Telescope results, Barnard's Star has a proper motion of $10.3700 \pm 0.0003''$ yr⁻¹ in $355.6 \pm 0.1^\circ$ (11). A value of $10.354 \pm 0.006''$ yr⁻¹ in $355.85 \pm 0.06^\circ$ is measured in Chapter 2.

^fAccording to Hubble Space Telescope results, GJ 876 has an absolute parallax of 214.6 ± 0.2 mas (12).

^gAccording to Hubble Space Telescope results, GJ 876 has a proper motion of $1.168 \pm 0.001''$ yr⁻¹ in $125.3 \pm 0.1^\circ$ (12).

^hConsidering the error in its parallax, this borderline star may not actually be within 5 pc although its formal distance places it closer.

ⁱConsidering the error in its parallax, this borderline star may actually be within 5 pc although its formal distance places it farther away.

REFERENCES.—(1) Gliese & Jahreiß 1991; (2) Hipparcos; (3) YPC; (4) RECONS 2006; (5) Soederhjelm 1999; (6) T. J. Henry 2006, private communication; (7) Scholz *et al.* 2003; (8) McCaughrean *et al.* 2004; (9) Ducurant *et al.* 1998; (10) Tinney 1996; (11) Benedict *et al.* 1999; (12) Benedict *et al.* 2002

the forty-nine systems listed by RECONS include three with their first parallax being published this year (Henry *et al.* 2006; Costa *et al.* 2006).

1.4.2 Ten-parsec Sample

Doubling the radius of the solar neighborhood to 10 pc increases the volume contained within eightfold. This sample should include an increased numbers of stars with greater variety while still being small and close enough that its complete census might be achievable. Reid and Gizis (1997, Reid *et al.* 1999) briefly promoted an 8-pc sample on the grounds it was 90% complete.

In 1997, Henry *et al.* reported the discovery of a star within four parsecs. At that time, they estimated that approximately 130 star systems within 10 pc were not yet discovered based on the stars then known within 5 pc. Since then, RECONS has concentrated on identifying and characterizing stars within 10 pc (Henry *et al.* 1997). In the intervening years, parallaxes have been measured for stars that place them within 5 pc of the Sun and between 5 and 10 pc. Consequently, the estimated number of missing systems actually increased during the intervening years. Chapter 4 describes preliminary results characterizing forty-three possible nearby stars as part of the Cerro Tololo Inter-American Observatory Parallax Investigation (CTIOPI), which is a RECONS endeavor, began in 1999. Of these, two stars, and possibly a third, are new members of the 10-pc sample.

1.4.3 Twenty-parsec Sample

Kuiper (1942) recommended that the nearby star sample be expanded to 20 pc in order to include more stars and improve its utility. This sample is expected to include

3,140 stellar systems or 4,290 individual objects. The Gliese catalogs of nearby stars (1957, 1969) attempted to describe all the stars known at the time within such volume; the second edition listed 1,328 stars including some borderline cases. However, Gliese did not rely solely on trigonometric parallaxes and included spectroscopic and photometric distance estimates to improve the completeness and to make the listings more comprehensive. Consequently, misidentified giants or undetected binaries may be inadvertently included. However, observing programs could select lists of stars without trigonometric parallaxes or photometry for further investigation from these catalogs. Some modern collaborations use a 20-pc limit to the solar neighborhood.

1.4.4 Twenty-five-parsec Sample

Woolley *et al.* (1970) extended the definition of the solar neighborhood another 5 pc with the Royal Observatory catalog of nearby stars and the preliminary version of Gliese's third catalog (Gliese & Jahreiß 1991) likewise moved outward. The NStars Database also uses a 25-pc radius to define the solar neighborhood; its limit was established to meet the requirements of the proposed Terrestrial Planet Finder (TPF). Even with the indefinite postponement of TPF, 25 pc currently remains a good outer limit to the solar neighborhood given the incompleteness of our knowledge of the region within 10 pc of the Sun and the reliability of distances given the precision of parallaxes measured with CCD's. From the list of forty-three possible nearby stars described in Chapter 4, twenty-eight stars are confirmed as new members of the solar neighborhood including two within 10 pc, as mentioned earlier.

1.5 NEW AND COOL MEMBERS OF THE SOLAR NEIGHBORHOOD

Previously unidentified members of the solar neighborhood may be so cool, red, and dim that they were missed in previous studies. Detailed observations, including accurate distances and luminosities, are important for the faint stars and brown dwarfs found at the cool end of the main sequence and least populated part of the mass-luminosity relationship. The search for unseen companions to known nearby stars is another important source of new stars and substellar objects.

1.5.1 M, L, and T Dwarfs

The M dwarfs make up about 70% of the solar neighborhood and about half the stellar mass in our Galaxy. The even-less massive L dwarfs are probably an equally numerous component but may have not been detected in large numbers due to their low luminosity (Henry *et al.* 2002). Many of the missing nearby stars may belong to the faint stars and cool end of the main sequence for which detailed observations are just becoming possible.

The late M and early L dwarfs are probably a mix of true stars and substellar brown dwarfs that will slowly cool to even later spectral types (Burrows *et al.* 2001). Theories about the structure and evolution of these objects are developing based on a relatively small number of examples, few of which have intrinsic luminosities derived from photometry and trigonometric parallaxes.

A significant population of these cool dwarfs was not included in the Hipparcos catalog. Some of the Hipparcos parallaxes are for stars as faint as 12.4 magnitude (Perryman *et al.* 1997) in V-band, which corresponds to an M5 dwarf just beyond 10

pc. Although this mission filled in the bright nearby stars, the Hipparcos catalog is known to be significantly incomplete for stars fainter than 9th magnitude in V (Perryman *et al.* 1997), corresponding to an M5 dwarf just beyond 2 pc. The YPC describes 2,300 stars that are not in the Hipparcos catalog.

Several larger modern surveys, especially the Two Micron All Sky Survey (Skrutskie *et al.* 2006, hereafter 2MASS), the Deep Near Infrared Survey of the Southern Sky (Epchtein *et al.* 1999, hereafter DENIS), and the Sloan Digital Sky Survey (York *et al.* 2000, hereafter SDSS), in combination with existing high-proper-motion studies, are revealing a wealth of candidates for the solar neighborhood. Many of these candidates belong to the faint M, L, and T dwarf classes. While excellent work is being done, the distances to these candidates are primarily estimates from photometry and spectroscopy. Obtaining trigonometric parallax measurements for these objects is highly desirable to reduce the uncertainties in both distances and, more importantly, absolute magnitudes.

The Virginia Astronomical Instrumentation Laboratory (VAIL) led by Skrutskie recently refurbished the 31-inch (0.8-meter) reflector at Fan Mountain Observatory and installed an infrared camera. Chapter 5 discusses the feasibility of using this instrument to measure parallaxes of cool stars and brown dwarfs at infrared wavelengths. Better understanding of the three-dimensional positions and two-dimensional motions of nearby, very low mass objects will improve our understanding of the luminosity function, mass-luminosity relationship, and velocity distribution for the lower end of the main sequence. These physical relationships can then constrain models for the

formation, structure, and evolution of the lowest mass stars and the highest mass substellar objects.

1.5.2 Low-mass Companions

Detection of stars in binary and multiple star systems provides measurements of stellar mass and, in eclipsing systems, also stellar radii. The primary star in an astrometric binary, such as Sirius or Procyon, exhibits a characteristic wobble as it orbits the center of mass of its system. Once the parallax and proper motion of a nearby star have been measured, the residuals may reveal an additional perturbation due to an unseen companion.

Van de Kamp (1969) successfully detected six astrometric companions to nearby stars using this method; until recently, astrometric programs were the primary source of very low mass stars. In addition, van de Kamp (1963b, 1969) described a very small amplitude oscillation in the motion of Barnard's Star that he attributed to a planet. Although no other study, including this one, has confirmed his claim, astrometric planet searches could provide valuable information about these smallest of companions.

To date, radial-velocity programs are the primary source of extrasolar planets orbiting main sequence stars with programs looking for transits and gravitational lenses also contributing. Like astrometric companions searches, radial-velocity programs look for the motion of the parent star in response to its planets.

The highly successful radial-velocity searches are most sensitive to massive planets close to their stars that produce high stellar velocities (Nelson 2001). However, this technique is detecting planets of decreasing mass and longer period at improved

precision with the least massive now projected to be only about eight times the mass of the Earth (Rivera *et al.* 2005). With time, the orbital axes of detected planets are also increasing; the most distant has a semi-major axis slightly greater than five astronomical units (AU) (Marcy *et al.* 2002). However, radial-velocity searches tend to focus on older main sequence stars later than F8V that are not rapidly rotating (McCarthy *et al.* 2004); these stars have a single-set of well-defined spectral lines that more easily reveal any Doppler shift. Radial-velocity programs cannot determine the inclination of the observed orbit. Therefore, they report estimated lower limits to planetary masses, or projected masses ($m \sin i$).

Astrometric planet searches, such as those discussed in Chapters 2 and 3, complement radial-velocity observations in a number of ways. They are sensitive to planets in larger orbits that produce noticeable stellar displacements, a bias opposite of radial-velocity searches. Therefore, they could confirm the presence of more distant planets in systems with short-period planets that are suggested by velocity residuals such as those described by Fischer *et al.* (2001). In addition, they are better suited to detect multiple planets in systems with masses decreasing with distance (Quirrenbach *et al.* 2004). The candidates for astrometric observations are not restricted by age, spectral type, or stellar rotation. Such programs can identify the frequency of planets around the low-mass stars that make up so much of the solar neighborhood and around more massive stars. The identification of planets around pre-main sequence stars could provide insight into planet formation mechanisms and the interactions of among young planets. Astrometric detections allow for the unambiguous determination of the orbital

elements, especially inclination. Knowing the orbital inclination of a system allows the determination of actual masses and whether multiple planets have co-planar orbits (Quirrenbach *et al.* 2004).

Despite the detection of at least 176 extrasolar planets since 1995 (IAU WG ESP 2006³), our knowledge of them is still rudimentary. Therefore, the non-detections discussed in this dissertation are also significant, if less exciting, and provide information about the frequency, distribution, and masses of extrasolar planets. While brown dwarfs are not as exciting as planets in the popular imagination, they are the transition region between stars and planets. The discovery of new brown dwarfs would improve our knowledge of the faint end of the main sequence and help fill in the census of the solar neighborhood.

1.6 FUTURE OF THE NEARBY STAR SAMPLE

The completion of the nearby star sample is a Sisyphean labor. Progress on the inner regions of the solar neighborhood reveals the incompleteness of the outer regions. Completing an inner volume allows the defining radius to be pushed outward to enclose more territory and additional stars. On the other hand, small improvements in our knowledge of the solar neighborhood ripple outward clarifying our understanding of many branches of astronomy. Despite the progress made in the last century in measuring parallaxes and determining the fundamental properties of nearby stars, the

³The International Astronomical Union (IAU) Working Group (WG) on Extrasolar Planets (ESP) maintains a list of extrasolar planets reported in refereed journals at <http://www.dtm.ciw.edu/boss/planets.html>

census is still incomplete and observations will continue to be needed well into this century. Each chapter mentions additional projects that grow naturally out of the work described herein and would enhance our knowledge of the nearest stars. Identifying the nearly 4,100 missing stellar systems expected within 25 pc is a daunting undertaking. However, the recently dedicated Panoramic Survey Telescope and Rapid Response System (Pan-STARRS)⁴ and planned Large Synoptic Survey Telescope (LSST)⁵ promise accurate positions for vast numbers of stars that could be mined in support of the solar neighborhood census along with traditional astrometric programs. The process of detecting and understanding the newest members of the solar neighborhood will also suggest new questions about the solar neighborhood and the Milky Way. How well, after all, can we mortals truly know our neighbors?

⁴The University of Hawai'i maintains a website describing their new telescope at <http://pan-starrs.ifa.hawaii.edu/public/>

⁵The LSST Corporation maintains a website detailing their proposed telescope at http://www.lsst.org/lsst_home.shtml

Chapter 2 Barnard's Star: Parallax, Proper Motion, And Possible Planetary Perturbation

2.1 INTRODUCTION

Barnard's Star is a fascinating object, not only because of its nearness and high proper motion, but also because of the earlier suggestions that it had planetary companions. Until the dramatic successes of the radial velocity searches for extrasolar planets, any hint of other planets attracted much interest. Such was the case with Barnard's Star. Its planetary saga began in 1963 with the first in a series of Sproul Observatory studies by van de Kamp suggesting the presence of a small amplitude astrometric perturbation. Later studies indicated that some portion of the perturbation was instrumental in nature and arose from a discontinuity in the imaging properties of the Sproul telescope. However, subsequent accounting for instrumental systematic errors in the Sproul data still yielded an astrometric perturbation, which could be represented by two circular orbits (van de Kamp 1975, 1977a, 1982). The most recent Leander McCormick Observatory (McCormick) investigation of Barnard's Star using photographic plate material is presented herein. Table 2.1 and Table 2.2 list the basic physical characteristics of Barnard's Star from the literature and from this study, respectively.

TABLE 2.1
 PROPERTIES OF BARNARD'S STAR FROM LITERATURE

Property	Value	Reference
Position RA (hh mm ss.sss)	17 57 48.498	1
(2000.0) Declination (dd mm ss.ss)	+04 41 35.40	
Other Designations	BD +4°3561, LHS 57, GJ 699, G 140-24, NLTT 45718, TYC 425-2502-1, HIP 87937	2
Spectral Type	M4 V	3
Apparent V_{JM} Magnitude	9.53 ± 0.03	4
Apparent K_{CIT} Magnitude	4.5 ± 0.1	5
Luminosity (L_{\odot})	0.0035 ± 0.0002	6
Radial Velocity (km s^{-1})	-110.5 ± 0.4	7
Metallicity [m/H]	-0.5 ± 0.5	8
Radius (R_{\odot})	0.200 ± 0.008	6
Effective Temperature (K)	3,100 ± 100	6
Population	Old Disk-Halo	5
	Intermediate population II	8

NOTE.—CIT system with $K=2.2 \mu\text{m}$ defined by (9)

REFERENCES.—(1) Tycho; (2) SIMBAD; (3) Kirkpatrick *et al.* 1991; (4) Weis 1993; (5) Leggett 1992; (6) Dawson & De Robertis 2004; (7) Nidever *et al.* 2002; (8) Gizis 1997; (9) Elias *et al.* 1982

TABLE 2.2
 PROPERTIES OF BARNARD'S STAR FROM THIS STUDY

Property	Value	Comments
Parallax (mas)	552 ± 7	
Proper Motion ($'' \text{yr}^{-1}$)	10.354 ± 0.006	
Position Angle (degrees)	355.85 ± 0.06	of proper motion
Secular Acceleration (mas yr^{-2})	1.253 ± 0.041	
Distance (parsecs)	1.81 ± 0.02	
Transverse Velocity (km/s)	89 ± 1	
Absolute V_{JM} Magnitude	13.240 ± 0.037	m_V from (1)
Absolute K_{CIT} Magnitude	8.2 ± 0.1	m_K from (2)
Mass (M_{\odot})	0.16 ± 0.04	K-band M-L relationship (3)
Luminosity (L_{\odot})	0.0032 ± 0.0007	(4) and radius below
Radius (R_{\odot})	0.196 ± 0.004	Radius-mass relationships (5, 6)

REFERENCES.—(1) Weis 1993; (2) Leggett 1992; (3) Delfosse *et al.* 2000 ; (4) Dawson & De Robertis 2004; (5) Caillault & Patterson 1990; (6) Neece 1984

2.2 HISTORY

E. E. Barnard discovered the star that bears his name in 1916 because of its large proper motion (Barnard 1916). In 1963, van de Kamp detected a perturbation in the proper motion of Barnard's Star that he explained by the presence of a planetary companion. Since that time, at least fourteen studies have attempted to confirm the presence of any planets. Although several techniques have been employed, none have been successful but only a few have been sensitive to low-mass objects in long-period orbits.

2.2.1 Astrometric Studies

Based on observations made with the Sproul Observatory 61-centimeter refractor between 1916 and 1962, van de Kamp's analysis had a planet with about 1.6 times the mass of Jupiter (M_{J1}) in an orbit with a period of 24 years and eccentricity of 0.6 (van de Kamp 1963b). In 1969, he updated his results with another single-planet solution and a two-planet alternative solution to the astrometric wobbles detected that fit the data equally well (van de Kamp 1969a, 1969b). Hershey's (1973) study of AC +65° 6955 indicated that physical changes made to the Sproul telescope in 1949 produced noticeable instrumental effects in plate series taken with the telescope that could give the appearance of a perturbation. After some accounting for these instrumental effects, van de Kamp (1975, 1977a, 1982) continued to assert that Barnard's Star had two planets. In his final 1982 analysis, he calculated that the detected planets had 0.7 and 0.5 M_{J1} with 12- and 20-year orbits, respectively. Van de Kamp (1986) estimated the errors on these masses to be $\pm 0.1 M_{J1}$.

Gatewood analyzed 610 exposures on 241 plates taken on 169 nights at the Allegheny and Van Vleck Observatories between 1916 and 1971 (Gatewood 1972, Gatewood & Eichhorn 1973). After accounting for differences between plates taken with different telescopes, Gatewood's analysis of the deviations between calculated and measured positions, or residuals, did not appear to indicate a perturbation greater than 11 milliseconds of arc (mas), which corresponds to a $1.2 \pm 0.2 M_{\text{J}}$ planet. In comparison, van de Kamp (1969a) used 10,452 exposures on 3,036 plates taken on 766 nights with a single instrument in his first 1969 analysis. Later investigation by Gatewood (1995) using his Multichannel Astrometric Photometer (MAP) hinted that a slight astrometric perturbation might exist in the proper motion of Barnard's Star. However, he thought the MAP residuals were most likely random measurement errors. According to Gatewood (1995), any planets present would have to be less massive than Jupiter or have either short or long orbital periods. Van de Kamp (1982) described just such planets.

Harrington and Harrington (1987) report an astrometric study of Barnard's Star at the United States Naval Observatory (USNO). Based on 400 plates taken in Flagstaff between 1972 and 1986, they reported that the residuals obtained appeared to approximate an unperturbed proper motion more closely than the periodic motion predicted by van de Kamp (1982). However, the data were inconclusive. In particular, observations made in 1977 were especially suggestive of a significant change in motion (Harrington & Harrington 1987). These observations cover a period slightly longer than the orbital period of the inner planet but less than a single orbit of the outer planet van

de Kamp described. When even a full orbital period has been observed, the linear component of a companion-induced perturbation may still be mistakenly included in the proper motion terms (Black & Scargle 1982).

Using the Fine Guidance Sensors (FGS) of the Hubble Space Telescope (HST), Benedict *et al.* (1999) observed Barnard's Star over three years. Using a periodogram technique similar to that described in section 2.3.3, they found significant power associated at a 0.5-year period. However, that signal appears to be associated with the rolling of the telescope. After additional corrections for motions of the telescope, they found no evidence of any companion with a mass slightly less than that of Jupiter and a period between 150 and 1,000 days, or between 0.4 and 3 years. This mass limit approaches that necessary to detect the planets described van de Kamp (1982). However, their observations and the periods they consider cover a fraction of the orbital periods van de Kamp calculated. This observation period is too short to decouple orbital and proper motion terms adequately if long-period planets were present.

Although McCormick has a substantial collection of photographic material for Barnard's Star, no previous investigation analyzed the complete collection. As shown in Figure 2.1, the preliminary analyses failed to detect any planetary companions (Fredrick & Ianna 1985; Ianna 1995; Bartlett & Ianna 2001) although some earlier reports (van de Kamp 1963a, 1969a; Harrington & Harrington 1987) hinted of a perturbation detected in this material.

A Barnard's Star Perturbation Search Using McCormick Observatory Photographic Plate Material

Jennifer Bartlett and Phillip Ianna, University of Virginia, Department of Astronomy

TABLE I. PARALLAX AND PROPER MOTION

Parameter	Value
McCormick Parallax	540.2 ± 1.7 milliarseconds
Hubble Space Telescope Parallax	545.4 ± 0.9 milliarseconds
Yale Parallax	545.6 ± 1.1 milliarseconds
Hipparcos Parallax	549.3 ± 1.6 milliarseconds
McCormick Proper Motion	103.12 ± 0.2 milliarseconds/yr
Hubble Space Telescope Proper Motion	107.70 ± 0.3 milliarseconds/yr
Hipparcos Proper Motion	105.66 ± 2.2 milliarseconds/yr

ABSTRACT

A time-series analysis of photographic plates taken of Barnard's Star at the Leander McCormick Observatory since 1969 reveals no evidence of periodic perturbations indicative of a planetary companion. Table I lists the proper motion and parallax of Barnard's Star calculated from these observations. Table II lists the resulting annual residuals, which are illustrated in Figure 1. The x- and y-residuals correspond to residuals in right ascension and declination, respectively. The error bars indicate a 95 percent confidence level. Figure 2 shows the periodograms corresponding to these residuals. In neither case does the power at any frequency indicate a signal at a significance level of 50 percent or better. However, this work does not absolutely rule out the possibility that Barnard's Star may have planets.

TABLE II. RESIDUALS FOR ANNUAL NORMAL POINTS

Year	X Residuals (microns)	Y Residuals (microns)	Image
1969	-1.0 ± 0.6	-0.1 ± 0.9	11
1970	-0.6 ± 0.4	-0.3 ± 0.5	50
1974	-0.2 ± 0.7	0.0 ± 0.7	41
1977	0.2 ± 0.4	0.3 ± 0.3	31
1978	-0.2 ± 0.3	0.1 ± 0.4	74
1979	0.1 ± 0.4	-0.7 ± 0.5	42
1980	0.4 ± 0.3	-0.1 ± 0.3	39
1981	-0.1 ± 0.4	-0.3 ± 0.4	67
1982	0.2 ± 0.4	-0.3 ± 0.4	59
1983	0.1 ± 0.4	-0.4 ± 0.4	84
1984	0.1 ± 0.9	-0.3 ± 0.7	21
1985	0.4 ± 0.9	-1.0 ± 1.1	8
1986	0.4 ± 0.5	0.4 ± 0.5	72
1988	-1.0 ± 0.7	0.0 ± 0.4	37
1989	0.5 ± 0.4	-0.3 ± 0.4	40
1990	-0.4 ± 0.3	0.6 ± 0.3	102
1992	-1.8 ± 0.9	-0.2 ± 1.2	8
1993	-1.4 ± 0.7	0.0 ± 0.9	17
1998	0.0 ± 0.6	-0.1 ± 0.7	59

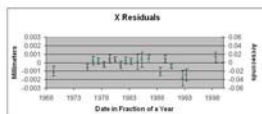


FIGURE 1. RESIDUALS FOR ANNUAL NORMAL POINTS

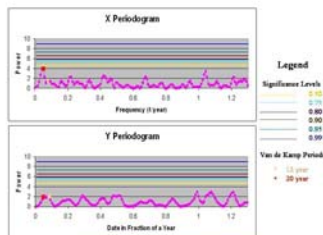


FIGURE 2. RESIDUAL PERIODOGRAMS

HISTORY

Barnard's Star is a particularly interesting object, not only because of its nearness and high proper motion, but also because of the early planet-detection claims. Table III lists several of the physical characteristics of this red dwarf. In 1963, Peter van de Kamp explained perturbations in its proper motion by the presence of a planetary companion. Based upon observations made at the Sproul Observatory between 1916 and 1962, Van de Kamp claimed the star had a planet with about 1.6 times the mass of Jupiter and an orbital period of 24 years. In 1969, he produced another single-planet solution and a two-planet solution to the astrometric wobble detected. After accounting for instrumentation effects that might have been partially responsible for his initial results, he continued to assert that Barnard's Star had two planets. Figures 3 and 4 illustrate the results of his 1982 analysis, in which he calculated that the detected planets had 0.7 and 0.5 Jupiter masses and 12- and 20-year orbits, respectively. However, the searches listed in Table IV have failed to confirm his results. Although the McCormick Observatory has a substantial collection of photographic material related to Barnard's Star, these plates have only been partially analyzed in the past. The earlier analyses involving fewer observations also failed to detect any planetary companions.



FIGURE 3. SPROUL RESIDUALS FOR ANNUAL NORMAL POINTS



FIGURE 4. SPROUL RESIDUALS AFTER REMOVING ORBITS

TABLE III. PHYSICAL CHARACTERISTICS

Parameter	Value
Distance	16.0 ± 0.1 pc
Proper Motion (μ)	103.12 ± 0.2 mas/yr
Parallax (π)	540.2 ± 1.7 mas
Magnitude	16.7 ± 0.1
Spectral Type	M4V
Mass	0.16 ± 0.01 M _J

TABLE IV. PARTIAL LIST OF BARNARD'S STAR STUDIES

Observer	Year of Publication	Method
Van de Kamp	1963, 1969, 1974, 1975	astrometric (Sproul plates)
Garnaud, Fuhrman	1977	astrometric (Albany and Van 13ck plates)
Frankik, Ianna	1985	astrometric (small set of McCormick plates)
Mary, Beuthe	1989	radial velocity
Shkolnik et al.	1990	radial velocity
Horne, McCarthy	1990	astrometric
Garnaud	1997	astrometric (Hubble Space Telescope Photometer)
Ianna	1997	astrometric (small set of McCormick plates)
Bartlett et al.	1999	Hubble Space Telescope interferometer
Bartlett, Ianna	2001	astrometric (complete set of McCormick plates)

TABLE V. MCCORMICK REFRACTOR CHARACTERISTICS

Parameter	Description
Overall Aperture	3.5-inch refractor mounted behind a 10-in. Clark and Sons Objective Star
Objective Star	67 centimeters
Focal Ratio	f/14.5
Focal Length	969 centimeters
Angular Field	0.74 degrees
Plate Scale	20.75 arcseconds per millimeter
Barnard's Star Plates	110 (1) plates with V filters (12 filters (100 - 100 nanometer band pass)
Mounting Equinox	EQ3 (H&M) Microdome mount

TABLE VI. MCCORMICK OBSERVATIONS

Parameter	Value
Run Date	April 1969 through August 1998 (c. 29 years)
Images	924
Plates	204
Aligns	165
Reference Stars	12

TABLE VII. POWER SPECTRA PEAKS

Frequency (1/years)	Power	False Alarm Probability
X Residuals	1.1 × 10 ⁻⁵	1.0%
Y Residuals	1.1	99%

METHOD AND RESULTS

The observers at McCormick Observatory obtained photographic plate images of Barnard's Star over many years with the 26.25-inch refractor. This analysis relies on those observations made since 1969 because the earlier material is too sparse and of such poor quality so as to be unusable for this study. Table V characterizes the McCormick refractor, which has been in operation since 1885. Table VI describes the observations upon which this analysis is based.

The McCormick fathomed microdome mount measured the positions of Barnard's Star and 12 reference stars on each of the photographic plates. From these measurements, the McCormick Parallax Reduction Program calculated the proper motion and parallax of Barnard's Star, which are listed in Table I. The proper motion calculation included significant secular acceleration terms. The program output included the residuals associated with each observation. The residuals were combined into the annual normal points listed in Table II and illustrated in Figure 1. The periodograms of the x- and y-residuals were calculated separately using the Lamb method described in *American Recipes in FORTRAN 77*. Frequencies up to four times the Nyquist frequency were searched to produce plots of power versus frequency. Figure 2 shows that the power at no frequency is indicative of a signal at a significance level of 50 percent or better. Table VII summarizes the characteristics of the highest peak in each power spectrum including the probability that the peak could be caused by noise. In both cases, the peaks are most likely false alarms. In addition, no signal is seen at the frequencies corresponding to 12 or 20 years, which are the periods associated with the planets reported by Van de Kamp in 1982.

DISCUSSION

This failure to replicate Van de Kamp's results, while not unexpected, does not completely eliminate the possibility that such planetary companions exist. The Sproul Observatory material available to Van de Kamp is unique. In 1982, his analysis used nearly 20,000 exposures on 4,580 plates taken on 1,200 nights between 1938 and 1981 at Sproul Observatory compared with this analysis of fewer exposures at McCormick Observatory. However, the McCormick refractor was not subjected to significant physical changes, such as the modifications made to the Sproul refractor in 1949. In addition, the baseline of the McCormick observations represents only slightly more than twice the period of the more massive, but shorter period, planet described by Van de Kamp. Even with smoothing to annual normal points, the residuals to the proper motion and parallax solutions obtained in this study show the noise typical of photographic plates. Nonetheless, this study further reduces the possibility that planets as massive as Jupiter orbit Barnard's Star.

ACKNOWLEDGEMENTS

We gratefully acknowledge support from NSF grant AST 98-20711 and from Littion Marine Systems, Incorporated.

REFERENCES

Bartlett, J. and Ianna, P. (Aug. 1999) "Astrometric Astronomy of Proxima Centauri and Barnard's Star Using Hubble Space Telescope Fine Guidance Sensor 3: Detection Limits for Sub-Jupiter Companions." *Astron. J.*, 118(2), 1086-1100.

Frankik, L. W. and Ianna, P. A. (Dec. 1985) "The Barnard's Star Perturbations." *Bull. American Astron. Soc.*, 17, 551.

Osmond, George. (1995) "A Study of the Astrometric Motion of Barnard's Star." *Astrophysics and Space Sciences*, 224, 91-101.

Osmond, George and Eshbach, Heinrich. (Oct. 1975) "An Unsuccessful Search for a Planetary Companion of Barnard's Star (HD + 37061)." *Astron. J.*, 70(8), 769-776.

Hony, Todd. "The One Hundred Nearest Star Systems." [Internet web page], last edited 1 January 2000, last visited 26 April 2001, available at <http://olympus.gsu.edu/OLYCON/TOP100.htm>

Hony, Todd and McCarthy, D. W. (Feb. 1995) "A Systematic Search for Brown Dwarfs Orbiting Nearby Stars." *Ap. J.*, 306, 334-347.

Ianna, P. A. (1997) "Twenty Years of McCormick Observations." *Astrophysics and Space Sciences*, 224, 136.

Mary, Geoffrey W. and Beuthe, Kerstin J. (Sept. 1989) "A Search for Substellar Companions to Low-Mass Stars." *Ap. J.*, 344, 451-453.

NASA. This research made use of NASA's Astrophysics Data System Abstract System.

Pear, W. H. et al. (1992) *Harvard Catalogue of Proper Motions* (2nd ed., Cambridge University Press), 509-577.

Shkolnik, M. F. et al. (Oct. 1989) "An Infrared Search for Low-Mass Companions of Stars Near the Sun." *Astron. J.*, 98(5), 1429-1437.

Van de Kamp, Peter. (Sept. 1963) "Astrometric Study of Barnard's Star from Plates Taken with the 24-inch Sproul Refractor." *Astron. J.*, 68(7), 513-521.

(March 1969) "Parallax, Proper Motion, Acceleration, and Orbital Motion of Barnard's Star." *Astron. J.*, 74(3), 228-240.

(Aug. 1969) "Astometric Dynamical Analysis of Barnard's Star." *Astron. J.*, 74(3), 797-799.

(Aug. 1975) "Astrometric Study of Barnard's Star from Plates Taken with the Sproul 61-cm Refractor." *Astron. J.*, 80(5), 616-643.

(1982) "The Planetary System of Barnard's Star." *Pulsar Astronomy*, 16, 141-147.

Fig. 2.1 – Results of Preliminary Time-series Analysis of Photographic Plates from Leander McCormick Observatory (Bartlett & Ianna 2001).

2.2.2 Radial-Velocity Studies

Marcy and Benitz (1989) made twenty-five radial velocity observations of Barnard's Star over about four years as part of a larger search for brown dwarfs. After analyzing their short-interval measurements using a periodogram technique similar to that described herein, they reported no companions to Barnard's Star with projected masses (mass times the sine of an unknown inclination angle, $m \sin i$) greater than or equal to about $11 M_{21}$. Their mass-detection sensitivity limit was many times greater than those calculated by van de Kamp (1982). Consequently, the California and Carnegie Planet Search continued radial velocity observations of Barnard's Star at the Lick and Keck Observatories. Their recent results appear to eliminate Jupiter-size planets with periods as long as eight years and also render a Jupiter-sized planet with an orbit of 11.5 years unlikely (C. McCarthy *et al.* 2006, in preparation).

Endl *et al.* (2002) used the European Southern Observatory Coudé Echelle spectrometer to take twenty-four radial-velocity measurements of Barnard's Star over nearly 4 years. Their observations are sensitive to planets within an astronomical unit of the central star, which is within the orbit of the inner planet described by van de Kamp (1982). They combined their estimated detectible mass limits with those of Benedict *et al.* (1999) in order to eliminate planets with projected masses ($m \sin i$) greater than $1.2 M_{21}$. Van de Kamp's planets fall below this mass limit.

More radial velocity measurements of Barnard's Star, this time by Kürster *et al.* (2003), were made using the Ultraviolet-Visual Echelle Spectrograph on the 8.2-meter Kueyen Unit Telescope of the Very Large Telescope (VLT-UT2+UVES). Using a

periodogram technique, they searched the hydrogen-alpha (H_α) index and radial-velocity residuals for signals indicative of companions with periods between 2–885 days, or up to nearly 2.5 years. They found no evidence of planets with projected masses ($m \sin i$) greater than $0.12 M_{21}$. Within the habitable zone of Barnard's Star, which they associated with periods between 5.75 days and 21.5 days, they found no evidence of planets with projected masses as small as $0.02 M_{21}$. They acknowledge the possibility of missing massive planets with highly eccentric orbits. Although the masses excluded by this work would include those described by van de Kamp (1982), the orbital periods considered are far less than his.

2.2.3 Direct Imaging Studies

Skrutskie, Forrest, and Shure (1989) undertook the earliest direct imaging search. They observed stars in the solar neighborhood, including Barnard's Star, in the infrared in order to detect low-mass companions. They observed Barnard's Star on three nights in 1985. Because of saturating light from the primary star, companions within 2 seconds of arc ($2''$) of the primary were undetectable. At the distance of Barnard's Star, this separation equals a linear separation of about 4 astronomical units (AU). Van de Kamp (1982) calculated orbital radii of 2.7 and 3.8 AU for the planets; the inner planet would be undetectable but the outer planet would be near the edge of the saturation region. In addition, this survey was sensitive to substellar companions with an apparent K-band (effective wavelength of 2.2 micrometers, μm) magnitude brighter than 15.0. This magnitude limit corresponds to an object with an effective temperature of approximately 1,000 Kelvin (K) and more massive than $50 M_{21}$. Therefore, this search

would miss cooler planets less massive than Jupiter, such as those described by van de Kamp.

Oppenheimer *et al.* (2001) used coronagraphic images taken with Gunn r and z filters ($r = 668$ nanometers, nm, and $z = 912$ nm per Schneider, Gunn, & Hoessel 1983) and direct images taken with J ($1.25 \mu\text{m}$) and K filters to search for common proper motion companions to northern stars within 8 parsecs (pc) of the Sun. They took the optical images of Barnard's Star in 1992 and 1994 using the Palomar 60-inch telescope and infrared images in 1996 and 1997 using the Palomar 200-inch telescope. Although they found no companion to Barnard's Star, they detected six new stellar companions in other nearby systems. In z-band, their survey could conceivably detect brown dwarfs with ages of about 1 gigayear (Gyr) and with masses as small as $15 M_{21}$ separated from the primary star by distances between 20 and 225 AU. In J-band, their survey could possibly sense brown dwarfs with ages of about 1 Gyr and masses as small as $16 M_{21}$ separated from the primary star by distances between 5 and 120 AU. The separations and masses that Oppenheimer *et al.* (2001) would have revealed are both too large for their survey to detect van de Kamp's planets (1982).

Van Buren and his team (1998) undertook another infrared survey using an N-band filter ($10.2 \mu\text{m}$) at Palomar Observatory on two non-photometric nights. They were seeking brown dwarfs or giant planets orbiting within $2\text{--}10''$ of selected primary stars, which translates to a separation of $4\text{--}18$ AU for Barnard's Star. They did not detect any companion in this range with a temperature greater than 1,000 K, which would correspond to a planetary mass between 70 and $80 M_{21}$. Although the outer planet

described by van de Kamp (1982) is near the inner boundary of this search, he calculated a mass much smaller than the limit set by this survey.

In 1991 and again in 1998, Hinz *et al.* (2002) imaged Barnard's Star in J-band as part of a survey of northern M dwarfs within 8 pc of the Sun. They were seeking brown dwarfs sharing common proper motions with these stars. They detected no new companions brighter than approximately 16.5 magnitudes within about 4 minutes of arc of any the stars in their sample. Similar to the work of Oppenheimer *et al.* (2001), their survey was sensitive to 1-Gyr-old brown dwarfs with masses as low as $16 M_{21}$ (Hinz *et al.* 2002). The planets described by van de Kamp (1982) fall well below this limit.

Schroeder *et al.* (2000) used the HST wide field planetary camera 2 (WFPC-2) to image directly faint companions to the seventeen nearest star systems. They observed 23 stars within 13 pc of the Sun, including Barnard's Star on five occasions, using the F814W, F675W, and F1042M filters (F814W = 792.4 nm, F675W = 669.7 nm, F1042M \approx 1,019 nm per Holtzman *et al.* 1995). They found no new companions. The sensitivity of their search was insufficient to identify planets that Benedict *et al.* (1999) would have missed. Therefore, Schroeder *et al.* (2000) would not have detected the planets described by van de Kamp (1982) either.

2.2.4 Miscellaneous Studies

Although astrometric, radial-velocity, and direct imaging searches have been the most common approaches to detecting companions to Barnard's Star, other techniques have been used including radio observations and speckle interferometry.

Winglee, Dulk, and Bastian observed Barnard's Star at 0.33 Gigahertz (GHz) and 1.47 GHz with the Very Large Array (VLA) in 1986. They hoped to detect cyclotron maser radiation from Barnard's Star or its possible companions; several planets within our Solar System produce such radiation. However, they detected neither Barnard's Star nor any companion.

Using speckle interferometry, Henry and McCarthy (1990) sought brown dwarfs orbiting M dwarfs within 5 pc of the Sun. With respect to Barnard's Star, they looked for companions separated from it by a minimum of 2 AU, or about 1", out to a maximum of 10 AU. The orbital radii calculated by van de Kamp (1982) fall within the inner half of this annulus. According to this study, any companion near the star would have to have an absolute K-band magnitude greater than 11.7 while any companion at the outer limit would have to have an absolute K-band magnitude greater than 12.2. However, their magnitude limits correspond to brown dwarfs with masses larger than $70 M_{21}$, which would miss the low-mass planets described by van de Kamp.

2.3 MEASUREMENT AND ANALYSIS

Observers at McCormick obtained Eastman Kodak 103a-G photographic plate images of Barnard's Star over many years with the 26.25-inch (67-centimeter) refractor and a Schott GG 495 filter giving a 495–600 nm passband (Schott 2006, Kodak 1989). The plate scale is $20.7484 \pm 0.0005''$ millimeter⁻¹ (Alden & van de Kamp 1927; Vyssotsky & van de Kamp 1937); the McCormick Parallax Reduction Program (sager; hereafter MPRP) uses the commonly adopted value of 20.75 mas millimeter⁻¹. On 107 nights between April 1969 and August 1998, observers obtained 919 good images on

293 plates. This analysis relies only on those observations made since 1969. The earliest material, including approximately sixty-three plates from 1916 to 1934 and eight plates from 1968, was excluded because it is too sparse and of inadequate quality to be usable for this study. In addition, different emulsions and filters were used from 1916 to 1934 (Mitchell *et al.* 1940). This exclusion eliminates all of the plates available to van de Kamp in 1963. The 1968 plates were among the first taken of Barnard's Star when it was reinstated in the parallax program at the request of P. A. Ianna (2006, private communication; L. Frederick 2006, private communication).

The McCormick Photometric Data Systems (PDS) 1010GM Microdensitometer, a granite-based and laser-encoded microdensitometer, measured the positions of Barnard's Star and twelve reference stars on each of the photographic plates. The microdensitometer scanned with a 20- μm square aperture and 10- μm step size to digitize a 71 by 71 pixel map centered on each reference star and Barnard's Star. Then, the relative image locations were obtained by fitting Gaussians to the sky subtracted marginal distributions. The plates were scanned in density mode in a boustrophedonic pattern. The repeatability of positions with this system is typically a few tenths of a micrometer and the accuracy of a single position with the somewhat noisy, coarse-grained emulsion is about $\pm 1.5 \mu\text{m}$. Guinan and Ianna (1983) provide further description of the reduction software.

2.3.1 Relative Motions

From these measurements, the MPRP calculated the relative parallax and proper motion of Barnard's Star to be $546.5 \pm 1.4 \text{ mas}$ and $10,361.25 \pm 0.20 \text{ mas yr}^{-1} (\text{yr}^{-1})$ in

355.9050 ± 0.0011 degrees ($^{\circ}$), respectively. The mean errors of unit weight were 1.3 and $1.5 \mu\text{m}$ in the x- and y-coordinates, respectively. Table 2.3 lists the individual components of each motion. The discrepancy of approximately 70 mas between the x- and y-components of the parallax, which correspond to right ascension and declination, appears to be due to the low signal in the y-direction. A very small-amplitude parallactic displacement is produced in the y-direction owing to the close proximity of Barnard's Star to the ecliptic. The calculation of relative parallax and proper motion used an iterative three plate-constant adjustment model, with scale, orientation, and origin terms. The program processed the reference star proper motions and plate constants twice to improve results. Several additional terms were tested using Tycho-2 (Høg *et al.* 2000, hereafter Tycho) V-band (510 nm) apparent magnitudes and B-V colors (B=420 nm). Individually, the coefficients of coma—magnitude times position—and color terms were not statistically significant as shown in Table 2.4. To be considered significant in a coordinate, a coefficient had to be greater than three times its associated error for the majority of exposures; the probability of such a comparatively large coefficient arising from noise alone is less than 1 percent (%) (Beers 1957). A magnitude term, however, was significant in x but not y. Including a magnitude term reduced the difference between the two parallactic components from 90 mas to 56 mas.

TABLE 2.3
COMPONENTS OF THE RELATIVE MOTION OF BARNARD'S STAR

Parameter	X		Y		Combined	
Parallax (mas)	547.9	± 1.4	474.6	± 9.9	546.5	± 1.4
Proper Motion (mas yr ⁻¹)	-739.9	± 0.2	10334.8	± 0.2	10361.25	± 0.20
Position Angle (degrees)		355.9050 \pm 0.0011	
Secular Acceleration (mas yr ⁻²)	-0.025 \pm 0.037		1.253 \pm 0.041		1.253 \pm 0.041	
Mean Error of Unit Weight (μ m)	1.3	...	1.5	
Mean Error of Unit Weight (mas)	27.1	...	32.1	

TABLE 2.4
ADDITIONAL PLATE MODEL TERMS CONSIDERED

Term	Significant in X?		Significant in Y?		Frames Considered	Comments
	(Frames)	(%)	(Frames)	(%)		
V _T Magnitude	495	54	188	21	916	slight improvement in solution
Coma	393	43	74	8	916	
(B-V) _T Color	454	50	284	31	916	does not improve solution
V _T Mag & Acceleration	518	56	217	24	919	greatest overall improvement in solution
Coma & Acceleration	393	43	74	8	916	
(B-V) _T Color & Acceleration	454	50	281	34	916	solution quality similar to no acceleration

Because Barnard's Star has a large absolute parallax ($\pi = 552 \pm 7$ mas as calculated in section 2.3.2), proper motion ($\mu = 10.354 \pm 0.006'' \text{ yr}^{-1}$), and radial velocity ($V_r = -110.5 \pm 0.4$ kilometers second⁻¹ per Nidever *et al.* 2002), significant secular acceleration ($\dot{\mu}$) was expected (van de Kamp 1977b). The equation

$$\dot{\mu} = -2.05'' \times 10^{-6} V_r \mu \pi \quad (2.1)$$

predicts 1.29 ± 0.02 mas yr⁻². The geocentric motion of Barnard's Star may be described by

$$X = c_x + \mu_x t + \pi_x P_\alpha + q_x t^2 \quad (2.2)$$

$$Y = c_y + \mu_y t + \pi_y P_\delta + q_y t^2 \quad (2.3)$$

where c_x and c_y are geocentric positions at the mean time of the observations (1983.7740), t is time lapsed since then in solar years, P_α and P_δ are the parallactic factors in right ascension and declination, and q_x and q_y are half of the secular acceleration in each direction. We measured a secular acceleration of 1.253 ± 0.041 mas yr⁻²; Table 2.3 lists the individual components of this motion as well. The y-component of this secular acceleration was statistically significant. Table 2.5 compares this value with earlier studies. The current McCormick measurement of the secular acceleration of Barnard's Star is within the errors of the predicted value and that measured by Benedict *et al.* (1999) based on three years of HST observations. Although the inclusion of a secular acceleration term increased the difference between the x- and y-components of the relative parallax, it reduced the uncertainty in the y-component from 14 mas to 10

mas, decreased the number of residuals greater than or equal to $4 \mu\text{m}$ from 72 to 33, and reduced the largest residual from $8.3 \mu\text{m}$ to $4.8 \mu\text{m}$.

TABLE 2.5
SECULAR ACCELERATION MEASUREMENTS OF BARNARD'S STAR

Measurement with Baseline	Secular Acceleration (mas yr ⁻¹)		Reference
Predicted	1.29	± 0.02	
McCormick, 1969–1998	1.25	± 0.04	
Hubble Space Telescope, 1993–1996	1.2	± 0.4	1
Sproul, 1916–1981	1.30	± 0.03	2
McCormick, 1916–1973	1.38	± 0.04	3

REFERENCES.—(1) Benedict *et al.* 1999; (2) van de Kamp 1986; (3) van de Kamp 1977b

Magnitude, coma, and color plate constants were also tested in conjunction with secular acceleration. Again, neither coma nor color terms made significant contributions to the solution as shown in Table 2.4. Using the magnitude term with secular acceleration produced a smaller discrepancy between two components of the parallax than using either no acceleration or acceleration alone; the difference was 68 mas rather than 90 mas or 100 mas. This combination of terms also produced a smaller error in y -component of the parallax than with no acceleration or with either acceleration or magnitude alone; the error was 9.7 mas rather than 14 mas, 10 mas, or 14 mas, respectively.

2.3.2 Reduction to Absolute

The relative parallax and proper motion of Barnard's Star are measured with respect to a reference frame of twelve stars, which are listed in Table 2.6 and shown in Figure 2.2. Several of these reference stars appear in other studies of Barnard's

TABLE 2.6
REFERENCE STARS

Reference Star	Tycho Identification	Coordinates (2000.0)		V_T (magnitude)	K_s (magnitude)	Other Designations
		Right Ascension (hh mm ss.sss)	Declination (dd mm ss.ss)			
1	TYC 425-262-1	17 57 51.948	+04 42 20.25	11.515 ± 0.119	10.575 ± 0.025	
2	TYC 425-1810-1	17 58 21.609	+04 36 09.90	11.100 ± 0.087	5.963 ± 0.017	
3	TYC 425-1467-1	17 58 56.021	+04 35 35.40	11.326 ± 0.103	10.484 ± 0.021	
4	TYC 425-1773-1	17 58 31.320	+04 30 53.67	11.838 ± 0.181	9.917 ± 0.021	
5	TYC 425-1397-1	17 58 36.252	+04 22 57.71	11.134 ± 0.096	10.115 ± 0.021	
6	TYC 425-802-1	17 58 24.420	+04 27 41.41	9.933 ± 0.034	6.794 ± 0.024	BD+4 3562, HIP 87991
7	TYC 425-22-1	17 57 19.878	+04 53 14.85	8.729 ± 0.016	7.102 ± 0.026	BD+4 3558, HIP 87901
8	TYC 425-187-1	17 56 43.618	+04 47 28.46	10.888 ± 0.078	9.793 ± 0.020	
9	TYC 425-1858-1	17 56 30.064	+04 37 37.66	10.785 ± 0.071	8.983 ± 0.022	
10	TYC 425-616-1	17 57 43.928	+04 26 23.60	8.831 ± 0.016	8.648 ± 0.023	BD+4 3560
11	TYC 425-214-1	17 57 34.938	+04 35 10.34	11.599 ± 0.131	8.772 ± 0.022	
12	TYC 425-1844-1	17 57 24.418	+04 36 09.29	10.522 ± 0.049	8.676 ± 0.022	BD+4 3559
Barnard's	TYC 425-2502-1	17 57 48.498	+04 41 35.40	9.776 ± 0.028	4.524 ± 0.020	BD+4 3561, HIP 87937

REFERENCES.—Positions and V_T magnitudes are from Tycho. K_s magnitudes are from 2MASS. Other designations are from SIMBAD.

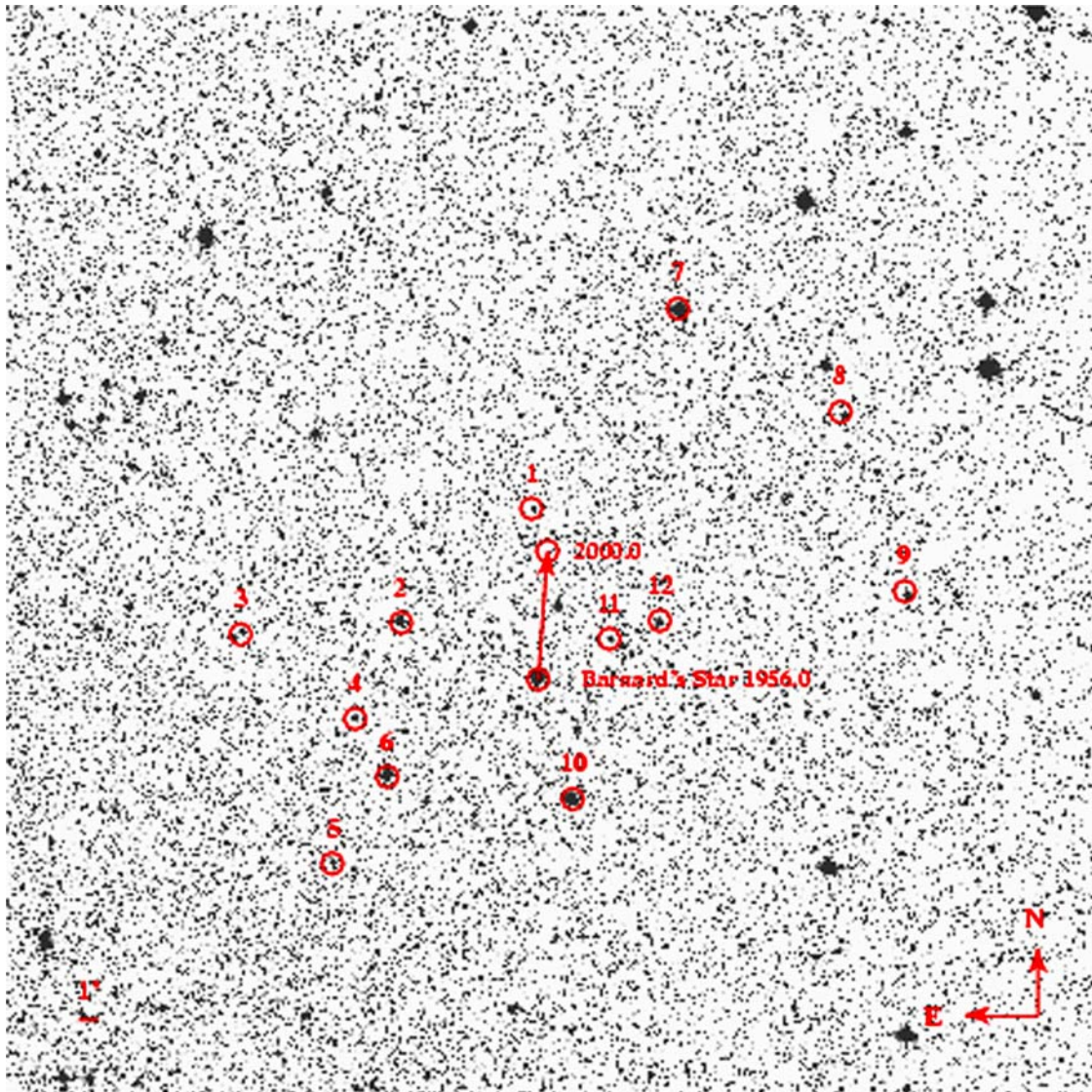


FIG. 2.2.— Barnard's Star (c. 1956.0) and Reference Frame. Image Source: Digitized Sky Survey via *SkyView* with annotations by R. Patterson, J. L. Bartlett, & J. L. Bartlett. Image Copyright © California Institute of Technology; digitized and compressed by Space Telescope Science Institute.

Star (van de Kamp 1935; Grossbacher, Mesrobian, & Upgren 1968; Gatewood & Eichhorn 1973; Castelaz *et al.* 1991; Benedict *et al.* 1999); Table 2.7 provides cross-references to the earlier studies.

Ideally, the reference stars should be sufficiently distant to show neither parallax nor proper motion themselves. In reality, these stars will have small parallaxes and proper motions over the period of observation. Therefore, a correction to account for the mean distance and motion of the reference frame is necessary to convert the relative parallax and proper motion to absolute ones. Because the MPRP corrects the measured positions for the relative proper motions of the reference stars, no additional correction is required for secular acceleration (van de Kamp 1977b).

Several methods exist for determining the necessary corrections to absolute parallax and proper motion ranging from statistical methods requiring little information about the individual reference stars to photometric and spectroscopic methods that are very specific to the reference stars used.

The Yerkes Galactic Model calculates mean and secular parallaxes based on the stellar luminosity function, the distribution of stars and dust, and solar and stellar kinematics. This model may be used to estimate corrections to convert relative parallaxes and proper motions to absolute ones using the galactic latitude and apparent visual magnitude of each reference star (van Altena 1974). To obtain comparable visual magnitudes, the Tycho V-band magnitudes were converted to the Johnson and Morgan (1951, 1953; hereafter Johnson-Morgan) system (VJM=550 nm) using the

TABLE 2.7
REFERENCE STAR CROSS-REFERENCES

Reference Star	Tycho Identification	van de Kamp ^a	Van Vleck Observatory ^b	Allegany Observatory ^c	Hubble Space Telescope ^d	References
1	TYC 425-262-1			13	36	1, 2
2	TYC 425-1810-1			16		1, 3
3	TYC 425-1467-1			20		1
4	TYC 425-1773-1					
5	TYC 425-1397-1					
6	TYC 425-802-1	4	2 nd π , BD +4°3562 ^e	17		4, 5, 1, 3
7	TYC 425-22-1			770		3
8	TYC 425-187-1			5		1
9	TYC 425-1858-1					
10	TYC 425-616-1	2	3, BD +4°3560	11		4, 5, 1, 3
11	TYC 425-214-1					
12	TYC 425-1844-1	1	2, BD +4°3559	10		4, 5, 1, 3

NOTES.— ^aReference star numbers used by van de Kamp in his various articles

^bVan Vleck Observatory reference star number and *Bonner Durchmusterung* (BD) identification

^cAllegany Observatory numbers

^dReference star identification number used by Benedict *et al.* 1999

^eVan Vleck Observatory used the same field to measure the parallax of Barnard's Star (BD +4°3561) and BD +4°3562.

REFERENCES.—(1) Gatewood & Eichhorn 1973; (2) Benedict *et al.* 1999; (3) Castelaz *et al.* 1991; (4) van de Kamp 1935; (5) Grossbacher, Mesrobian, & Upgren 1968

transformations in *The Hipparcos and Tycho Catalogues* (ESA 1997, hereafter Hipparcos). However, reference star 2 (TYC 425-1810-1) appears to be an M star (Castelaz *et al.* 1991) for which these transformations are not recommended. The V_{JM} magnitudes listed in Table 2.8 were assumed to correspond to van Altena's (1974) visual magnitude.

According to the Yerkes Galactic Model, 4.0 ± 1.6 mas should be added to the relative parallax and $1.7 \pm 6.3'' \text{ yr}^{-1}$ to the relative proper motion of Barnard's Star. *The General Catalogue of Trigonometric Stellar Parallaxes* (van Altena, Lee, & Hoffleit 1995, hereafter YPC) uses a more detailed galactic model (van Altena *et al.* 1988). Benedict *et al.* (1999) estimate their correction to absolute from Table 2 of this catalog. According to this table, a star at a galactic latitude of approximately 14.0° and with an average reference frame V magnitude of about 10.6 would require a correction of approximately 2.6 ± 0.2 mas added to the relative parallax (YPC; Benedict *et al.* 1999).

With Méndez, van Altena (1998) updated his galactic models once more. Méndez and van Altena offer to calculate the appropriate corrections upon request. In this instance, van Altena (2005, private communication) declined with the recommendation that calculating photometric distances for the reference stars and comparing their proper motions with those in the Hipparcos or Tycho catalogs would provide more reliable corrections.

Distances to stars may also be estimated assuming the apparent motion of their class is actually due to the motion of the Sun. Such secular parallaxes provide

TABLE 2.8
BRIGHTNESS OF REFERENCE STARS

Reference Star	Tycho Identification	B_{JM} (magnitude)	V_{JM} (magnitude)	K_{BB} (magnitude)	Comments
1	TYC 425-262-1	11.61 ± 0.19	11.50 ± 0.13	10.614 ± 0.026	
2	TYC 425-1810-1	12.71 ± 0.36	10.89 ± 0.15	6.001 ± 0.019	M3I star (ref 1), poor B and V transformations
3	TYC 425-1467-1	11.70 ± 0.17	11.28 ± 0.11	10.523 ± 0.022	
4	TYC 425-1773-1	12.38 ± 0.32	11.77 ± 0.20	9.956 ± 0.022	
5	TYC 425-1397-1	11.71 ± 0.16	11.07 ± 0.11	10.154 ± 0.022	
6	TYC 425-802-1	11.120 ± 0.080	9.792 ± 0.043	6.832 ± 0.025	
7	TYC 425-22-1	9.264 ± 0.028	8.666 ± 0.018	7.141 ± 0.027	
8	TYC 425-187-1	11.19 ± 0.13	10.852 ± 0.084	9.832 ± 0.021	
9	TYC 425-1858-1	11.42 ± 0.13	10.710 ± 0.079	9.021 ± 0.023	
10	TYC 425-616-1	8.845 ± 0.028	8.829 ± 0.017	8.687 ± 0.024	
11	TYC 425-214-1	12.57 ± 0.29	11.48 ± 0.16	8.810 ± 0.023	
12	TYC 425-1844-1	11.036 ± 0.087	10.461 ± 0.054	8.715 ± 0.023	
Barnard's	TYC 425-2502-1	11.178 ± 0.085	9.589 ± 0.039	4.562 ± 0.022	M4V star (ref 2), poor B and V transformations

REFERENCES.— B_{JM} and V_{JM} magnitudes from Tycho using Hipparcos transformations. K_{BB} magnitudes from 2MASS using Carpenter (2006) transformations. (1) Castelaz *et al.* 1991; (2) Kirkpatrick *et al.* 1991

another statistical approach to converting a relative parallax to an absolute one. Because the apparent solar motion varies with spectral type (Vyssotsky & Williams 1948b), knowledge of the spectral types of the reference stars is needed to convert the appropriate secular parallax to a mean parallax.

Because only five reference stars have published spectral types, spectral types were estimated from broadband photometry. Tycho B- and V-band apparent magnitudes were converted to the standard Johnson-Morgan system using the Hipparcos transformations. K_s -band ($2.159 \mu\text{m}$) magnitudes from the Two Micron All Sky Survey (Skrutskie *et al.* 2006, hereafter 2MASS) were converted to the Bessell and Brett system of 1988 ($K_{\text{BB}}=2.19 \mu\text{m}$) using the transformations from the *Explanatory Supplement to the 2MASS All Sky Data Release* (Carpenter 2006). Table 2.8 lists these transformed magnitudes. Then, the resulting B-V and V-K colors were de-reddened using dust maps derived from Diffuse Infrared Background Experiment (DIRBE) and Infrared Astronomy Satellite (IRAS) data with the Cerro Tololo Inter-American Observatory (CTIO) and United Kingdom Infrared Telescope (UKIRT) systems ($V_{\text{CTIO}}=551.9 \text{ nm}$ and $K_{\text{UKIRT}}=2.2152 \mu\text{m}$) representing the standard optical and infrared bands (Schlegel, Finkbeiner, & Davis 1998).

The $(B-V)_0$ colors were compared to those provided by Drilling and Landolt in *Allen's Astrophysical Quantities* (2000, Table 15.7) to estimate spectral type and absolute V-band magnitude ($V_{\text{DL}}=550 \text{ nm}$) on a homogenized system closely related to the Johnson-Morgan system (Cousins 1976; Landolt 1992; Bessell 1979, 1976; Menzies *et al.* 1991). The $(V-K)_0$ colors were compared to those provided by Tokunaga in

Allen's Astrophysical Quantities (2000, Tables 7.6 through 7.8) to estimate spectral type and temperature. The resulting temperatures were used to calculate absolute V-band magnitudes (Drilling & Landolt 2000). Although the various transformations to V_{JM} magnitudes should result in consistent results, the definition of the Johnson-Morgan system itself evolved as it was applied to fainter and redder stars. Subsequent standards in that system by different observers show systematic differences (Menzies *et al.* 1991; Cousins 1984). The definition of K_{BB} appears less confused in the literature, but additional inconsistencies in those transformations may be revealed in time.

The assumption that all of the reference stars are main sequence stars produced reasonable distances, except for reference star 2 (TYC 425-1810-1) that appears to be a supergiant (Castelaz *et al.* 1991). The spectral types estimated from these colors were adopted for the reference stars without published spectral types. These estimated spectral types are probably accurate to within one spectral class. For those with published spectral types, the types determined by narrow-band photometry at Allegany Observatory (Castelaz *et al.* 1991), which are accurate to within 2.5 spectral subclasses, or determined by spectroscopy at the WIYN⁶ Observatory (Benedict *et al.* 1999) were adopted. Table 2.9 lists the broadband colors used, the initial estimated spectral types, and the final adopted spectral types.

Vyssotsky and Williams (1948a) provide two tables of secular parallaxes. In the first, they calculated secular parallaxes for stars grouped by photovisual magnitude

⁶WIYN stands for University of Wisconsin-Madison, Indiana University, Yale University, and National Optical Astronomy Observatories (NOAO).

TABLE 2.9
SPECTRAL TYPES FOR BARNARD'S STAR FIELD

Reference Star	Tycho Identification	(B-V) ₀ (mag)	(V-K) ₀ (mag)	Initial	van de Kamp	Spectral Types			Adopted	
						Kuiper	Allegany	Michigan	WIYN	
1	TYC 425-262-1	-0.0852	0.3759	A1V					A9III	A9III
2	TYC 425-1810-1	1.6140	4.3516	M3V			M3I			M3I
3	TYC 425-1467-1	0.2069	0.2089	A5V						A5V
4	TYC 425-1773-1	0.4136	1.2945	F4V						F4V
5	TYC 425-1397-1	0.4456	0.3883	F1V:						F1V:
6	TYC 425-802-1	1.1342	2.4479	K4V	F2	K4	K5V			K5V
7	TYC 425-22-1	0.3969	0.9915	F4V			G0V	F7V		G0V
8	TYC 425-187-1	0.0947	0.3682	A4V						A4V
9	TYC 425-1858-1	0.4720	1.0611	F5V						F5V
10	TYC 425-616-1	-0.1606	-0.3234	B6V	B8		B8I	B8/9III		B8I
11	TYC 425-214-1	0.8977	2.1648	K2V						K2V
12	TYC 425-1844-1	0.3828	1.2386	F4V	G0		G0V			G0V
Barnard's	TYC 425-2502-1	1.3938	4.5104	M3V						M4V

REFERENCES.—Spectral types from van de Kamp 1963b; Bidelman 1985 (Kuiper); Castelaz *et al.* 1991 (Allegany); Houk & Swift 1999 (Michigan); Benedict *et al.* 1999 (WIYN); and Kirkpatrick *et al.* 1991 (adopted for Barnard's Star).

and galactic latitude. In the second, they further divided the stars by spectral class. The secular parallaxes were converted to mean parallaxes using the solar velocities measured by Vyssotsky and Williams (1948b). Equating the V_{JM} and photovisual magnitudes and using the first table, a correction of 3.47 ± 0.43 mas should be added to the relative parallax to correct it to an absolute one using just the average reference frame brightness of 10.6 ± 1.0 magnitudes and galactic latitude of $30.93 \pm 0.11^\circ$. Averaging the corrections for each reference star should provide a more accurate correction. In this case, the first table produces a correction of 2.76 ± 0.85 mas to the relative parallax. According to the second table, the correction should be 3.2 ± 2.5 mas. In the latter two cases, the error represents the dispersion in mean parallaxes assigned to each reference star.

Photometric distances, which are calculated for each reference star, should give a better correction to convert a relative parallax to an absolute one than general statistical methods. Absolute V-band magnitudes were estimated from $(B-V)_0$ and $(V-K)_0$ when spectral types were determined for the reference stars. These values were converted to photometric parallaxes using the distance modulus formula and an interstellar absorption term (Schlegel, Finkbeiner, & Davis 1998). According to these distances, a correction of 6.8 ± 9.6 mas should be added to the relative parallax to convert it to an absolute parallax. These broadband photometric distances can be improved by the inclusion of trigonometric parallaxes from Hipparcos, narrow-band photometric distances from Allegany Observatory (Castelaz *et al.* 1991), and spectroscopic distances from WIYN (Benedict *et al.* 1999) where available. Using these

improved distances, a correction of 5.6 ± 6.7 mas is obtained. Table 2.10 lists broadband colors, apparent and absolute V-band magnitudes, estimated interstellar extinction, and parallaxes calculated from broadband photometry or provided by Hipparcos, Allegany, or WIYN.

The MPRP calculates relative proper motions for each of the reference stars as well as the star under investigation. The differences between the relative proper motions of the reference stars and known absolute proper motions provide a means of correcting the relative proper motion of Barnard's Star. Although absolute proper motions from Hipparcos are available for only two reference stars, absolute proper motions from Tycho are available for all twelve. According to the two Hipparcos values listed in Table 2.11, corrections of -20.6 ± 2.7 and -19.6 ± 2.2 mas yr⁻¹ should be added to the relative proper motion in right ascension and declination, respectively. According to the absolute proper motions from Tycho listed in Table 2.12, corrections of -9 ± 11 and -8.0 ± 5.6 mas yr⁻¹ should be added to the relative proper motion in right ascension and declination, respectively. The poor agreement between these corrections arises from the discrepancies in absolute proper motions available from these sources. As shown in Table 2.11 and Table 2.12, Hipparcos and Tycho report very different proper motions for two stars they have in common, reference stars 6 and 7 (TYC 425-802-1 and TYC 425-22-1). Tycho proper motions were calculated from a combination of ground-based observations and Hipparcos observations.

TABLE 2.10
PHOTOMETRIC PARALLAXES FOR REFERENCE STARS AND BARNARD'S STAR

Reference Star	Tycho Identification	(B-V) ₀ (mag)	(V-K) ₀ (mag)	V _{JM} (mag)	M _V (mag)	A _V (mag)	Photo.	Parallaxes (mas)			Final
								Hipparcos	Allegany	WIYN	
1	TYC 425-262-1	-0.0852	0.3759	0.5794	0.964	0.5794	1.0			1.0	1.0
2	TYC 425-1810-1	1.6140	4.3516	0.6055	-5.6	0.6055	0.1		0		0.0
3	TYC 425-1467-1	0.2069	0.2089	0.6207	1.853	0.6207	1.7				1.7
4	TYC 425-1773-1	0.4136	1.2945	0.5900	3.738	0.5900	3.2				3.2
5	TYC 425-1397-1	0.4456	0.3883	0.5908	2.652	0.5908	2.7				2.7
6	TYC 425-802-1	1.1342	2.4479	0.5777	6.898	0.5777	34.4	24.3	35		24.3
7	TYC 425-22-1	0.3969	0.9915	0.6016	3.607	0.6016	12.8	6.4	15		6.4
8	TYC 425-187-1	0.0947	0.3682	0.7352	1.784	0.7352	2.2				2.2
9	TYC 425-1858-1	0.4720	1.0611	0.7075	3.627	0.7075	5.3				5.3
10	TYC 425-616-1	-0.1606	-0.3234	0.5253	-0.958	0.5253	1.4		2		2.0
11	TYC 425-214-1	0.8977	2.1648	0.5735	6.228	0.5735	11.6				11.6
12	TYC 425-1844-1	0.3828	1.2386	0.5728	3.659	0.5728	5.7		7		7.0
Barnard's	TYC 425-2502-1	1.3938	4.5104	0.5828	9.728	0.5828	139.4	549.0			...

REFERENCES.—Parallaxes are from Hipparcos; Castelaz *et al.* 1991 (Allegany); and, Benedict *et al.* 1999 (WIYN).

TABLE 2.11
COMPARISON OF RELATIVE PROPER MOTIONS WITH HIPPARCOS PROPER MOTIONS

Reference Star	Tycho Identification	Relative Proper Motion (mas yr ⁻¹)		Hipparcos Proper Motion (mas yr ⁻¹)		Correction (mas yr ⁻¹)	
		Right Ascension	Declination	Right Ascension	Declination	RA	Dec
1	TYC 425-262-1	0.6 ± 0.2	-2.7 ± 0.2				
2	TYC 425-1810-1	7.5 ± 0.2	8.3 ± 0.2				
3	TYC 425-1467-1	20.1 ± 0.2	10.4 ± 0.2				
4	TYC 425-1773-1	16.3 ± 0.2	-3.8 ± 0.2				
5	TYC 425-1397-1	10.1 ± 0.3	2.6 ± 0.3				
6	TYC 425-802-1	-39.5 ± 0.1	-31.3 ± 0.2	-63.49 ± 2.46	-58.51 ± 1.93	-23.99	-27.21
7	TYC 425-22-1	0.5 ± 0.1	-2.6 ± 0.1	-16.74 ± 1.23	-14.68 ± 1.01	-17.24	-12.08
8	TYC 425-187-1	-6.3 ± 0.2	-8.3 ± 0.2				
9	TYC 425-1858-1	10.2 ± 0.2	-8.7 ± 0.2				
10	TYC 425-616-1	21.1 ± 0.1	8.4 ± 0.1				
11	TYC 425-214-1	-21.5 ± 0.3	-19.1 ± 0.2				
12	TYC 425-1844-1	-4.5 ± 0.2	38.7 ± 0.1				
					10326.9		
Barnard's	TYC 425-2502-1	-739.9 ± 0.2	10334.8 ± 0.2	-797.84 ± 1.61	3 ± 1.29

REFERENCE.—Hipparcos

TABLE 2.12
COMPARISON OF RELATIVE PROPER MOTIONS WITH TYCHO PROPER MOTIONS

Reference Star	Tycho Identification	Relative Proper Motion (mas yr ⁻¹)		Tycho Proper Motion (mas yr ⁻¹)		Correction (mas yr ⁻¹)	
		Right Ascension	Declination	Right Ascension	Declination	RA	Dec
1	TYC 425-262-1	0.6 ± 0.2	-2.7 ± 0.2	-3.6 ± 1.9	-6.4 ± 1.9	-4.2	-3.7
2	TYC 425-1810-1	7.5 ± 0.2	8.3 ± 0.2	-2.4 ± 2.3	0.8 ± 2.3	-9.9	-7.5
3	TYC 425-1467-1	20.1 ± 0.2	10.4 ± 0.2	4.2 ± 2.0	-3.0 ± 2.0	-15.9	-13.4
4	TYC 425-1773-1	16.3 ± 0.2	-3.8 ± 0.2	9.3 ± 2.1	-12.6 ± 2.0	-7	-8.8
5	TYC 425-1397-1	10.1 ± 0.3	2.6 ± 0.3	-8.8 ± 2.0	-6.4 ± 2.0	-18.9	-9
6	TYC 425-802-1	-39.5 ± 0.1	-31.3 ± 0.2	-62.4 ± 1.6	-46.3 ± 1.6	-22.9	-15
7	TYC 425-22-1	0.5 ± 0.1	-2.6 ± 0.1	-17.3 ± 1.0	-14.5 ± 1.1	-17.8	-11.9
8	TYC 425-187-1	-6.3 ± 0.2	-8.3 ± 0.2	0.7 ± 1.6	-5.9 ± 1.6	7	2.4
9	TYC 425-1858-1	10.2 ± 0.2	-8.7 ± 0.2	19.6 ± 1.9	-9.8 ± 1.8	9.4	-1.1
10	TYC 425-616-1	21.1 ± 0.1	8.4 ± 0.1	-2.1 ± 2.5	-6.2 ± 2.3	-23.2	-14.6
11	TYC 425-214-1	-21.5 ± 0.3	-19.1 ± 0.2	-19.7 ± 2.1	-27.9 ± 2.1	1.8	-8.8
12	TYC 425-1844-1	-4.5 ± 0.2	38.7 ± 0.1	-7.6 ± 1.7	34.0 ± 1.6	-3.1	-4.7
Barnard's	TYC 425-2502-1	-739.9 ± 0.2	10334.8 ± 0.2	-798.8 ± 1.6	10277.3 ± 1.5

REFERENCE.—Tycho

The various corrections proposed to convert the relative parallax and proper motion of Barnard's Star are summarized in Table 2.13 and Table 2.14, respectively. The improved photometric distances were adopted for the parallax correction and the proper motions from Tycho were adopted for the proper motion correction because these values reflect the best available information on the reference stars overall. Applying these corrections, Barnard's Star has an absolute parallax of 552 ± 7 mas and an absolute proper motion of $10.354 \pm 0.006''$ yr⁻¹ in $355.85 \pm 0.06^\circ$, which puts it at a distance of 1.81 ± 0.02 pc with a transverse velocity of 89 ± 1 kilometers second⁻¹. Table 2.15 compares the McCormick relative and absolute parallaxes with those available in the literature while Table 2.16 provides similar comparisons for proper motion.

TABLE 2.13
CORRECTIONS OF RELATIVE PARALLAX TO ABSOLUTE PARALLAX FOR BARNARD'S STAR

Technique	Correction (mas)		References
Mean Parallaxes, Yerkes Galactic Model	4.0	± 1.6	1
Yale Parallax Catalog	2.6	± 0.2	2
Secular Parallax of Mean Reference Frame	3.47	± 0.43	3, 4
Secular Parallaxes of Reference Stars (galactic longitude, apparent magnitude)	2.76	± 0.85	3, 4
Secular Parallaxes of Reference Stars (galactic longitude, apparent magnitude, spectral type)	3.2	± 2.5	3, 4
Photometric Parallaxes	6.8	± 9.6	5
Improved Photometric Parallaxes	5.6	± 6.7	5, 6, 7, 8

REFERENCES.—(1) van Altena 1974; (2) YPC; (3) Vyssotsky & Williams 1948a; (4) Vyssotsky & Williams 1948b; (5) see text for details; (6) Benedict *et al.* 1999; (7) Castelaz *et al.* 1991; (8) Hipparcos

TABLE 2.14
CORRECTIONS FROM RELATIVE TO ABSOLUTE PROPER MOTION FOR BARNARD'S STAR

Technique	Correction (mas yr ⁻¹)		Reference
Average Residual Proper Motions, Yerkes Galactic Model	1650	± 630	1
Hipparcos Absolute Proper Motions, Right Ascension	-20.6	± 2.7	2
Hipparcos Absolute Proper Motions, Declination	-19.6	± 2.2	2
Tycho Absolute Proper Motions, Right Ascension	-9	± 11	3
Tycho Absolute Proper Motions, Declination	-8.0	± 5.6	3

REFERENCES.—(1) van Altena 1974; (2) Hipparcos; (3) Tycho

TABLE 2.15
PARALLAX OF BARNARD'S STAR

Study	Parallax (mas)		Reference
McCormick, relative	546.5	± 1.4	
Hubble Space Telescope, relative	544.2	± 0.2	1
US Naval Observatory, relative	544.8	± 1.5	2
Sproul Observatory, relative	543.6	± 0.9	3
Van Vleck Observatory, relative	559	± 14	4
Allegany Observatory, relative	553	± 3.8	5
McCormick, absolute	552	± 7	
Hubble Space Telescope, absolute	545.4	± 0.3	1
Hipparcos, absolute	549	± 2	6
Yale Parallax Catalog, absolute	546	± 1	7
US Naval Observatory, absolute	547	± 2	2
Sproul Observatory, absolute	548	± 1	3

References.—(1) Benedict *et al.* 1999; (2) Harrington *et al.* 1993; (3) van de Kamp 1981; (4) Grossenbacher, Mesrobian, & Upgren 1968; (5) Beardsley *et al.* 1973; (6) Hipparcos; (7) YPC

TABLE 2.16
PROPER MOTION OF BARNARD'S STAR

Study	Proper Motion (mas yr ⁻¹)	Position Angle (degrees)	Ref.
McCormick, relative	10,361.3 ± 0.2	355.905 ± 0.001	
Hubble, relative	10,370.0 ± 0.3	355.6 ± 0.1	1
Yale Parallax Catalog, relative	10,310 ...	356 ...	2
US Naval Observatory, relative	10,360.3 ± 0.3	355.8 ± 0.0	3
Sproul, relative	10,307.0 ± 0.1	355.5277 ± 0.0006	4
Allegany, relative	10,318.7 ± 0.3	356.044 ± 0.002	5
Van Vleck, relative	10,349 ± 7	355.98 ± 0.07	6
McCormick, absolute	10,354 ± 6	355.85 ± 0.06	
Tycho, absolute	10,308 ± 2	355.556 ± 0.009	7
Hipparcos, absolute	10,358 ± 1	355.582 ± 0.009	8

REFERENCES.—(1) Benedict *et al.* 1999; (2) YPC; (3) Harrington *et al.* 1993; (4) van de Kamp 1981; (5) Beardsley *et al.* 1973; (6) Grossenbacher, Mesrobian, & Upgren 1968; (7) Tycho; (8) Hipparcos

The relative parallax for Barnard's Star from McCormick falls towards the middle of the published relative parallaxes from other programs. It is slightly larger than that measured by the Benedict *et al.* (1999), but its lower limit is within the upper range of the relative parallax measured at the USNO (Harrington *et al.* 1993). The absolute parallax from this study is larger than any of the absolute parallaxes found in literature; however, its lower limit is within the upper range of all the published values.

The absolute parallax resulting from this study suffers from a large correction to absolute (5.6 mas), nearly three times greater than used by the USNO (Harrington *et al.* 1993) and nearly five times greater than used by Benedict *et al.* (1999), along with a large associated error (± 6.7 mas). Benedict *et al.* (1999) obtained their correction to absolute from the YPC, which was within 0.2 mas of spectrophotometric correction. Van Altena (2005, private communication), the primary author of the YPC, discouraged

such a statistical approach in favor of a more tailored approach, such as photometric or spectroscopic distance estimates for the actual reference stars used. The reference frame selected includes two stars within 100 pc, reference stars 6 (TYC 425-802-1) and 11 (TYC 425-214-1), without which the correction would be reduced by more than a half. Based on the parallaxes listed in Table 2.17, reference star 6 has a parallax of 25 ± 2 mas, which puts it as a distance of about 41 pc. Removing reference star 6 from the analysis degrades the parallax solution. The distance estimate for reference star 11, approximately 86 pc, used herein relies solely on broadband photometry. Recent spectra obtained for this star with the 40-inch telescope at Fan Mountain Observatory may increase this distance estimate, reduce the correction to absolute, and improve the absolute parallax obtained. Alternatively, the example of Benedict *et al.* (1999) could be followed and the correction estimated from the YPC be adopted, which would result in an absolute parallax of 549 ± 1 mas.

TABLE 2.17
PARALLAX OF REFERENCE STAR 6 (TYC 425-802-1)

Study	Parallax (mas)	Reference
McCormick, relative	16 \pm 1	byproduct of this analysis
Hipparcos, absolute	24.32 \pm 2.28	1
Yale Parallax Catalog, absolute	27.2 \pm 2.8	2
Allegany, absolute	22 \pm 3	3

NOTE.—Reference star 6 (TYC 425-802-1) is also known as HIP 87991, Plx 4102, Allegany 17, BD +4°3562, and Kuiper 84.

REFERENCES.—(1) Hipparcos; (2) YPC; (3) Gatewood 1973

The relative proper motion of Barnard’s Star measured at McCormick is larger than all the other published measurements except that by Benedict *et al.* (1999). The relative proper motions calculated by McCormick, the USNO (Harrington *et al.* 1993),

and Benedict *et al.* (1999) do not overlap even considering all their formal errors. The position angles associated with the published proper motions all lie within 5° west of due north with the value measured herein towards the middle of the published values. In most published studies, the observers have been content to provide relative proper motions and position angles without attempting to correct these measurements for any motion in the reference frame. Hipparcos and Tycho provide absolute proper motions and position angles; their proper motions bracket the value measured at McCormick. The McCormick position angle indicates a slightly more northerly motion than the other two measurements. However, the McCormick relative proper motion was converted to an absolute one through comparison with Tycho proper motions.

2.3.3 Time-Series Analysis

The MPRP also calculates the residuals associated with each observation, which are shown in Figure 2.3. Lacking an obvious periodic signal, a time-series analysis of these residuals should reveal whether they result from random measurement error or from a periodic perturbation such as van de Kamp (1982) described. The frequency domain provides mathematical tools for identifying a signal with an unknown period from a collection of measurements. When observations occur at uneven intervals, as is the case with the photographic plates in this study and for many other astronomical observations, a least-squares spectrum reveals the relative spectral power that each evaluated frequency, or its associated period, contributes to the measurements

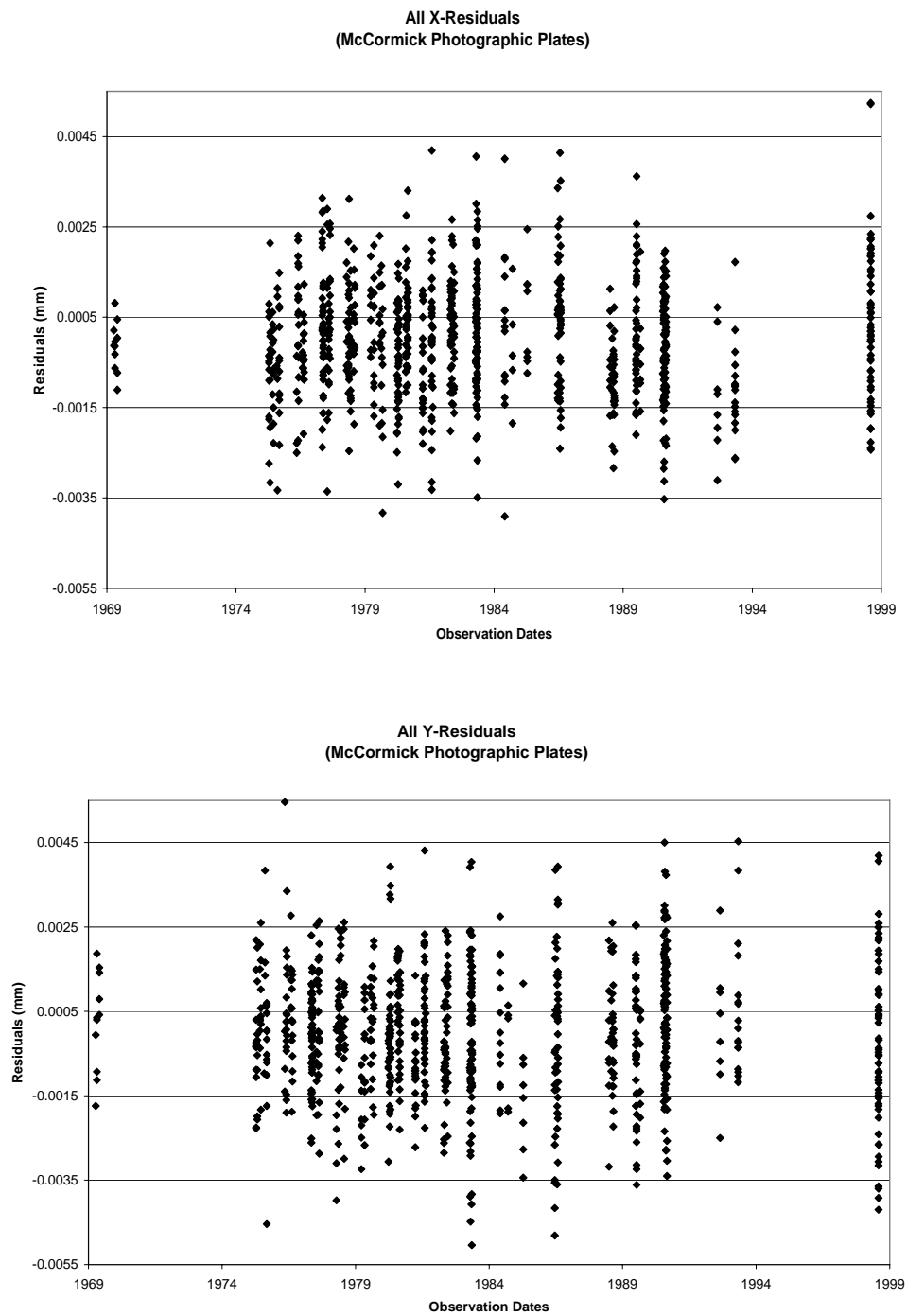


FIG. 2.3.—All X- and Y-Residuals for Barnard's Star. Top chart contains all x-residuals. Bottom chart contains all y-residuals.

(Barning 1963; Lomb 1976). This least-squares spectrum is calculated by fitting sine waves to the data so as to minimize the squares of the resulting residuals (Barning 1963). Alternatively, the classical periodogram, which works well for evenly sampled data, provides estimates of the spectral power of tested frequencies in irregularly sampled sets (Lomb 1976).

However, the classical periodogram may be modified in such a way that it becomes equivalent to the corresponding least-squares spectrum; this modified periodogram, known as the Lomb-Scargle normalized periodogram, reduces to the classical one when even time intervals are used (Scargle 1982). Press and Rybiki (1989) reduced the computational burden of calculating the Lomb-Scargle normalized periodogram by replacing single measurements with multiple, evenly spaced values that approximate the original quantity.

To test this approach, the Ephemeris2 program was altered to calculate the positions of planets van de Kamp (1982) described for the time of each observation using the modified Thiele-Innes constants he provided, which are listed in Table 2.18.

TABLE 2.18
ORBITAL PARAMETERS FOR VAN DE KAMP'S PLANETS

Parameter	Primary Solution		Single Planet Solution
	Inner Planet	Outer Planet	
(B) in milliseconds of arc	2.1 ± 1.1	-4.0 ± 1.1	2.1 ± 1.1
(G) in milliseconds of arc	5.3 ± 1.1	-0.9 ± 1.1	6.4 ± 1.1
(A) in milliseconds of arc	-0.8 ± 1.3	-4.5 ± 1.3	-2.1 ± 1.3
(F) in milliseconds of arc	4.5 ± 1.3	-3.4 ± 1.3	5.5 ± 1.3
Period in years	12.0 ± 1.0	20 ± 3	12.0 ± 0.5
Eccentricity	0.0	0.0	0.0
Periastron Time	N/A	N/A	N/A

REFERENCE.—van de Kamp 1982

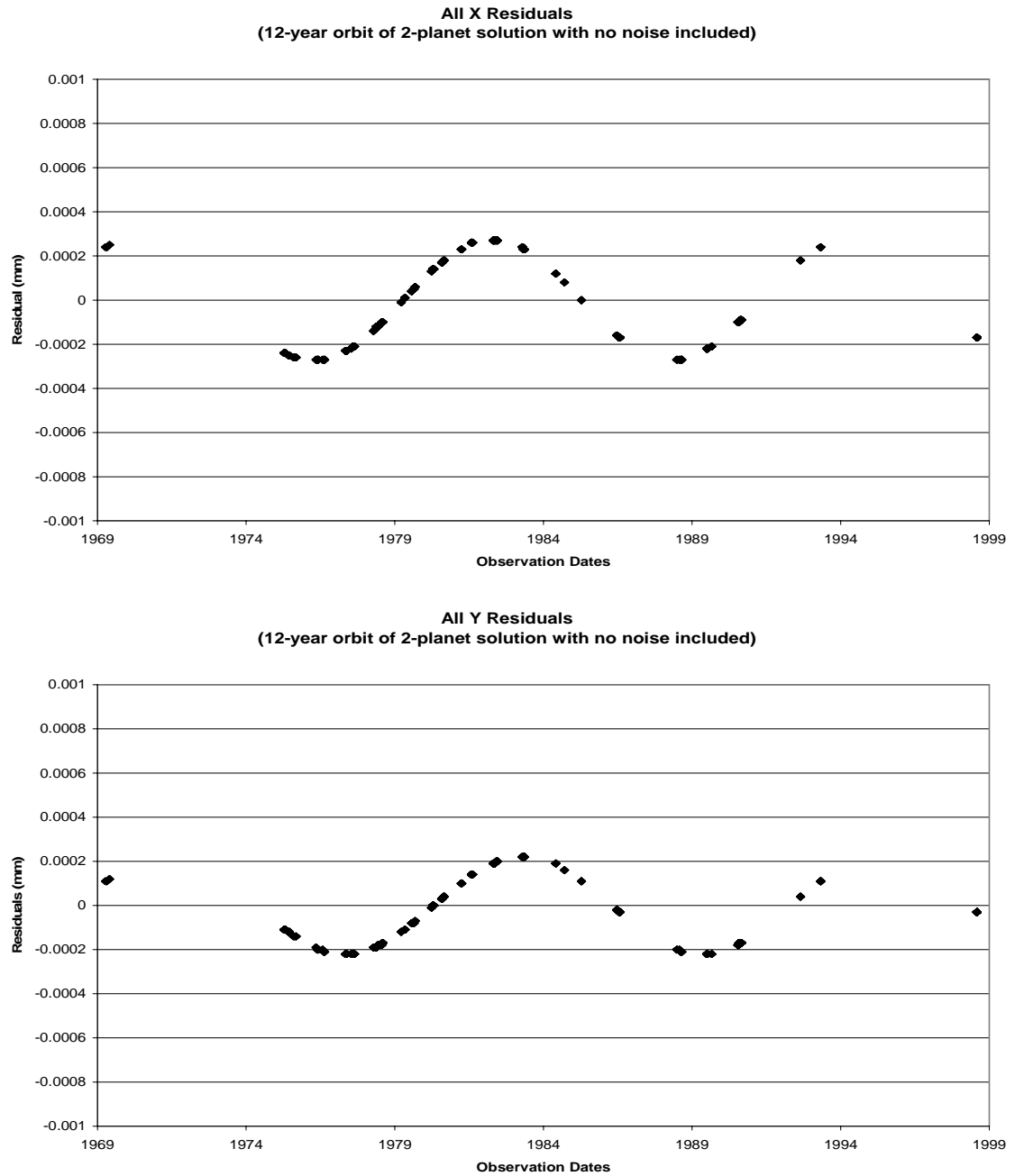


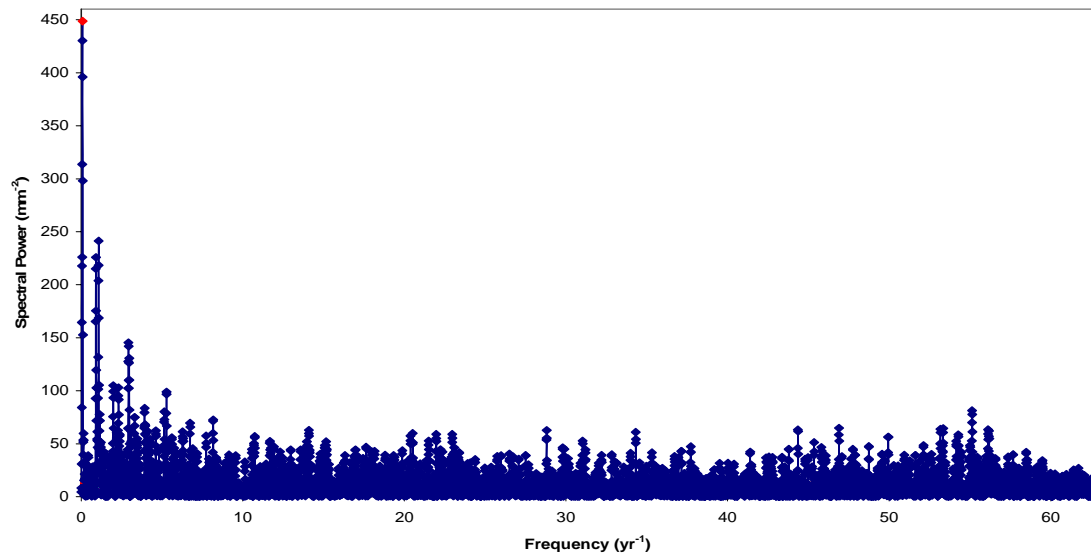
FIG. 2.4.— Theoretical Displacement of Barnard's Star due to Planet in 12-year Orbit Described by van de Kamp (1982). Top chart contains theoretical x-residuals resulting from the perturbation alone. bottom panel contains theoretical y-residuals.

Figure 2.4 shows the displacement of Barnard's Star due to the inner planet of the two-planet solution, ignoring any additional perturbation due to the outer planet and without the addition of any noise. Their periodic signals were recovered by calculating separate Lomb-Scargle periodograms for the x- and y-positions using the spreading technique of Press and Rybiki (1989; Press *et al.* 1996). The 12-year period is easily recovered from the corresponding periodograms in Figure 2.5.

When separate Lomb-Scargle periodograms were calculated for the x- and y-residuals produced by MPRP, the periodograms shown in Figure 2.6 resulted. These periodograms are very noisy and show the spurious peaks expected when a large number of frequencies are searched (Scargle 1982).

Scargle (1982) discusses two ways of improving detection efficiency: obtaining additional observations and averaging the data. The former method was not an option because the photographic plates used in this study are no longer manufactured. Therefore, we resorted to the latter by combining the residuals into nightly and annual normal points and re-calculating periodograms for the averaged data. Figure 2.7 and Figure 2.8 show the nightly normal points and the corresponding periodograms. Table 2.19 lists the annual normal points, which are illustrated in Figure 2.9. The Nyquist frequency is the highest frequency that can be recovered at a given even sampling rate. Averaging the data reduces the effective Nyquist frequency, which may drop below the signal frequency making detection more difficult (Scargle 1982). Fortunately, as shown in Table 2.20, the frequency of either a 12- or a 20-year period perturbation

Periodogram for All X Residuals
(12-year orbit of 2-planet solution with no noise included)



Periodogram for All Y Residuals
(12-year orbit of 2-planet solution with no noise included)

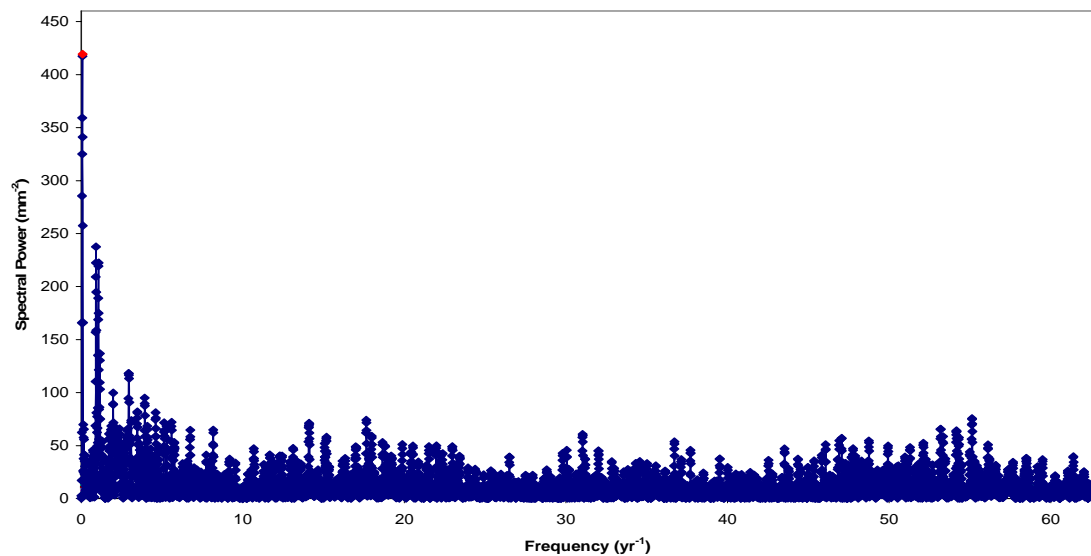


FIG. 2.5.—Periodograms of Theoretical Displacement of Barnard’s Star due to Planet in 12-year Orbit Described by van de Kamp (1982). Top chart is a periodogram calculated for theoretical x-residuals. Bottom chart is a periodogram calculated for theoretical y-residuals. The maxima in both periodograms at 0.0853 yr^{-1} (11.7 years) tower so far above the 99% confidence level at 12.8 mm^{-2} that the confidence levels cannot be distinguished on this scale.

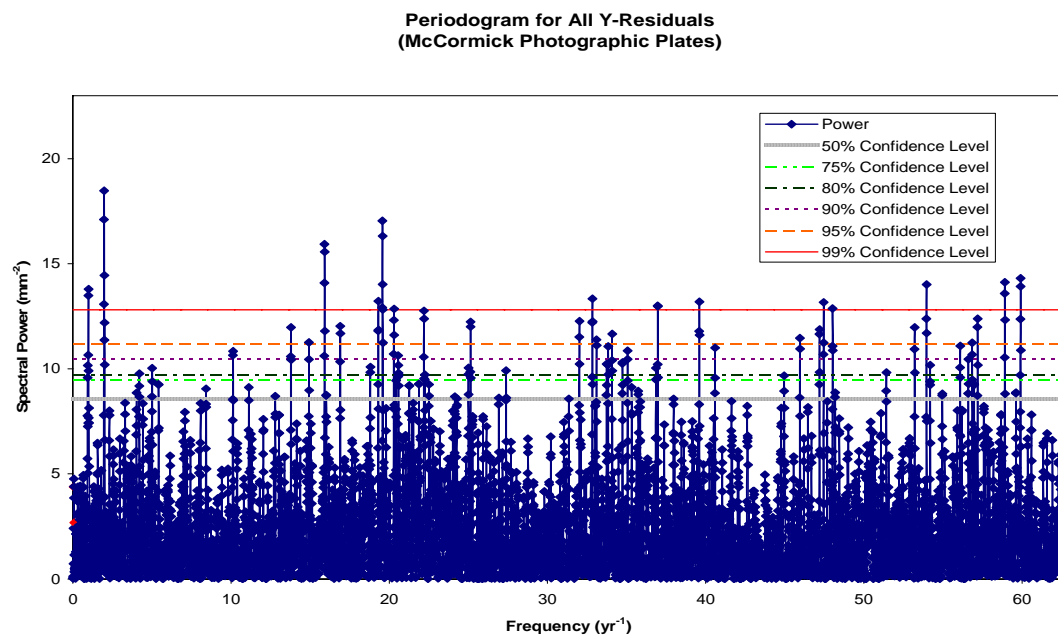
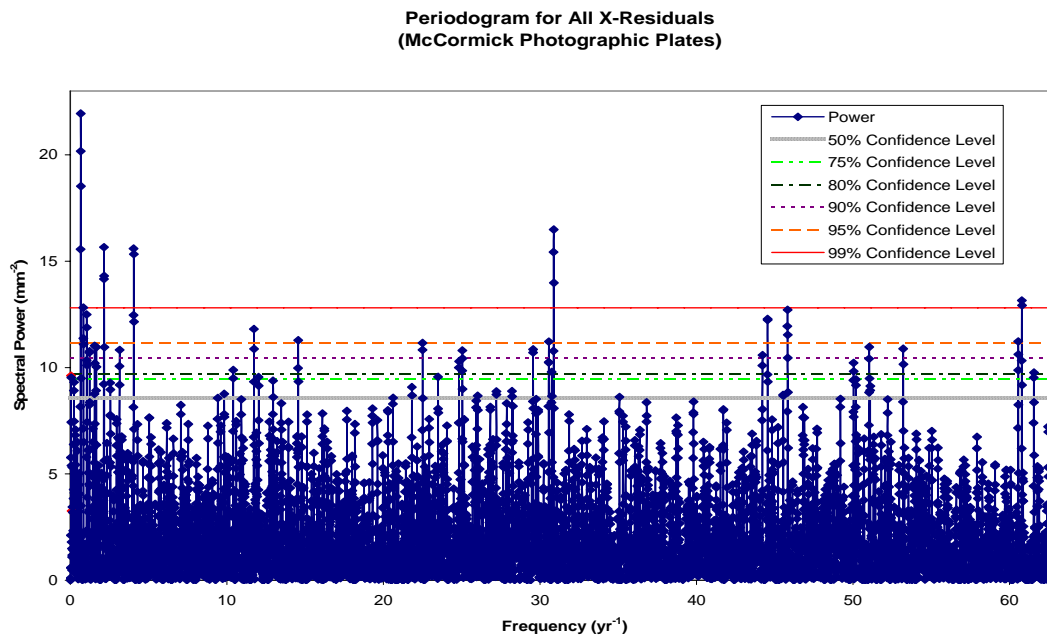


FIG. 2.6.— Periodograms for All X- and Y-Residuals for Barnard’s Star. Top chart is a periodogram calculated for all x-residuals. Bottom chart is a periodogram calculated for all y-residuals. Horizontal lines in the periodograms indicate likelihood that spectral peaks exceeding that power are real and not caused by noise only. Solid line is 99% confidence, dashed line 95% confidence, dotted line 90% confidence, dash dotted line is 80% confidence, dash double-dotted line is 75% confidence, and hashed line is 50% confidence.

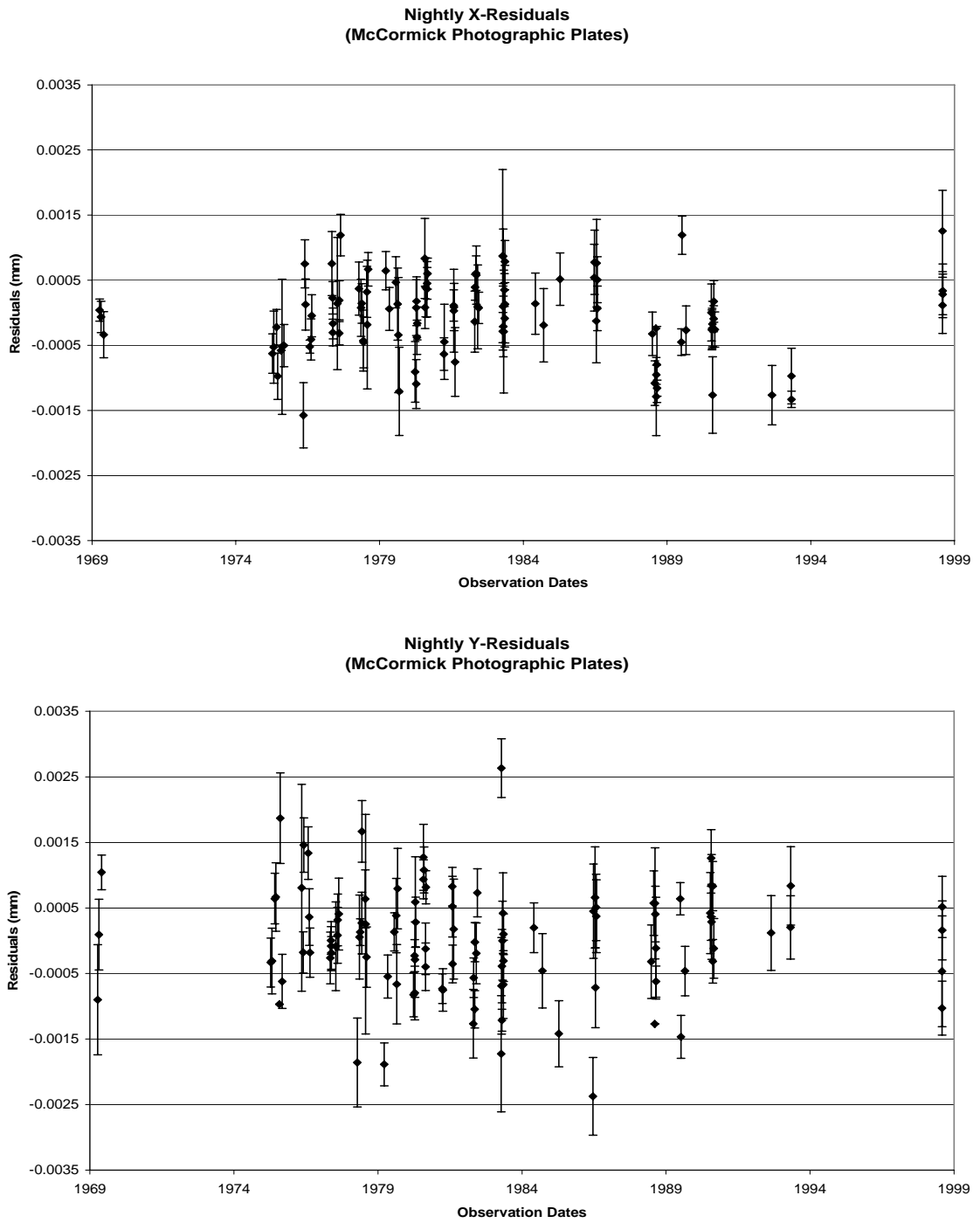


Fig. 2.7.— Nightly X- and Y-Residuals for Barnard’s Star. Top chart contains x-residuals averaged by night. Bottom chart contains y-residuals averaged by night.

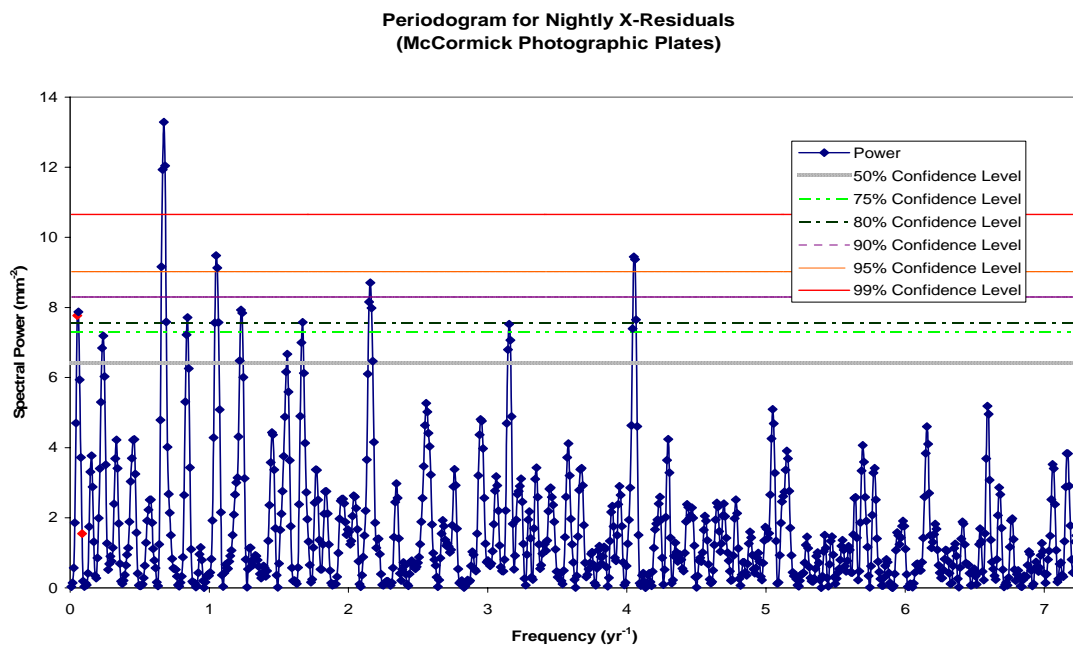


Fig. 2.8.— Top chart is a periodogram calculated for nightly x-residuals. Bottom chart is a periodogram calculated for nightly y-residuals. Horizontal lines in the periodograms indicate likelihood that spectral peaks exceeding that power are real and not caused by noise only. Solid line is 99% confidence, dashed line 95% confidence, dotted line 90% confidence, dash dotted line is 80% confidence, dash double-dotted line is 75% confidence, and hashed line is 50% confidence.

TABLE 2.19
ANNUAL NORMAL POINTS FOR BARNARD'S STAR

Observations (Year Fraction)	X Residuals (millimeters)	Y Residuals (millimeters)	Images
1969.339 ± 0.017	-0.00015 ± 0.00017	0.00026 ± 0.00035	11
1975.455 ± 0.022	-0.00057 ± 0.00016	0.00002 ± 0.00021	50
1976.494 ± 0.017	-0.00005 ± 0.00018	0.00047 ± 0.00023	41
1977.458 ± 0.013	0.00028 ± 0.00015	0.00000 ± 0.00013	81
1978.431 ± 0.013	0.00009 ± 0.00015	0.00009 ± 0.00020	54
1979.470 ± 0.027	0.00004 ± 0.00020	-0.00035 ± 0.00021	42
1980.439 ± 0.018	-0.00003 ± 0.00011	0.00011 ± 0.00014	93
1981.464 ± 0.021	-0.00020 ± 0.00017	-0.00006 ± 0.00016	64
1982.377 ± 0.008	0.00025 ± 0.00015	-0.00017 ± 0.00018	50
1983.327 ± 0.003	0.00028 ± 0.00015	-0.00024 ± 0.00020	82
1984.489 ± 0.029	0.00006 ± 0.00038	0.00003 ± 0.00032	20
1985.278 ± 0.000	0.00052 ± 0.00040	-0.00142 ± 0.00050	8
1986.536 ± 0.006	0.00048 ± 0.00020	-0.00021 ± 0.00028	53
1988.597 ± 0.010	-0.00088 ± 0.00014	-0.00004 ± 0.00022	37
1989.532 ± 0.009	0.00020 ± 0.00019	-0.00033 ± 0.00022	48
1990.600 ± 0.004	-0.00023 ± 0.00011	0.00045 ± 0.00016	102
1992.648 ± 0.000	-0.00127 ± 0.00046	0.00012 ± 0.00057	8
1993.327 ± 3.3x10 ⁻⁴	-0.00112 ± 0.00025	0.00058 ± 0.00040	17
1998.584 ± 3.5x10 ⁻⁴	0.00040 ± 0.00022	-0.00028 ± 0.00027	58

TABLE 2.20
COMPARISONS OF ORBITAL PERIODS TO EFFECTIVE NYQUIST FREQUENCIES

Parameter	Frequency (yr ⁻¹)
12-year Orbital Period	0.083
20-year Orbital Period	0.050
Effective Nyquist Frequency, all observations	15.671
Effective Nyquist Frequency, nightly normal points	1.808
Effective Nyquist Frequency, annual normal points	0.325

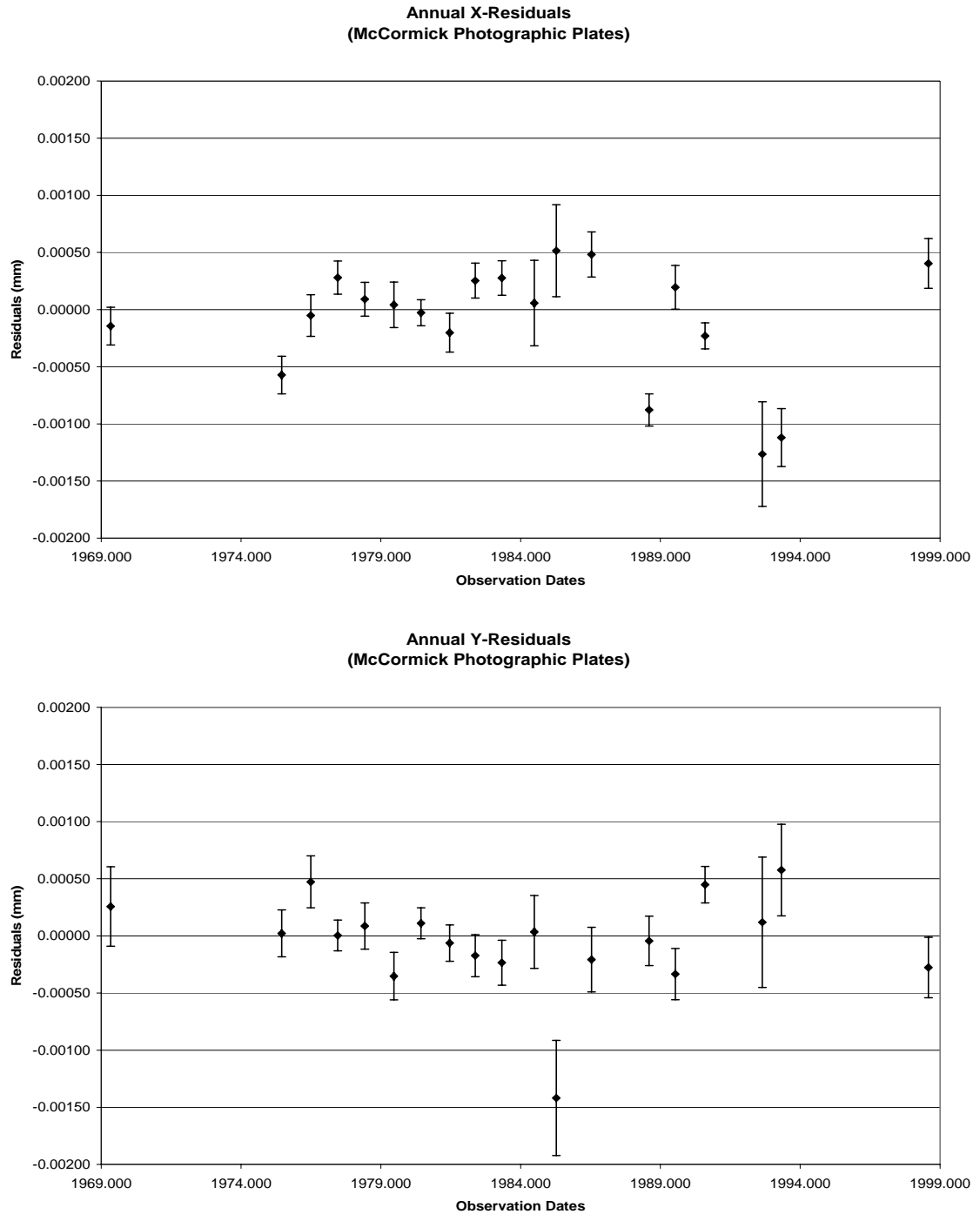


FIG. 2.9.—Annual X- and Y-Residuals for Barnard's Star. Top chart contains x-residuals averaged by year. Bottom chart contains y-residuals averaged by year.

The algorithm used searched frequencies up to four times the effective Nyquist frequency to produce plots of spectral power versus frequency. In addition, the algorithm calculated the false alarm probability, or the probability that noise rather than a true signal caused a particular peak in power (Press *et al.* 1996). Figure 2.10 shows that the power at no frequency is indicative of a signal at a significance level of 50% or better. The peak power of 3.951 millimeters⁻² (mm⁻²) in the x-residuals and of 2.966 mm⁻² in the y-residuals occurs at a frequency of 0.051 yr⁻¹, corresponding to a period of 19 years. Van de Kamp (1982) suggested a range of 17–23 years for the outer planet. As intriguing as these peaks may be, the corresponding false alarm probabilities are 77% and 98%. In the periodogram for all x-residuals, this frequency corresponds to a local peak that has a greater than 75% chance of being real but the corresponding y-frequency is adjacent to a local peak that has a less than 50% chance of being real. In the periodogram for nightly x-residuals, the frequency is adjacent to a local peak that has a greater than 80% chance of being real but the corresponding y-frequency is a local peak that has a less than 50% chance of being real. The outer planet described by van de Kamp (1982) should produce a perturbation of Barnard's Star on the order of 6 mas, which corresponds to about 0.3 μm at the plate scale of the McCormick refractor. Therefore, these intriguing peaks are most likely caused by noise. Table 2.21 also lists the primary peaks in all the periodograms. Table 2.22 describes the features of all the periodograms that correspond to the 12 and 20-year orbits described by van de Kamp (1982).

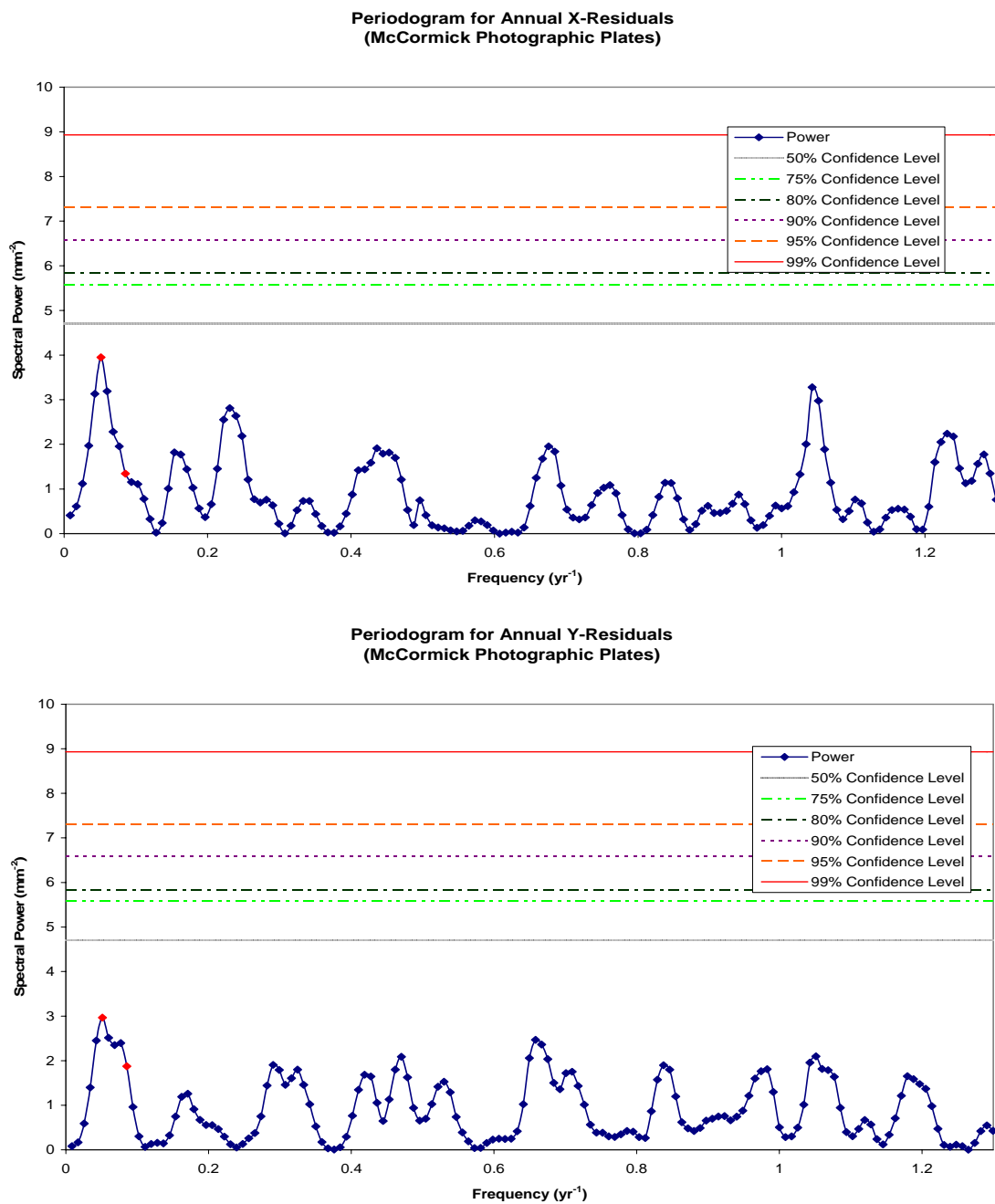


FIG. 2.10.—Periodograms for Annual Barnard Star Residuals. Bottom left panel is a periodogram calculated for annual x-residuals. Bottom right panel is a periodogram calculated for annual y-residuals. Horizontal lines in the periodograms indicate likelihood that spectral peaks exceeding that power are real and not caused by noise only. Solid line is 99% confidence, dashed line 95% confidence, dotted line 90% confidence, dash dotted line is 80% confidence, dash double-dotted line is 75% confidence, and hashed line is 50% confidence.

TABLE 2.21
PRIMARY SPECTRAL PEAKS IN PERIODOGRAMS FOR BARNARD'S STAR

Periodogram	Freq. (yr ⁻¹)	Power (mm ⁻²)	Period (yr)	False Alarm Prob. (%)	Comments
All X	0.674	21.943	1.48	11	multiple of 6 month observing cycle?
All Y	1.978	18.474	0.5055	51	6 month observing cycle
Nightly X	0.674	13.285	1.48	72	multiple of 6 month observing cycle?
Nightly Y	1.978	7.961	0.5055	14	6 month observing cycle
Annual X	0.051	3.951	19	77	within 17–23 year range
Annual Y	0.051	2.966	19	98	within 17–23 year range

NOTE.—Van de Kamp (1982) suggests a range of 17–23 years for the orbit of the outer planet.

TABLE 2.22
PERIODOGRAM POINTS CORRESPONDING TO 12 AND 20-YEAR ORBITS

Periodogram	Freq. (yr ⁻¹)	Power (mm ⁻²)	Period ^a (yr)	False Alarm Prob. (%)	Comments
All X	0.051	9.616	20	< 25	local peak
All X	0.085	3.263	12	> 50	
All Y	0.051	4.386	20	> 50	adjacent to local peak
All Y	0.085	2.683	12	> 50	
Nightly X	0.051	7.766	20	< 20	adjacent to local peak
Nightly X	0.085	1.545	12	> 50	
Nightly Y	0.051	2.448	20	> 50	local peak
Nightly Y	0.085	0.968	12	> 50	
Annual X	0.051	3.951	19	> 50	primary peak within 17–23 yr range
Annual X	0.085	1.345	12	> 50	
Annual Y	0.051	2.966	19	> 50	primary peak within 17–23 yr range
Annual Y	0.085	1.873	12	> 50	

NOTE.—Van de Kamp (1982) suggests a range of 11.5–13 years for period of the inner planet and 17–23 years for the period of the outer planet.

as described by van de Kamp (1982) is less than any of effective Nyquist frequencies (f_{Neff})

$$f_{\text{Neff}} = \frac{N}{2T} \quad (2.4)$$

where N is the number of observations taken over total time (T). In comparison to the noisy periodograms calculated from the residuals produced by the MPRP, the periodograms calculated for a simulated perturbation clearly reveal a periodic signal. The 12-year period is easily recovered from the simulated, noise-free data as illustrated in Figure 2.4 and Figure 2.5.

2.3.4 Companion Mass Limits

The majority of the planet searches described above that failed to detect the planets described by van de Kamp (1982) were insensitive to such low mass planets in long period orbits. Assuming a circular orbit for a planet as described by van de Kamp, Kepler's third law describes the minimum detectable companion mass (M_p)

$$M_p = \left(\frac{M_*}{P} \right)^{\frac{2}{3}} \frac{\alpha}{\pi} \quad (2.5)$$

where M_* is the stellar mass ($M_* = 0.16 \pm 0.04 M_\odot$ per Delfosse *et al.* 2000), P is the period (12.0 ± 0.5 yr), π is the parallax (552 ± 7 mas), and α is the minimum detectable perturbation of the photocenter in milliseconds of arc.

Several α values have been suggested in literature, which predict sensitivity to planets with minimum masses between 1.1 and 2.1 M_{21} shown in Table 2.23. Campbell, Walker, & Yang (1988) settled on 10 mas based on astrometric studies of the stars

TABLE 2.23
MINIMUM DETECTABLE PERTURBATIONS AND CORRESPONDING MASSES

Alpha (mas)	Planetary Mass (M_{21})	Reference
10	1.1 \pm 0.2	1
20	2.1 \pm 0.3	2
21.3 \pm 3.5	2.2 \pm 0.5	periodogram trial

REFERENCES.—(1) Campbell, Walker, & Yang 1988; (2) Heintz 1988

included in their radial-velocity program. Heintz (1988) suggested 20 mas because astrometric perturbations would reveal themselves as extremely large residuals.

To determine whether this investigation specifically could have detected the planets van de Kamp (1982) described, 1.1- μ m noise, assumed as typical of photographic data and represented by the MPRP residuals, was added to the positions shown in Figure 2.4 producing the positions shown in Figure 2.11. The McCormick residuals averaged $1.02 \pm 0.81 \mu\text{m}$ in x and $1.21 \pm 0.96 \mu\text{m}$ in y with corresponding maxima of $5.2 \mu\text{m}$ and $5.5 \mu\text{m}$ compared with the perturbation amplitudes of $0.72 \mu\text{m}$ and $1.20 \mu\text{m}$, respectively described by van de Kamp (1982). The noise in the McCormick nightly normal points averaged $0.550 \pm 0.046 \mu\text{m}$. As shown in Figure 2.12, the 12-year period is no longer obvious in the corresponding periodograms. Therefore, this study would not detect the planets van de Kamp described.

Using the same observation times and orbital parameters, the distance between the central star and its hypothetical planets was increased until the 12-year period began to appear in the related periodograms. Figure 2.13 shows a combination of displacements twice as large those associated with the inner planet

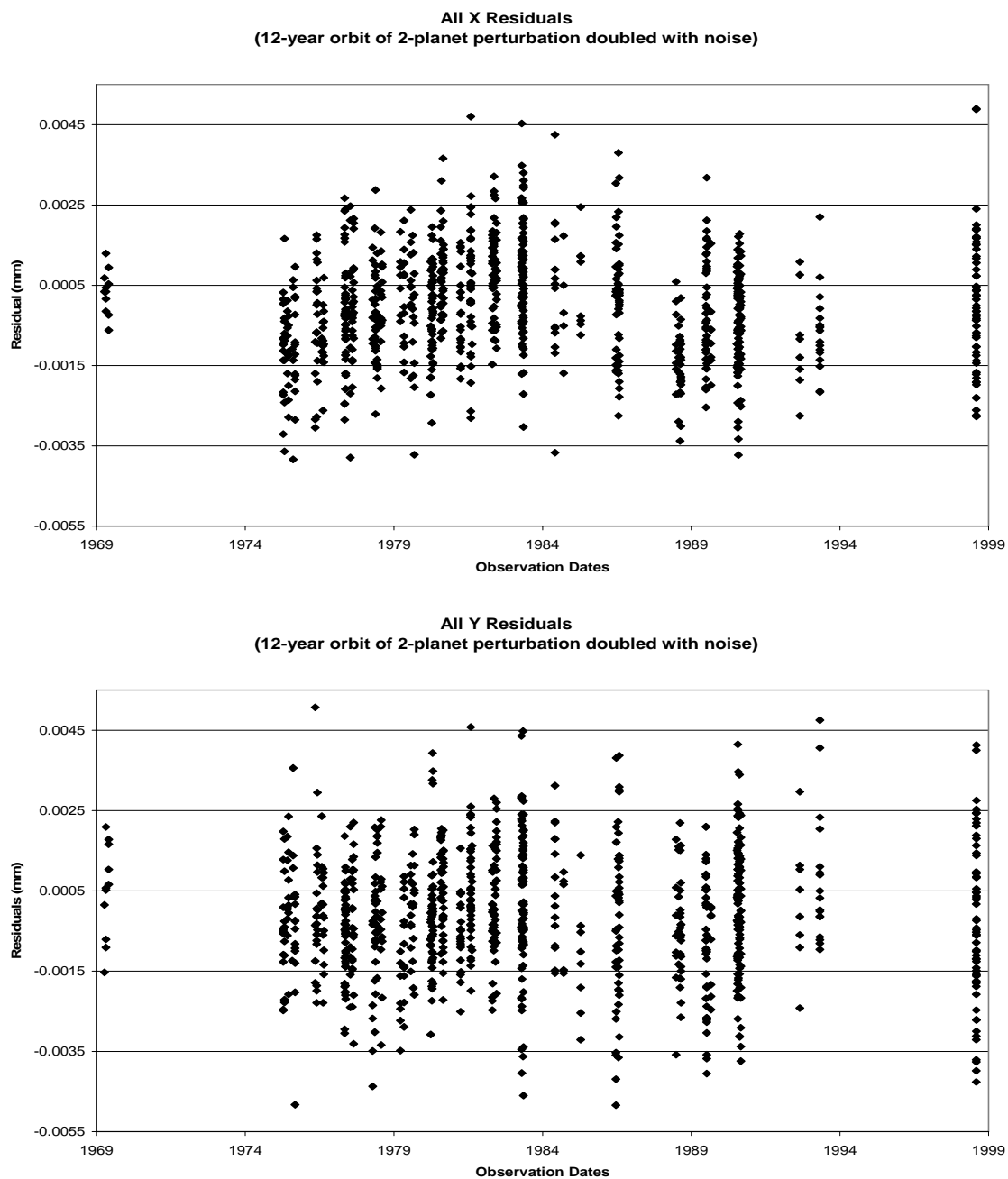


FIG. 2.13.— Theoretical Displacement Doubled with Noise Added. Top chart contains expected x-residuals combining the theoretical perturbation doubled and noise. Bottom chart contains expected y-residuals.

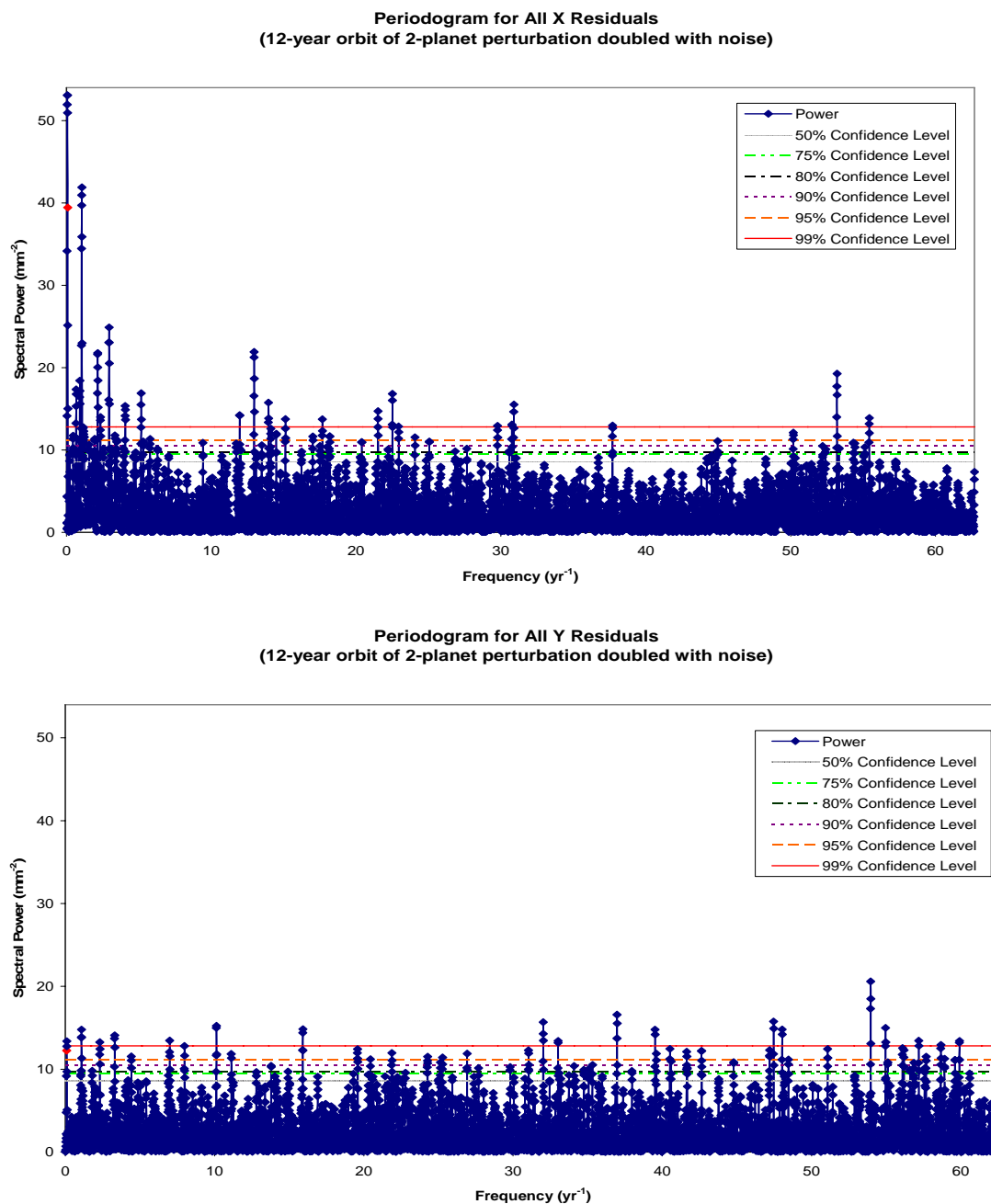


FIG. 2.14.—Periodograms of Theoretical Displacement Doubled with Noise Added. Top chart is a periodogram calculated for expected x-residuals. Bottom chart is a periodogram calculated for expected y-residuals. Horizontal lines in the periodograms indicate likelihood that spectral peaks exceeding that power are real and not caused by noise only. Solid line is 99% confidence, dashed line 95% confidence, dotted line 90% confidence, dash dotted line is 80% confidence, dash double-dotted line is 75% confidence, and hashed line is 50% confidence.

of the two-planet described by van de Kamp (1982) and the residuals of this study. The corresponding periodograms are displayed in Figure 2.14 as well.

For Figure 2.15, the orbital amplitude was increased three-fold. In the corresponding periodograms, also shown in Figure 2.16, the 12-year period begins to emerge from the noise represented by the McCormick residuals. In the periodograms for the all x- and nightly x-residuals, the maximum peak occurs at a frequency of 0.077 yr^{-1} , which corresponds to a period of 13 years. The maximum peak in the nightly y-residual periodogram occurs at a frequency of 0.085 yr^{-1} , which corresponds to a period of 12 years. For Figure 2.17, the planetary residuals were increased four-fold and the 12-year period is clearly visible in the periodograms of Figure 2.18. The maximum peak in each of the x-residual periodogram occurs at a frequency of 0.077 yr^{-1} , which corresponds to a period of 13 years. The maximum peaks in the all y- and nightly y-residual periodograms occur at 0.085 yr^{-1} , which corresponds to a period of 12. years. Continuing to increase the size of the perturbation does not change the frequency at which the x-residual periodograms peak but the power at 0.077 yr^{-1} increases.

From this simple test, we deduce that this study could detect a planet as small as $2.2 \pm 0.5 M_{21}$, which would produce a perturbation of $1.03 \pm 0.17 \mu\text{m}$, or $21.3 \pm 3.5 \text{ mas}$. A perturbation of this size is essentially the same as the 1.6- M_{21} planet initially reported by van de Kamp (1963b) and three times greater than the more massive planet

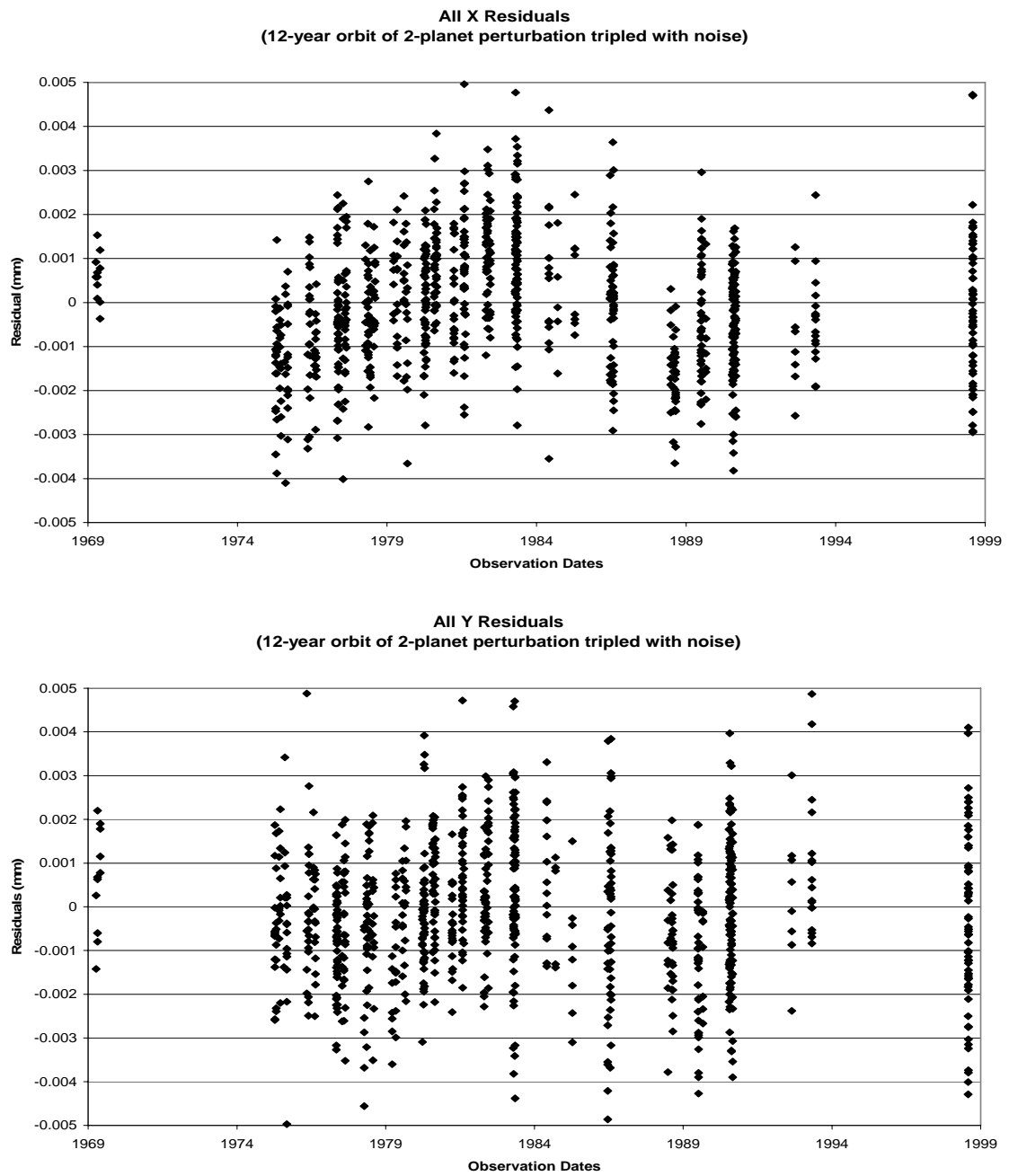
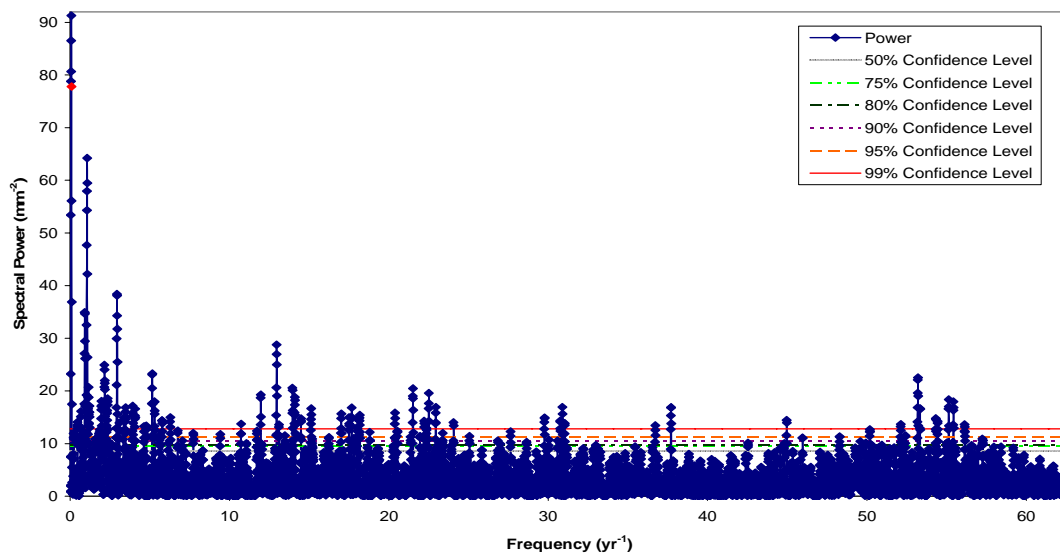


FIG. 2.15.— Theoretical Displacement Tripled with Noise Added. Top chart contains expected x-residuals combining the theoretical perturbation tripled and noise. Bottom chart contains expected y-residuals.

Periodogram for All X Residuals
(12-year orbit of 2-planet perturbation tripled with noise)



Periodogram for All Y Residuals
(12-year orbit of 2-planet perturbation tripled with noise)

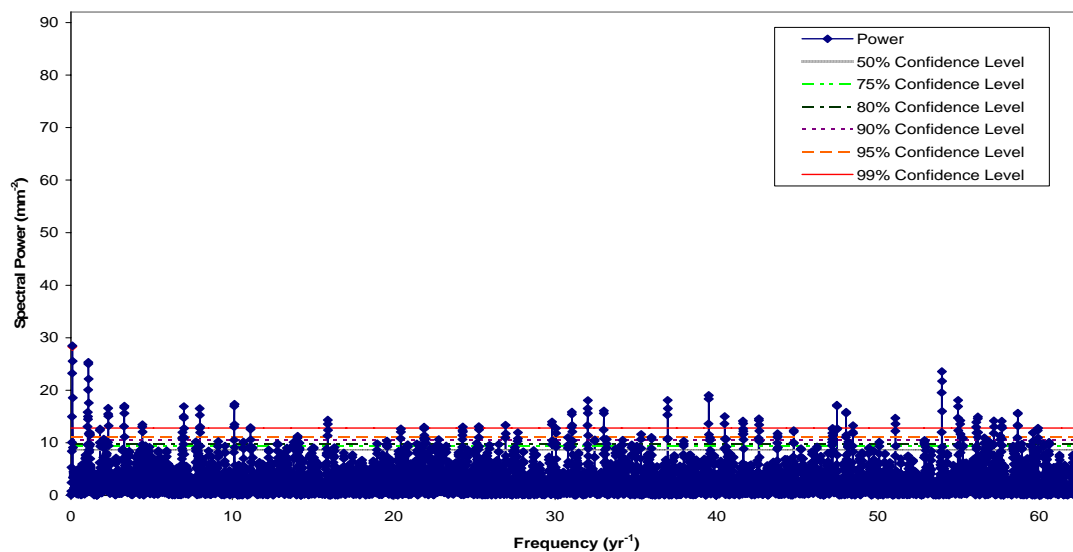


FIG. 2.16.— Periodograms of Theoretical Displacement Tripled with Noise Added. Top chart is a periodogram calculated for expected x-residuals. Bottom chart is a periodogram calculated for expected y-residuals. Horizontal lines in the periodograms indicate likelihood that spectral peaks exceeding that power are real and not caused by noise only. Solid line is 99% confidence, dashed line 95% confidence, dotted line 90% confidence, dash dotted line is 80% confidence, dash double-dotted line is 75% confidence, and hashed line is 50% confidence.

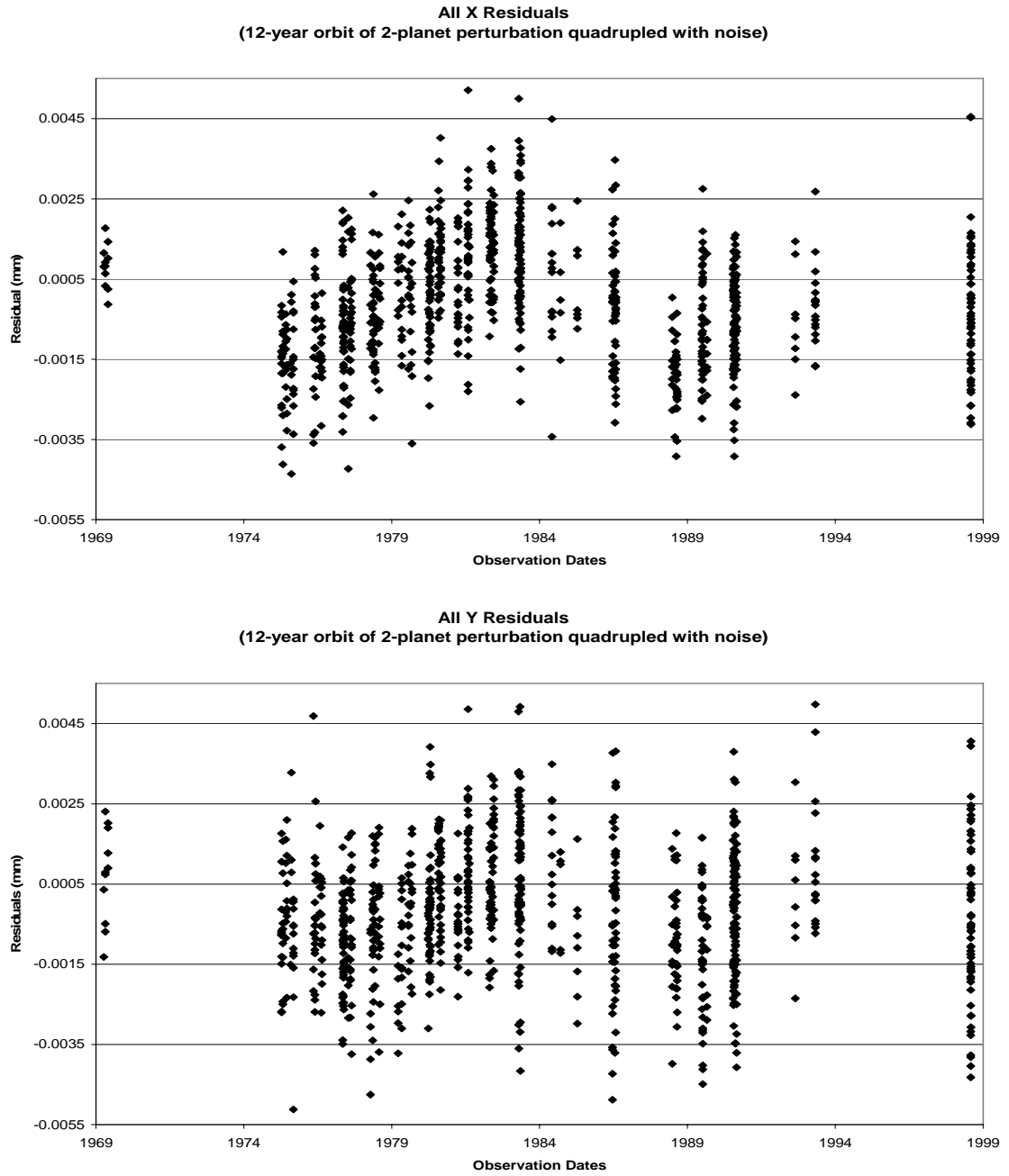
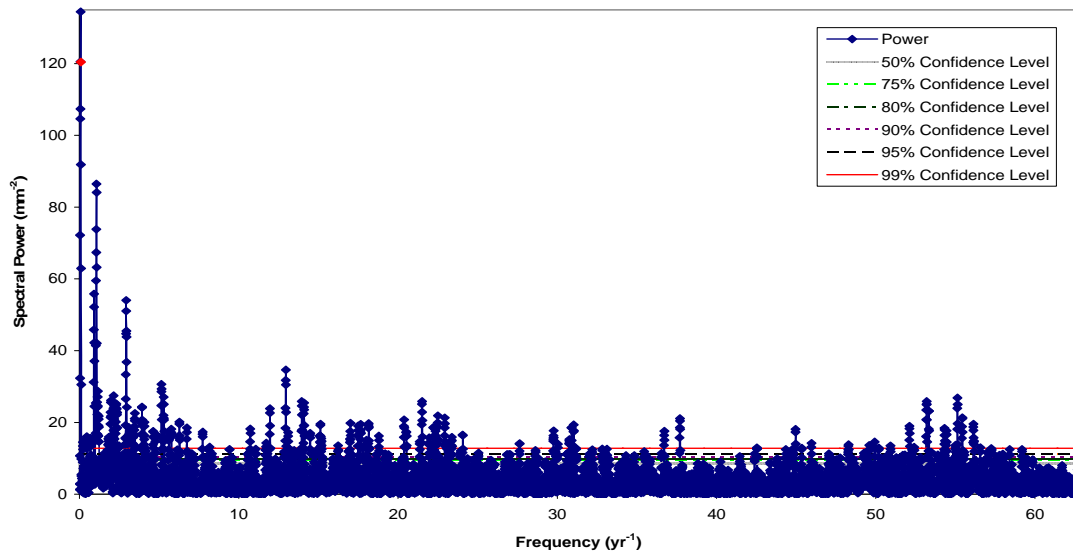


FIG. 2.17.— Theoretical Displacement Quadrupled with Noise Added. Top chart contains expected x-residuals combining the theoretical perturbation quadrupled and noise. Bottom chart contains expected y-residuals.

Periodogram for All X Residuals
(12-year orbit of 2-planet perturbation quadrupled with noise)



Periodogram for All Y Residuals
(12-year orbit of 2-planet perturbation quadrupled with noise)

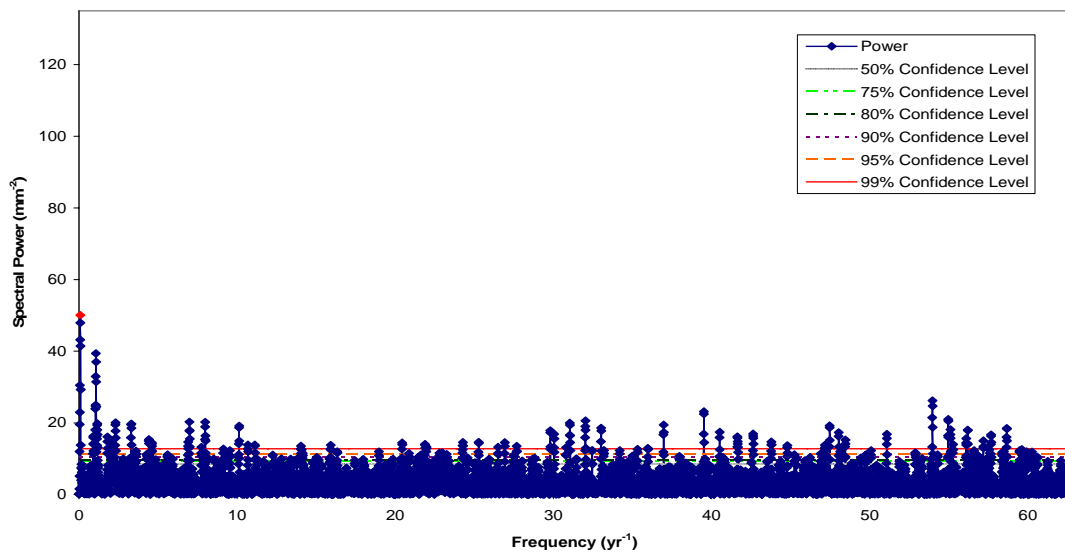


FIG. 2.18.— Periodograms of Theoretical Displacement Quadrupled with Noise Added. Top chart is a periodogram calculated for expected x-residuals. Bottom chart is a periodogram calculated for expected y-residuals. Horizontal lines in the periodograms indicate likelihood that spectral peaks exceeding that power are real and not caused by noise only. Solid line is 99% confidence, dashed line 95% confidence, dotted line 90% confidence, dash dotted line is 80% confidence, dash double-dotted line is 75% confidence, and hashed line is 50% confidence.

of the two described in his final analysis (1982). This low mass limit demonstrates the potential of astrometry to detect planets as well as larger companions.

2.4 DISCUSSION

This failure to replicate van de Kamp's results, while not unexpected considering the other searches to date, does not completely eliminate the possibility that such planetary companions exist. The Sproul Observatory material has similar precision to the McCormick photographic plates but the quantity of Sproul plates is unique. In 1982, van de Kamp analyzed nearly 20,000 exposures on 4,580 plates taken on 1,200 nights between 1938 and 1981. Although many other studies have attempted without success to confirm his results, no study has completely ruled out the possibility of low-mass companions to Barnard's Star.

Previous investigations of the photographic plate material at the McCormick have achieved similar negative results (Fredrick & Ianna 1985; Ianna 1995; Bartlett & Ianna 2001) despite van de Kamp's (1963a, 1969a) earlier analyses. Although containing far fewer observations than those taken at Sproul Observatory, McCormick is thought to have the second largest collection of Barnard's Star observations. In addition, the baseline of the McCormick observations represents slightly more than twice the period of the more massive, but shorter period, planet described by van de Kamp (1982). Furthermore, the McCormick refractor did not undergo significant physical changes, such as the modifications made to the Sproul refractor (van de Kamp 1975). Even with smoothing to annual normal points, the residuals to the proper motion and parallax solutions obtained in this study show the noise typical of photographic

plates. Nonetheless, this study further reduces the possibility that giant planets orbit Barnard's Star. Recent radial velocity results indicate such planets are even more unlikely leaving a remote possibility that smaller planets are present (C. McCarthy *et al.* 2007, in preparation).

Chapter 3 Planets In The South: Astrometric Search For Companions To Stars On The University Of Virginia Southern Parallax Program

3.1 INTRODUCTION

Although the presence of planets orbiting Barnard's Star described by van de Kamp (1963b, 1982) remains unconfirmed, an increasing number of extrasolar planets are being detected and confirmed. As of 2006 August 28, the International Astronomical Union (IAU) Working Group (WG) on Extrasolar Planets (ESP) listed 176 planets orbiting main sequence stars.⁷ Marcy *et al.* (2005) estimate that 12 percent (%) of stars host at least one giant planet within 20 astronomical units (AU) based on their radial-velocity studies of 1,330 F, G, K, and M stars with multiple planets in approximately 1% of those systems. This detection rate suggests that as many as eleven stars out of the approximately ninety stars observed in the University of Virginia (UVA) Southern Parallax Program (SPP) might have a planet. The subsample of thirteen stars studied herein might be expected to host up to two planets. However, Butler *et al.* (2004) have detected fewer than expected giant planets orbiting M dwarfs. Because radial-velocity programs have only studied a small sample of such cool stars so far, Endl *et al.* (2003) have begun a program focused on these late types.

Although a wealth of information about extrasolar planets may be obtained by an astrometric planet search, the SPP was not designed specifically for those goals. The SPP sought to identify new stellar members of the solar neighborhood. However, having measured the parallaxes and proper motions of possible nearby stars, the

⁷The IAU WG ESP maintains a list of extrasolar planets at <http://www.dtm.ciw.edu/boss/planets.html>

analysis of the residuals from the parallax solutions for any periodic perturbations that might indicate unseen companions is a reasonable extension of the program. Because these stars have low masses, their reflex displacement will be greater. Also, because these stars are close, the angular size of that displacement will be more easily detected. Sozzetti (2005) discusses the corresponding astrometric signature (α_{sig} in seconds of arc)

$$\alpha_{sig} = \frac{M_p a}{M_* d} \quad (3.1)$$

at length, where M_p and M_* are the masses of the planet and its host, respectively, in solar mass units, a is the semi-major axis in AU, and d is the distance in parsecs. The detection or non-detection of such planets would provide additional insight into the frequency of planets around low mass stars. Until recently, all very low luminosity stars were found through their associated astrometric perturbations, mostly at Sproul Observatory (Lippincott 1978). Therefore, the detection of any companions, regardless of mass, would be of scientific significance and improve our knowledge multiplicity within the solar neighborhood.

3.2 MEASUREMENT AND ANALYSIS

The SPP observed approximately ninety stars from 1987 until 2002 using the 1-meter reflector at Siding Springs Observatory, which is described in Table 3.1. Over the course of observations, several different charge-coupled device (CCD's) detectors were used with the 1-meter reflector. Of these, the two used primarily were CCD #1 and CCD #6; only images taken with either of these were considered for astrometric reduction. The first, GEC P8603 EEV, operated from 1987 through early 1994. Its

replacement, a GEC P88500, functioned from 1994 until the end of the project in 2002.

Table 3.2 details the two astrometric detectors. Observations were made through the V_C , R_C , and I_C filters (M. Bessell 1999, private communication) specified in Table 3.3.

Begam, Ianna, and Patterson (2006, in preparation; hereafter BIP) provide additional details of the SPP.

TABLE 3.1
CHARACTERISTICS OF THE SIDING SPRING REFLECTOR

Parameter	Description
Objective Size (meter)	1
(inches)	40
Optics	Ritchey-Chrétien
Focal Ratio	f/8
Focal Length (meters)	~8.1
Focal Plane Scale ($''$ mm ⁻¹)	25.55

NOTE.—Table 3.2 details the CCD's used with this telescope. Table 3.3 describes the filters.

REFERENCES.—Patterson, Ianna, & Begam 1998; BIP; MSSSO 2006⁸

TABLE 3.2
CHARACTERISTICS OF CCD'S USED

Parameter	CCD #1	CCD #6
Dates	1987 Jul—1994 Feb	1994 Jan—2002 Jul
Chip	GEC P8603 EEV	GEC P88500 EEV
Size (pixels)	380 x 578	2186 x 1152
CCD Pixel Size (μ m)	22.0	22.5
CCD resolution ($''$ pixel ⁻¹)	0.5621	0.5749
Description	thick, front-illuminated	thick, front-illuminated, uncoated
Grade	A	Engineering

REFERENCES.—RSAA Detector Lab. 2006⁹; M. Begam 2006, private communication; BIP

⁸Mount Stromlo and Siding Spring Observatories maintain a telescope specifications on-line at <http://www.mso.anu.edu.au/observing/telescopes/40inch.php>

⁹Details of various CCD's maintained by the Research School of Astronomy and Astrophysics Detector Laboratory may be found at <http://www.mso.anu.edu.au/observing/detectors/ccdlab/ccdinstr/ccdinstr.htm>

TABLE 3.3
CHARACTERISTICS OF FILTERS USED

Filter (Cousins)	Passband (nanometers)	Effective Wavelength (nanometers)
V	470.00 – 650.00	551.28
R	550.00 – 880.00	654.82
I	690.00 – 1,060.00	816.10

REFERENCE.—M. Bessell 1999, private communication

The use of CCD's to record the images of stars by the SPP, rather than photographic plates as was used to record images of Barnard's Star, is especially appropriate for low mass stars. The quantum efficiency of CCD's can reach 90% for wavelengths close to 750 nanometers (nm) compared with about 1% for photographic emulsions (Kitchen 1998). The greater sensitivity of CCD's to longer wavelengths of light is better than photographic plates for the many M dwarfs that the SPP observed and for the filters employed. In addition, CCD's have a greater dynamic range than photographic plates. Because of their low noise, CCD's can reach a similar signal-to-noise ratio 20–30 times faster than a photographic plate (Kitchen 1998). However, photographic plates have the advantage of a longer stable life. Eastman Kodak 103a-G photographic plates were used to image Barnard's Star for over twenty-nine years while multiple CCD's were used with the Siding Spring reflector during the fifteen years of SPP operations.

From the overall SPP program, eight stars, with spectral types from early to middle M that lie between 3.5 and 22 parsecs (pc) away, were initially selected for time series analysis. The stars in this first subsample were observed at least eighty-one times over a minimum of two years; in most cases, observations continued after the selection

of this subsample. The longest baseline for any of these stars was 8.2 years. The resulting errors in the relative parallaxes calculated for these stars are less than 3 mas. This subsample was the subject of a preliminary analysis using the McCormick Parallax Reduction Program (sager; hereinafter MPRP), which is discussed by Bartlett, Ianna, and Begam (2002). The preliminary periodograms produced no clear indication of unseen companions, but those for LHS 288 and LHS 2813 displayed some interesting features, as illustrated in Figure 3.1.

The especially noisy periodograms calculated for LHS 288 led to a complete re-reduction of this field. For some fields, additional observations became available after the preliminary analysis. After the SPP concluded operations, an additional five stars were selected based on the quality of their parallax solutions. The single stars in this second subsample were observed at least fifteen times over a minimum of five years also producing a relative parallax with an error of 3 mas or less. These stars, which lie between 6.5 and 22 pc, also have spectral types between early and middle M plus one white dwarf. Table 3.4 and Table 3.5 describe the selected stars. The SPP previously published photometry for LHS 337 and LHS 532, which can be found in Table 3.6.

Selecting stars based on the quality of their parallax solution can be approached in one of two ways. As done here, potential hosts may be selected for small errors associated with their final parallax that should be accompanied by small residuals. A perturbation due to a companion should stand out from the noise in the

A Search for Astrometric Companions to Southern Nearby Stars

Jennifer L. Bartlett (Hampden-Sydney College and University of Virginia), Philip A. Ianna (National Science Foundation), Michael C. Began (University of Virginia)

TABLE II. PARALLAXES AND PROPER MOTIONS

Star	Spectral Type	Parallax (mas)	Proper Motion μ (mas/yr)	Position Angle θ (deg)	Observations
LHS 288	M5.5	0.0 ± 0.11^{138}	0.2154 ± 0.0016	1.639° in 348.5°	01 nights on 18 nights May 1991 - March 1996
LHS 337	M4.5	0.0 ± 12.36^{49}	0.1448 ± 0.0016	1.439° in 206.4°	104 plates on 14 nights Feb. 1994 - June 1997
LHS 532	M4.5	0.0 ± 67.03^{700}	0.0946 ± 0.0014	1.072° in 209.6°	104 plates on 14 nights Feb. 1994 - Oct. 1997
LHS 1134	M3	0.0 ± 41.17^{360}	0.1002 ± 0.0028	0.761° in 221.0°	49 plates on 11 nights July 1996 - Nov. 2001
LHS 1565	M3.5	0.0 ± 44.70^{360}	0.2841 ± 0.0014	0.830° in 117.4°	137 plates on 22 nights Oct. 1995 - Aug. 2002
LHS 2739	M3.5	0.0 ± 31.10^{420}	0.0446 ± 0.0009	0.581° in 254.7°	137 plates on 22 nights May 1994 - June 1997
LHS 2813	M2	0.0 ± 53.73^{318}	0.0575 ± 0.0014	0.532° in 138.7°	112 plates on 14 nights Feb. 1994 - June 1997
LHS 3064	M3	0.0 ± 12.22^{12}	0.0845 ± 0.0010	0.724° in 342.2°	112 plates on 14 nights Feb. 1994 - March 1996

NOTES: Values in bold face are significant at the 95% level. Values in italics are significant at the 90% level. Values in regular face are not significant.

What if a companion were present?
 - different peaks in both x- and y-ventral spectra at same frequency
 - similar peaks remain when nightly normal points used instead of individual observations
 - predicted perturbation of LHS 288 by various companions calculated, Table IV

TABLE IV. PREDICTED PERTURBATIONS OF LHS 288

Companion (Optical Masses)	Distance from Star (AU)	Period (years)	Amplitude (milliarcseconds)	Comments
40	1.0	4.21	0.0793	0.00154
	1.0	4.21	0.391	0.0154
	0.5	1.88	0.0793	0.00307
80	1.0	5.33	0.157	0.00614
	5.0	26.6	0.793	0.0307

NOTES: Values in bold face are significant at the 95% level. Values in italics are significant at the 90% level. Values in regular face are not significant.

What about LHS 288?
 - Ask good explanation for differences between periodograms for LHS 288 and the rest of the sample, Figure 3 vs. Figure 2, 5, and 6
 - Signals detected are probably spurious but require additional investigation to understand all of the features, Table V along with Figure 2 and 3
 - One line in very crowded region near galactic plane

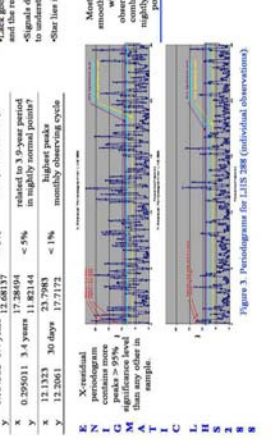


Figure 3. Periodograms for LHS 288 (individual observations).

TABLE III. SPECTRAL FEATURES OF LHS 283

Star	Star (Distance)	Period (years)	Power	False Alarm Probability	Comments
right ascension (h) \rightarrow x	0.529258	1.9 years	2.208903	> 5%	Period \sim 1.9 years with additional investigations
y	56.5550	6 days	11.0853	4.4%	different peaks at slightly normal points, peaks remain but with less than 50% significance level
Declination (d) \rightarrow y	36.5188	10 days	12.1798	2.7%	companion unlikely

What if a companion were present?
 - Higher power indicates stronger signal
 - Significance level indicates likelihood that a peak identifies a real "signal"
 - False Alarm Probability is likelihood that noise produces "signal"



Figure 2. Periodograms for LHS 283.

Method
 University of Virginia southern hemisphere parallax program
 - Observations: Siding Spring Observatory, Figures 1 and Table I
 - Redundant observations using standard plate constant, central overlap problem
 - Selected stars
 - Parameters and proper motions measured, Table II
 - Reducible in x and y: coordinates treated separately
 - Non-reducible in x and y: coordinates treated separately
 - Spectrograms up to 6x Nyquist frequency searched
 - Periodograms prepared using
 - Individual observations, Figure 2, 3, 5, and 6
 - Nightly normal points, Figure 4

What if a companion were present?
 - Higher power indicates stronger signal
 - Significance level indicates likelihood that a peak identifies a real "signal"
 - False Alarm Probability is likelihood that noise produces "signal"

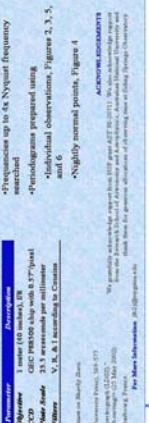


Figure 4. Periodograms for LHS 283 (nightly normal points).

TABLE V. QUODDISH SPECTRAL PEAKS OF LHS 337 AND LHS 1565

Star	Star (Distance)	Period (years)	Power	False Alarm Probability	Comments
LHS 337	x	57.2084	6 days	5.77027	73% prob. due noise
	y	58.3435	6 days	6.53899	45% companion unlikely
LHS 1565	x	9.91148	37 days	8.88650	4.4% different periods
	y	6.75220	34 days	8.26741	8.0% companion unlikely

No peak > 50% significance level when combined into nightly normal points

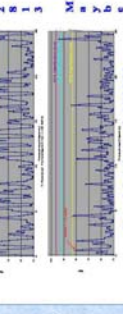


Figure 5. Periodograms for LHS 337.

The other side
 - Periodograms for LHS 337 and LHS 1565 are typical, Table VI along with Figures 5 and 6
 - Similar peaks have high false alarm probabilities or do not appear in both x- and y-ventral spectra
 - Periodograms for nightly normal points contain no peaks > 50% significance level
 - No clear indication of any companions

What if a companion were present?
 - Higher power indicates stronger signal
 - Significance level indicates likelihood that a peak identifies a real "signal"
 - False Alarm Probability is likelihood that noise produces "signal"

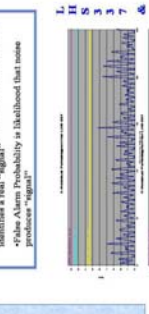


Figure 6. Periodograms for LHS 1565.

What if a companion were present?
 - Higher power indicates stronger signal
 - Significance level indicates likelihood that a peak identifies a real "signal"
 - False Alarm Probability is likelihood that noise produces "signal"

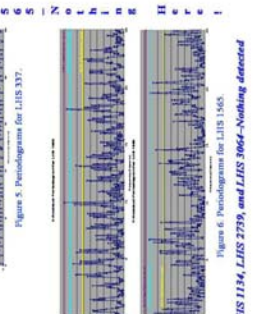


Figure 7. Periodograms for LHS 2739.

TABLE VI. QUODDISH SPECTRAL PEAKS OF LHS 337 AND LHS 1565

Star	Star (Distance)	Period (years)	Power	False Alarm Probability	Comments
LHS 337	x	57.2084	6 days	5.77027	73% prob. due noise
	y	58.3435	6 days	6.53899	45% companion unlikely
LHS 1565	x	9.91148	37 days	8.88650	4.4% different periods
	y	6.75220	34 days	8.26741	8.0% companion unlikely

No peak > 50% significance level when combined into nightly normal points

All the rest are similar - LHS 532, LHS 1134, LHS 2739, and LHS 3064 - Nothing detected

FIG. 3.1. — Summary of Results from the Preliminary Analysis (Bartlett, Ianna, & Began 2002).

TABLE 3.4
POTENTIAL HOST STARS FROM THE SPP

Star (LHS)	Position (2000.0) ^a		Spectral Type	Apparent Visual Magnitude ^b	Sample ^c	References
	RA (hh mm ss.ss)	Dec (dd mm ss.s)				
34	07 53 08.16	-67 47 31.5	DQ9	13.6 ± 0.3	2	1, 2
271	09 42 46.36	-68 53 06.1	M4.5 V	12.72 ± 0.03	2	3, 4
288	10 44 21.24	-61 12 35.6	M5.5 V	13.90 ± 0.03	1	5, 4
337	12 38 49.10	-38 22 53.7	M4.5 V	12.78 ± 0.05	1	6, 7
532	22 56 24.66	-60 03 49.2	M5.0 V	14.01 ± 0.05	1+	4, 7
1134	00 43 26.01	-41 17 34.0	M3.0 V	13.1 ^d ± 0.4 ^e	1+	6, 8
1565	03 35 59.72	-44 30 45.5	M5.5 V	13.03 ± 0.01 ^f	1	9, 10
2310	10 47 38.69	-79 27 45.9	M3.0 V	13.45 ± 0.01 ^f	2	6, 11
2739	13 27 19.59	-31 10 39.7	M3.5 V	13.58 ± 0.015	1+	6, 12
2813	13 51 21.75	-53 32 46.0	M2.0 V	12.9 ± 0.01 ^f	1+	6, 11
3064	15 22 12.98	-27 49 42.7	M3:	13.28 ± 0.01 ^f	1+	13, 14
3242	16 48 24.49	-72 58 34.1	M0.5 V	11.44 ± 0.01	2	6, 15
3418	18 52 00.17	-60 46 11.3	M3.5 V	13.4 ^d ± 0.4 ^e	2	6, 9

NOTES.—^aCoordinates from 2MASS were updated with preliminary relative proper motions from BIP using addpm routine from Jao 2004

^bApparent visual magnitude on the Johnson-Morgan system (16, 17) with V=550 nm; V_{Cousins} , V_{Kron} , and V_{Eggen} are substantially the same according to 18 and are used here where appropriate

^cPlus (+) in this column indicates that additional frames became available after the initial analysis of this star as part of sample 1

^dAssumed to be Johnson-Morgan V-band magnitude

^ePhotometric error estimated from quality of reported absolute V magnitude

^fPhotometric error estimated from 19

REFERENCES.—(1) McCook & Sion 2003; (2) Bessell 1990; (3) Henry *et al.* 2002; (4) Henry *et al.* 2004; (5) Bessell 1991; (6) Hawley, Gizis, & Reid 1996; (7) Patterson, Ianna, & Begam 1998; (8) Gliese & Jahreiß 1991; (9) Henry *et al.* 1997; (10) Rodgers & Eggen 1974; (11) Eggen 1987; (12) Reid, Kilkenny, & Cruz 2002; (13) Bidelman 1985; (14) Eggen 1969; (15) ESA 1997; (16) Johnson & Morgan 1951; (17) Johnson & Morgan 1953; (18) Bessell and Weis 1987; (19) Ryan 1989

TABLE 3.5
PRELIMINARY RELATIVE PARALLAXES AND PROPER MOTIONS FROM THE SPP

Star (LHS)	Parallax (mas)	Proper Motion (mas year ⁻¹)	Position Angle (degrees)	Mean Error ^a (μm)		Images	Observations		
				X	Y		Nights	Start	Stop
34	117.9 ± 1.8	2102.65 ± 0.70	135.804 ± 0.019	0.38	0.38	106	23	1995 Feb	2001 Dec
271	153.8 ± 1.4	1118.51 ± 0.60	356.160 ± 0.015	0.39	0.75	131	27	1992 Jan	2002 Jan
288	213.4 ± 1.7	1641.99 ± 0.61	348.513 ± 0.028	0.54	0.37	105	18	1991 May	1998 Mar
337	145.9 ± 1.4	1432.30 ± 0.86	206.375 ± 0.030	0.33	0.43	104	14	1994 Feb	1997 Jun
532	94.2 ± 1.4	1074.27 ± 0.70	209.672 ± 0.037	0.37	0.36	101 ^b	20	1994 Jul	2001 Aug
1134	99.2 ± 2.2	764.55 ± 0.70	221.001 ± 0.052	0.33	0.42	51	12	1996 Jul	2002 Jun
1565	284.5 ± 1.4	830.83 ± 0.45	117.404 ± 0.039	0.29	0.46	81	18	1995 Oct	2002 Jan
2310	71.1 ± 2.8	483.62 ± 0.95	244.224 ± 0.091	0.56	0.58	114 ^b	20	1994 Apr	2001 Jan
2739	43.6 ± 0.9	581.37 ± 0.50	254.639 ± 0.049	0.3	0.31	141 ^b	24	1994 Apr	2001 Jun
2813	59.8 ± 1.7	533.70 ± 0.60	138.608 ± 0.064	0.51	0.45	136	19	1994 Feb	2002 Apr
3064	82.7 ± 1.0	729.00 ± 0.47	36.117 ± 0.034	0.31	0.37	121	16	1994 Feb	2002 Apr
3242	64.6 ± 1.3	712.49 ± 0.66	222.429 ± 0.052	0.39	0.45	127	20	1994 Feb	2001 May
3418	45.2 ± 0.9	724.82 ± 0.42	298.064 ± 0.038	0.27	0.33	123	20	1994 Apr	2000 Sep

NOTES.—^aMean error of unit weight

^bOne questionable image was used in calculating positions and motions of reference stars only. This frame was dropped from the relative parallax and proper motion calculation and did not produce residuals. Therefore, the time-series analysis considered one residual fewer.

REFERENCE.—BIP

TABLE 3.6
SPP PHOTOMETRY OF POTENTIAL HOST STARS

Star (LHS)	V_C (mag)	R_C (mag)	I_C (mag)
337	12.78 \pm 0.05	11.48 \pm 0.06	9.75 \pm 0.06
532	14.01 \pm 0.05	12.50 \pm 0.06	10.75 \pm 0.06

REFERENCE.—Patterson, Ianna, & Begam 1998

residuals. On the other hand, the small errors may be an indication that no orbital component is present. In the alternative approach, larger errors may identify host candidates. The corresponding large residuals may be evidence of the presence of an orbital component. The large error, however, may merely reflect noisy or sparse data. In this study, we selected candidate hosts with “clean” parallaxes in the hopes of finding clear evidence of companions.

The observations for each star in this study were made over only a few years; for LHS 271 with the longest baseline, images were taken over 10 years. Therefore, annual normal points were not considered. The results for each individual star are discussed below. The reference stars relative to which the parallax and proper motion of the possible nearby star of interest were measured were selected so that they surrounded the star of interest and shared a common apparent brightness with it. Potential reference stars that were identifiable close binaries were excluded. However, the colors are rarely identical and, consequently, their apparent positions change slightly relative to one another as the atmosphere refracts their light differently as a function of hour angle. Such differential color refraction (DCR) may be minimized by restricting analysis of frames to images taken within 30 minutes of the transit. However, observational circumstances may require the consideration of frames taken at somewhat larger hour

angles; Table 3.7 lists the number of frames used for each star that were taken either 30 minutes or more east or west of the meridian. When possible, the SPP used photometry and weather records to model and correct the positions of stellar images for DCR before the calculation of parallaxes and proper motions. BIP discusses the approach used to model DCR, which is essentially that of Stone (1996). Table 3.7 also provides the status of DCR corrections for the stars in this study.

TABLE 3.7
DCR CORRECTION STATUS FOR SPP STARS

Star (LHS)	Filter (Cousins)	Large HA (# frames)	DCR Status	Comment
34	I	6	Uncorrected	unreduced I and R photometry exists
271	R	24	Uncorrected	no photometry exists
288	R	19	Corrected	
337	R	16	Corrected	
532	R	9	Corrected	
1134	R	5	Uncorrected	unreduced photometry exists
1565	V	4	Uncorrected	unreduced photometry exists
2310	R	9	Uncorrected	no photometry exists
2739	R	10	Corrected	photometry missing for 3/14 ref. stars weather missing for 30/141 frames
2813	R	27	Corrected	
3064	R	17	Corrected	
3242	V	3	Uncorrected	current photometry inadequate
3418	R	20	Corrected	

NOTE.—An exposure is considered to have a large hour angle (HA) if it was taken at 30 minutes or more east or west of the meridian.

REFERENCE.—BIP

The MPRP, the least-squares adjustment program that was used for the study of Barnard's Star and for the preliminary analysis, was designed for photographic plates scanned by a Photometric Data Systems (PDS) microdensitometer. P.A. Ianna prepared a new version (2005; hereinafter MPRP2) to calculate the parallaxes and proper

motions from observations recorded on CCD's, such as used with the Siding Spring Observatory 1-meter telescope.

The modernized MPRP2 used an iterative three plate-constant adjustment model to calculate the preliminary relative parallaxes and proper motions listed in Table 3.5. To improve the results, the program iterated over the plate constants and relative proper motions seven times for each field. In most cases, small fluctuations in the least significant digit of the resulting relative parallax and proper motions continue with each iteration; the most significant improvements appear in the first few iterations. The mean errors of unit weight range from 0.3 to 0.8 μm , or 7 to 20 milliseconds of arc (mas), with an average of $0.4 \pm 0.1 \mu\text{m}$, or $10 \pm 2 \text{ mas}$, in the x-coordinate (right ascension) and of $0.4 \pm 0.1 \mu\text{m}$, or $11 \pm 3 \text{ mas}$, in the y-coordinate (declination).

Following the removal of proper motion and parallax, the x- and y-residuals associated with each observation were subjected to a time-series analysis using the Lomb-Scargle normalized periodogram method (Press *et al.* 1996). The x- and y-residuals for each single night were combined and a new set of periodograms were calculated for each star. A similar approach was used for the photographic observations of Barnard's Star in Chapter 2. Frequencies up to four times the effective Nyquist frequency were searched; the Nyquist frequency is the highest frequency recoverable from evenly sampled data. Although averaging the data can improve detection efficiency, it also reduces the effective Nyquist frequency, which may drop below the signal frequency and make detection more difficult (Scargle 1982). The effective Nyquist frequency (f_{Neff}) for unevenly sampled data may be expressed as

$$f_{Neff} = \frac{N}{2T} \quad (3.2)$$

where N is the number of observations taken over total time (T). The lowest independent frequency (f_{low}) is

$$f_{low} = \frac{1}{T} \quad (3.3)$$

and the observation time defines a single period. When a companion is suspected, more than a single full orbital period should be observed in order to decouple the linear component of the companion-induced perturbation from the proper motion terms adequately (Black & Scargle 1982). Table 3.8 lists the effective Nyquist and lowest independent frequencies for each star.

3.2.1 Concerns Regarding Time and Parallax Factor Calculations

When graphing the residuals and associated periodograms for LHS 2813 and LHS 3064, a discrepancy in the order of some recent frames was detected. The frame numbers for each field were sequential but the associated observation dates, expressed as fractional years, were not. No other regions had such obvious temporal discontinuities. A comparison of the handwritten observation logs, the on-line catalogs, and the parallax input files (pif's) indicated that the problem occurred when the observation date was converted to a fractional year during the pif-generation process. The parallax factors, which are calculated based on observation time, were also affected, but the hour angles did not appear to be. The problem appeared to occur during observations that

TABLE 3.8
FREQUENCIES ASSOCIATED WITH AVAILABLE OBSERVATIONS

Star (LHS)	Lowest Independent				Effective Nyquist				Observational Baseline (years)
	Frequency (yr ⁻¹)		Period (yr)		Frequency (yr ⁻¹)		Period (yr)		
	All	Nightly	All	Nightly	All	Nightly	All	Nightly	
34	0.14574179	0.1457418	6.8614500	6.861450	7.7243	1.603	0.1295	0.6238	6.8614500
271	0.10023248	0.1002325	9.9768060	9.976806	6.5652	1.353	0.15232	0.7390	9.9768060
288	0.14762488	0.14762754	6.7739260	6.7738040	7.7503	1.329	0.129027	0.7526	6.7739260
337	0.30268991	0.30268991	3.3037110	3.3037110	15.740	2.119	0.063533	0.4720	3.3037110
532	0.14092067	0.31036190	7.0961910	3.2220450	7.0460	2.948	0.14192	0.3392	7.0961910
1134	0.16731000	0.1673134	5.9769290	5.976807	4.266	1.004	0.2344	0.9961	5.9769290
1565	0.15986262	0.1598657	6.2553710	6.255249	6.474	1.439	0.1545	0.6950	6.2553710
2310	0.14942908	0.1494345	6.6921380	6.691894	8.4427	1.494	0.11844	0.6692	6.6921380
2739	0.14016358	0.1401660	7.1345210	7.134399	9.8115	1.682	0.10192	0.5945	7.1345210
2813	0.12253201	0.1225320	8.1611330	8.161133	8.3322	1.164	0.12002	0.8591	8.1611330
3064	0.12257051	0.1225742	8.1585690	8.158325	7.4155	0.981	0.13485	1.02	8.1585690
3242	0.14173746	0.1417424	7.0552980	7.055054	9.0003	1.417	0.11111	0.7055	7.0552980
3418	0.15624644	0.1562494	6.4001460	6.400024	9.6092	1.562	0.10407	0.6400	6.4001460

spanned local midnight. In addition to the obvious discontinuities initially discovered within the files for the two specific regions, the discontinuity in one field was found to continue in the observations of another field. In this case, the observations of LHS 2813 suffered a discontinuity at local midnight. Observations of LHS 3064 immediately followed LHS 2813 and continued the incorrect times. Identifying this more subtle type of temporal reversal in the other regions would require checking each observation.

As of 2006 June 29, the data reduction software was still being investigated for the source of these errors and an eventual program-wide solution (M. Begam 2006, private communication). To circumvent this problem, a stand-alone program, “pfnly,” was used to calculate the fractional year and parallax factors manually for each frame of LHS 2813 and LHS 3064. The existing times and parallax factors were compared with the new values and the pif’s updated appropriately. Eventually, 4 out of 136 frames for LHS 2813 and 39 out of 121 frames for LHS 3064 were changed; the average magnitude of the changes was 0.0021 ± 0.0012 year and 0.0024 ± 0.0052 in parallax factor.

Although LHS 288 lacks an obvious discontinuity, its observation times and parallax factors were checked against pfnly-calculated values because its periodograms are noisy. As a result of this check, no frames for LHS 288 were changed.

New relative parallaxes and proper motions for LHS 2813 and LHS 3064 were calculated based on the revised times and parallax factors. Table 3.9 compares the relative parallaxes and proper motions obtained from the uncorrected data to those obtained after the corrections. The changes are all within the errors of the original values.

TABLE 3.9
EFFECT OF CORRECTIONS FOR TEMPORAL DISCONTINUITY IN DATA

Star (LHS)	Parallax (mas)		Proper Motion (mas yr ⁻¹)		Position Angle (deg)		Comment
	Uncorrected	Corrected	Uncorrected	Corrected	Uncorrected	Corrected	
2813	59.9 ± 1.7	59.8 ± 1.7	533.80 ± 0.60	533.72 ± 0.60	138.615 ± 0.064	138.608 ± 0.064	changes in y-coordinate
3064	82.7 ± 1.0	82.7 ± 1.0	729.16 ± 0.47	729.00 ± 0.47	36.108 ± 0.034	36.117 ± 0.034	changes in y-coordinate

The residuals from updated relative parallax and proper motion were, then, subjected to time-series analysis as discussed earlier.

Before the publication of the final SPP parallaxes and proper motions (BIP), the year fraction and parallax factors for each observation will need to be verified. The time-series analysis used herein to identify possible perturbations is not as sensitive to small errors in these values. The order of the residuals is more important than the time of observation with which they are associated. Beutler (1970) demonstrated that a power spectrum may be estimated when only the sampling order is recorded for an infinite baseline. Correcting LHS 2813 and LHS 3064 restored temporal order to the plate sequences; the discontinuities might otherwise have seriously affected the detection of a perturbation. None of the other fields appear to have frames out of order; LHS 288 was manually checked and found to be free of this particular error. Therefore, no other fields were manually corrected.

3.2.2 Periodograms

None of the periodograms calculated for any of the stars clearly indicated the presence of any unseen companions. LHS 288 and 2813 showed some interesting features in the preliminary analysis (Bartlett, Ianna, & Begam 2002), and LHS 288 retains most of them at the end of this final reduction.

Significant peaks in both the x- and y-residual periodograms at the same frequency would indicate the possible presence of a companion. In rare cases, such as an orbital inclination near 90 degrees ($^{\circ}$), a strong peak in only one coordinate might also signal the presence of a companion. When the individual residuals are combined

into nightly normal points, the resulting periodograms should also show similar peaks. Parallax observations are made primarily in the morning and evenings and in this case were usually scheduled during bright observing time. The cyclical nature of this observing schedule may produce signals at frequencies close to the synodic month, six months, and one year (Black & Scargle 1982).

When individual observations are considered, a larger range of frequencies is sampled than when nightly normal points are analyzed. Therefore, some high-frequency peaks in the periodograms for individual residuals cannot be compared with similar points on the periodograms for nightly residuals. In all cases, the high frequencies correspond to periods less than one year, which are most likely spurious. Because in most cases the effective Nyquist frequency corresponds to periods of less than one year, the algorithm may extract potential periods less than a year. However, astrometric techniques are more sensitive to long-period planets (Quirrenbach *et al.* 2004).

3.2.2.1 LHS 34

Although the other stars in this study are M dwarfs, LHS 34 is a white dwarf. Its reasonable parallax and moderate coverage were sufficient to include it in the second subsample; Figure 3.2 illustrates the residuals for LHS 34. It also has the highest measured proper motion of any star in this study. DCR corrections were not applied to LHS 34 as explained in Table 3.7. However, it was observed in I-band, where atmospheric refraction is minimal (Jao *et al.* 2005)

A white dwarf may not appear as an ideal primary to host planetary companions, but they do appear in binaries and are, therefore, worth investigating. Farihi, Becklin,

and Zuckerman (2005) identified two L-dwarf companions and nine M-dwarf companions later than spectral type M4.5 in a survey of 261 white dwarfs. In addition, a planet with a projected mass (mass times the sine of an unknown inclination angle, $m \sin i$) 2.5 times greater than that of Jupiter (M_{21}) orbits the neutron star-white dwarf binary system, PSR B1620-26 + WD J1623-266 (Thorsett, Arzoumanian, & Taylor 1993; Joshi & Rasio 1997) while a neutron star, PSR 1257+12, appears to host a system of several planets (Wolszczan & Frail 1992). However, LHS 34 does not appear to have companions, as shown in Figure 3.3.

At best, the periodograms for LHS 34 hint at something occurring with a period of 2–2.5 years; the minimum detectable companion by this study would have a mass of $13.8 \pm 0.8 M_{21}$ as discussed in section 3.2.2. No spectral peak is clearly of physical origin and most probably arise from noise alone; Table 3.10 lists the major features of the periodograms for individual and nightly residuals in x and y. The all x- and y-periodograms have points at a frequency of 0.47366 yr^{-1} , which corresponds to a period of 2.1112 years, with a greater than 50% chance of being real but the corresponding points in the periodograms for nightly residuals do not. The maximum power in the nightly x-residuals is found nearby at a frequency of 0.4008 yr^{-1} , which corresponds to a period of 2.495 years, and has a greater than 50% chance of being real. Although the corresponding point of the all x-residual periodogram is a local peak, the corresponding points in both y-periodograms have a less than 50% chance of being real.

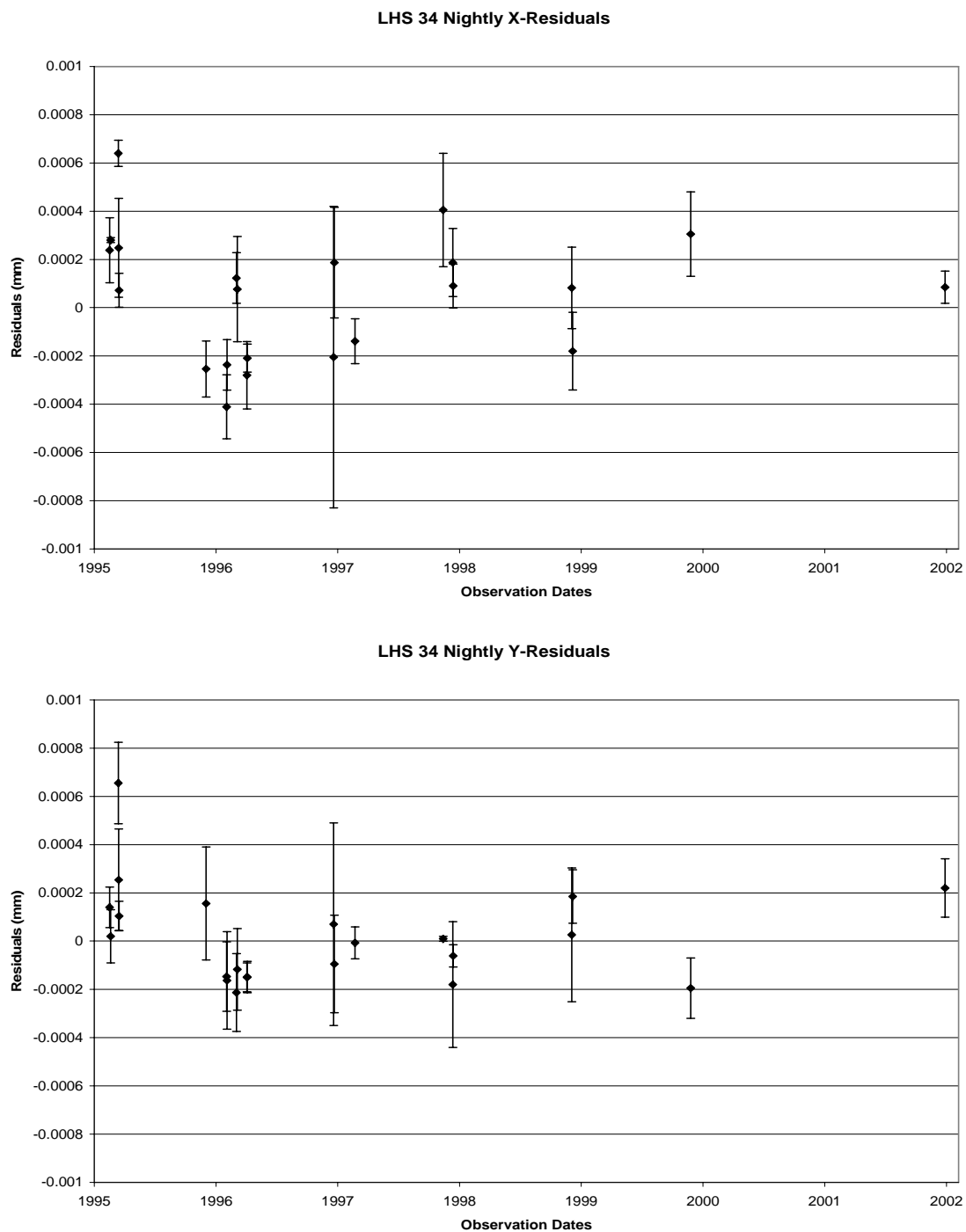


FIG. 3.2.—Nightly X- and Y-Residuals for LHS 34. Top chart contains x-residuals averaged by night. Bottom chart contains y-residuals averaged by night.

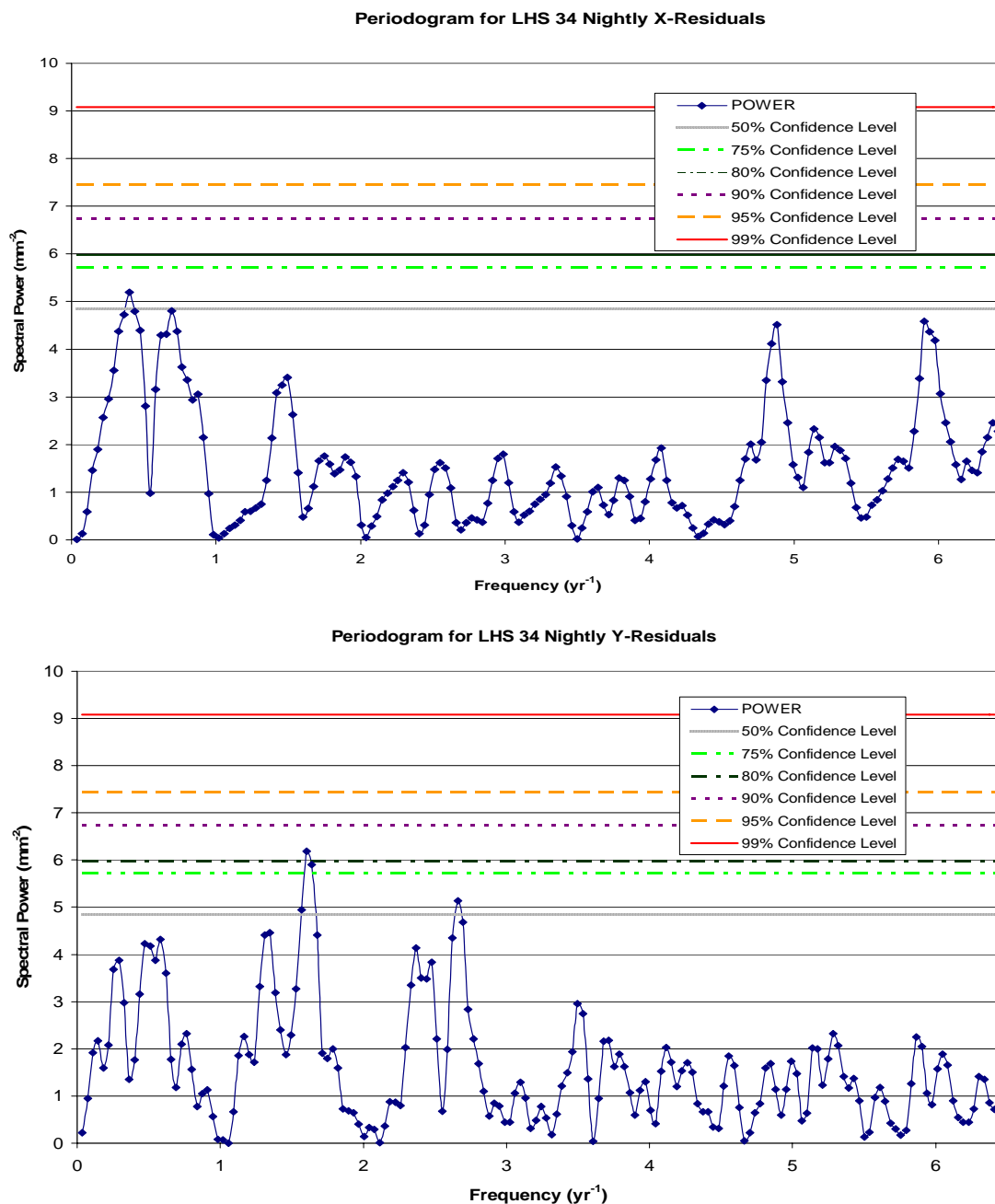


Fig. 3.3.— LHS 34 Periodograms. Top chart is a periodogram calculated for nightly x-residuals. Bottom chart is a periodogram calculated for nightly y-residuals. Horizontal lines in the periodograms indicate likelihood that spectral peaks exceeding that power are real and not caused by noise only. Solid line is 99% confidence, dashed line 95% confidence, dotted line 90% confidence, dash dotted line is 80% confidence, dash double-dotted line is 75% confidence, and hashed line is 50% confidence.

TABLE 3.10
FEATURES OF PERIODOGRAMS FOR LHS 34

Feature	Frequency (yr ⁻¹)	Period (yr)	Power (mm ⁻²)	False Alarm Probability (%)	Comment
All X, maximum	28.748	0.034786	11.115	<1	frequency too high for nightly x
All X, local peak	0.40079	2.4951	9.0149	<10	corresponds to maximum in nightly x
All X	0.47366	2.1112	7.8254	<20	corresponds to local peak in all y
All Y, maximum	1.6032	0.62377	8.4863	8	matches maximum in nightly y
All Y	0.40079	2.4951	3.3113	<50	corresponds to maximum in nightly y
All Y, local peak	0.47366	2.1112	6.4906	<50	
Nightly X, maximum	0.4008	2.495	5.199	39	corresponds to local peak in all x
Nightly X	0.4737	2.111	4.397	>50	corresponds to local peak in all y
Nightly Y, maximum	1.603	0.6238	6.181	17	matches maximum in all y
Nightly Y	0.4737	2.111	4.227	>50	corresponds to local peak in all y

3.2.2.2 LHS 271

LHS 271, a M4.5 V star (Henry *et al.* 2002), has the longest baseline and was observed on the most nights of any of the stars in this study. This coverage along with an adequate parallax solution prompted the inclusion of LHS 271 in the second sample. Jao *et al.* (2005) determined an absolute parallax of 153 ± 2 mas and a relative proper motion of $1.120 \pm 0.003'' \text{ yr}^{-1}$ in $365.7 \pm 0.2^\circ$, which generally agrees with the preliminary relative parallax and proper motion listed in Table 3.5

Figure 3.4 illustrates the residuals that were calculated without the benefit of DCR corrections as discussed in Table 3.7. DCR is a concern for LHS 271, which was observed through the R_C filter and for which 18% of the exposures used were taken at large hour angles. DCR is greatest for red stars observed in R-band (Jao *et al.* 2005). The SPP also made eighty-two I-band observations of LHS 271 but the error associated with the resulting parallax was greater than 3 mas (156.9 ± 4.4 mas) and the baseline was much shorter (4.8 years).

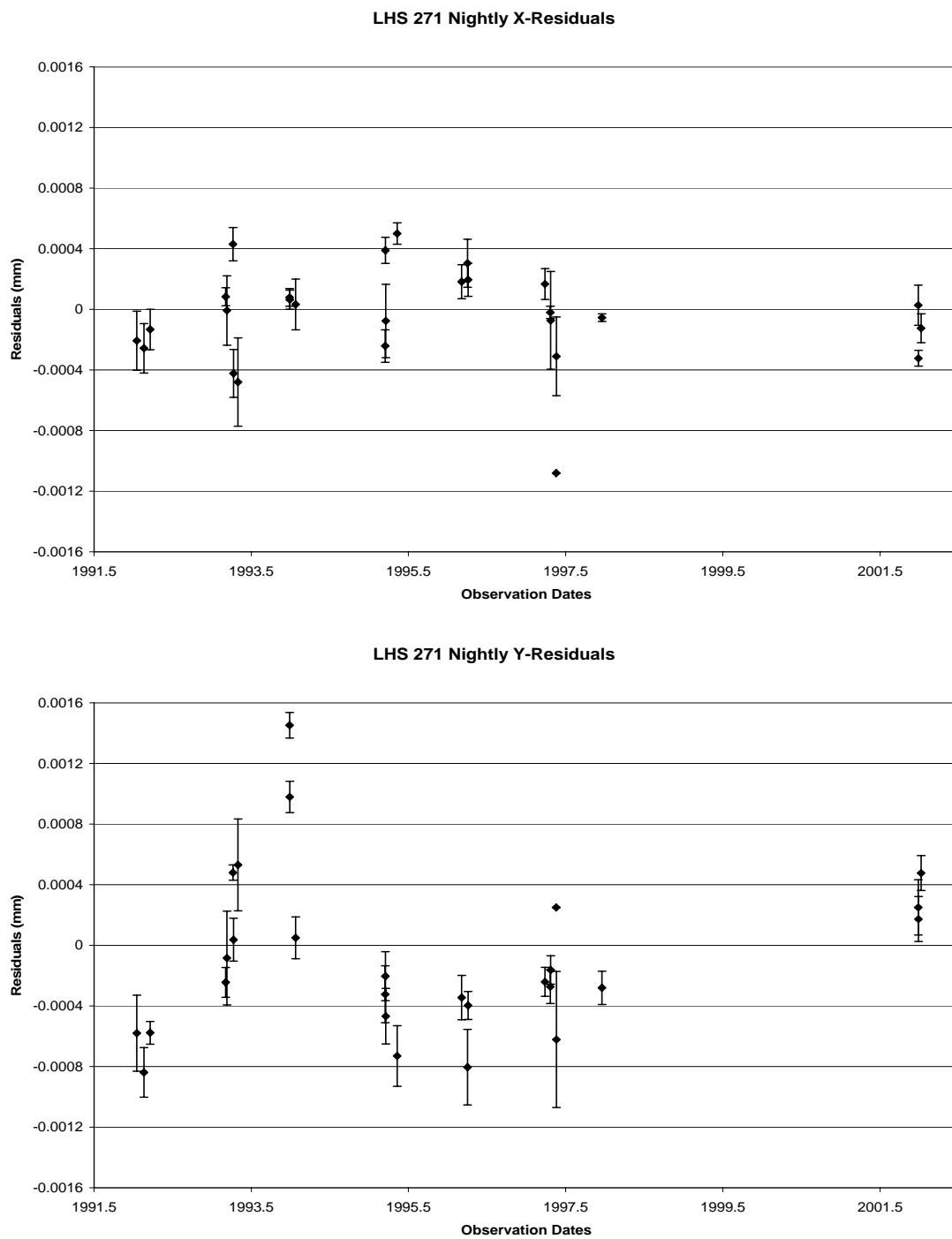


FIG. 3.4.— Nightly X- and Y-Residuals for LHS 271. Top chart contains x-residuals averaged by night. Bottom chart contains y-residuals averaged by night.

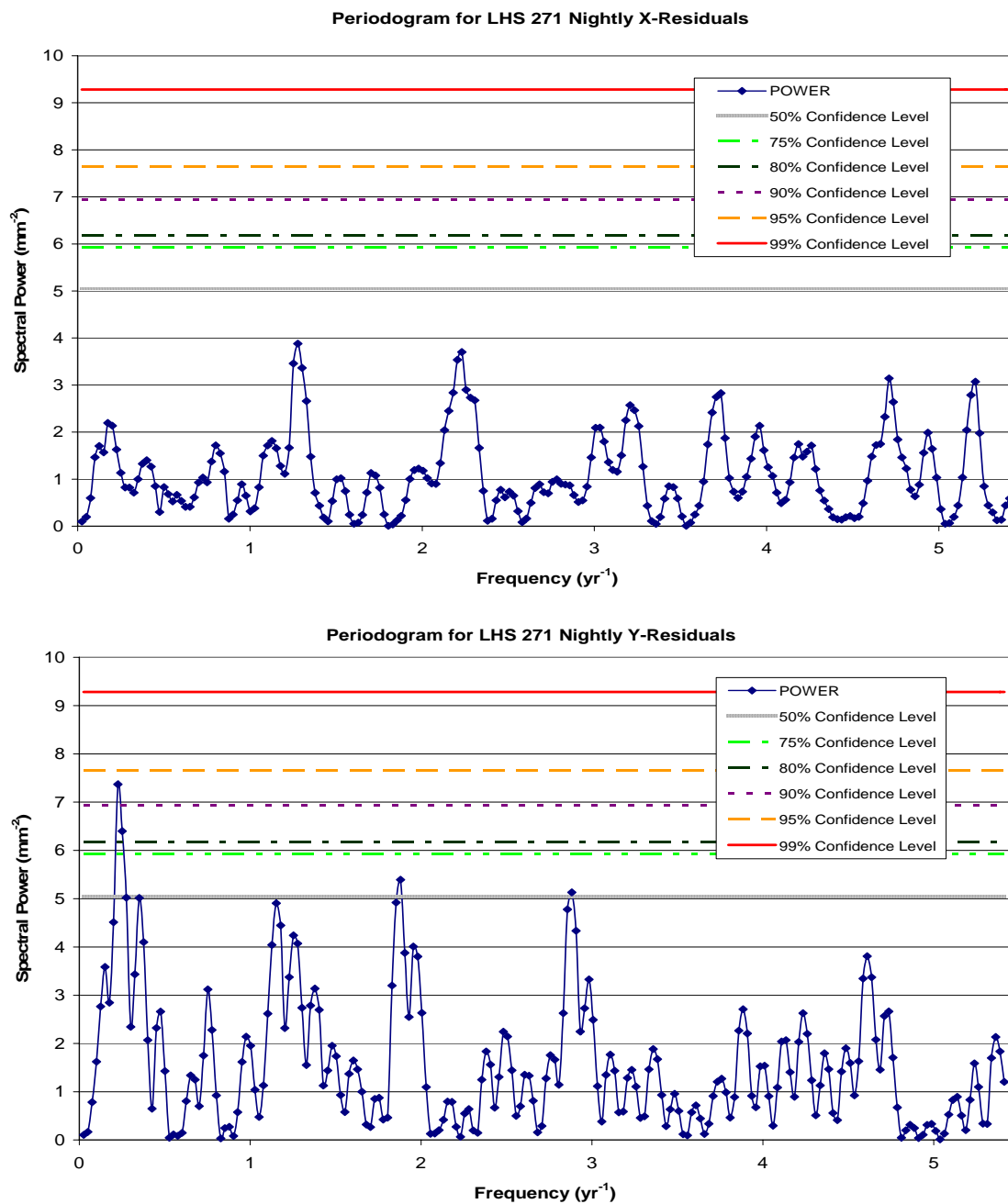


FIG. 3.5.— LHS 271 Periodograms. Top chart is a periodogram calculated for nightly x-residuals. Bottom chart is a periodogram calculated for nightly y-residuals. Horizontal lines in the periodograms indicate likelihood that spectral peaks exceeding that power are real and not caused by noise only. Solid line is 99% confidence, dashed line 95% confidence, dotted line 90% confidence, dash dotted line is 80% confidence, dash double-dotted line is 75% confidence, and hashed line is 50% confidence.

TABLE 3.11
 FEATURES OF PERIODOGRAMS FOR LHS 271

Feature	Frequency (yr ⁻¹)	Period (yr)	Power (mm ⁻²)	False Alarm Probability (%)	Comment
All X, maximum	23.655	0.042275	7.6379	22	frequency too high for nightly x
All X, local peak	0.20047	4.9884	5.3863	>50	adjacent to frequency of interest
All X, adjacent to local peak	0.22552	4.4341	3.7702	>50	corresponds to maxima in y
All X, local peak	1.2780	0.78249	5.0507	>50	corresponds to maximum in nightly x
All Y, maximum	0.22552	4.4341	32.103	<1	matches maximum in nightly y
All Y, local peak	1.2780	0.78249	14.138	<1	corresponds to maximum in nightly x
Nightly X, maximum	1.278	0.7825	3.879	90	corresponds to weak local peak in all x
Nightly X	0.2255	4.434	1.629	>50	corresponds to maxima in y
Nightly Y, maximum	0.2255	4.434	7.370	7	matches maximum in all y
Nightly Y, local peak	1.253	0.7981	4.238	>50	adjacent to frequency of interest
Nightly Y, adjacent to local peak	1.278	0.7825	4.071	>50	corresponds to maximum in nightly x

LHS 271 does not appear to have any unseen companions as shown in Figure 3.5. As discussed in section 3.2.3, the minimum detectable companion by this study would have a mass of $4.8 \pm 0.8 M_{21}$. Table 3.11 lists the important features of the periodograms. Although the maximum peaks in both y-periodograms occur at a frequency of 0.2255 yr^{-1} , which corresponds to a 4.434-yr period, no significant power appears at that frequency on either of the x-periodograms. Some orbital orientations to our line of sight might result in a perturbation of only one coordinate; however, such alignments are unlikely.

3.2.2.3 LHS 288

LHS 288 was an intriguing candidate in the preliminary analysis (Bartlett, Ianna, & Begam 2002) that continues to perplex. It is a nearby, M5.5 V star (Bessell 1991). The photographic SPP previously measured an absolute parallax of $221 \pm 8 \text{ mas}$, which puts it at a distance of about 4.5 pc, and a relative proper motion of 1.648 ± 0.005 seconds of arc ($''$) yr^{-1} in $347.6 \pm 0.1^\circ$ with the Yale-Columbia 66-centimeter refractor at Mount Stromlo Observatory (Ianna & Bessell 1986). Recent results from the Cerro Tololo Inter-American Observatory Parallax Investigation (CTIOPI) place it slightly farther away with an absolute parallax of $209 \pm 3 \text{ mas}$ but similar proper motion of $1.643 \pm 0.001'' \text{ yr}^{-1}$ in $347.70 \pm 0.07^\circ$ (Henry *et al.* 2006)

As part of the CCD program, LHS 288 was imaged 105 times on 18 nights between 1991 May and 1998 March using the R_C filter; however, only 104 images were used for the preliminary periodograms. Figure 3.1 shows the results of the preliminary analysis along with some estimates of the potential perturbations due to hypothetical

brown dwarf companions. The periodograms calculated for LHS 288 were dramatically noisier than any of the others. Significant power appeared to be present at frequencies of 0.14751 and 0.29501 yr^{-1} , which correspond to periods of 6.7794 and 3.3897 years, in the all x- and all y-periodograms. Because the longer period is twice the shorter, these peaks may be related. The nightly x- and y-periodograms have features on either side of 0.2950 yr^{-1} , a local peak in the nightly x-periodogram and the maximum peak in the nightly y-periodogram. While the features in the periodograms for all residuals have a greater than 99% chance of being real, the corresponding features in the periodograms for nightly normal points have a less than 50% chance. Although the features are most likely spurious, the initial results bore further investigation in order to understand all the features presented.

LHS 288 was one of the first fields reduced using CCD images during the SPP. Therefore, some changes in software and methodologies occurred during its reduction, (M. Begam 2002, private communication; P. Ianna 2002, private communication). To eliminate these changes in the data reduction pipeline as a possible noise source in LHS 288 periodograms, LHS 288 was re-reduced beginning with the archived, flat-fielded images.

During this re-analysis of the LHS 288 field, all 105 images were used. DCR corrections were applied to LHS 288 and its eleven reference stars, which are identified in Figure 3.6 and Table 3.12. Ianna and Bessell (1986) used a magnitude term in addition to the standard three-plate constant model to improve the earlier

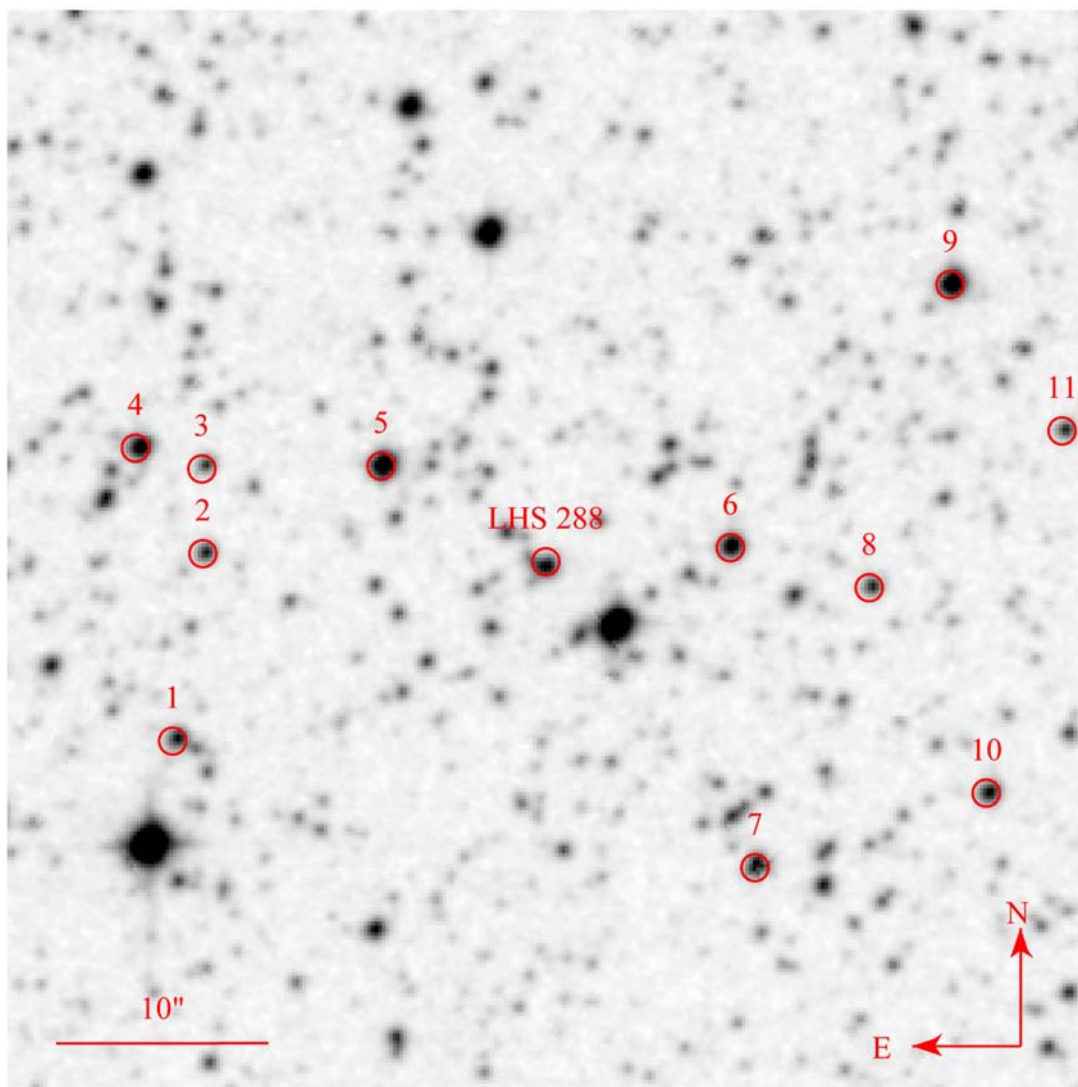


FIG. 3.6.— LHS 288 and Reference Frame. Image Source: Second Generation Digitized Sky Survey via *SkyView* with annotations by J. L. Bartlett & J. L. Bartlett. Image © 1993-2004 Anglo-Australian Observatory Board; compressed and distributed by the Space Telescope Science Institute.

parallax measurement of LHS 288. When MPRP2 calculated the relative parallax and proper motion of LHS 288, additional terms were considered for inclusion in the plate adjustment model

$$\begin{aligned}\varepsilon &= ax + by + c + gm + hmx + kC \\ \eta &= dx + ey + f + lm + nmy + pC\end{aligned}\tag{3.4}$$

where (x, y) are the coordinates of the reference star in the system of its own plate; (ε, η) are the coordinates of the reference stars in the system of the trail plate; $a, b, c, d, e, f, g, h, k, l, n, p$ are the plate constants; m is the apparent magnitude of the reference star; and, C is the color of the reference star. The potential terms of magnitude (gm, lm), coma (hmx, nmy), and color (kC, pC) were tested individually based on the photometry listed in Table 3.12; Patterson, Ianna, and Begam (1998) describe the reduction of SPP photometry to the Cousins system (Bessell 1995; Bessell 1990; Menzies *et al.* 1989; Cousins 1980a; Cousins 1980b; hereafter Cousins). The photometry for LHS 288 is consistent with other published values listed in Table 3.13. Table 3.14 summarizes the results; the number of frames for which a particular higher order term was considered statistically significant out of the 105 total frames is listed for each term separately by coordinate. A prospective term was considered statistically significant for a particular frame if the calculated coefficient was greater than three times the associated error; the probability of such a comparatively large coefficient arising from noise alone is less than 1% (Beers 1957). Although coma is generally reduced in a Ritchey-Chrétien

TABLE 3.12
PHOTOMETRY OF REFERENCE STARS FOR LHS 288

Star	2MASS Designation ^a	V _C (mag) ^b	R _C (mag) ^b	I _C (mag) ^b	(R-I) _C (mag) ^b
Reference 1	10443567-6113281	13.648 ± 0.008	13.044 ± 0.007	12.56 ± 0.008	0.48
Reference 2	10443450-6112361	13.900 ± 0.007	13.529 ± 0.009	13.20 ± 0.020	0.33
Reference 3	10443454-6112125	14.180 ± 0.010	13.960 ± 0.020	13.95 ± 0.040	0.01
Reference 4	10443709-6112067	12.297 ± 0.001	12.182 ± 0.002	12.03 ± 0.005	0.15
Reference 5 ^c	10442763-6112120	...	11.437 ± 0.001	11.13 ± 0.003	0.31
Reference 6	10441423-6112345	13.037 ± 0.003	12.305 ± 0.003	11.57 ± 0.004	0.73
Reference 7	10441326-6114033	13.819 ± 0.007	12.998 ± 0.004	12.21 ± 0.006	0.79
Reference 8	10440888-6112456	15.050 ± 0.010	13.396 ± 0.007	11.62 ± 0.004	1.78
Reference 9 ^d	10440577-6111215	...	11.386 ± 0.001	11.19 ± 0.003	0.20
Reference 10	10440438-6113425	13.244 ± 0.003	12.932 ± 0.006	12.60 ± 0.008	0.33
Reference 11	10440148-6112019	14.800 ± 0.010	13.890 ± 0.010	12.92 ± 0.010	0.97
LHS 288	10442131-6112384	13.966 ± 0.007	12.306 ± 0.003	10.33 ± 0.001	1.98

NOTES.—^a2MASS designations have the form hhmmss.ss-ddmmss.s

^bThe errors listed herein are from the raw fitting based on the standard stars observed. Based on other SPP photometry, the expected internal error for V_C ~ ± 0.02 mag, external error for V_C ~ ± 0.04 mag, and the error of the fit ~ ± 0.02 mag.

^cReference star 5 is also Tycho 8957-3132-1.

^dReference star 9 is also Tycho 8957-1309-1.

REFERENCE.—Photometry is from BIP with SPP errors from Patterson, Ianna, & Begam (1998). Other designations are from 2MASS and Høg *et al.* 2000.

reflector and by the small field, the R and I coma terms appeared significant in x (right ascension). Early frames were taken with no guiding until the autoguider system on the 1-meter telescope was functioning properly and reliably (P. Ianna 2006, private communication). Insufficient guiding could produce positional errors that are a function of magnitude (Schlesinger 1910). No extra term produced a significant improvement in the overall parallax and proper motion solution; consequently, none were used in the final reduction.

TABLE 3.13
COMPARISON OF LHS 288 PHOTOMETRY

Source	V_C (mag)	R_C (mag)	I_C (mag)	$(R-I)_C$ (mag)	Ref
SPP ^a	13.966 ± 0.049	12.306 ± 0.049	10.330 ± 0.057	1.98	1
RECONS	13.90 ^b ± 0.03	12.31 ± 0.03	10.27 ± 0.03	2.04	2
Bessell	13.92 ...	12.33 ...	10.31 ...	2.02	3

NOTES.—^aErrors for SPP values are estimated from 4.

^b V_{JM} is quoted here. It is substantially the same as V_C according to 5.

REFERENCES.—(1) BIP; (2) Henry *et al.* 2004; (3) Bessell 1991; (4) Patterson, Ianna, & Begam 1998; (5) Bessell & Weis 1987

TABLE 3.14
ADDITIONAL PLATE MODEL TERMS CONSIDERED FOR LHS 288

Term	Significant in X?		Significant in Y?		Comment
	(frames)	(percent)	(frames)	(percent)	
V magnitude	not tested, incomplete photometry
R magnitude	69	66	13	12	improved solution insignificantly
I magnitude	49	47	8	8	term statistically insignificant
R coma	71	68	13	12	improved solution insignificantly
I coma	68	65	12	11	solution slightly worsened
R-I color	3	3	0	0	term statistically insignificant

NOTE.—A total of 105 frames were used for LHS 288.

Although the LHS 288 pif did not contain any obvious temporal discontinuities like those found for LHS 2813 and LHS 3064, the observation year fraction and

parallax factors were manually checked for each observation as discussed in 3.2.1. No problems were found with any of these values.

The values listed in Table 3.5 were determined after seven iterations when the solutions appeared to converge; five individual residuals greater than $1 \mu\text{m}$ resulted but all nightly residuals were less than $1 \mu\text{m}$. Skipping the frame with the largest residual produced a slightly better solution overall but the image itself, the observing log, and the reduction notes provide no reason for doing so and it was retained. In half the images taken that particular night, reference star 9 was definitely saturated and dropped from the reduction. On further examination of the images, the contours of reference star 5 and 9 indicated possible saturation. However, dropping reference stars 5 and 9 from those frames worsened the solution so these stars were retained.

The residuals from the final reduction of LHS 288 are shown in Figure 3.7, individually, and in Figure 3.8, combined into nightly normal points. Figure 3.9 and Figure 3.10 are the corresponding periodograms. The highest power in both x-periodograms occurs at 0.2952 yr^{-1} , which corresponds to a 3.4-year period, with a greater than 80% chance of being real in both cases. The corresponding frequency in the periodogram for all y-residuals has a greater than 99% chance of being real and is adjacent to a local peak. The highest power in both y-periodograms occurs at 0.1476 yr^{-1} , which corresponds to a 6.8-year period, with a greater than 80% chance of being real in both cases. The corresponding frequency in the periodogram for all x-residuals has a greater than 99% chance of being real and is adjacent to a local peak. Aliasing

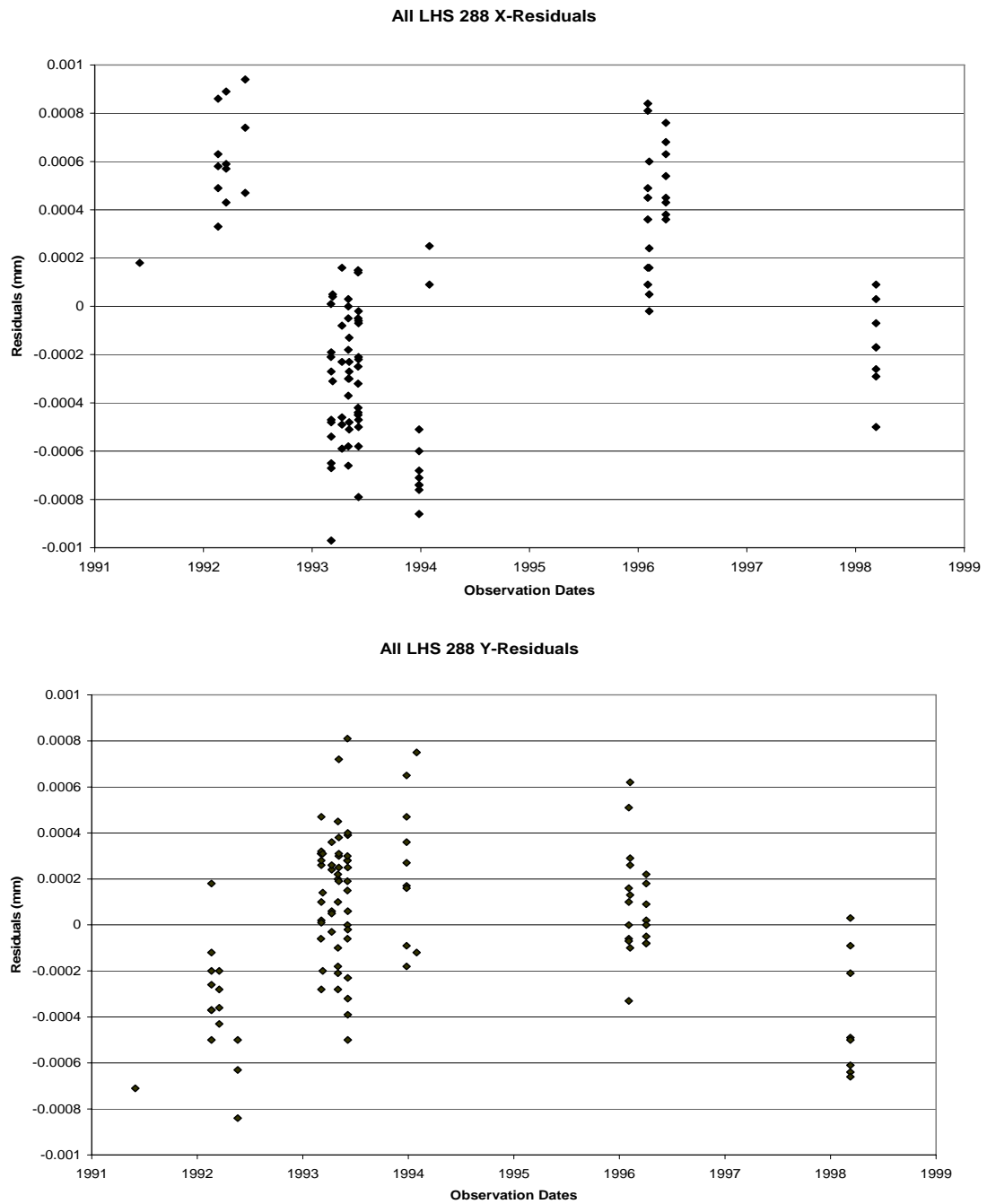


FIG. 3.7.— All X- and Y-Residuals for LHS 288. Top chart contains all x-residuals. Bottom chart contains all y-residuals.

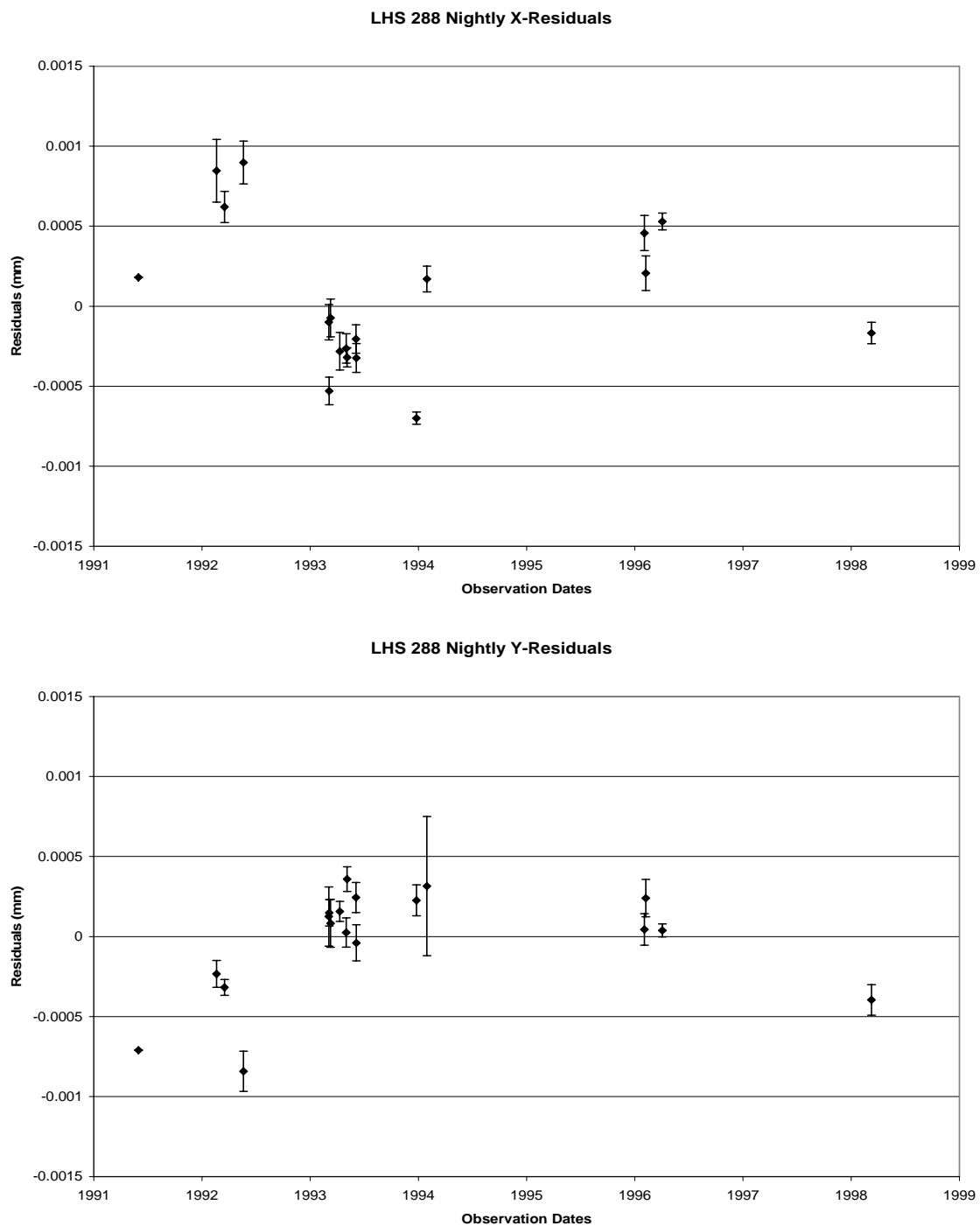


FIG. 3.8.—Nightly X- and Y-Residuals for LHS 288. Top chart contains x-residuals averaged by night. Bottom chart contains y-residuals averaged by night.

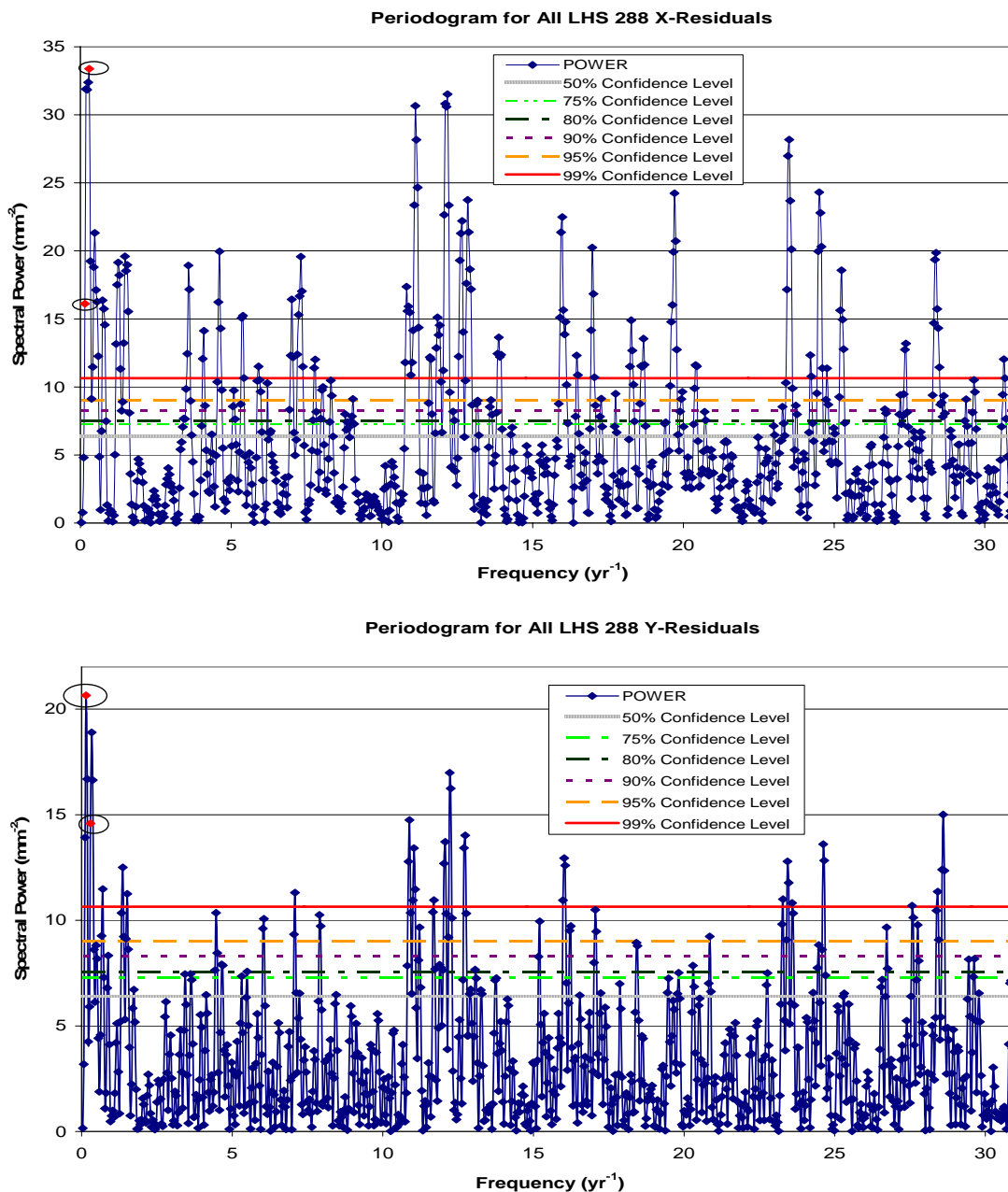


FIG. 3.9.—LHS 288 Periodograms. Top chart is a periodogram calculated for all x-residuals. Bottom chart is a periodogram calculated for all y-residuals. Ovals mark points of interest implying a companion with an orbit of 3.4 or 6.8 years. Horizontal lines in the periodograms indicate likelihood that spectral peaks exceeding that power are real and not caused by noise only. Solid line is 99% confidence, dashed line 95% confidence, dotted line 90% confidence, dash dotted line is 80% confidence, dash double-dotted line is 75% confidence, and hashed line is 50% confidence.

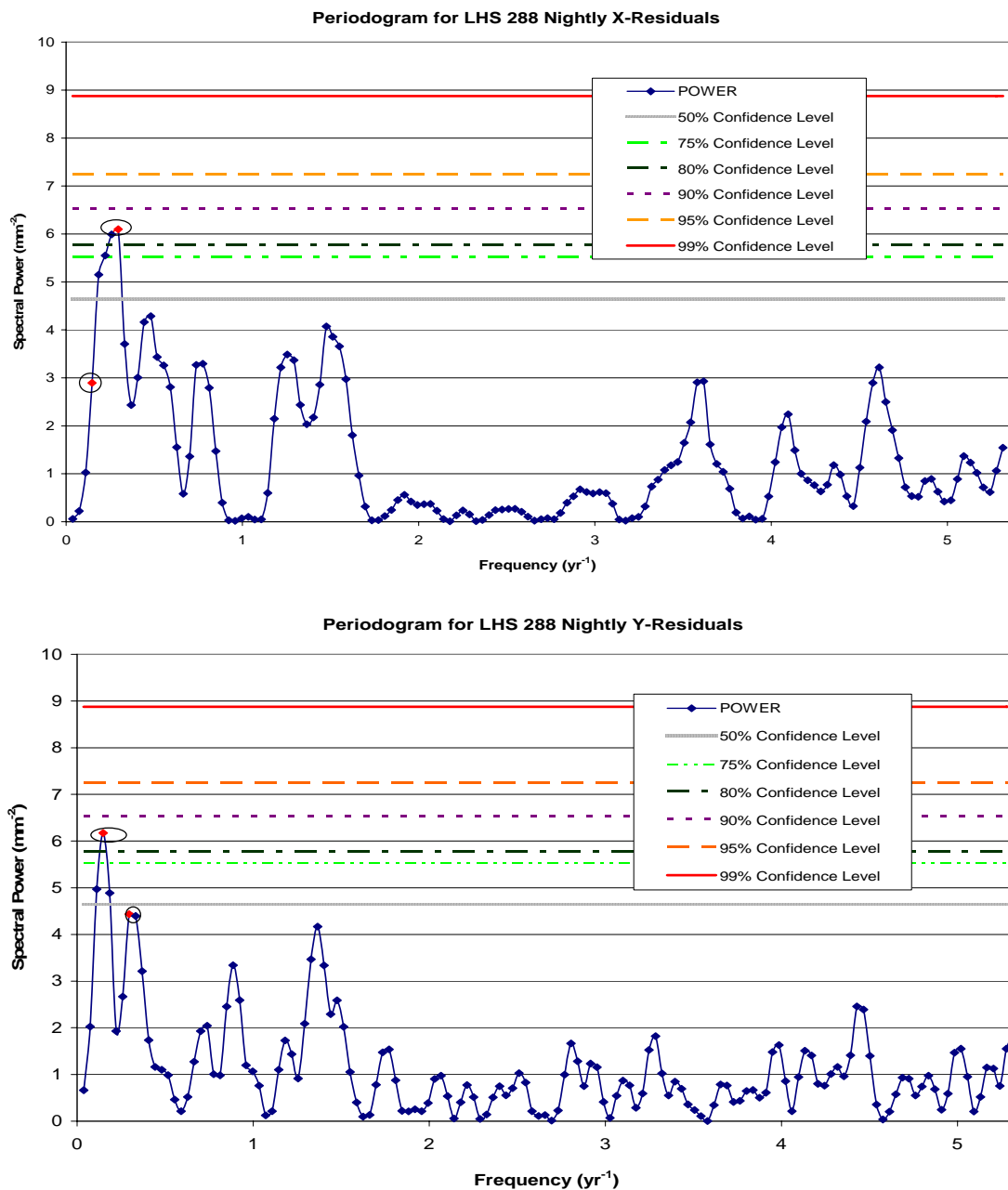


FIG. 3.10.—LHS 288 Nightly Periodograms. Top chart is a periodogram calculated for nightly x-residuals. Bottom chart is a periodogram calculated for nightly y-residuals. Ovals mark points of interest implying a companion with an orbit of 3.4 or 6.8 years. Horizontal lines in the periodograms indicate likelihood that spectral peaks exceeding that power are real and not caused by noise only. Solid line is 99% confidence, dashed line 95% confidence, dotted line 90% confidence, dash dotted line is 80% confidence, dash double-dotted line is 75% confidence, and hashed line is 50% confidence.

TABLE 3.15
 FEATURES OF PERIODOGRAMS FOR LHS 288

Feature	Frequency (yr ⁻¹)	Period (yr)	Power (mm ⁻²)	False Alarm Probability (%)	Comment
All X, maximum	0.29525	3.3870	33.380	<1	matches maximum in nightly x
All X, adjacent to local peak	0.14762	6.7739	16.116	<1	corresponds to maxima in y
All X, local peak	0.18453	5.4192	31.895	<1	adjacent to frequency of interest
All Y, maximum	0.14762	6.7739	20.651	<1	matches maximum in nightly y
All Y, adjacent to local peak	0.29525	3.3870	14.581	<1	corresponds to maxima in x
All Y, local peak	0.33216	3.0106	18.898	<1	adjacent to frequency of interest
Nightly X, maximum	0.2953	3.387	6.099	15	matches maximum in all x
Nightly X	0.1476	6.774	2.895	>50	corresponds to maxima in y
Nightly Y, maximum	0.1476	6.774	6.173	14	matches maximum in all y
Nightly Y, local peak	0.2953	3.387	4.435	>50	corresponds to maxima in x

can move spectral power to a lower frequency than the actual signal but is generally reduced by uneven sampling (Scargle 1982) like the observations of LHS 288. Table 3.15 lists the features of the periodograms for LHS 288.

The periodograms for LHS 288 may indicate a perturbation with a 3.4-year or 6.8-year period. These potential signals are stronger than any others detected in this study. However, they do not clearly indicate the presence of an unseen companion. The multiplication of the residuals by an appropriate data windowing function might reduce any spectral leakage present and smooth the periodogram further (Scargle 1982). With its low mass and proximity to the Earth, a Jupiter-mass planet orbiting LHS 288 with these periods would produce perturbations of 2–3 mas as discussed in 3.2.3.2. The minimum detectable planet in this study would be $2.4 \pm 0.7 M_{\text{J}}$. Because LHS 288 is a high proper-motion star in a rich field, the possibility that it passed over an undetected faint star during the SPP observations cannot be eliminated; such a distorted point-spread function might mimic a perturbation. Additional observations from an independent data set would provide the best determination of the validity of these spectral peaks. The Research Consortium on Nearby Stars (RECONS 2006, private communication) remains interested in LHS 288 as a potential planetary host and continues to observe it at CTIO. Observing it with the Fine Guidance Sensors (FGS) of the Hubble Space Telescope (HST) would be another possibility.

3.2.2.4 LHS 337

LHS 337 is a nearby, M4.5 V (Hawley, Gizis, & Reid 1996), high-proper motion star at a distance of about 6.9 pc (BIP). Recent CTIOPI results place it slightly closer with an absolute parallax of 157 ± 2 mas and proper motion of $1.464 \pm 0.002''$ yr⁻¹ in $206.4 \pm 0.1^\circ$ (Henry *et al.* 2006). As shown in Figure 3.1, LHS 337, along with LHS 1565, served as an example of a star with no hint of perturbation detected by the preliminary analysis. It has the shortest baseline of any star in this study, only 3.3 years. However, it was imaged 104 times on 14 nights resulting in a relative parallax with an error less than 1.5 mas and mean errors of unit weight less than 0.5 μ m; these error values fall in the mid-range of such errors in this study. Earlier SPP photometry can be found in Table 3.6.

Before calculating the final periodograms, DCR corrections were applied to LHS 337 and its reference stars. As shown in Figure 3.11 and Figure 3.12, LHS 337 still shows no sign of any perturbation. Any companion would need to be less than $6 \pm 1 M_{21}$ as discussed in 3.2.3. Table 3.16 lists the features of the periodograms for LHS 337, all of which correspond to periods of less than one year and are most likely the result of noise. No point in the periodograms for nightly residuals has a 50% or greater possibility of being real. Jao *et al.* (2003) found no companions to LHS 337 during an examination of CTIOPI images.

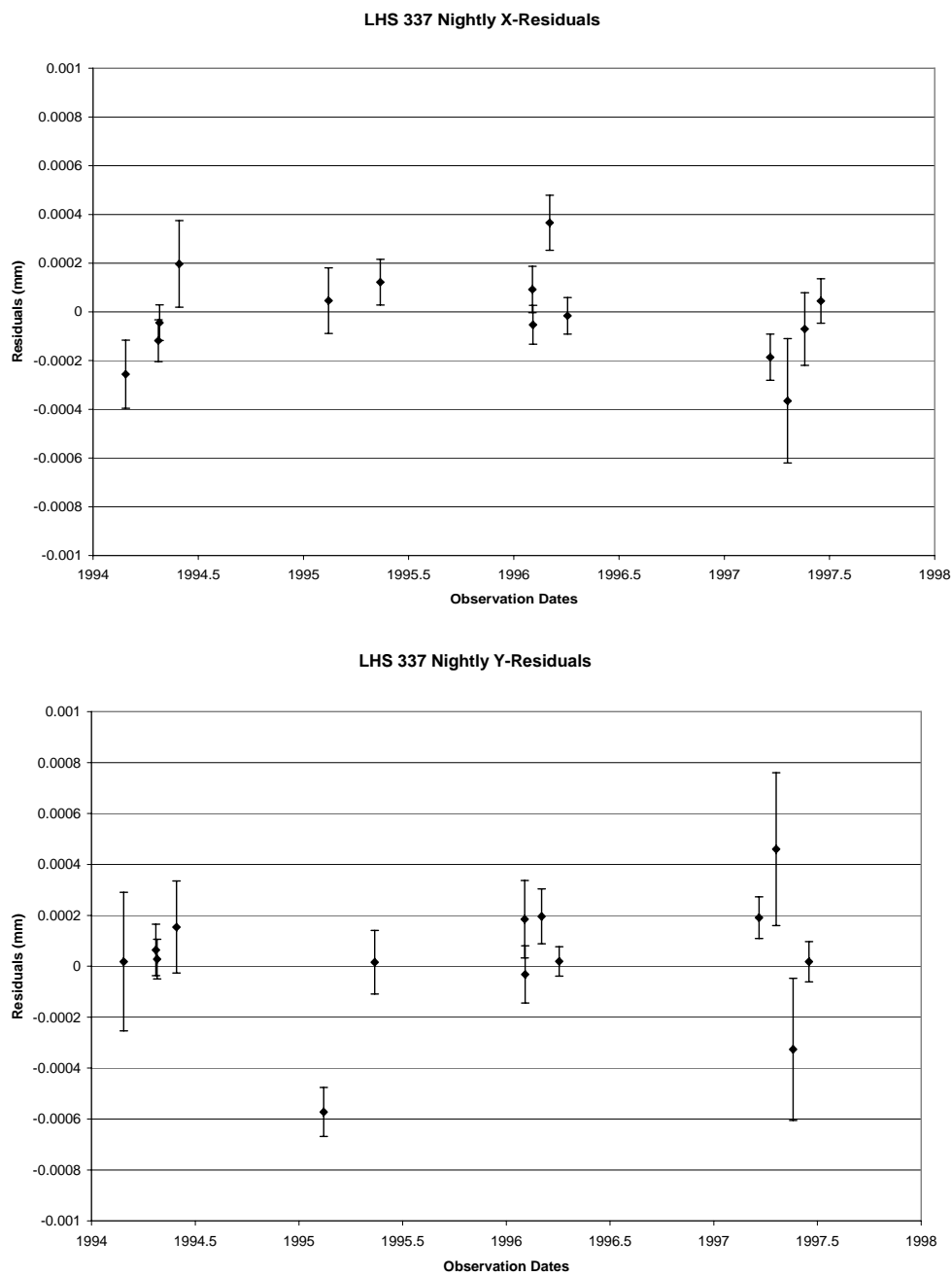


FIG. 3.11.—Nightly X- and Y-Residuals for LHS 337. Top chart contains x-residuals averaged by night. Bottom chart contains y-residuals averaged by night.

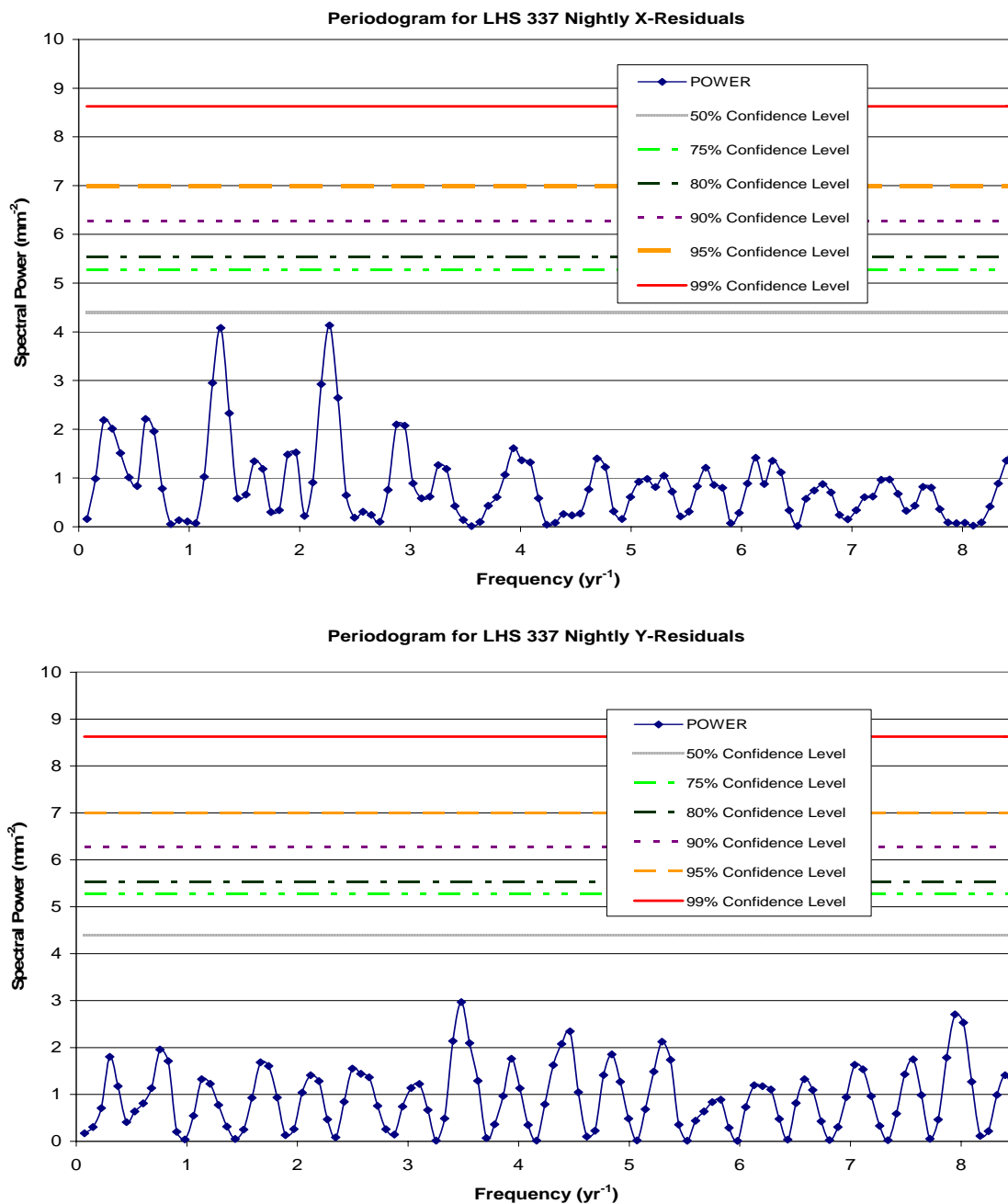


FIG. 3.12.—LHS 337 Periodograms. Top chart is a periodogram calculated for nightly x-residuals. Bottom chart is a periodogram calculated for nightly y-residuals. Horizontal lines in the periodograms indicate likelihood that spectral peaks exceeding that power are real and not caused by noise only. Solid line is 99% confidence, dashed line 95% confidence, dotted line 90% confidence, dash dotted line is 80% confidence, dash double-dotted line is 75% confidence, and hashed line is 50% confidence.

TABLE 3.16
 FEATURES OF PERIODOGRAMS FOR LHS 337

Feature	Frequency (yr ⁻¹)	Period (yr)	Power (mm ⁻²)	False Alarm Probability (%)	Comment
All X, maximum	13.7	0.07	7.3	23	27-day period, monthly observing cycle?
All Y, maximum	58.3	0.02	6.5	47	6-day period
Nightly X, maximum	2.3	0.44	4.1	60	
Nightly Y, maximum	3.5	0.29	3.0	95	

3.2.2.5 LHS 532

LHS 532 is the faintest star in this study as shown in Table 3.4 and Table 3.6. DCR corrections were applied to LHS 532 and all its reference stars. Because of the questionable nature of one new frame, only 100 out of 101 frames produced useable residuals (P. Ianna 2006, private communication; M. Begam 2006, private communication).

As shown in Figure 3.13 and Figure 3.14, LHS 532 still shows no sign of any perturbation. According to section 3.2.3, this study could detect companions more massive than $6 \pm 1 M_{21}$. Although a strong local peak in the periodogram for all x-residuals at 2.9 yr^{-1} , which corresponds to a 0.35-year period, matches the highest peak in the nightly x-residual periodogram, the nightly residual maximum has a 77% false alarm probability making these features mostly noise-related. In addition, neither of the y-residual periodograms have any points with even a 50% chance of being real. Table 3.17 lists the features of the periodograms for LHS 532.

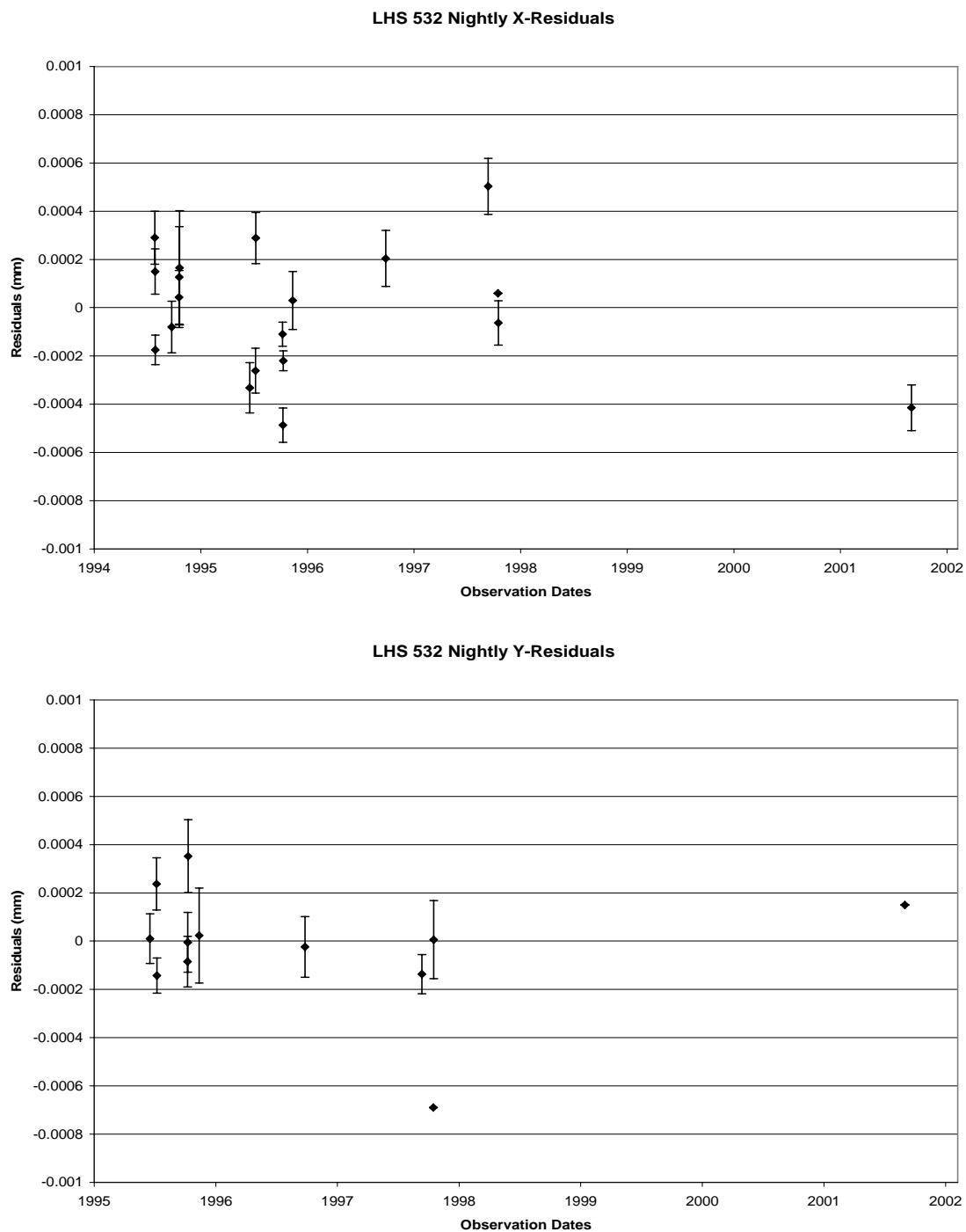


FIG. 3.13.— Nightly X- and Y-Residuals for LHS 532. Top chart contains x-residuals averaged by night. Bottom chart contains y-residuals averaged by night.

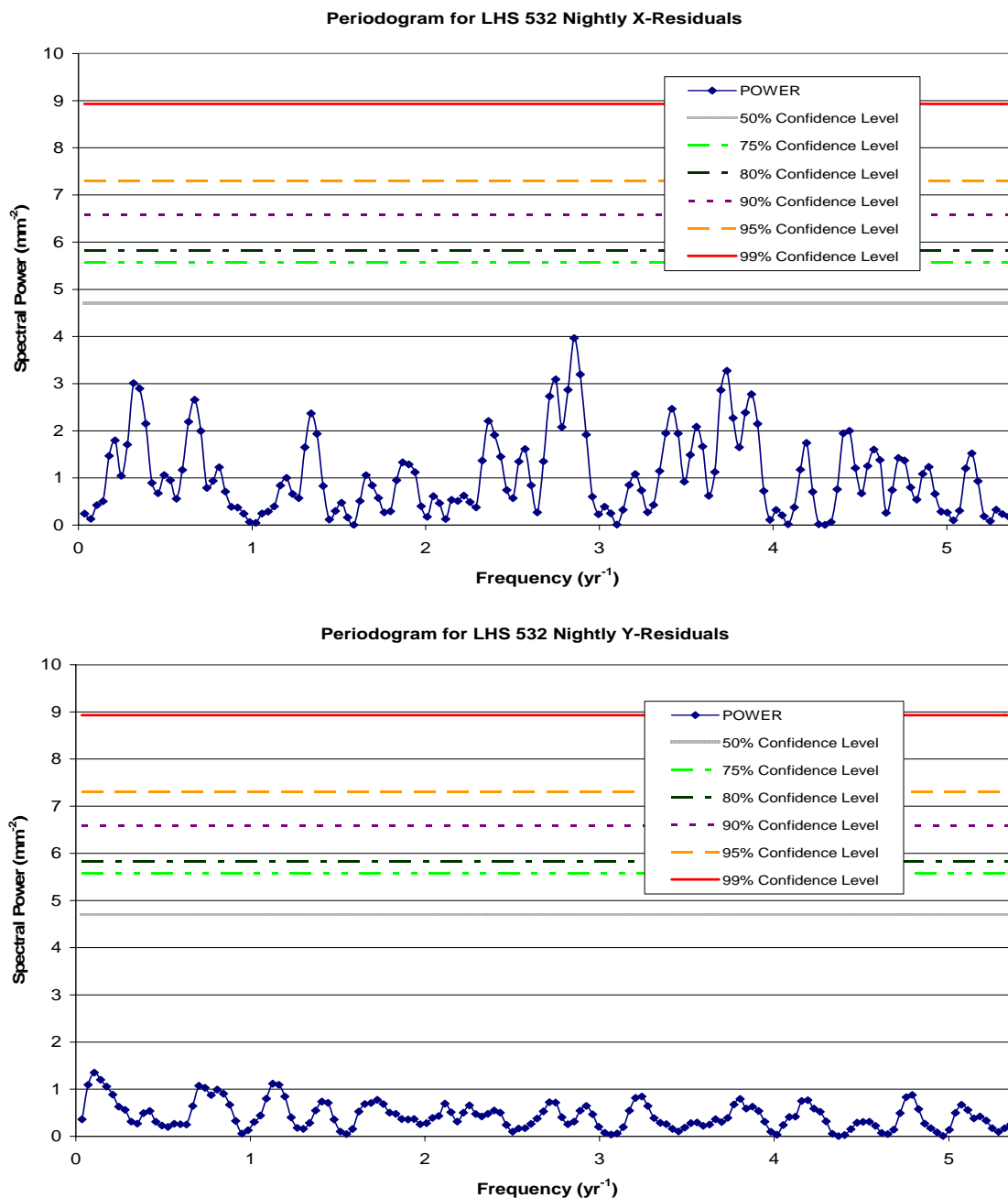


FIG. 3.14.— LHS 532 Periodograms. Top chart is a periodogram calculated for nightly x-residuals. Bottom chart is a periodogram calculated for nightly y-residuals. Horizontal lines in the periodograms indicate likelihood that spectral peaks exceeding that power are real and not caused by noise only. Solid line is 99% confidence, dashed line 95% confidence, dotted line 90% confidence, dash dotted line is 80% confidence, dash double-dotted line is 75% confidence, and hashed line is 50% confidence.

TABLE 3.17
 FEATURES OF PERIDOGRAMS FOR LHS 532

Feature	Frequency (yr ⁻¹)	Period (yr)	Power (mm ⁻²)	False Alarm Probability (%)	Comment
All X, maximum	7.0	0.14	14.2	<1	
All X, local peak	2.9	0.35	11.0	<1	matches maximum in nightly x
All Y, maximum	22.2	0.05	3.2	>99	
Nightly X, maximum	2.9	0.35	4.0	77	corresponds to local peak in all x
Nightly Y, maximum	0.1	9.46	1.3	>99	

3.2.2.6 LHS 1134

With fifty-one images taken on twelve nights, LHS 1134 has fewest of both spread over a 6-year baseline. Despite the paucity of exposures, the relative parallax calculated for LHS 1134 has an error less than 2.5 mas but it is the second largest such error in this study. The associated mean errors of unit weight are less than 0.5 μm and fall near the median value for this study. DCR corrections were not applied to LHS 1134 and its reference stars as noted in Table 3.7. LHS 1134 was observed using the R_C filter so DCR may be significant for the five frames that were taken at high hour angles.

During the preliminary analysis, no hint of a perturbation or any interesting features in the periodograms were noted. As shown in Figure 3.15 and Figure 3.16, LHS 1134 continues to show no sign of any periodic motion due to companions more massive than $7 \pm 1 M_{21}$ as discussed in section 3.2.3. The maxima in both y-residual periodograms occur at 1.1 yr^{-1} , which corresponds to a 0.92-year period but the nightly residual maximum has a 73% false alarm probability making these features mostly noise-related. In addition, neither of the x-residual periodograms have any points with even a 50% chance of being real. Table 3.18 lists the features of the periodograms for LHS 1134.

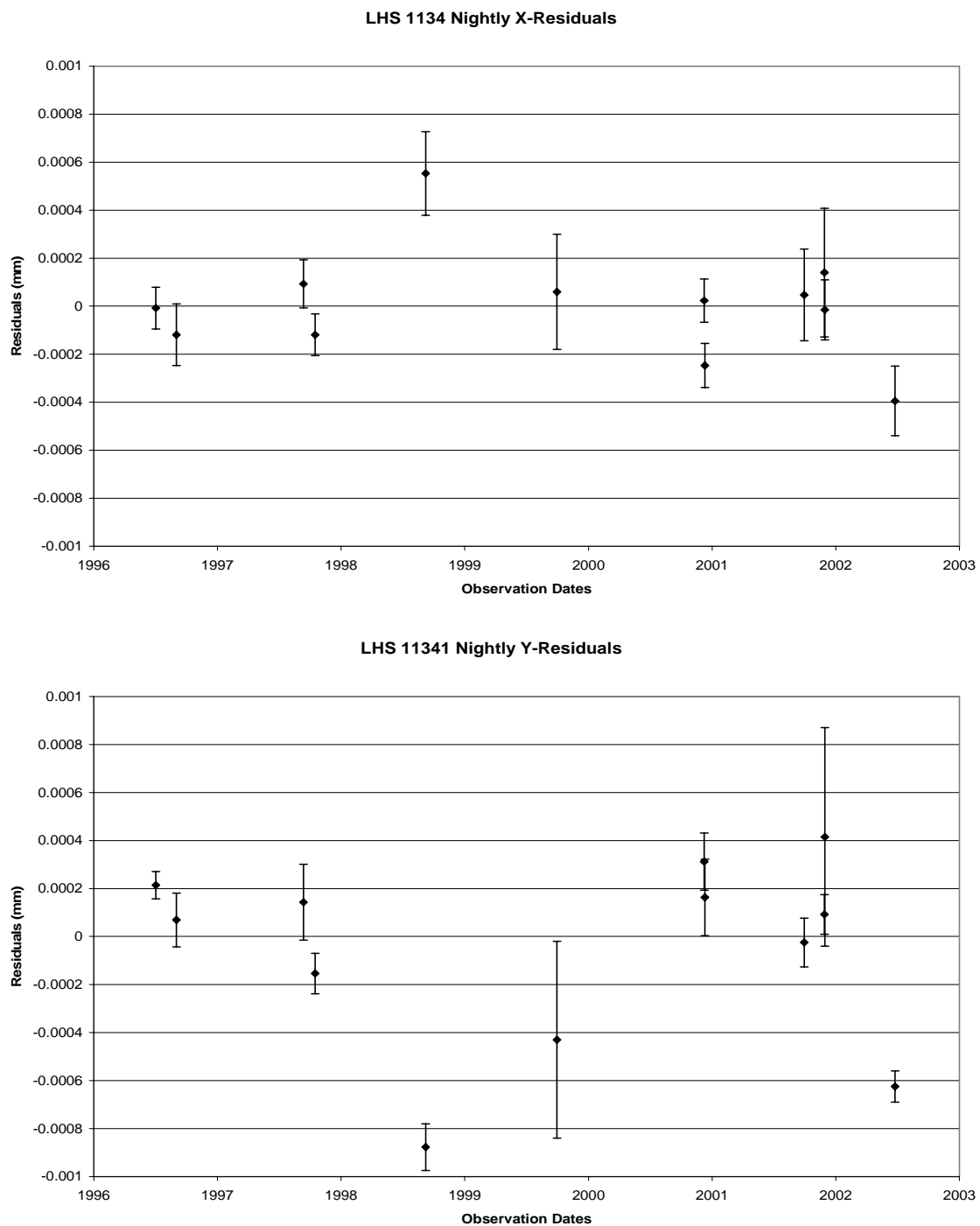


FIG. 3.15.— Nightly X- and Y-Residuals for LHS 1134. Top chart contains x-residuals averaged by night. Bottom chart contains y-residuals averaged by night.

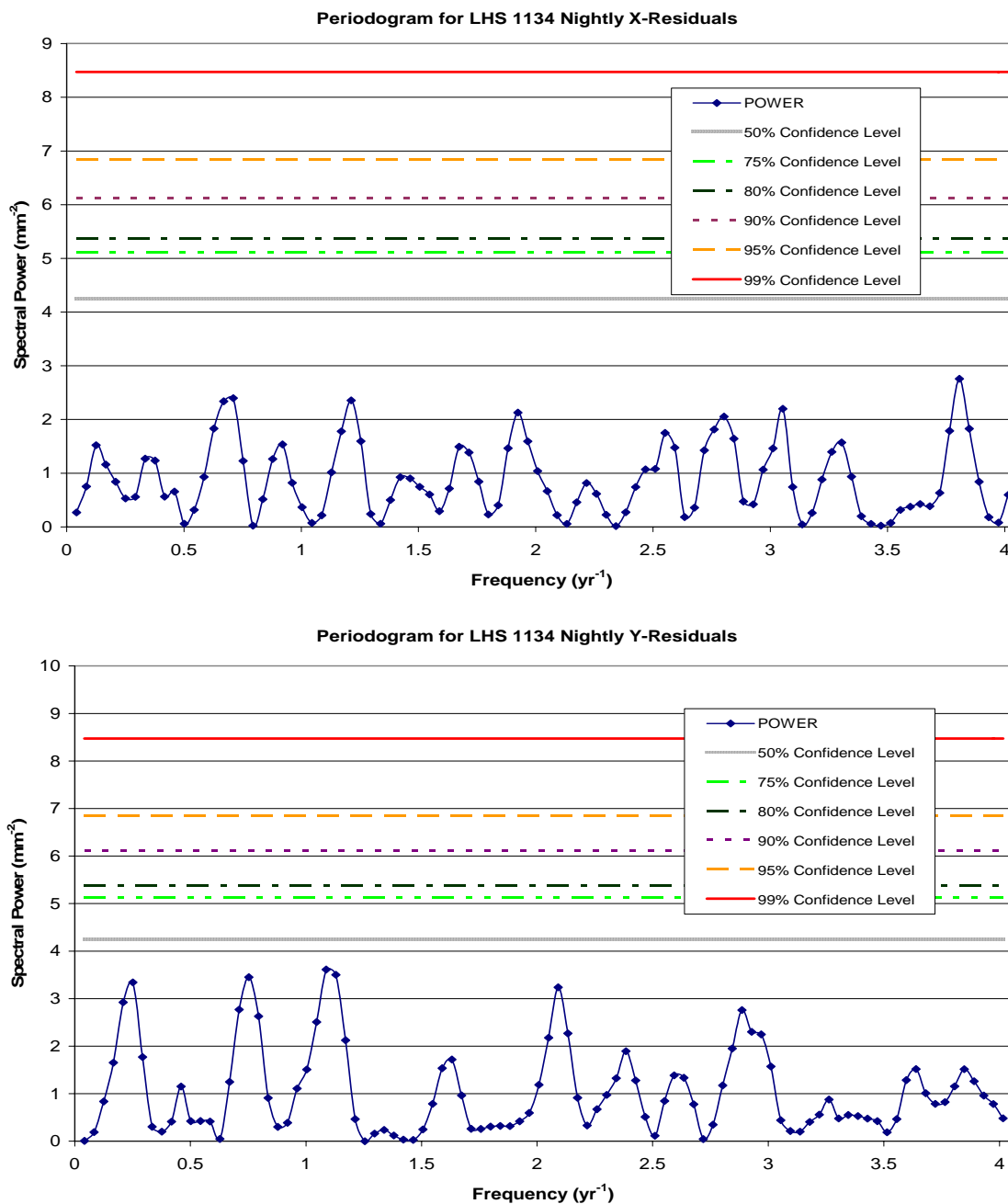


FIG. 3.16.— LHS 1134 Periodograms. Top chart is a periodogram calculated for nightly x-residuals. Bottom chart is a periodogram calculated for nightly y-residuals. Horizontal lines in the periodograms indicate likelihood that spectral peaks exceeding that power are real and not caused by noise only. Solid line is 99% confidence, dashed line 95% confidence, dotted line 90% confidence, dash dotted line is 80% confidence, dash double-dotted line is 75% confidence, and hashed line is 50% confidence.

TABLE 3.18
 FEATURES OF PERIODOGRAMS FOR LHS 1134

Feature	Frequency (yr ⁻¹)	Period (yr)	Power (mm ⁻²)	False Alarm Probability (%)	Comment
All X, maximum	17.0	0.06	4.4	91	
All Y, maximum	1.1	0.92	8.3	5	matches maximum in nightly y
Nightly X, maximum	3.8	0.26	2.8	96	
Nightly Y, maximum	1.1	0.92	3.6	73	matches maximum in all y

3.2.2.7 LHS 1565

LHS 1565 is the nearest star in this study. The photographic SPP previously measured a preliminary absolute parallax of 273 ± 5 mas, which put it at a distance of 3.7 pc (Ianna 1997) and ranked it twentieth among the nearest star systems (Henry *et al.* 1997). It also has the latest spectral type of the main sequence stars in this study, M5.5 V (Henry *et al.* 1997), which it shares with LHS 288.

As shown in Figure 3.1, LHS 1565, like LHS 337, served as an example of a star with no hint of perturbation detected by the preliminary analysis. As explained in Table 3.7, no DCR correction was applied to LHS 1565 and its reference stars. LHS 1565 was observed using the V_C filter. Because photon count changes little for red stars in V-band, DCR is reduced (Jao *et al.* 2004). In addition, only 5% of the exposures for LHS 1565 were taken at large hour angles.

As shown in Figure 3.17 and Figure 3.18, LHS 1565 still shows no sign of any perturbation by a planet more massive than $1.7 \pm 0.4 M_{21}$ as shown in section 3.2.2. Table 3.19 lists the features of the periodograms for LHS 1565. As in the preliminary periodograms, the highest peaks for all x- and y-residuals occurred at frequencies corresponding to periods of less than two months with false alarm possibilities less than 10%. The pattern of observations makes such short periods unlikely to be real; neither frequency was sampled when the individual residuals are combined as nightly normal

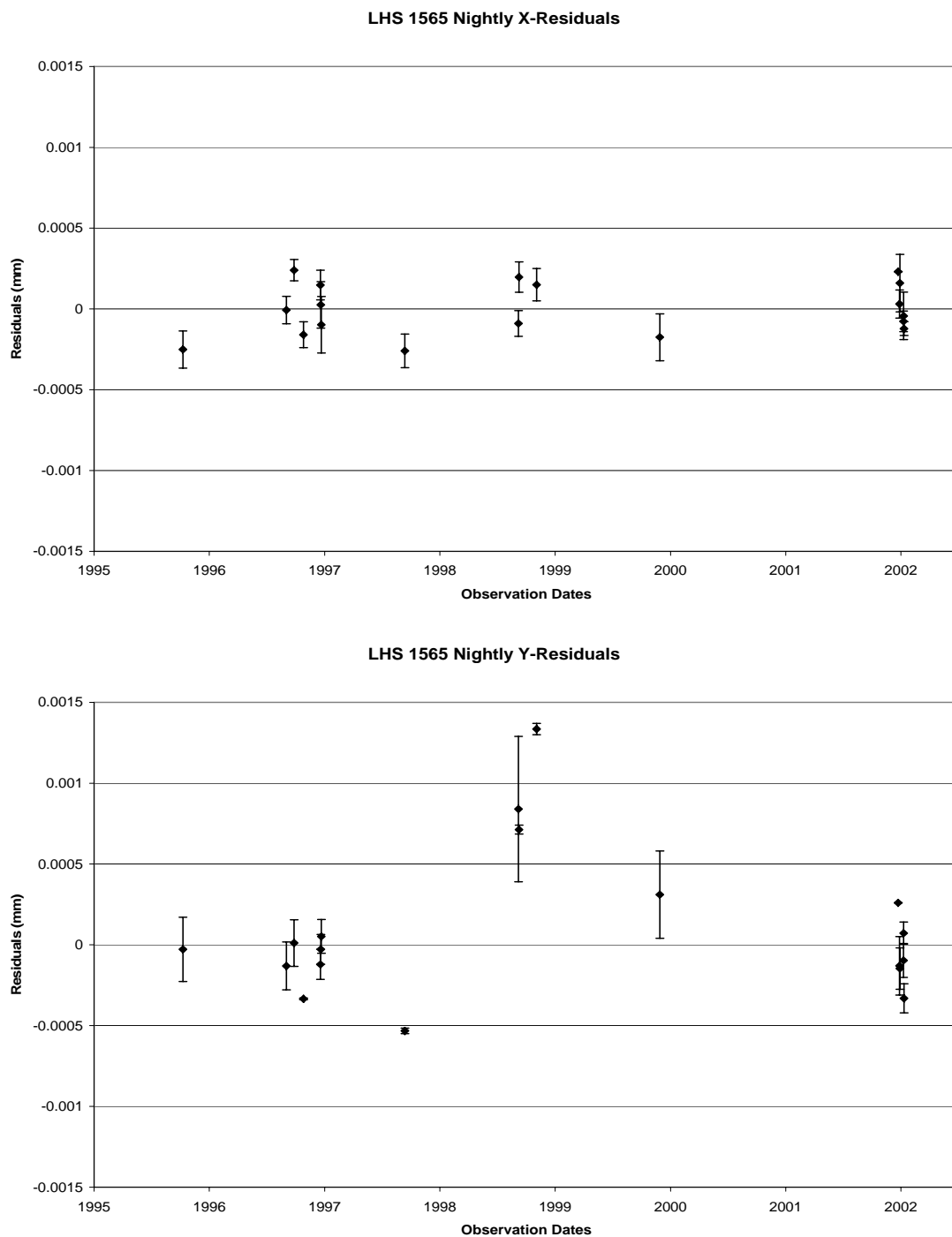


FIG. 3.17.— Nightly X- and Y-Residuals for LHS 1565. Top chart contains x-residuals averaged by night. Bottom chart contains y-residuals averaged by night.

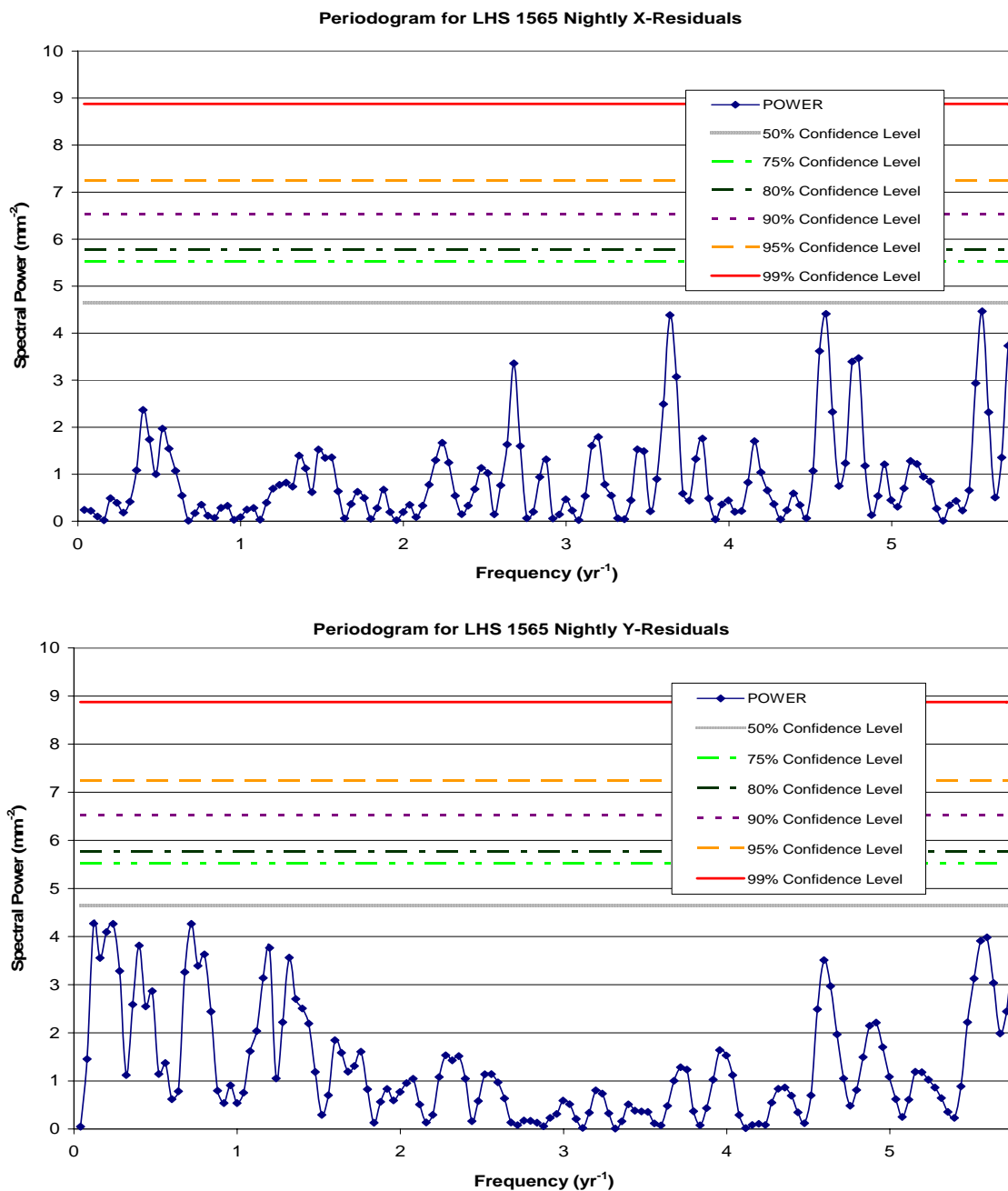


FIG. 3.18.— LHS 1565 Periodograms. Top chart is a periodogram calculated for nightly x-residuals. Bottom chart is a periodogram calculated for nightly y-residuals. Horizontal lines in the periodograms indicate likelihood that spectral peaks exceeding that power are real and not caused by noise only. Solid line is 99% confidence, dashed line 95% confidence, dotted line 90% confidence, dash dotted line is 80% confidence, dash double-dotted line is 75% confidence, and hashed line is 50% confidence.

TABLE 3.19
 FEATURES OF PERIODOGRAMS FOR LHS 1565

Feature	Frequency (yr ⁻¹)	Period (yr)	Power (mm ⁻²)	False Alarm Probability (%)	Comment
All X, maximum	9.911	0.1009	8.814	5	frequency too high for nightly residuals
All X, local peak	0.1599	6.255	1.293	>50	adjacent to frequency of interest
All X, adjacent to local peak	0.1199	8.340	0.7255	>50	corresponds to maximum in nightly y
All X, local peak	5.555	0.1800	7.007	<50	corresponds to maximum in nightly x
All Y, maximum	6.754	0.1481	8.237	8	frequency too high for nightly residuals
All Y, local peak	0.1199	8.340	7.390	<20	corresponds to maximum in nightly y
All Y, local peak	5.595	0.1787	6.526	<50	adjacent to frequency of interest
All Y, adjacent to local peak	5.555	0.1800	5.624	>50	corresponds to maximum in nightly x
Nightly X, maximum	5.555	0.1800	4.464	57	corresponds to local peak in all x
Nightly X	0.1199	8.340	0.09870	>50	corresponds to maximum in nightly y
Nightly Y, maximum	0.1199	8.340	4.272	64	corresponds to local peak in all y

points. When the residuals were combined into nightly normal points, the periodograms show no peaks that had as much as a 50% chance of being real.

3.2.2.8 LHS 2310

LHS 2310 has the smallest proper motion of any star in this study. Although it has the largest error in parallax and largest unit error of mean weight in x , the overall quality of its parallax and proper motion solution along with its 6.7-year baseline was sufficient to ensure its inclusion in the second sample. In computing the relative parallax and proper motion of LHS 2310, 114 images taken on 20 nights between 1994 April and 2001 January were used. Because of the questionable nature of one exposure, only 113 frames were used to determine the parallax and proper motion of LHS 2310. The observations were made exclusively with CCD #6.

As explained in Table 3.7, no DCR correction was available for LHS 2310 and its reference stars, which were observed using the R_C filter. Although significant DCR might be expected for a red star observed in R-band (Jao *et al.* 2005), only 8% of the exposures used were taken at large hour angles.

At best, Figure 3.19 and Figure 3.20 hint of a 3.0 to 3.4-year period perturbation in LHS 2310. According to section 3.2.3, this study could detect brown dwarfs more massive than $16 \pm 2 M_{21}$. The maxima for all y - and nightly y -residuals occur at the same frequency, 3.7 yr^{-1} , which corresponds to a period of approximately 99 days but no matching peaks occur in either x -periodogram. The periodograms for nightly residuals have no points with a 50% or greater likelihood of being real. Table 3.20 lists the features of the periodograms for LHS 2310.

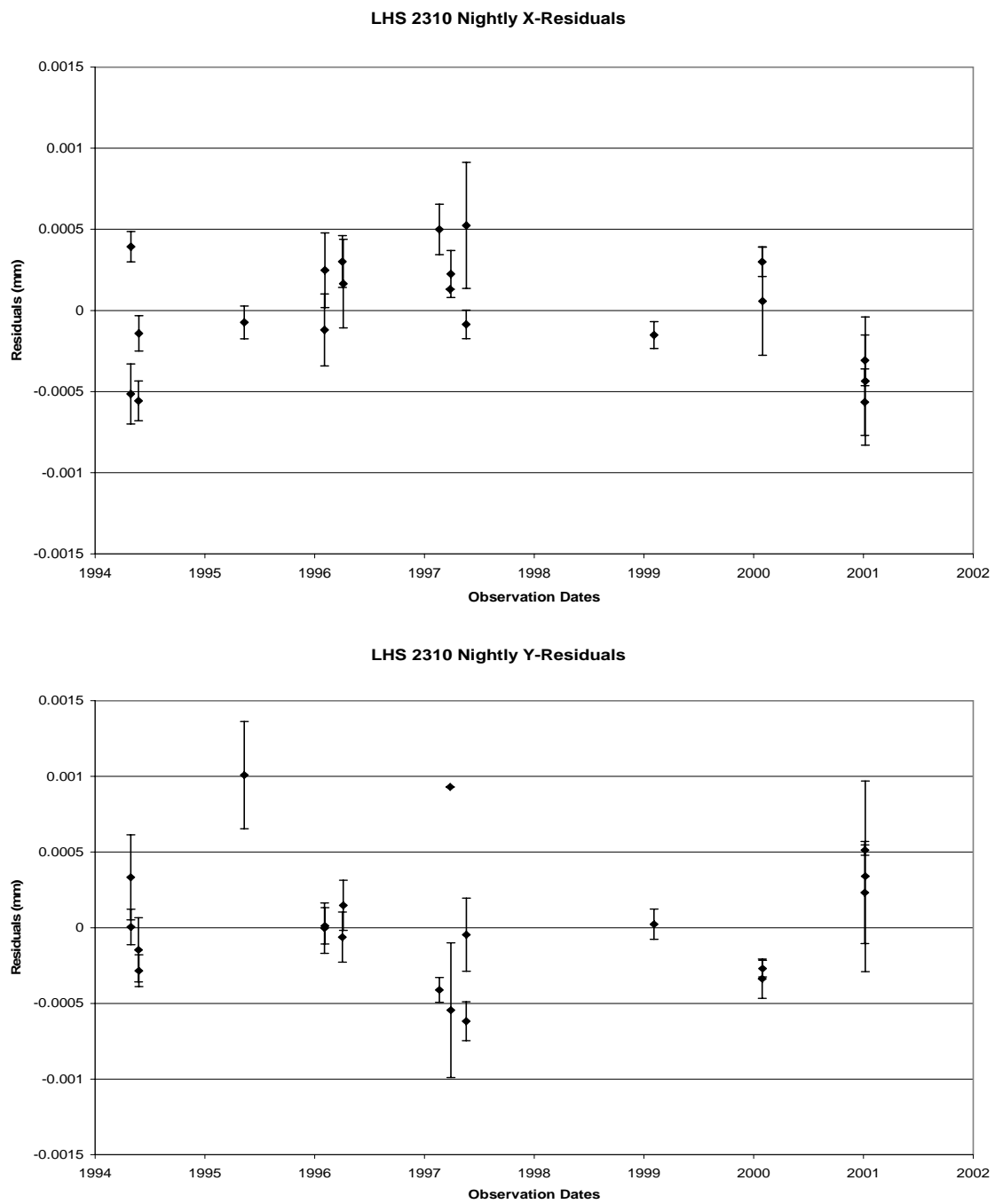


FIG. 3.19.— Nightly X- and Y-Residuals for LHS 2310. Top chart contains x-residuals averaged by night. Bottom chart contains y-residuals averaged by night.

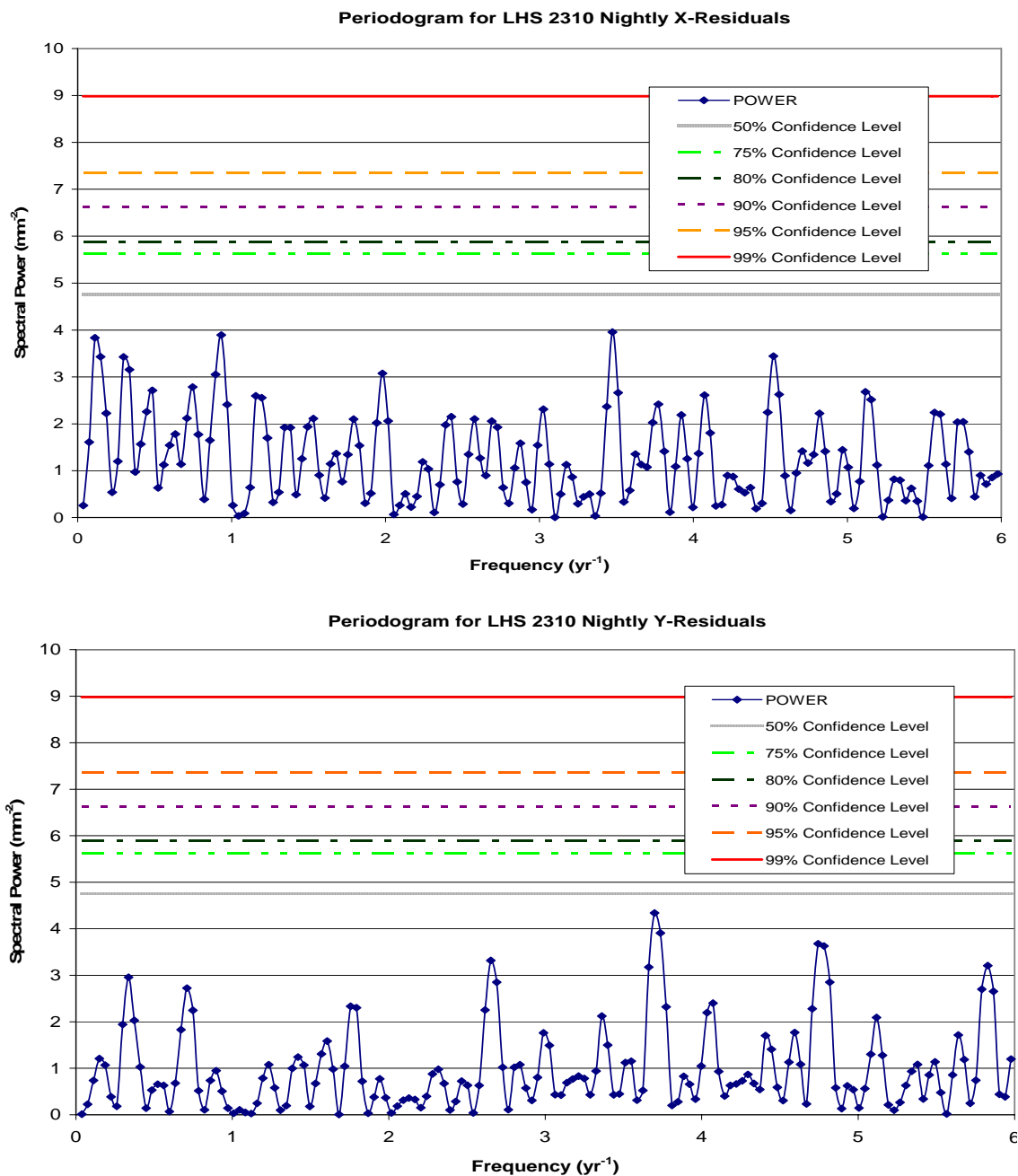


FIG. 3.20.— LHS 2310 Periodograms. Top chart is a periodogram calculated for nightly x-residuals. Bottom chart is a periodogram calculated for nightly y-residuals. Horizontal lines in the periodograms indicate likelihood that spectral peaks exceeding that power are real and not caused by noise only. Solid line is 99% confidence, dashed line 95% confidence, dotted line 90% confidence, dash dotted line is 80% confidence, dash double-dotted line is 75% confidence, and hashed line is 50% confidence.

TABLE 3.20
FEATURES OF PERIODOGRAMS FOR LHS 2310

Feature	Frequency (yr ⁻¹)	Period (yr)	Power (mm ⁻²)	False Alarm Probability (%)	Comment
All X, maximum	27.2	0.04	14.4	<1	
All X, local peak	0.3	3.35	7.5	<25	possible corresponding signal in all y
All Y, maximum	3.7	0.27	11.4	1	matches maximum in nightly y
All Y, adjacent to local peak	0.3	3.35	6.7	<50	corresponds to local peak in all x
All Y, local peak	0.3	2.97	7.7	<20	adjacent to interesting frequency in all x and y
Nightly X, maximum	3.5	0.29	4.0	79	
Nightly Y, maximum	3.7	0.27	4.3	65	matches maximum in all y

3.2.2.9 LHS 2739

LHS 2739 is the most distant star in this study; its relative parallax places it at a distance of about 23 parsecs. LHS 2739 benefits from the largest number of images available for a star in this study; it shares the smallest error in parallax of 0.9 mas with LHS 3418 and has the smallest mean error of unit weight in y . Between 1994 April and 2001 June, 140 useable observations were made of LHS 2739. Before calculating the final periodograms, DCR corrections were applied to LHS 2739 and its reference stars.

As shown in Table 3.7, the DCR correction for LHS 2739 suffered from two problems: no photometry for 3 out of 14 reference stars and no weather data for 30 out of 141 frames. The reference stars without photometry were assumed to have spectral type G0V. Because weather data were also unavailable on days adjacent to those observation dates without weather, weather from the same day in another year was used. LHS 2739 was observed using the R_C filter for which DCR can be significant. However, only ten frames were taken at large hour angles and the largest was less than 42 minutes west. In addition, the majority of frames were taken within 20 minutes of the meridian.

The preliminary analysis identified no interesting features in the periodograms calculated for LHS 2739. Figure 3.21 and Figure 3.22 indicate that LHS 2739 is without companions more massive than the limit of $17 \pm 2 M_{24}$ set in section 3.2.3 for this study. The maximum peak in the periodograms for nightly residuals has a greater than 50% chance of being real and has a corresponding local peak in all x -residuals.

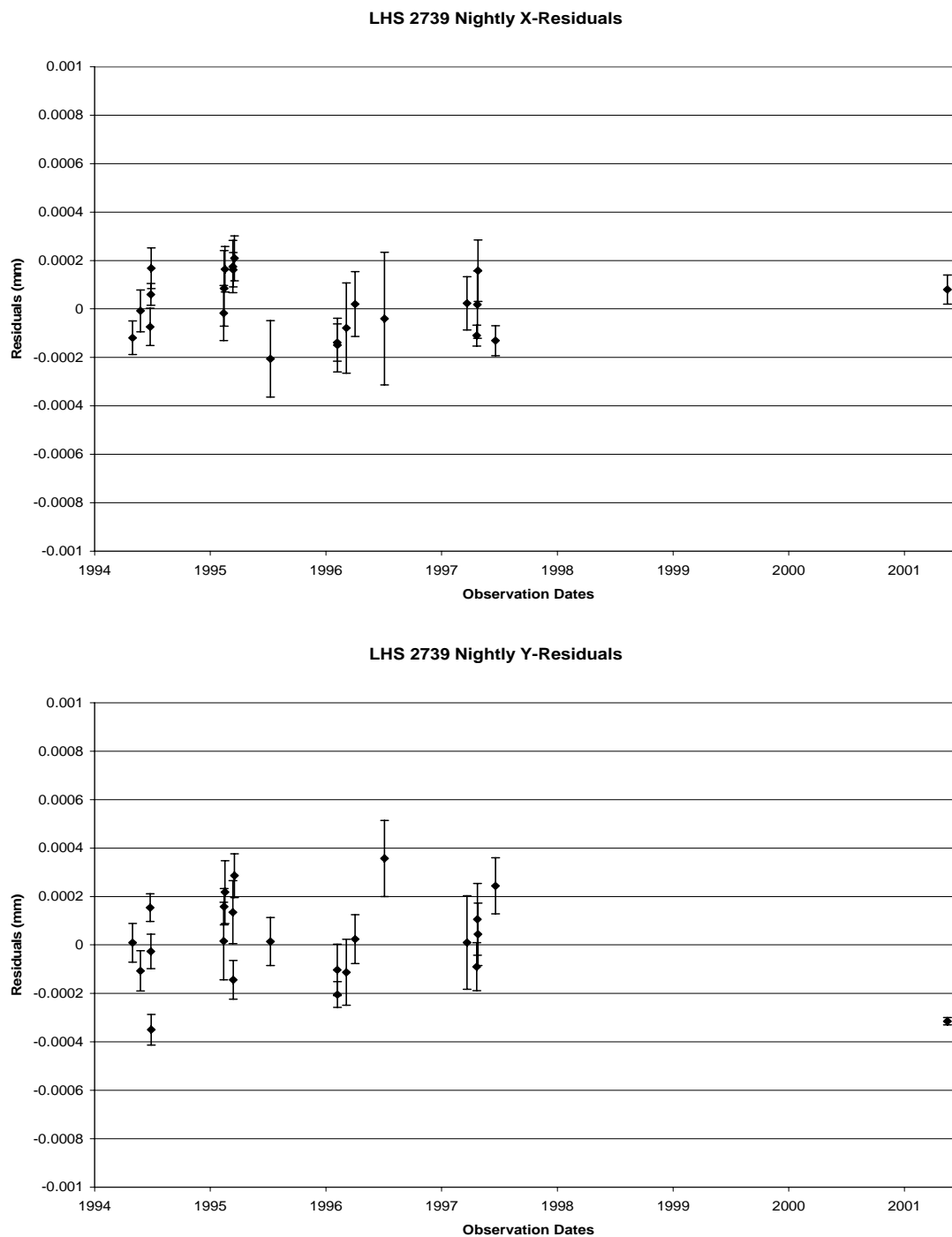


FIG. 3.21.— Nightly X- and Y-Residuals for LHS 2739. Top chart contains x-residuals averaged by night. Bottom chart contains y-residuals averaged by night.

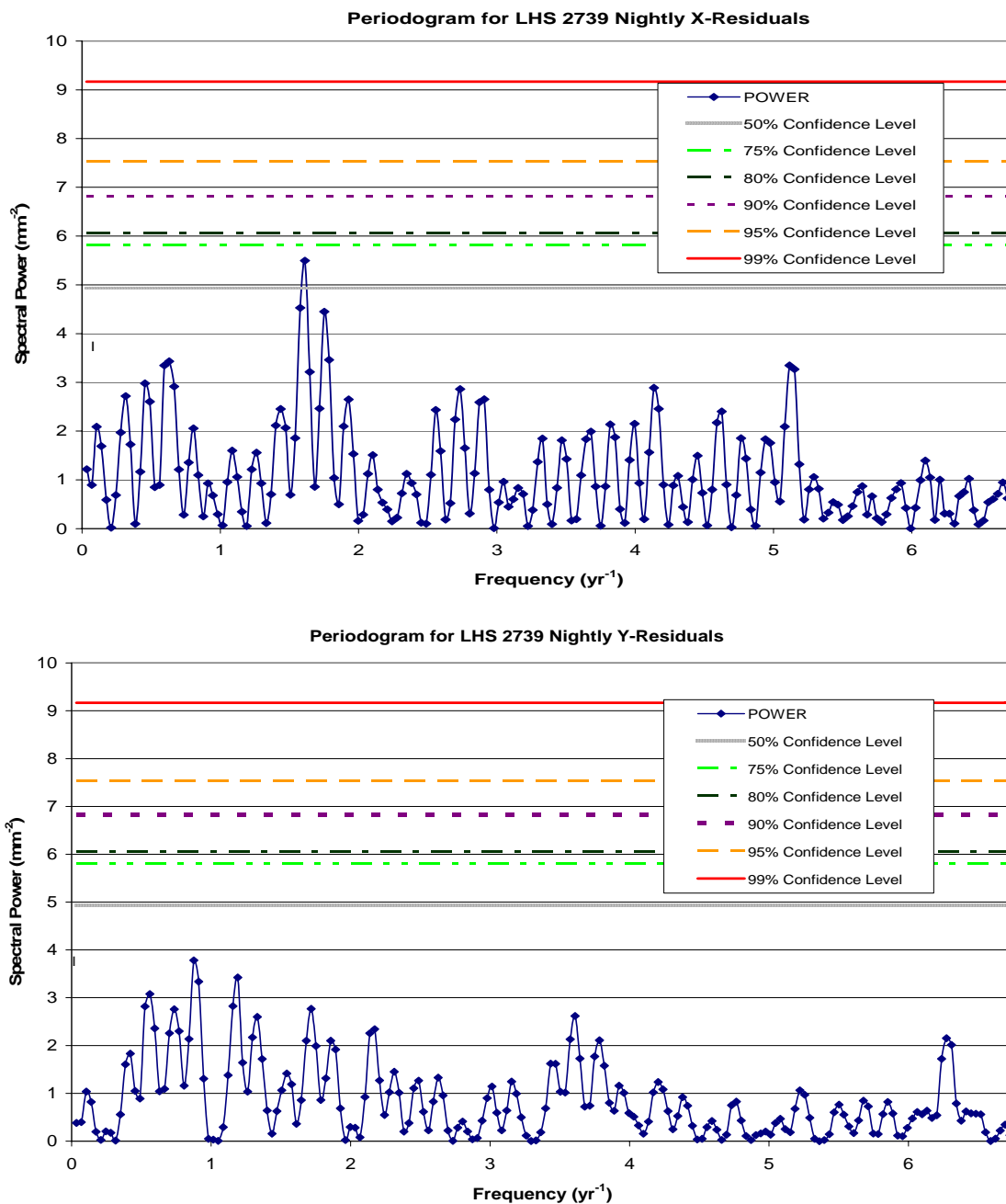


FIG. 3.22.—LHS 2739 Periodograms. Top chart is a periodogram calculated for nightly x-residuals. Bottom chart is a periodogram calculated for nightly y-residuals. Horizontal lines in the periodograms indicate likelihood that spectral peaks exceeding that power are real and not caused by noise only. Solid line is 99% confidence, dashed line 95% confidence, dotted line 90% confidence, dash dotted line is 80% confidence, dash double-dotted line is 75% confidence, and hashed line is 50% confidence.

TABLE 3.21
 FEATURES OF PERIODOGRAMS FOR LHS 2739

Feature	Frequency (yr ⁻¹)	Period (yr)	Power (mm ⁻²)	False Alarm Probability (%)	Comment
All X, maximum	14.1	0.07	7.8	21	
All X, local peak	1.6	0.62	7.6	<25	corresponds to maximum in nightly x
All Y, maximum	35.5	0.03	11.6	1	
All Y, local peak	0.9	1.14	7.4	<50	corresponds to maximum in nightly y
Nightly X, maximum	1.6	0.62	5.5	33	corresponds to local peak in all x
Nightly Y, maximum	0.9	1.14	3.8	89	corresponds to local peak in all y

These peaks occur at a frequency of 1.6 yr^{-1} , which corresponds to a period of approximately 227 days. The short period represented and the lack of corresponding signals in the y-periodograms make noise the most likely origin of these peaks. The nightly y-residual maximum has a matching local peak in the periodogram for all y-residuals. These peaks occur at a frequency of 0.9 yr^{-1} , which corresponds to a period of approximately 1.14 year. Table 3.21 summarizes these features.

3.2.2.10 LHS 2813

LHS 2813 was the star with the most promising periodograms during the preliminary analysis, which covered observations made between 1994 and mid-1997. It is one of the more distant stars in this study at about 17 pc. It also has the second smallest proper motion in Table 3.5 based on slightly more than eight years of observations (BIP). It is also a relatively early red dwarf with spectral type M2.0 V (Hawley, Gizis, & Reid 1996).

Figure 3.1 shows local peaks that occur in all four periodograms at a frequency of 0.5293 yr^{-1} , which corresponds to a period of approximately 1.889 years. For the nightly x-residual periodogram, this peak is also the maximum but one with less than 50% chance of being real. For the y-periodograms, these local peaks are weak; both have less than a 50% chance of being real. Although a companion might be expected to produce signals of similar strength in both coordinates, some orientations would produce a signal primarily in the x-coordinate. Although the potential signal at this frequency is probably due to noise, it was worth further investigation.

After the preliminary analysis, five more observations taken in 2002 were added to the calculation of relative parallax and proper motion calculation for LHS 2813. Then, all the observations were corrected for DCR. The resulting pif was found to have frames that appeared to be out of order; this temporal discontinuity was corrected as discussed in 3.2.1. The results of these updated calculations are shown in Figure 3.23 and Figure 3.24.

In the final periodograms, the situation for LHS 2813 is less clear. The maxima for the y-residual periodograms have moved to 0.5208 yr^{-1} , which corresponds to a period of approximately 1.920 years—close to the earlier period of interest. However, the maxima for the x-residual periodograms both have moved away from the earlier frequency of interest to a frequency of 0.3676 yr^{-1} , which corresponds to a period of approximately 2.720 years. The new maximum in the nightly x-residual periodogram has a false alarm probability of only 14%. The all x-residual periodogram retains high power near the earlier frequency of interest but no peak occurs there or adjacent to that frequency. The nightly x-residual periodogram has a local peak adjacent to the earlier frequency of interest but it is a weak one with a less than 50% chance of being real. The all y-residual periodogram point that corresponds to the new maxima in the x-residual periodograms is adjacent to a local peak and has a greater than 50% chance of being real. In the nightly y-residuals, the frequency corresponding to the new maximum in the x-residual periodograms is adjacent to a weak local peak with a less than 50% chance of being real.

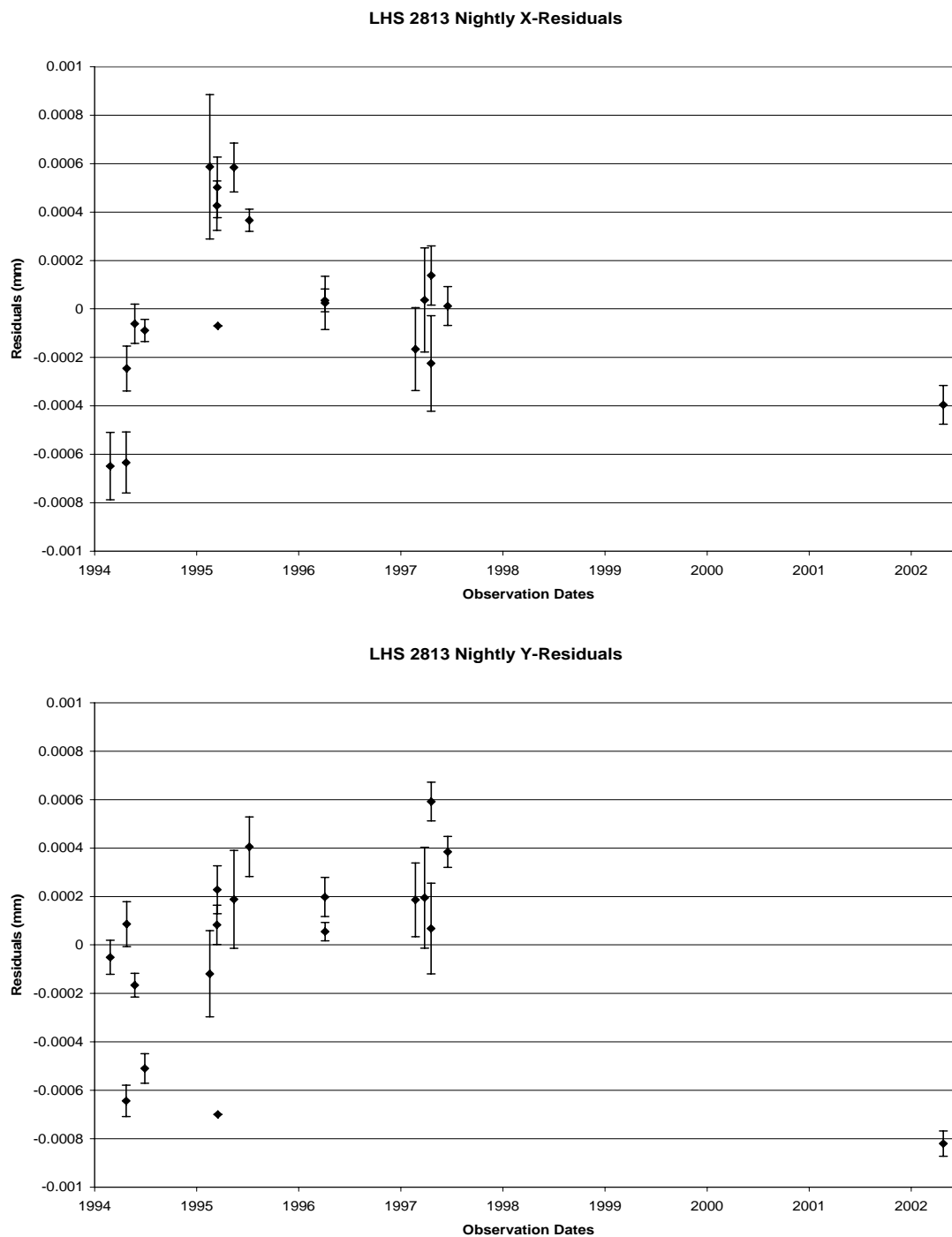


FIG. 3.23.—Nightly X- and Y-Residuals for LHS 2813. Top chart contains x-residuals averaged by night. Bottom chart contains y-residuals averaged by night.

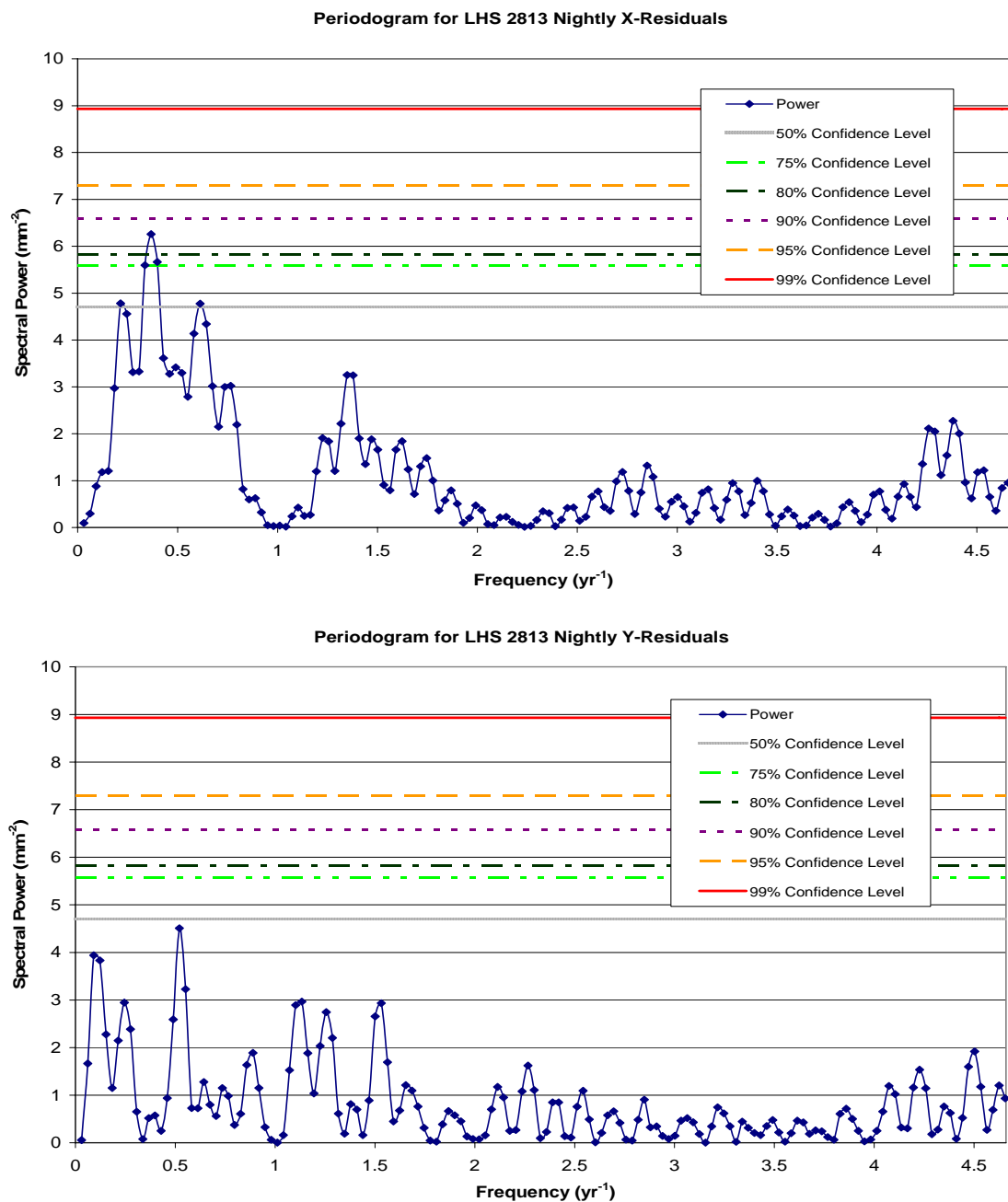


FIG. 3.24.—LHS 2813 Periodograms. Top chart is a periodogram calculated for nightly x-residuals. Bottom chart is a periodogram calculated for nightly y-residuals. Horizontal lines in the periodograms indicate likelihood that spectral peaks exceeding that power are real and not caused by noise only. Solid line is 99% confidence, dashed line 95% confidence, dotted line 90% confidence, dash dotted line is 80% confidence, dash double-dotted line is 75% confidence, and hashed line is 50% confidence.

TABLE 3.22
 FEATURES OF PERIODOGRAMS FOR LHS 2813

Feature	Frequency (yr ⁻¹)	Period (yr)	Power (mm ⁻²)	False Alarm Probability (%)	Comment
All X, maximum	0.36760	2.7204	30.033	<1	matches maximum in nightly x
All X, high power but no peak	0.52076	1.9203	18.661	<1	corresponds to maxima in both y
All Y, maximum	0.52076	1.9203	24.252	<1	matches maximum in nightly y
All Y, local peak	0.39823	2.5111	7.6087	<25	adjacent to frequency of interest (x maxima)
All Y, adjacent to local peak	0.36760	2.7204	7.3540	<50	corresponds to maxima in both x
Nightly X, maximum	0.3676	2.720	6.259	14	matches maximum in all x
Nightly X, local peak	0.4901	2.040	3.417	>50	adjacent to frequency of interest (y maxima)
Nightly X, adjacent to local peak	0.5208	1.920	3.297	>50	corresponds to maxima in both y
Nightly Y, maximum	0.5208	1.920	4.508	57	matches maximum in all y
Nightly Y, local peak	0.3982	2.511	0.5745	>50	adjacent to frequency of interest (x maxima)
Nightly Y, adjacent to local peak	0.3676	2.720	0.5168	>50	corresponds to maxima in both x

NOTE.—Preliminary study found possible perturbation with frequency of 0.5293 yr⁻¹ or a period of about 1.889 years; the potential signal was more distinct in the x-residuals than the y-residuals.

The 8.16-year baseline for LHS 2813 is more than twice either period of interest, the frequencies of interest are both greater than the lowest independent frequency and less than the Nyquist frequency. Table 3.22 summarizes the features discussed. Brown dwarf companions more massive than $17 \pm 2 M_{\text{J}}$ should have been detectable by this study according to section 3.2.3. Although the weak signals identified here are most likely spurious, additional observations of LHS 2813 in a future study could further clarify the situation.

3.2.2.11 LHS 3064

LHS 3064 is a modest M3 star (Bidelman 1985) with the median apparent brightness (V_J) for this study and a relative parallax and proper motion close to the median values, as shown in Table 3.4 and Table 3.5. The preliminary periodograms for LHS 3064 contained no interesting features. Before the final reduction, an additional six observations made in 2001 and 2002 were included in the relative parallax and proper motion calculations for LHS 3064. Its final baseline was longer than eight years. The LHS 3064 pif appeared to have several frames out of order; this temporal discontinuity was corrected as discussed in 3.2.1. In addition, DCR corrections were applied to LHS 3064 and its reference stars.

After the additional frames were added and DCR corrections made, LHS 3064 still shows no sign of a perturbation, as displayed in Figure 3.25 and Figure 3.26. According to section 3.2.3, perturbations due to companions more massive than $6 \pm 1 M_{\text{J}}$ should have been revealed. The maxima in the all x- and all y-residual periodograms occur at very high frequencies, which are unlikely to be real. The

frequency in the all y-residual periodogram that corresponds to the maximum of the all x-residual periodogram is adjacent to a weak local peak. The maximum in the nightly x-residual periodogram has a less than 50% chance of being real as do the corresponding frequencies in the other three periodograms. The maximum in the nightly y-residual periodogram occurs at frequency of 1.99 yr^{-1} , which corresponds to a period of approximately 0.502 years; it has a less than 50% chance of being real. The corresponding frequency on all y-residual periodogram has a greater than 95% chance of being real and is adjacent to a local peak. The corresponding frequency on the nightly x-residual periodogram is a weak local peak with a less than 50% chance of being real. The semi-annual period may be a result of the parallax observing cycle, which requires images be taken in the mornings and evenings when the parallax factors are large. Table 3.23 lists the features of the LHS 3064 periodograms.

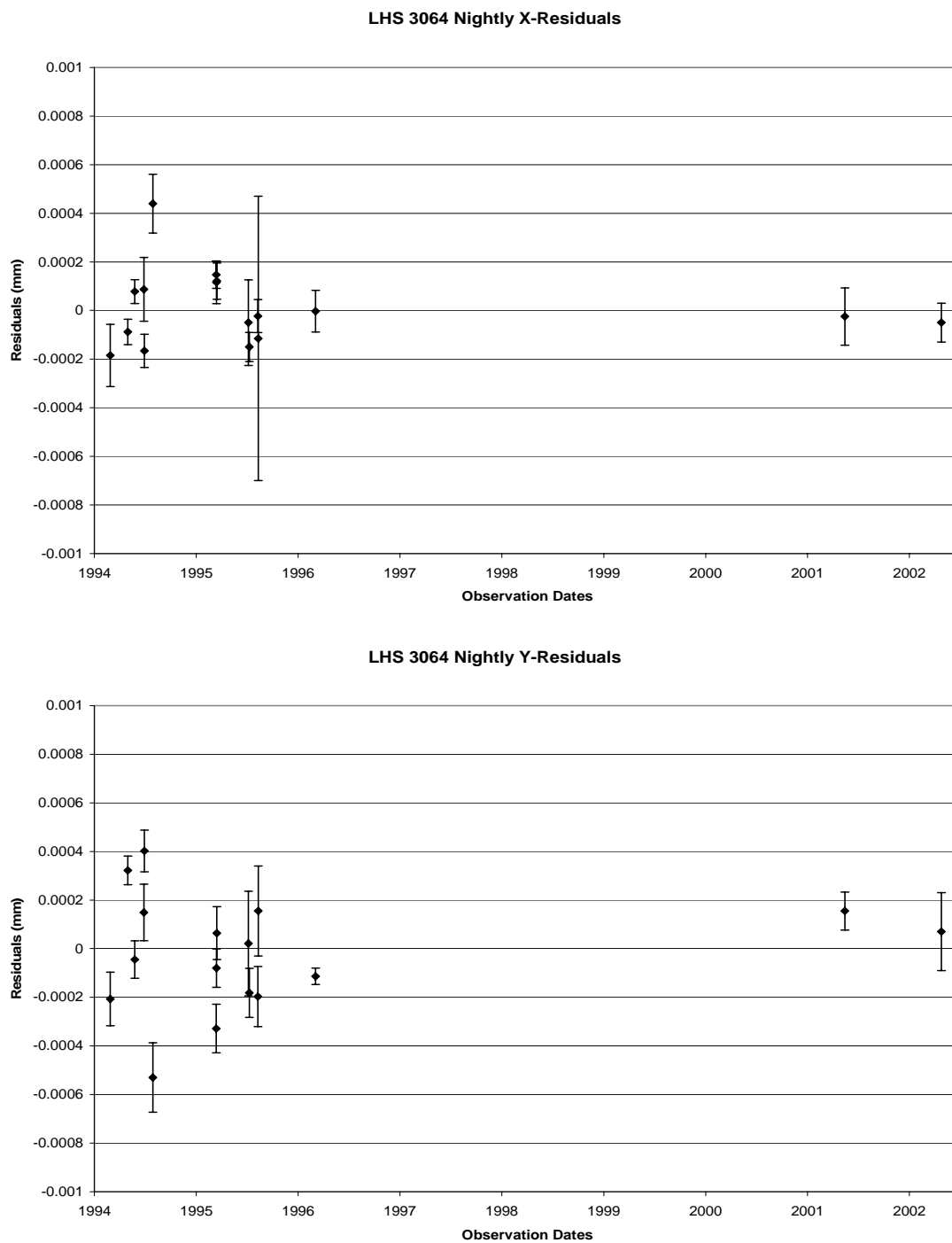


FIG. 3.25.— Nightly X- and Y-Residuals for LHS 3064. Top chart contains x-residuals averaged by night. Bottom chart contains y-residuals averaged by night.

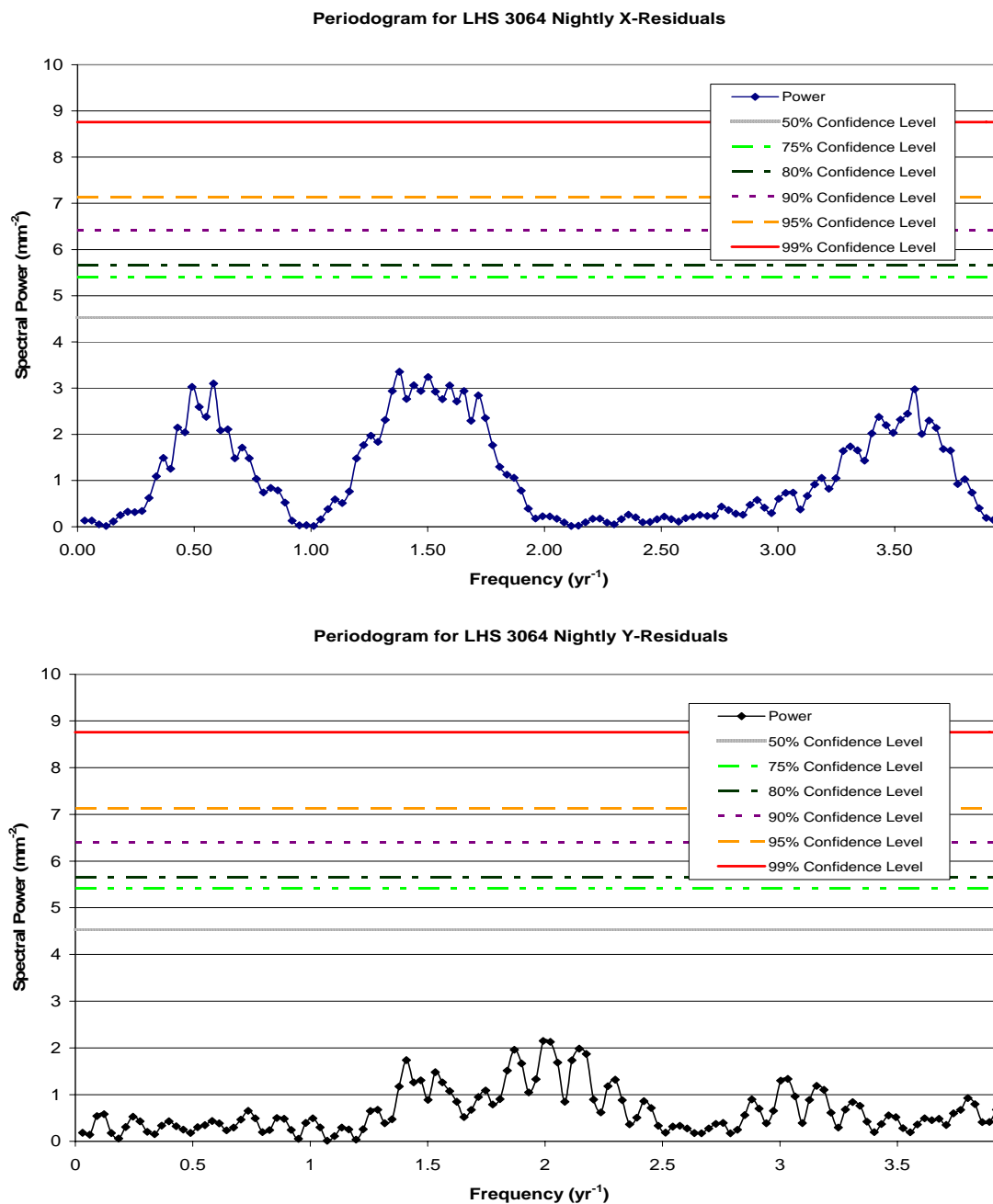


FIG. 3.26.— LHS 3064 Periodograms. Top chart is a periodogram calculated for nightly x-residuals. Bottom chart is a periodogram calculated for nightly y-residuals. Horizontal lines in the periodograms indicate likelihood that spectral peaks exceeding that power are real and not caused by noise only. Solid line is 99% confidence, dashed line 95% confidence, dotted line 90% confidence, dash dotted line is 80% confidence, dash double-dotted line is 75% confidence, and hashed line is 50% confidence.

TABLE 3.23
FEATURES OF PERIODOGRAMS FOR LHS 3064

Feature	Frequency (yr ⁻¹)	Period (yr)	Power (mm ⁻²)	False Alarm Probability (%)	Comment
All X, maximum	11.062	0.090400	7.6433	21	~33 days, frequency too high for nightly residuals
All Y, maximum	19.182	0.052131	14.797	<1	~19 days, frequency too high for nightly residuals
All Y, local peak	2.0224	0.49446	10.058	<5	adjacent to frequency of interest (all y maximum)
All Y, adjacent to local peak	1.9918	0.50207	9.9274	<5	corresponds to maximum in nightly y
Nightly X, maximum	1.38	0.725	3.35	90	
Nightly X, local peak	1.99	0.502	0.228	>50	corresponds to maximum in nightly y
Nightly Y, maximum	1.99	0.502	2.15	<1	~6 months, probably related to observing cycle

3.2.2.12 LHS 3242

LHS 3242 is the brightest star in this study as shown in Table 3.4 and has the earliest spectral type of the main sequence stars, M0.5 V (Hawley, Gizis, & Reid 1996). The moderate errors associated with its relative parallax and a baseline longer than eight years contributed to its inclusion in the second sample.

Although DCR correction is not yet possible for LHS 3242 and its reference stars as explained in Table 3.7, only 2% of the exposures used were made at large hour angles. LHS 3242 was observed with the V_C filter; DCR is reduced because the photon count changes little for red stars across this passband (Jao *et al.* 2005).

The residuals after the calculation of relative parallax and proper motion for LHS 3242 are shown in Figure 3.27 along with their associated periodograms in Figure 3.28. No pattern that might indicate the presence of brown dwarf companions more massive than $18 \pm 1 M_{24}$ is present; the minimum detectable companion mass is discussed in section 3.2.3. The maxima in the all x- and all y-residual periodograms occur at high frequencies that are not sampled when the data is averaged by night. No point on either nightly periodogram has a 50% or greater chance of being real. Table 3.24 lists the features of these periodograms.

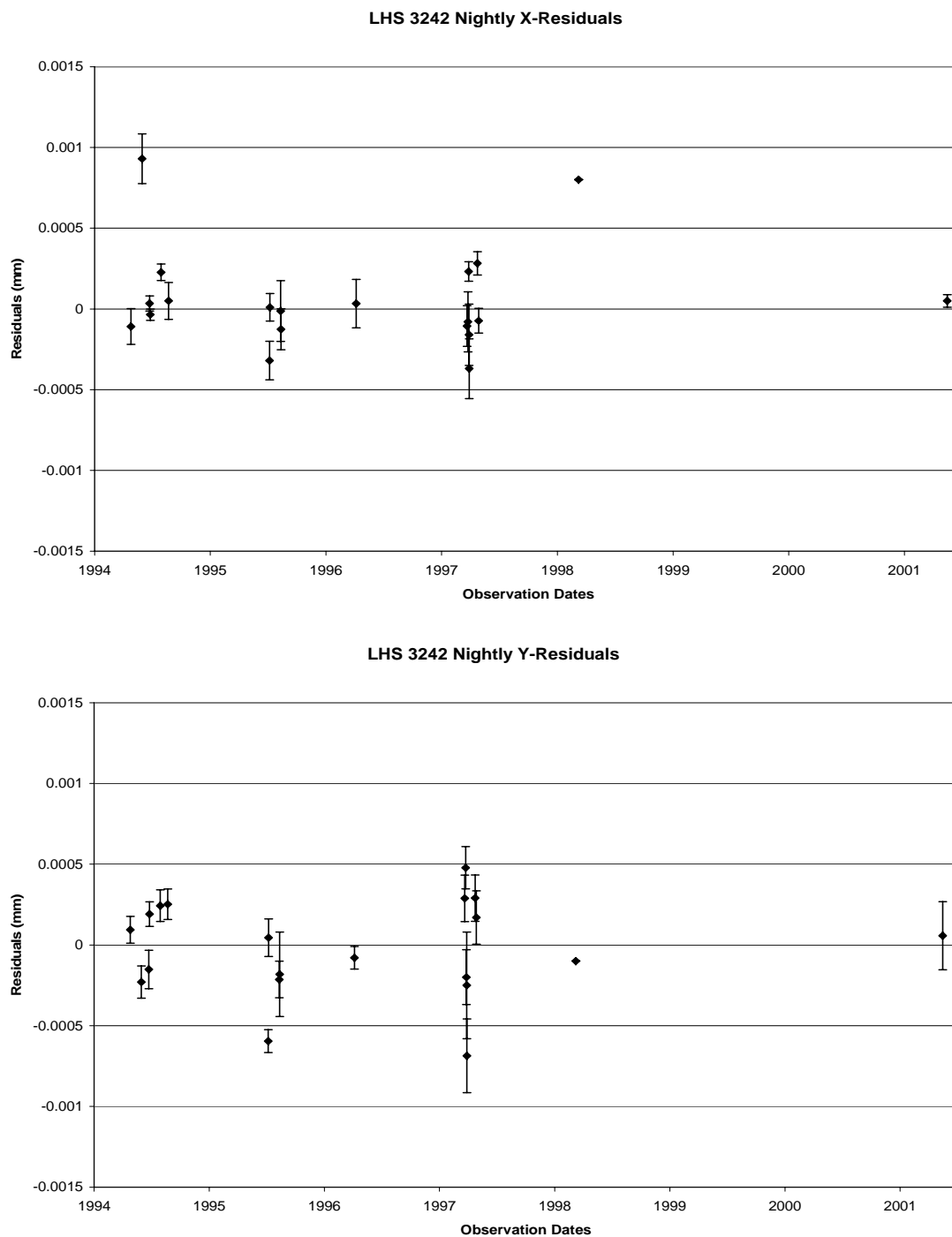


FIG. 3.27.—Nightly X- and Y-Residuals for LHS 3242. Top chart contains x-residuals averaged by night. Bottom chart contains y-residuals averaged by night.

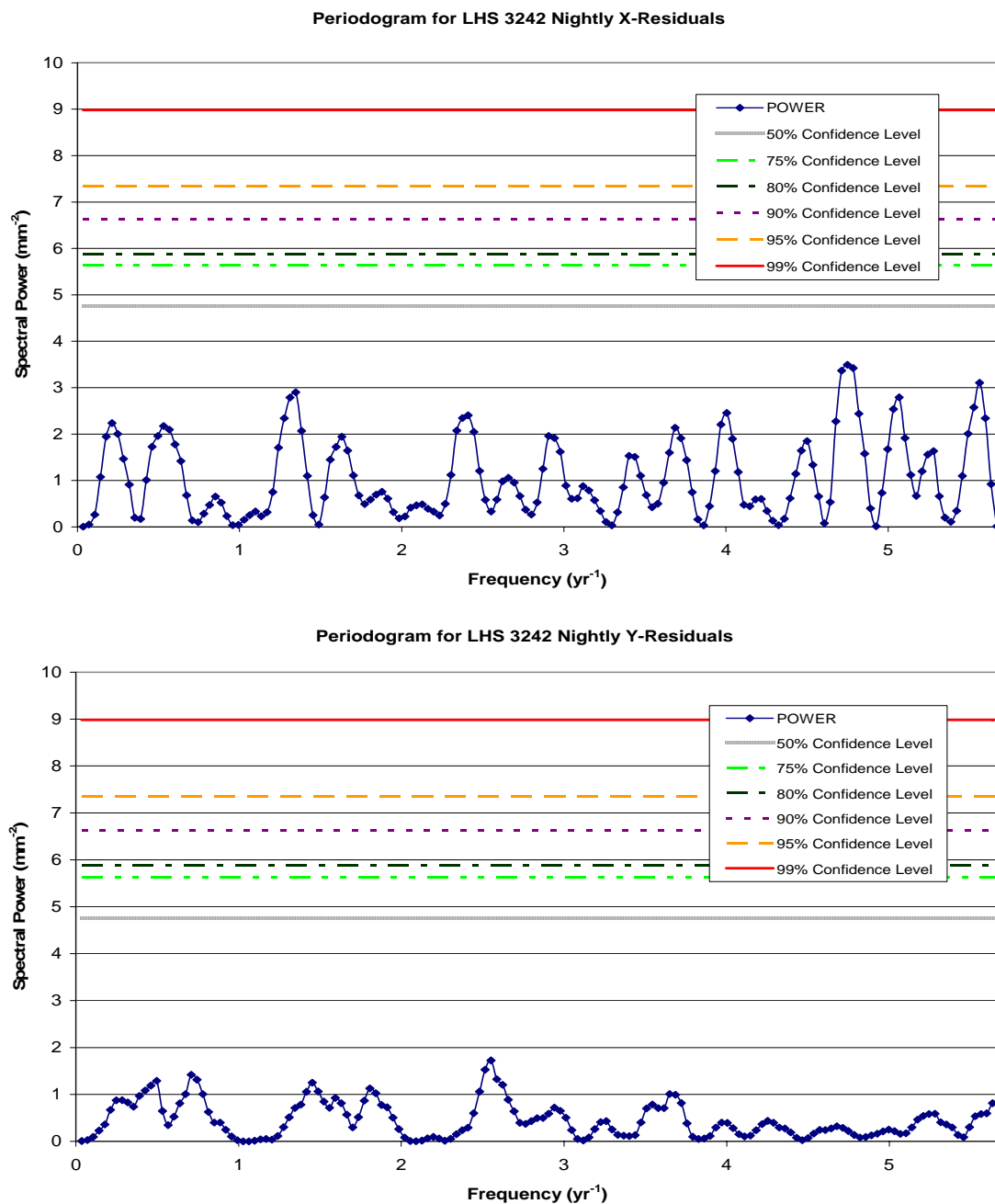


FIG. 3.28.—LHS 3242 Periodograms. Top chart is a periodogram calculated for nightly x-residuals. Bottom chart is a periodogram calculated for nightly y-residuals. Horizontal lines in the periodograms indicate likelihood that spectral peaks exceeding that power are real and not caused by noise only. Solid line is 99% confidence, dashed line 95% confidence, dotted line 90% confidence, dash dotted line is 80% confidence, dash double-dotted line is 75% confidence, and hashed line is 50% confidence.

TABLE 3.24
 FEATURES OF PERIODOGRAMS FOR LHS 3242

Feature	Frequency (yr ⁻¹)	Period (yr)	Power (mm ⁻²)	False Alarm Probability (%)	Comment
All X, maximum	6.2	0.16	8.1	15	frequency too high for nightly residuals
All Y, maximum	33.6	0.03	14.7	<1	frequency too high for nightly residuals
Nightly X, maximum	4.8	0.21	3.5	92	
Nightly Y, maximum	2.6	0.39	1.7	>99	

3.2.2.13 LHS 3418

LHS 3418 is approximately 22 pc away (BIP), slightly closer than the other M3.5 V (Hawley, Gizis, & Reid 1996) star in this study, LHS 2739. LHS 3418 also ties LHS 2739 for the smallest error associated with the calculation of its relative parallax. Its mean error of unit weight in y is also the smallest. The quality of the parallax and proper motion solution along with its moderate baseline contributed to the inclusion of LHS 3418 in the second subsample. LHS 3418 and its reference stars were all corrected for DCR.

The residuals displayed in Figure 3.29 and analyzed in Figure 3.30 do not indicate the presence of any companions. A limit to the size of any companions missed by this study is set in section 3.2.3 at $17 \pm 2 M_{21}$. The maxima in the nightly x - and nightly y -residuals occur at adjacent frequencies, 5.20 yr^{-1} and 5.23 yr^{-1} respectively, which correspond to periods of approximately 70 days, but both have high false alarm probabilities. The corresponding points in periodograms for all residuals have a greater than 50% chance of being real and are adjacent to local peaks. The distribution of observations makes periods less than one year highly unlikely. The maxima for the both periodograms for all residuals occur at frequencies too high to appear in the nightly periodograms. Table 3.25 summarizes the features discussed.

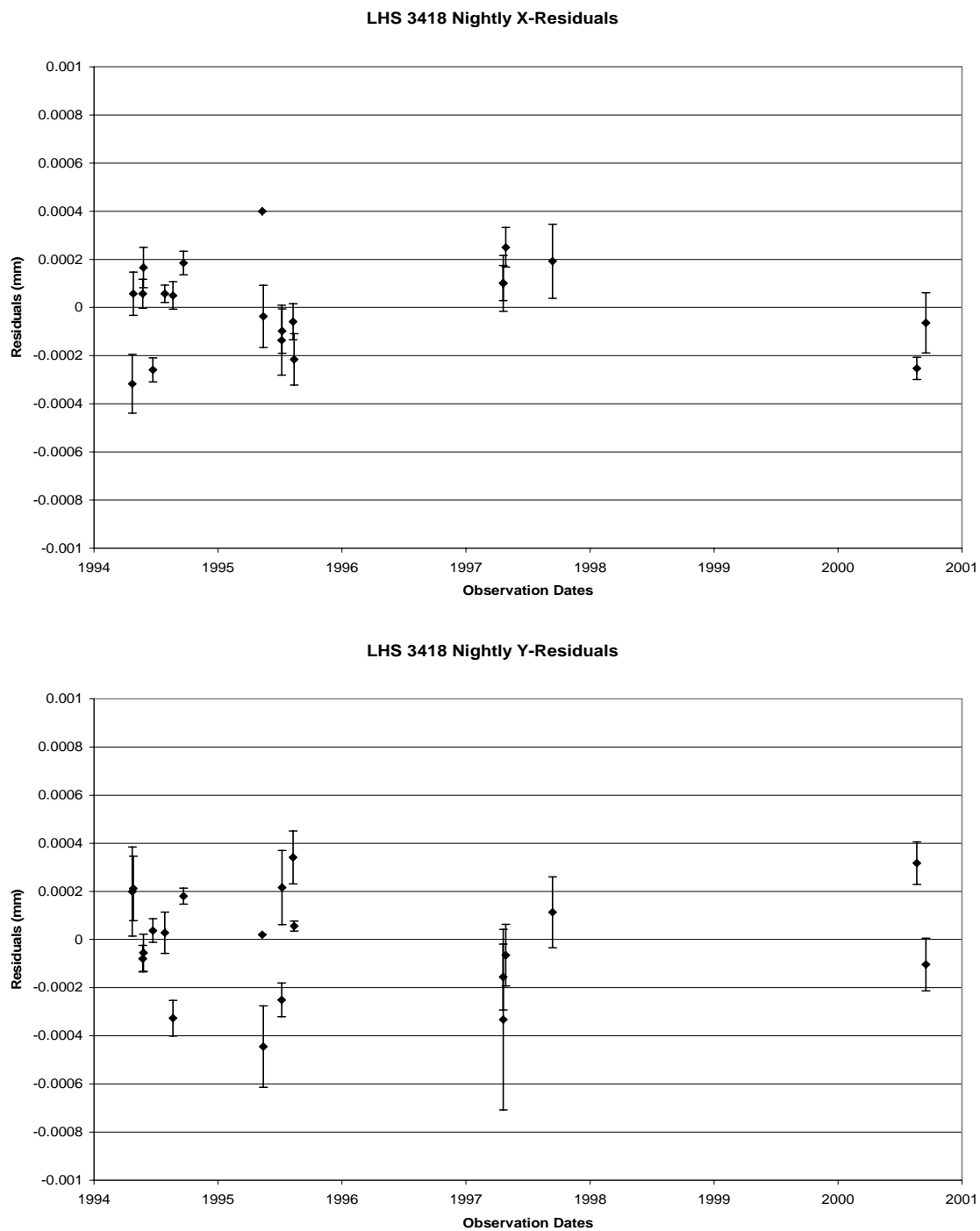


FIG. 3.29.—Nightly X- and Y-Residuals for LHS 3418. Top chart contains x-residuals averaged by night. Bottom chart contains y-residuals averaged by night.

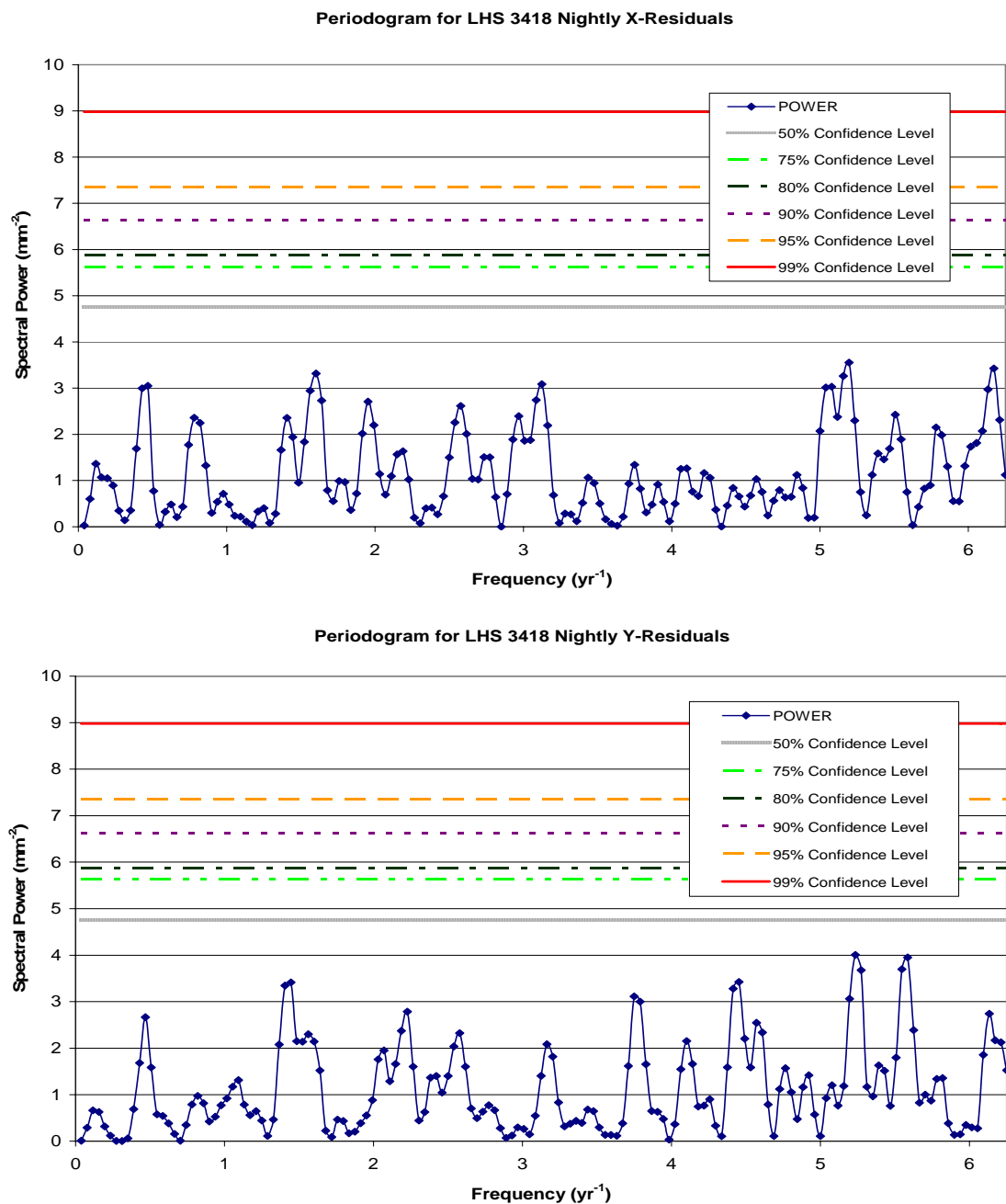


FIG. 3.30.—LHS 3418 Periodograms. Top chart is a periodogram calculated for nightly x-residuals. Bottom chart is a periodogram calculated for nightly y-residuals. Horizontal lines in the periodograms indicate likelihood that spectral peaks exceeding that power are real and not caused by noise only. Solid line is 99% confidence, dashed line 95% confidence, dotted line 90% confidence, dash dotted line is 80% confidence, dash double-dotted line is 75% confidence, and hashed line is 50% confidence.

TABLE 3.25
FEATURES OF PERIODOGRAMS FOR LHS 3418

Feature	Frequency (yr ⁻¹)	Period (yr)	Power (mm ⁻²)	False Alarm Probability (%)	Comment
All X, maximum	30.038	0.033291	14.240	<1	frequency too high for nightly residuals
All X, local peak	5.1561	0.19394	8.7494	<10	adjacent to frequency of interest
All X, adjacent to local peak	5.1952	0.19249	8.6350	<10	corresponds to maximum in nightly x
All X	5.2343	0.19105	5.3922	>50	correspond to maximum in nightly y
All Y, maximum	6.7967	0.14713	12.424	<1	frequency too high for nightly residuals
All Y, local peak	5.2733	0.18963	9.4221	<5	adjacent to frequency of interest
All Y, adjacent to local peak	5.2343	0.19105	8.5760	<10	corresponds to maximum in nightly y
All Y	5.1952	0.19249	5.9664	>50	corresponds to maximum in nightly x
Nightly X, maximum	5.195	0.1925	3.553	90	adjacent to maximum in nightly y
Nightly X, adjacent to maximum	5.234	0.1910	2.297	>50	corresponds to maximum in nightly y
Nightly Y, maximum	5.234	0.1910	4.007	77	adjacent to maximum in nightly x
Nightly Y, adjacent to maximum	5.195	0.1925	3.063	>50	corresponds to maximum in nightly x

3.2.3 Companion Mass Limits

Despite expectations to find at least one substellar companion amongst the stars observed by the CCD extension of the SPP, no such unseen body was clearly detected. Because the numbers of extrasolar planets found to date remains small, non-detections contribute to the understanding of planetary frequency. Therefore, the sensitivity of this study to planets must be established. Assuming a circular orbit for simplicity, Kepler's third law estimates the minimum detectable companion mass (M_p)

$$M_p = \left(\frac{M_*}{P} \right)^{\frac{2}{3}} \frac{\alpha}{\pi} \quad (3.5)$$

where M_* is the stellar mass in solar mass units (M_\odot), P is the period in years, π is the absolute parallax in milliseconds of arc (mas), and α is the minimum detectable perturbation in mas.

Known binary systems were excluded from this study so the masses of potential host stars must be estimated from an appropriate mass-radius relationship or mass-luminosity relationship. The former applies only to LHS 34, the sole white dwarf in this study. Bergeron, Leggett, and Ruiz (2001) obtained a mass of $0.72 \pm 0.06 M_\odot$ for this stellar remnant. Through astrophysical modeling, they obtained the effective temperature and the solid angle. Using an absolute parallax of 141.2 ± 8.4 mas (van Altena, Lee, & Hoffleit 1995), they converted the solid angle to a radius, which they fit to their cooling sequences to determine the mass. Because their radius assumes LHS 34 is nearer than indicated by the SPP relative parallax of 117.9 ± 1.8 (BIP), their mass may be considered an upper limit. The calculated radius of LHS 34 will increase with

estimated distance and, for white dwarfs, larger radii correspond to smaller masses. Although when corrected to an absolute parallax the SPP value will increase, it will remain smaller than 141 mas.

The majority of the stars in this study are M dwarfs so Table 3.26 lists mass estimates based on the K-band relationship derived by Delfosse *et al.* (2000). Their mass-luminosity relationship is based on the hybrid photometric system described by Leggett (1992), who adopted California Institute of Technology infrared colors defined by Elias *et al.* (1982, hereafter CIT). J (1.235 μm) and K_S (2.16 μm) photometry from the Two Micron All Sky Survey (Skrutskie *et al.* 2006, hereafter 2MASS; Cohen, Wheaton, and Megeath 2003) was converted to K_{CIT} (2.2 μm). The absolute K_{CIT} magnitudes were estimated using the preliminary relative parallaxes in Table 3.5. These absolute magnitudes are upper limits. The eventual correction to absolute will increase the parallaxes slightly, which would produce a larger absolute magnitude. The absolute K_{CIT} magnitudes were then converted to stellar masses using the K-band mass-luminosity relationship (Delfosse *et al.* 2000). These masses are also upper limits; an increase in absolute luminosity will decrease the corresponding mass. Using absolute parallaxes can be expected to reduce the masses herein by less than 2.5%.

TABLE 3.26
 STELLAR MASSES ESTIMATED FROM INFRARED PHOTOMETRY

Star (LHS)	2MASS J (mag)	2MASS K _S (mag)	CIT K (mag)	CIT M _K (mag)	Mass (M _☉)	Comment
34	12.726 ± 0.023	12.362 ± 0.024	12.381 ± 0.024	12.738 ± 0.042	...	white dwarf
271	7.953 ± 0.024	7.037 ± 0.017	7.055 ± 0.018	7.990 ± 0.027	0.176 ± 0.043	
288	8.492 ± 0.021	7.728 ± 0.027	7.746 ± 0.028	9.392 ± 0.033	0.096 ± 0.043	
337	8.174 ± 0.024	7.386 ± 0.021	7.404 ± 0.022	8.225 ± 0.030	0.157 ± 0.043	
532	8.984 ± 0.026	8.108 ± 0.023	8.126 ± 0.024	7.996 ± 0.040	0.175 ± 0.043	
1134	8.572 ± 0.019	7.710 ± 0.016	7.728 ± 0.017	7.711 ± 0.052	0.201 ± 0.043	
1565	7.523 ± 0.020	6.610 ± 0.021	6.628 ± 0.022	8.899 ± 0.024	0.116 ± 0.043	
2310	9.052 ± 0.029	8.139 ± 0.023	8.157 ± 0.024	7.416 ± 0.092	0.233 ± 0.044	
2739	9.329 ± 0.029	8.517 ± 0.027	8.535 ± 0.028	6.733 ± 0.053	0.324 ± 0.043	
2813	8.926 ± 0.027	8.123 ± 0.024	8.141 ± 0.025	7.025 ± 0.068	0.282 ± 0.044	
3064	9.094 ± 0.024	8.274 ± 0.023	8.292 ± 0.024	7.880 ± 0.036	0.185 ± 0.043	
3242	8.04 ± 0.024	7.224 ± 0.020	7.242 ± 0.021	6.293 ± 0.049	0.397 ± 0.043	
3418	9.305 ± 0.020	8.457 ± 0.024	8.475 ± 0.025	6.751 ± 0.050	0.322 ± 0.043	

REFERENCES.—CIT K magnitudes calculated from listed 2MASS photometry in accordance with Carpenter 2006. Masses calculated from CIT M_K according to Delfosse *et al.* 2000.

The periods considered also affect the ability of a program to detect companions of various sizes. Ideally, the observations should be span more than a single orbit in order to adequately separate the companion-induced perturbation from the proper motion term (Black & Scargle 1982). Radial-velocity surveys are sensitive to short-period planets that produce a large velocity change in the host star. Astrometric techniques, however, are best suited to finding planets with longer orbital periods that produce larger displacements in the host star (Quirrenbach *et al.* 2004). The longest period considered for each stars is its observational baseline, listed in Table 3.8. A planet with a one-year period is likely to be missed because of confusion with the annual cycle associated with parallax observing. Therefore, the shortest period considered is 1.5 years in every case.

Setting the minimum detectable perturbation (α) is the most subjective step because of the quality and quantity of available data varies and because misleading peaks will appear in periodogram when a large number of frequencies are evaluated (Scargle 1982). Minimum detectable perturbations (α) of 10–20 mas have been suggested in literature (Campbell, Walker, & Yang 1988; Heintz 1988) and are discussed in Chapter 2. Chapter 2 indicates a slightly larger minimum detectable perturbation of 21.3 ± 3.5 mas for photographic plates taken with the Leander McCormick Observatory (McCormick) 26.25-inch (67-centimeter) refractor, which has a plate scale of about $20,750$ mas millimeter⁻¹. Expressed in micrometers, the perturbation would be 1.03 ± 0.17 μm , which is a little less than the size of the average residual, which was 1.12 ± 0.89 μm .

The digital images available from CCD's may be measured more precisely than photographic plates measured on a microdensitometer. Positions on a CCD image may be repeatable to about one-fiftieth (~ 0.02) of a pixel (Monet *et al.* 1992), which translates to 0.44–0.45 micrometer (μm) or 11.2–11.5 milliseconds seconds of arc (mas) for the Siding Spring Observatory 1-meter reflector. The CCD's and telescope used by the SPP may be considered typical of such programs; the best endeavors may achieve positions better than 0.3 μm (Monet *et al.* 1992). In comparison, positions of McCormick photographic plates were measured by the Photometric Data Systems (PDS) 1010GM Microdensitometer with an accuracy of about 1.5 μm , which translates to 31 mas for that telescope. Consequently, the average residuals for the SPP planet search were less than 0.5 μm , less than 0.4 μm for nightly normal points, while the average residual for the Barnard's Star study was over 1 μm , or about 0.6 μm for nightly normal points. Therefore, the SPP will be more sensitive to smaller perturbations. Assuming a similar ratio of minimum detectable perturbations to average residuals, Table 3.27 provides estimates of the minimum detectable perturbation for each potential host, which range from 5.4 to 10 mas.

TABLE 3.27
MINIMUM DETECTABLE PERTURBATIONS FOR POTENTIAL HOST STARS

Star (LHS)	Average Residual (μm)	Alpha (μm)	Alpha (mas)
34	0.30 \pm 0.23	0.27 \pm 0.31	7.0 \pm 7.8
271	0.44 \pm 0.40	0.40 \pm 0.49	10 \pm 13
288	0.36 \pm 0.28	0.33 \pm 0.37	8.4 \pm 9.6
337	0.29 \pm 0.24	0.26 \pm 0.31	6.7 \pm 7.9
532	0.29 \pm 0.21	0.26 \pm 0.29	6.7 \pm 7.4
1134	0.29 \pm 0.22	0.26 \pm 0.30	6.7 \pm 7.6
1565	0.28 \pm 0.25	0.26 \pm 0.31	6.7 \pm 8.0
2310	0.43 \pm 0.36	0.39 \pm 0.46	10 \pm 12
2739	0.24 \pm 0.19	0.22 \pm 0.25	5.6 \pm 6.3
2813	0.39 \pm 0.30	0.36 \pm 0.40	9 \pm 10
3064	0.27 \pm 0.21	0.25 \pm 0.27	6.3 \pm 7.0
3242	0.32 \pm 0.27	0.29 \pm 0.34	7.5 \pm 8.8
3418	0.23 \pm 0.19	0.21 \pm 0.24	5.4 \pm 6.3

Finally, the parallax used in calculating the minimum mass of a detectable planet should ideally be the absolute parallax. However, absolute parallaxes are not yet available for the SPP so the preliminary relative parallaxes from Table 3.5 are used with the understanding that the correction to absolute will increase the parallax values slightly. Typical corrections to absolute are on the order of 1 mas, which would bring these stars up to about 2.3% nearer, so the lack of such correction has a minimal effect.

3.2.3.1 Limits for the Sample Generally

With values for each of the terms in Equation 3.5, the minimum detectable companion mass may be calculated. Table 3.28 lists the minimum detectable masses for short and long periods detectable for each potential host star. For low mass stars, such as those studied herein, the detection of a companion of any size would be significant.

Additional nearby low-mass binaries would help define the mass-luminosity

relationship for the lower main sequence and provide constraints on formation theories for brown dwarfs and planets (Delfosse *et al.* 2000; Henry 2004).

TABLE 3.28
MINIMUM DETECTABLE COMPANION MASSES FOR POTENTIAL HOST STARS

Star (LHS)	Short Period (M_{21})		Longest Period (M_{21})		Comment
34	38.1	± 2.2	13.84	± 0.80	sensitive to brown dwarfs
271	16.8	± 2.7	4.75	± 0.77	
288	6.6	± 2.0	2.42	± 0.72	sensitive to planets
337	10.7	± 1.9	6.3	± 1.1	sensitive to planets
532	17.9	± 2.9	6.3	± 1.0	
1134	18.6	± 2.7	7.4	± 1.1	
1565	4.5	± 1.1	1.72	± 0.42	sensitive to planets
2310	42.8	± 5.6	15.8	± 2.1	sensitive to brown dwarfs
2739	48.0	± 4.4	17.0	± 1.5	sensitive to brown dwarfs
2813	52.1	± 5.6	16.9	± 1.8	sensitive to brown dwarfs
3064	19.6	± 3.0	6.4	± 1.0	
3242	50.0	± 3.8	17.8	± 1.3	sensitive to brown dwarfs
3418	44.5	± 4.1	16.9	± 1.6	sensitive to brown dwarfs

NOTE.—Short period is 1.5 years for all stars. The longest period is equal to the observational baseline listed in Table 3.8.

For short period orbits, the SPP is only capable of detecting planets around LHS 288, LHS 337, and LHS 1565. For the other stars, the minimum detectable mass is greater than $13 M_{21}$, which is the current upper mass limit set by the IAU WG ESP for a planet; planets should not have enough mass to support thermonuclear fusion of deuterium.¹⁰ Even for periods as long their observational baseline, nearly half the sample remains insensitive to planetary perturbations. In most cases, brown dwarfs with periods of a few years may be ruled out as companions to these stars. In addition, these

¹⁰The IAU WG ESP provides their current definition of planet at <http://www.dtm.ciw.edu/boss/definition.html>

periods correspond to separations smaller than 4 AU. Planets, especially moderate gas giants and smaller, may still be present.

Again, the correction of the relative parallaxes used herein to absolute parallaxes will slightly reduce the minimum detectable masses through the direct application of parallax and, for the red dwarfs, through its effect on the estimation of stellar masses. Assuming a typical correction of about 1 mas, the minimum detectable masses will be reduced by less than 4%, or no more than $2 M_{21}$, which does not significantly improve the SPP detection capability.

3.2.3.2 Limits for LHS 288

This study identified potential astrometric signals with periods of approximately 3.4 and 6.8 years in the final periodograms calculated for LHS 288. Figure 3.1 includes estimates of the perturbation for LHS 288 due to brown dwarfs. Although these strong peaks do not establish the presence of an unseen companion, the mass associated with any such hypothetical companion is worth considering. The minimum detectable perturbation estimated for LHS 288 above was based on the size of residuals in the final analysis of the SPP data. Therefore, it can also be taken as the size of the perturbation detected if either the 3.4- or 6.8-year period is real. The latter period is the same as the observational baseline. As shown in Table 3.29, these periods correspond to planets with masses of $2\text{--}7 M_{21}$. Such planets would lie within about 2 AU. Assuming the correction to absolute for LHS 288 is about 1 mas, the minimum detectable mass would decrease by less than 1%. A planet with a mass similar to Jupiter in a 1.5-year orbit

would produce a displacement of about 1.3 mas, which is well below the SPP sensitivity threshold.

TABLE 3.29
POTENTIAL MASSES FOR LHS 288 COMPANIONS CORRESPONDING TO DIFFERENT PERIODS

Period (years)	Companion Mass (M_{21})	Comment
1.5 ...	6.6 \pm 2.0	shortest period considered
3.39 \pm .48	3.8 \pm 1.2	corresponds to x-periodogram maxima
6.8 \pm 1.8	2.42 \pm 0.84	baseline, corresponds to y-periodogram maxima

Leinert *et al.* (1997) used K-band speckle interferometry to search for companions orbiting LHS 288. They set lower limits for the absolute K magnitude of possible companions at various orbital distances, which are listed in Table 3.30 on the following page. They based their absolute magnitudes on an absolute parallax of 220 ± 10 mas from the *Preliminary Version of the Third Catalogue of Nearby Stars* (Gliese & Jahreiß 1991). From these magnitude limits, corresponding masses and periods were calculated. First, the absolute K magnitudes were adjusted to the SPP parallax of 213.4 ± 1.7 mas for consistency with other LHS 288 estimates. The magnitudes in Table 3.30 are too large for the K-band mass-luminosity relationship used elsewhere in this study (Delfosse *et al.* 2000) and for the relationships from related speckle interferometric studies (Henry & McCarthy 1993). Therefore, masses were estimated using an earlier

TABLE 3.30
 COMPANION MASS LIMITS FOR LHS 288 FROM SPECKLE INTERFEROMETRY

Distance (AU)	M_K (mag)	Mass (M_{\odot})	Period (years)	Comment
1	11.6	35.0 \pm 2.2	2.8 \pm 2.1	brown dwarf, short period
2	12.1	28.2 \pm 1.8	8.1 \pm 9.1	brown dwarf, period longer than baseline
5	13.4	16.1 \pm 1.0	34 \pm 25	
10	14.1	11.87 \pm 0.75	97 \pm 73	planet, period much longer than baseline

REFERENCE.—Distance and absolute magnitude from Leinert *et al.* 1997

mass-luminosity relationship from a speckle interferometric study of northern-hemisphere red dwarfs (Henry & McCarthy 1990). Once companion masses were computed, corresponding periods were calculated using Kepler's third law. With periods accessible to SPP observations, their study would primarily have found brown dwarfs. The lowest mass to which they would have been sensitive is a planet with a mass of approximately 12 M_{\odot} orbiting at 10 AU with a period of nearly 98 years. Although this mass is well above the minimum detectible companion masses found for LHS 288, the period far exceeds the observational baseline.

In addition, Jao *et al.* (2003) examined astrometric images of 209 stars taken as part of the CTIOPI for companions within 20'' of the parallax star. For LHS 288, this separation translates to about 94 AU, which corresponds to a period of approximately 2,900 years. The R_C images of LHS 288 revealed no companions. Of the eight new multiples detected by this study, LTT 7419 AB had the largest magnitude difference, 6.1 magnitudes in V_{JM} . The new companions are all probably low-mass main sequence stars or white dwarfs. Their investigation is unlikely to have imaged gas giants.

If the periodograms for LHS 288 reflect the presence of physical companions, those bodies are too small to have been detected by the earlier investigations of this star. If the peaks are the result of noise, then this study further narrows the possibilities that LHS 288 hosts giant planets.

3.3 DISCUSSION

The failure to detect the clear signal of a companion of any kind in this selection of the SPP stars is disappointing; it may be an indication that gas giants are less common around M dwarfs than Sun-like stars. If the suggested perturbation of LHS 288 is not spurious, then the detection of a single planet in this sample is well within expectations. The detection of astrometric companions is biased towards large long-period orbits. Although the baselines available here are sufficient to determine adequate parallaxes, they do not appear to be adequate for planet detection; the average baseline is 6.9 ± 1.5 years. Another 2–6 years would bring the long-period perturbation sensitivity to planets around all the stars. More observations over the course of the SPP would have reduced the residuals and improved the sensitivity to lower mass companions. When the second subsample was selected, another nine stars were considered for inclusion but failed to meet the final criteria. Perhaps one of these harbors an unseen companion.

Chapter 4 Solar Neighborhood Census: Identifying and Characterizing New Nearby Stars

4.1 INTRODUCTION

Distance provides the third dimension to the sky, converting the celestial sphere into a vast, three-dimensional array. It places objects within specific regions and creates the volume-limited samples that underlie the stellar luminosity function, the mass-luminosity relationship, local stellar velocity distribution, and the stellar multiplicity fraction. The resulting understanding of stellar populations, stellar evolution, and star formation history contributes to the larger picture of galactic structure. However, this fundamental parameter of distance is unknown, or at best only estimated, for many stars and most substellar objects. Trigonometric parallax is the only direct means of measuring distances to stars and brown dwarfs, but requires time and patience. It is the method that identifies nearby stars and establishes their membership in the solar neighborhood.

Table 1.2 provides a current listing of seventy-nine objects in forty-nine stellar systems known to lie within 5 parsecs (pc) of the Sun, which implies a density of 0.0936 ± 0.0057 systems pc^{-3} . Extending this density to larger volumes, between 368 and 416 stellar systems should exist within 10 pc of the Sun and between 5,750 and 6,500 systems within 25 pc. However, only 249 stellar systems within 10 pc have been identified (RECONS 2006¹¹), leaving between 119 and 167 stellar systems yet to be found. The 25-pc volume appears to be missing about 4,100 systems (Backman *et al.*

2000; Henry *et al.* 2000; hereafter NStars Database¹²). The forty-three possible nearby stars studied herein will eventually account for some of these missing systems.

When a star is identified as belonging to the solar neighborhood, quantifying its fundamental properties increases in importance: spectral type, luminosity, motion, and metallicity. Determining whether it is truly a single star is also necessary. Its discovery may increase the census through the inclusion of stellar, brown dwarf, or planetary companions. Each new companion will also need its own fundamental properties measured. RECONS seeks to identify and thoroughly characterize all the stars within 10 pc. As part of these efforts, the Cerro Tololo Inter-American Observatory (CTIO) Parallax Investigation (CTIOPI) focuses on astrometric, photometric, and spectroscopic observations that identify nearby stars.

The parallax obtained from the astrometric observations will confirm whether these stars are truly part of the solar neighborhood and will clarify their three-dimensional position in space. In conjunction with the distance, the proper motion derived from the astrometric observations will provide the tangential component of the space velocity for each of these stars. CTIOPI stars are usually observed for 2–2.5 years (Jao *et al.* 2005), which is a short-baseline for determining proper motions. This information will help define stellar populations and the stellar velocity distribution, which together provide insight into the star formation history of the Galactic disk.

¹¹“The One Hundred Nearest Star Systems” is available at <http://www.chara.gsu.edu/RECONS/TOP100.htm>

¹²The NStars Database may be accessed at <http://nstars.arc.nasa.gov/index.cfm>

The relative parallax and proper motion of each star in this program is measured with respect to a reference frame of between five and fifteen stars, selected in accordance with the general rules adopted for CTIOPI and explained in Jao *et al.* (2005). Ideal reference stars are sufficiently distant to show neither parallax nor proper motion themselves and have apparent brightnesses similar to the possible nearby star. The actual stars selected will have small parallaxes and proper motions over the period of observation. Therefore, a correction to account for the mean distance and motion of the reference frame is necessary to convert the relative parallax and proper motion to an absolute one. Chapter 2 explores several methods of correcting relative values to absolute ones for Barnard's Star. As explained in Jao *et al.* (2005), CTIOPI adopted commonly used broadband photometric distance estimates for the reference stars to correct the relative parallax to absolute. No corrections are made to the proper motions at this time. In addition, the reference stars will not be uniform in color, which causes their apparent positions to change slightly as their light is refracted differently by the atmosphere as a function of hour angle and color. Jao *et al.* (2005) describes the model used by CTIOPI to correct this differential color refraction (DCR).

Photometry in the Johnson V band (V_J , centered on 547.5 nm) and the Kron-Cousins R and I bands (R_{KC} and I_{KC} centered on 642.5 nm and 807.5 nm) combined with an accurate distance will reveal the absolute magnitude of each star in these bands (Jao *et al.* 2005). In addition to providing a fundamental characteristic of each star, photometry is required to ensure the accuracy of the astrometric results. First, the photometry is used to make DCR corrections during the astrometric data reductions.

Then, the photometric distance to each reference star is used to convert a relative parallax to an absolute one.

4.2 SELECTION

Henry *et al.* (1997) describes the RECONS procedure by which the membership of a star in the solar neighborhood is established. Potential nearby stars are identified based on photometric or spectroscopic distances or based on high proper motion. Probable nearby stars have photometric distances based on both optical and near infrared observations plus spectroscopy to eliminate reddened giants. Henry *et al.* (1997) find that photometric distances generally provide better distance estimates than spectroscopy. Proven nearby stars have absolute parallaxes that place them in the solar neighborhood. This CTIOPI subsample seeks to advance possible nearby stars to proven nearby stars, but invested little effort on the intermediate step to establish them as probable nearby stars before proceeding to parallax measurements.

4.2.1 Possible Nearby Stars

The Two Micron All Sky Survey (Skrutskie *et al.* 2006, hereafter 2MASS), the Deep Near Infrared Survey of the Southern Sky (Epchtein *et al.* 1999, hereafter DENIS), and the Sloan Digital Sky Survey (York *et al.* 2000, hereafter SDSS) provide a wealth of new photometric data that can be used alone or in combination with other data sets to identify cool M and L dwarfs. The dim M dwarfs are currently about 70% of the stellar population of the solar neighborhood (Henry *et al.* 1997). The missing members of the solar neighborhood are likely to belong to this class and to the even fainter L class. Because of their inherent low luminosity, these very cool stars and brown dwarfs

may have been missed by earlier optical surveys. Programs seeking to identify these stars in the large infrared surveys are an excellent potential source of new possible nearby stars as they frequently include photometric and spectroscopic distance estimates.

An initial list of possible, nearby very low mass stars was compiled from the literature available in 2003 October. The review of literature concentrated on the work of I. N. Reid and collaborators (Reid *et al.* 2003; Cruz *et al.* 2003; Gizis *et al.* 2003; Reid, Kilkenny, & Cruz 2002; Reid & Cruz 2002; Cruz & Reid 2002; Gizis *et al.* 2000) in the proceeding five years. The published details were extracted for any star that the literature indicated was within 25 pc and for which no trigonometric parallax was currently available. The 25-pc limit was selected to match that of the NStars Database and is also the limit of some earlier nearby star catalogs (Woolley *et al.* 1970; Gliese & Jahreiß 1991). No effort was made to include stars with measured distances greater than 25 pc but with associated errors that might bring them within that radius. These stars were supplemented with lists of unpublished brown dwarfs suggested by K. Cruz (2003, private communication).

CTIO is located in the southern hemisphere. CTIOPI can and does observe stars north of the celestial equator (Jao *et al.* 2005; Costa *et al.* 2005). However, 42% of the expected systems are known in the northern hemisphere while only 31% of those expected in the southern hemisphere are known (Henry *et al.* 2002). At the time of sample selection, the United States Naval Observatory was actively measuring parallaxes in the northern hemisphere. Therefore, all stars with declinations greater than

0 degrees ($^{\circ}$) were excluded from the proposed sample. Approximately 305 possible nearby stars were identified this way.

Initially, CTIOPI operated both the 0.9-meter and 1.5-meter CTIO telescopes. In 2002, CTIO canceled the 1.5-meter program. Therefore, the stars in the proposed subsample needed to be bright enough to be observed with the 0.9-meter telescope using integration times no greater than 1,200 seconds (20 minutes). In general, CTIOPI science stars have R_{KC} magnitudes between 9 and 16. Objects fainter than sixteenth magnitude in I band were removed. Because not all stars had published I-band photometry, stars with published V-band magnitudes greater than 15 or J-band magnitudes greater than 13.1 were also eliminated. However, these brightness limits only reduced the proposed sample slightly; about 243 possible nearby stars remained.

To avoid duplicating the University of Virginia Southern Parallax Program (SPP), which is discussed in Chapter 3 and described further in Begam, Ianna, and Patterson (2006, in preparation; hereinafter BIP), the proposed sample was compared with that observing list. All stars on that program with the exception of LP 993-116, LP 888-18, and LHS 2397a were removed. LP 993-116 was excluded subsequently as a wide companion to LP 993-115, which was already included in CTIOPI (Jao *et al.* 2003).

To restrict the proposed sample further and to reduce the possibility of including stars from outside the solar neighborhood, stars with photometric or spectroscopic distance estimates greater than 15 pc were eliminated from the sample. The proposed sample now contained a manageable forty-three possible nearby star systems, which are

listed in Table 4.1, including three previously identified binary systems and four members of common proper motion pairs. Throughout this work, 2MASS designations are abbreviated 2MA hhmm-ddmm rather than 2MASS Jhhmmssss-ddmmss.

4.2.2 Probable Nearby Stars

Ideally, the possible nearby stars would be promoted to probable nearby stars by the acquisition of photometry and spectroscopy to confirm and refine the published distance estimates. Then, the probable nearby stars would be candidates for CTIOPI or other future parallax programs.

Previous experience with spectroscopic and photometric distance estimates from literature has indicated that widely varying values may be obtained depending on the quality of the relationships and observational data used. Table 4.2 provides a comparison among distances obtained by these methods for three stars, including a common proper motion pair. The distances for BD -44°836 and LP 993-116 (LP 993-15A and B) range from 6.0 to 611 pc and from 5.8 to 1,201 pc, respectively. To improve the photometric and spectroscopic distance estimates available from literature, a spectroscopic distance was calculated based on absolute I-magnitude relationships derived from RECONS stars. T. Henry (2003, private communication) initially provided the plots of absolute I-magnitude versus spectral type and (I-J) color shown in Figure 4.1 and Figure 4.2. Incomplete I and J photometry for the proposed sample of nearby stars made using the latter alone difficult. Rather than rely on values estimated from Figure 4.1, T. Henry (2003, private communication) later provided the data listed in Table 4.3.

TABLE 4.1
PROPOSED SAMPLE OF POSSIBLE NEARBY STARS FOR PARALLAX MEASUREMENT

Star	Alternate Name	Position (2000.0) ^a		Apparent Visual ^b Magnitude	Spectral Type	Estimated Distance (pc)	References	Notes ^c
		RA (hh mm ss.s)	Dec (dd mm ss.s)					
LP 991-84		01 39 21.72	-39 36 09.1	14.517 ± 0.007	...	8 ± 1	1, 2, 2	
LHS 1363	LP 649-72	02 14 12.56	-03 57 43.6	...	M6.5V	10.1 ± 1.4	1, 3, 3	
G 75-35		02 41 15.14	-04 32 17.8	13.800 ± 0.002	M4.0V	11.2 ± 0.8	1, 2, 4, 4	
2MA 0251-0352		02 51 14.99	-03 52 48.1	...	L3	12.1 ± 1.1	1, 3, 3	
LP 888-18	2MA 0331-3042	03 31 30.26	-30 42 38.7	18.26 ± 0.25	M7.5V	12.1 ± 1.2	1, 5, 3, 3	
LP 889-37		04 08 55.58	-31 28 54.0	14.52 ± 0.02	...	13.4 ± 1.0	1, 6, 6	
LHS 5094	LP 890-27	04 26 32.64	-30 48 01.8	14.02 ± 0.02	...	11.0 ± 0.8	1, 6, 6	
2MA 0429-3123		04 29 18.43	-31 23 56.7	...	M7.5V	9.7 ± 0.9	1, 3, 3	binary
LP 834-32		04 35 36.19	-25 27 34.9	12.38 ± 0.02	...	12.0 ± 1.4	1, 6, 6	
LP 655-43		04 38 02.52	-05 56 13.4	14.44 ± 0.02	...	14.7 ± 1.2	7, 6, 6	
LP 716-10		04 52 03.98	-10 58 22.1	15.97 ^d ± 0.25	M5.5V	14.3 ± 1.8	7, 5, 4, 4	
LP 776-25		04 52 24.42	-16 49 22.2	11.61 ± 0.02	...	12.4 ± 1.3	1, 6, 6	
2MA 0517-3349	LEHPM 2-0183	05 17 37.70	-33 49 03.1	...	M8V	14.7 ± 1.2	1, 3, 3	
LP 717-36		05 25 41.67	-09 09 12.6	12.56 ± 0.02	...	12.9 ± 1.5	1, 6, 6	
LHS 2024	LP 725-15	08 31 23.45	-10 29 53.8	15.0 ^e ± 0.01 ^f	M4V	13.9 ± 1.8	8, 9, 10, 11	
LHS 6167		09 15 36.40	-10 35 47.2	13.76 ± 0.02	M4-5	6.7 ± 0.5	1, 6, 12, 6	
2MA 0921-2104		09 21 14.10	-21 04 44.4	...	L2	12.4 ...	1, 13, 13	
G 161-71		09 44 54.18	-12 20 54.4	13.73 ± 0.02	M5Ve	6.2 ± 0.5	1, 6, 14, 6	
LP 671-8	G 163-21	10 54 41.97	-07 18 33.1	13.24 ± 0.02	M3-4	13.3 ± 1.8	15, 6, 12, 6	
LP 731-76		10 58 27.99	-10 46 30.5	14.39 ± 0.02	M4-5	11.6 ± 0.8	1, 6, 12, 6	poss cpm pair
LHS 2397a	LP 732-94	11 21 49.19	-13 13 08.5	18.26 ^d ± 0.25	M8.5V	12.0 ^g ± 2.0	16, 5, 17, 17	binary

TABLE 4.1 (CONTINUED)
 PROPOSED SAMPLE OF POSSIBLE NEARBY STARS FOR PARALLAX MEASUREMENT

Star	Alternate Name	Position (2000.0) ^a		Apparent Visual ^b Magnitude	Spectral Type	Estimated Distance (pc)		References	Notes ^c
		RA (hh mm ss.s)	Dec (dd mm ss.s)						
2MA 1155-3727		11 55 39.53	-37 27 35.7	...	L2e	12.6	...	18, 19, 13	
LP 734-34		12 10 28.37	-13 10 24.1	13.75 ± 0.02	...	12.9 ± 1.1	5, 6, 6		
LP 615-149		12 27 44.70	-03 15 00.6	12.82 ± 0.02	...	15.0 ± 1.7	15, 6, 6		
LHS 5226	LP 735-29	12 44 00.73	-11 10 30.3	14.18 ± 0.02	...	12.5 ± 0.9	8, 6, 6		
CE 303	2MA 1309-2330	13 09 21.85	-23 30 35.7	...	M8V	13.3 ± 1.1	20, 3, 3		
LHS 2783	LP 798-25	13 42 09.84	-16 00 23.4	13.39 ± 0.02	M4V	13.3 ± 1.8	1, 6, 10, 6		binary
LP 739-2		13 58 16.18	-12 02 59.1	14.41 ± 0.02	...	13.8 ± 1.0	1, 6, 6		
LHS 2880	GJ 540.2	14 13 04.86	-12 01 26.8	13.83 ± 0.02	M4.5V	9.8 ± 0.7	1, 6, 10, 6		
2MA 1507-2000		15 07 27.81	-20 00 43.3	...	M7.5V	14.2 ± 1.4	1, 3, 3		
LHS 3056	LP 742-61	15 19 11.72	-12 45 06.5	12.84 ± 0.02	M4V	11.6 ± 1.3	1, 6, 10, 6		
2MA 1534-1418		15 34 56.93	-14 18 49.2	...	M8V	13.5	...	1, 19, 13	
LP 869-19		19 42 00.66	-21 04 05.6	13.210 ± 0.020	...	10 ± 1	1, 2, 2		
LP 869-26		19 44 53.80	-23 37 59.4	14.078 ± 0.016	...	9 ± 1	1, 2, 2		poss new binary
LP 870-65		20 04 30.79	-23 42 02.4	13.0 ± 0.3	...	10 ± 2	1, 2, 2		
LP 756-3		20 46 43.64	-11 48 13.3	13.762 ± 0.024	M5-6	14 ± 2	1, 2, 21, 2		
LP 984-92		22 45 00.07	-33 15 26.0	13.381 ± 0.026	...	8 ± 1	1, 2, 2		poss cpm pair
LP 876-10		22 48 04.50	-24 22 07.8	12.618 ± 0.012	...	7.2 ± 0.8	1, 2, 2		
LP 932-83		22 49 08.41	-28 51 20.1	13.93 ± 0.02	...	14.1 ± 2.4	1, 22, 11		poss cpm pair
2MA 2306-0502 ^h		23 06 29.36	-05 02 29.2	...	M7.5V	11.3 ± 2.0	1, 3, 17		
LP 822-101		23 31 25.04	-16 15 57.8	13.122 ± 0.000	...	15 ± 2	1, 2, 2		
2MA 2351-2537	LEHPM 1-6334	23 51 50.48	-25 37 36.5	...	L1	13.2	...	23, 13, 13	

TABLE 4.1 (CONTINUED)
 PROPOSED SAMPLE OF POSSIBLE NEARBY STARS FOR PARALLAX MEASUREMENT

Star	Alternate Name	Position (2000.0) ^a		Apparent Visual ^b Magnitude	Spectral Type	Estimated Distance (pc)	References	Notes ^c
		RA (hh mm ss.s)	Dec (dd mm ss.s)					
LP 704-15	G 273-186	23 57 20.59	-12 58 48.7	12.93 ± 0.02	M3V	13.2 ± 1.7	15, 24, 10, 11	poss cpm pair

NOTES.—^aCoordinates from 2MASS updated with proper motion from the listed reference using addpm routine (25)

^bApparent visual magnitude (V_{JM}) on the Johnson-Morgan system (26, 27) with $V=550$ nm

^c“poss cpm pair” identifies one member of a possible common proper motion pair; the other star is identified in 4.6.

^d(5) was not consulted during the initial compilation of possible nearby stars. If it had been, this star would have been excluded as too faint.

^e V_{Eggen} is substantially the same as V_{JM} according to (28).

^fPhotometric error estimated from (29).

^gFurther investigation of the literature revealed an absolute trigonometric parallax for LHS 2397a of 70 ± 2 mas (30).

^hCTIOPI also observed this star with the 1.5-meter telescope and measured an absolute parallax is 82.6 ± 2.6 mas (31).

REFERENCES.—(1) this work, see section 4.3 and Table 4.6; (2) Reid *et al.* 2003; (3) Cruz *et al.* 2003; (4) Cruz & Reid 2002; (5) Salim & Gould 2003; (6) Reid, Kilkenny, & Cruz 2002; (7) *NLTT*; (8) Bakos, Sahu, & Nemeth 2002; (9) Eggen 1987; (10) Reid, Hawley, & Gizis 1995; (11) Reid & Cruz 2002; (12) Gigoyan, Hambaryan, & Azzopardi 1998; (13) K. I. Cruz 2003, private communication; (14) Torres *et al.* 2000; (15) Giclas, Burnham, & Thomas 1978; (16) Tinney 1996; (17) Gizis *et al.* 2000; (18) Deacon, Hambly, & Cooke 2005; (19) Gizis 2002; (20) Lodieu *et al.* 2005; (21) Abrahamyan *et al.* 1997; (22) Ryan 1992; (23) Pokorny, Jones, & Hambly 2003; (24) Weis 1991; (25) Jao 2004; (26) Johnson & Morgan 1951; (27) Johnson & Morgan 1953; (28) Bessell & Weis 1987; (29) Ryan 1989; (30) Monet *et al.* 1992; (31) Costa *et al.* 2006

TABLE 4.2
COMPARISON OF DISTANCE ESTIMATES

Star	Alternate Name	Photometric Distances (pc)			Other Distances (pc)			References
		RECONS 1998	Non-RECONS	RECONS 2003	RECONS Spectroscopic	Relative or Absolute Parallax ^a		
BD -44°836	LP 993-115A	611	10.5 ± 1.2	9.8	6.0 ± 2.1	10.7 ± 0.4	pr	1,2,3,4,3
LP 993-116	LP 993-115B	1201	7 ± 0.6	9.8	5.8 ± 2.0	10.7 ± 0.3	pr	1,2,3,4,3
LHS 2397a		...	12.0 ± 2.0	...	12.2 ± 3.5	14.3 ± 0.4	a	5,4,6

NOTE.—^aA “pr” indicates a preliminary, relative parallax was used. An “a” indicates a final absolute parallax was used.

REFERENCES.—(1) Patterson, Ianna, & Begam 1998; (2) Reid, Kilkenny, & Cruz 2002; (3) T. Henry 2003, private communication (4) method discussed in 4.2.2; (5) Gizis *et al.* 2000; (6) Monet *et al.* 1992

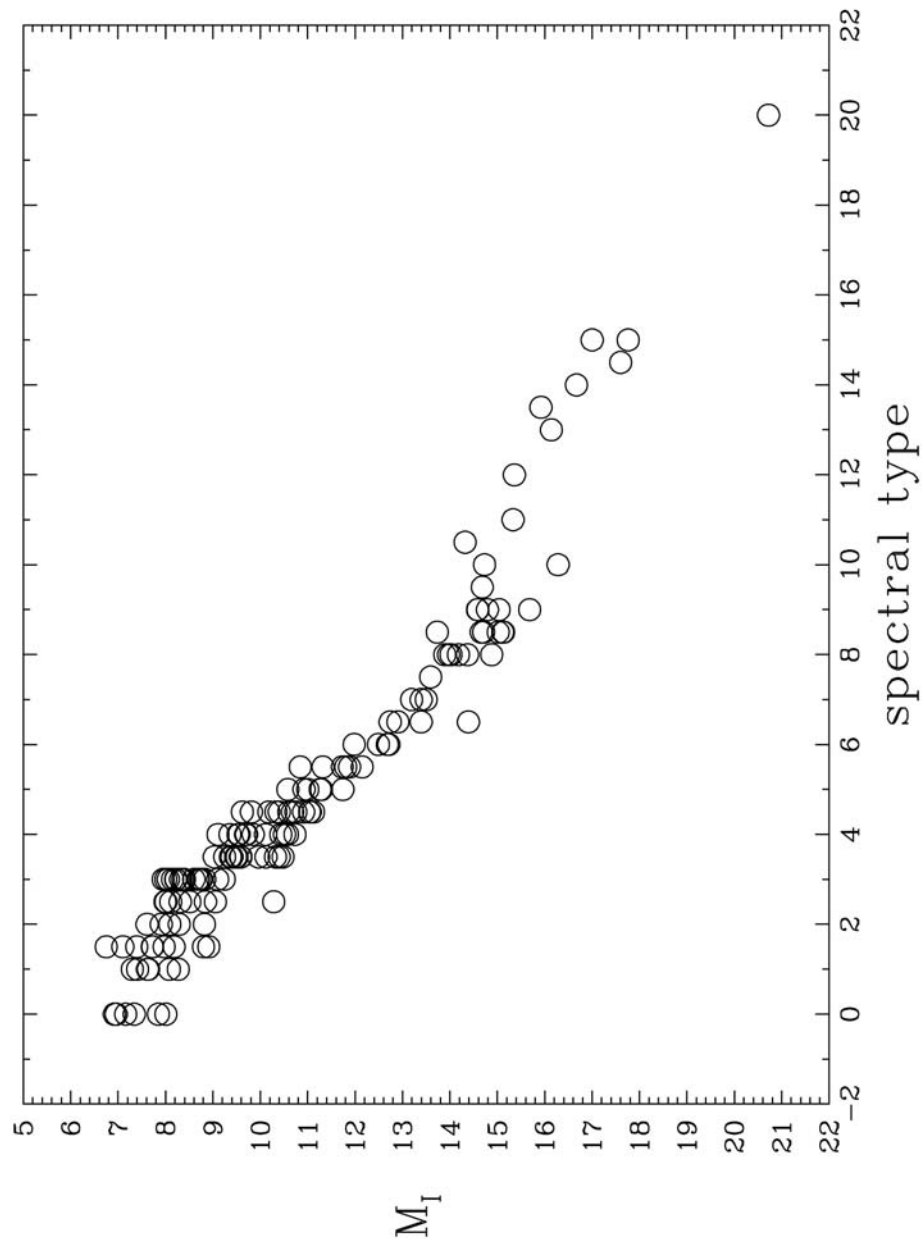


FIG. 4.1.— Absolute I-Magnitude versus Spectral Type (T. Henry 2003, private communication).

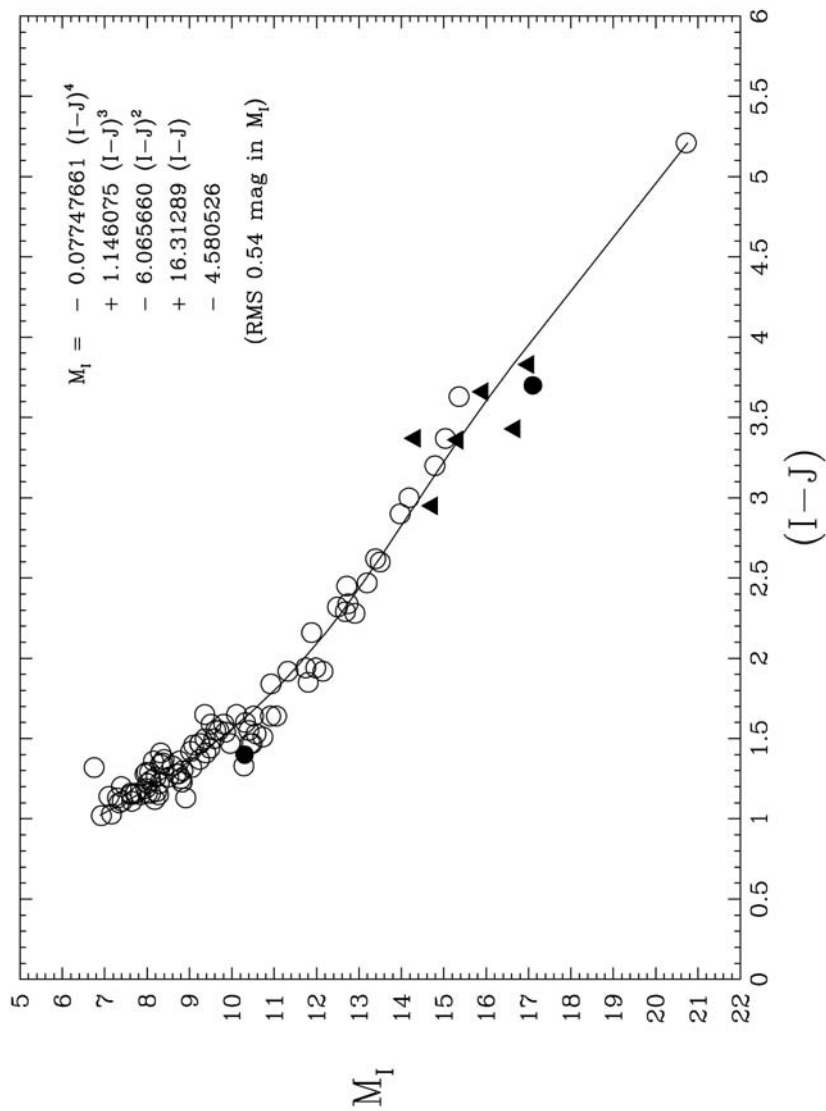


FIG. 4.2.— Absolute I-Magnitude versus (I-J) Color for Known Nearby Stars. Open circles are main sequence stars; filled circles are possibly subdwarfs; and filled triangles are possibly brown dwarfs (T. Henry 2003 & 2006, private communication).

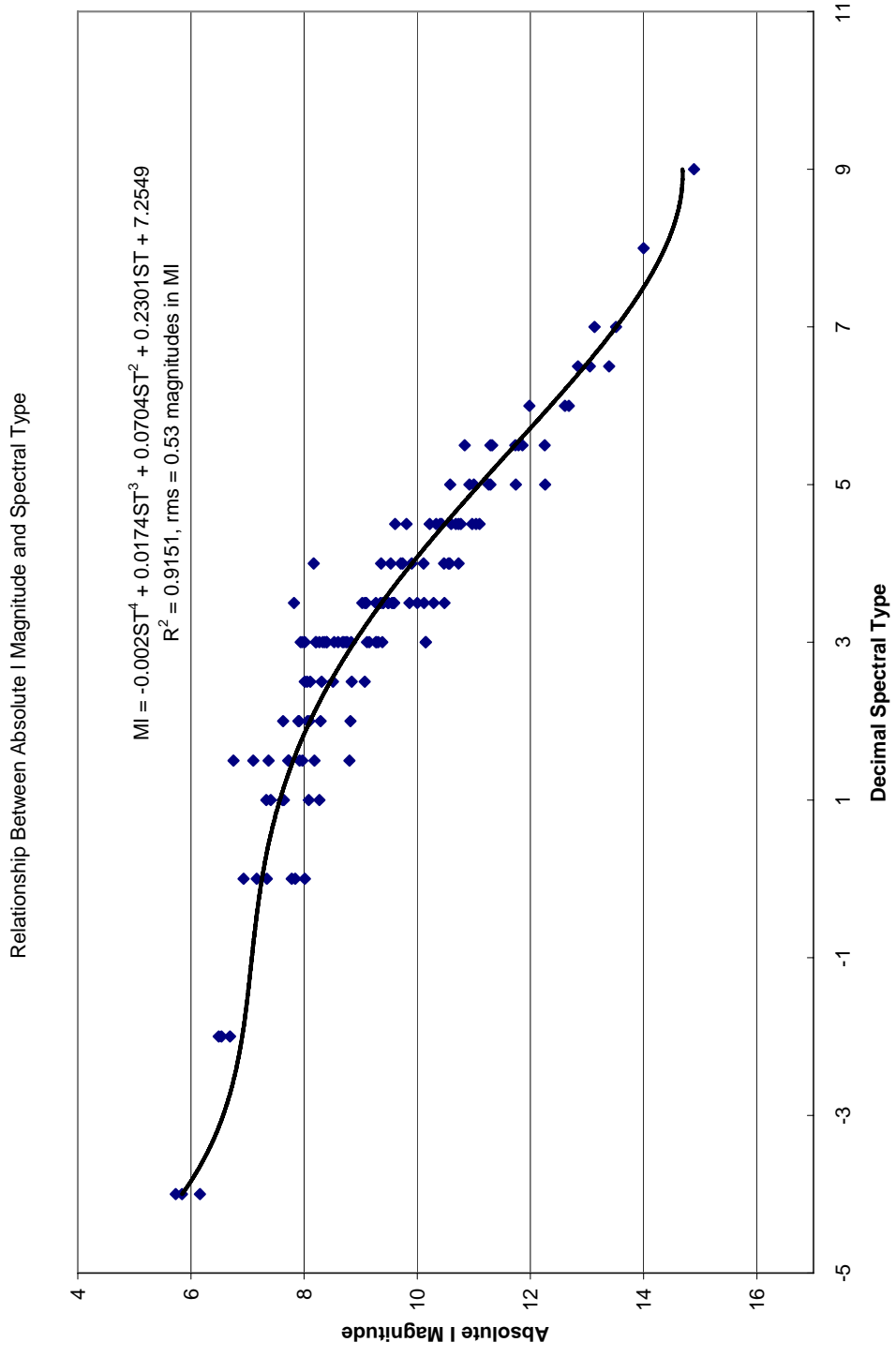


FIG. 4.3.— Absolute I-Magnitude versus Spectral Type for Known Nearby Files. Plot is based on data in Table 4.3, which was provided by T. Henry (2003, private communication).

TABLE 4.3
NEARBY STAR DATA FOR SPECTROSCOPIC AND PHOTOMETRIC DISTANCE ESTIMATES (1)

Star (GJ)	Alternate Name	Spectral Type	M _I (mag)	I-J (mag)	I-H (mag)	I-K (mag)	J-H (mag)	J-K (mag)	H-K (mag)	Comments
1		M3.0 V	8.21	1.08	...	1.89	...	0.81	...	
15 A		M1.5 V	8.18	1.92	
15 B		M3.5 V	10.48	1.45	2.05	2.29	0.6	0.84	0.24	41" visible orbit (2)
17		F9 V	3.9	
33		K2 V	5.4	
48		M2.5 V	8.01	1.27	1.87	2.12	0.6	0.85	0.25	
54.1		M4.5 V	11.1	1.69	2.2	2.53	0.51	0.84	0.33	
71		G8 V _p	4.86	
83.1		M4.5 V	10.97	1.7	2.24	2.56	0.54	0.87	0.32	
84		M3.0 V	7.97	1.3	1.94	2.18	0.64	0.88	0.24	
102		M4.0 V	10.11	1.59	2.15	2.43	0.56	0.85	0.29	
105 B		M3.5 V	9.58	1.55	2.09	2.31	0.54	0.76	0.22	165" visible orbit (3)
109		M3.0 V	8.7	1.36	1.91	2.15	0.55	0.79	0.24	
137		G5 Ve	4.29	
139		G5 V	4.56	
144	ε Eridani	K2 V	5.25	cold dust
166 A		K1 Ve	5.03	
166 C		M4.5 V	9.81	1.57	2.04	2.36	0.47	0.79	0.32	7" visible orbit (3)
169.1 A		M4.0 V	9.53	possibly corrupted by B in 2MASS
176		M2.0 V	7.91	1.27	1.91	2.12	0.64	0.86	0.22	
178		F6 V	3.13	
183		K3 V	5.4	

TABLE 4.3 (CONTINUED)
NEARBY STAR DATA FOR SPECTROSCOPIC AND PHOTOMETRIC DISTANCE ESTIMATES (1)

Star (GJ)	Alternate Name	Spectral Type	M _I (mag)	I-J (mag)	I-H (mag)	I-K (mag)	J-H (mag)	J-K (mag)	H-K (mag)	Comments
190		M3.5 V	7.82	1.49	2.08	2.36	0.58	0.86	0.28	
203		M3.5 V	9.86	1.49	1.96	2.26	0.47	0.77	0.3	
205		M1.5 V	7.1	
213		M4.0 V	9.9	1.62	2.11	2.35	0.5	0.74	0.24	
216 A		F6 V	3.26	19' possible cpm companion (3)
216 B		K2 V	5.4	96'' visible orbit (3)
226		M2.5 V	8.31	1.31	1.89	2.12	0.57	0.81	0.23	
229 A		M1.0 V	7.33	1.04	
232		M4.0 V	10.57	1.52	...	2.27	...	0.75	...	
239		M0.0 V	7.78	1.08	1.72	1.89	0.64	0.81	0.17	
244 A	Sirius	A1 V	1.49	
250 A		K3 V	5.74	1.34	
250 B		M2.5 V	8.11	1.24	...	2.1	...	0.86	...	58'' visible orbit (3)
251		M3.0 V	8.76	1.39	1.96	2.21	0.58	0.83	0.25	
273		M3.5 V	9.27	1.45	...	2.3	...	0.86	...	
283 B		M6.0 V	12.68	2.28	2.8	3.14	0.53	0.86	0.34	21'' visible orbit (3)
285		M4.0 V	9.36	1.66	2.23	2.54	0.58	0.88	0.31	
299		M4.0 V	10.73	1.48	1.97	2.24	0.5	0.76	0.27	
358		M3.0 V	8.4	1.39	1.97	2.23	0.58	0.85	0.26	
380		K7.0 V	6.54	
382		M2.0 V	7.63	1.22	1.85	2.1	0.63	0.87	0.24	

TABLE 4.3 (CONTINUED)
 NEARBY STAR DATA FOR SPECTROSCOPIC AND PHOTOMETRIC DISTANCE ESTIMATES (1)

Star (GJ)	Alternate Name	Spectral Type	M_I (mag)	I-J (mag)	I-H (mag)	I-K (mag)	J-H (mag)	J-K (mag)	H-K (mag)	Comments
388		M3.0 V	8.36	1.36	1.97	2.22	0.61	0.86	0.25	
393		M2.0 V	8.09	1.22	1.8	2.09	0.57	0.87	0.29	
406		M6.0 V	12.61	2.41	3.02	3.42	0.6	1	0.4	
408		M2.5 V	8.51	1.32	1.87	...	0.55	
411		M2.0 V	8.29	
412 A		M1.0 V	8.27	1.16	1.7	1.93	0.54	0.77	0.23	
412 B		M5.5 V	12.25	1.94	2.5	2.84	0.56	0.9	0.34	28" visible orbit (3)
424		M1.0 V	7.64	1.12	1.7	1.9	0.58	0.77	0.2	
432 A		K0 V	5.19	1.07	
433		M2.0 V	7.9	1.22	1.83	2.07	0.62	0.85	0.23	possible brown dwarf companion (4)
442 A		G5 V	4.33	
445		M3.5 V	9.48	1.41	1.91	2.18	0.51	0.77	0.26	
447		M4.0 V	10.55	1.66	2.22	2.52	0.56	0.85	0.29	
450		M1.5 V	7.97	1.22	1.81	2.03	0.59	0.81	0.22	
465		M3.0 V	9.27	1.28	1.76	2.06	0.49	0.78	0.3	
479		M3.0 V	8.33	1.38	1.95	2.22	0.58	0.84	0.26	
480.1		M3.0 V	10.15	1.4	1.92	2.21	0.51	0.8	0.29	
486		M3.0 V	9.11	1.49	2.01	2.32	0.53	0.83	0.3	
493.1		M4.5 V	10.73	1.73	2.31	2.62	0.59	0.89	0.31	
506		G6 V	4.31	
514		M1.0 V	7.62	1.11	1.71	1.97	0.6	0.87	0.26	

TABLE 4.3 (CONTINUED)
NEARBY STAR DATA FOR SPECTROSCOPIC AND PHOTOMETRIC DISTANCE ESTIMATES (1)

Star (GJ)	Alternate Name	Spectral Type	M _I (mag)	I-J (mag)	I-H (mag)	I-K (mag)	J-H (mag)	J-K (mag)	H-K (mag)	Comments
526		M1.5 V	7.72	1.21	...	1.97	...	0.77	...	
551	Proxima Centauri	M5.5 V	11.86	2.07	...	3.05	...	0.97	...	7,849'' visible orbit (3)
555		M3.5 V	9.55	1.65	2.23	2.55	0.58	0.9	0.32	
559 A	α Centauri A	G2 V	3.69	
559 B	α Centauri B	K0 V	4.83	18'' visible orbit (5)
581		M2.5 V	9.07	1.35	1.97	2.22	0.61	0.87	0.26	
588		M2.5 V	8.05	1.27	1.89	2.16	0.62	0.89	0.27	
595		M3.0 V	9.38	1.42	1.92	2.17	0.5	0.75	0.25	
609		M4.0 V	9.74	1.6	2.08	2.36	0.48	0.76	0.28	
618 A		M3.0 V	8.53	1.37	1.94	2.21	0.57	0.84	0.27	
618 B		M5.5 V	11.29	9'' visible orbit (3)
625		M1.5 V	8.8	1.28	1.83	2.06	0.54	0.77	0.23	
628		M3.0 V	9.28	1.47	2.05	2.35	0.58	0.88	0.3	
631		K0 Ve	4.94	
643		M3.5 V	10	1.5	...	2.33	...	0.83	...	72'' visible orbit (3)
644 C	VB 8	M7.0 V	13.13	2.4	2.98	3.36	0.57	0.96	0.39	221'' visible orbit (3)
664		K5 Ve	6.16	732'' visible orbit, poss. RV variable (3)
667 C		M2.5 V	8.84	1.29	1.82	2.1	0.53	0.81	0.29	31'' visible orbit (3)
673		K7.0 V	6.49	1	1.59	...	0.59	
674		M3.0 V	8.68	1.26	1.82	2.11	0.56	0.86	0.3	
678.1		M1.0 V	7.41	1.16	1.75	1.98	0.59	0.82	0.23	

TABLE 4.3 (CONTINUED)
NEARBY STAR DATA FOR SPECTROSCOPIC AND PHOTOMETRIC DISTANCE ESTIMATES (1)

Star (GJ)	Alternate Name	Spectral Type	M _I (mag)	I-J (mag)	I-H (mag)	I-K (mag)	J-H (mag)	J-K (mag)	H-K (mag)	Comments
680		M1.5 V	7.92	1.21	1.8	2.05	0.59	0.84	0.25	
682		M4.5 V	9.61	1.57	2.19	2.5	0.63	0.94	0.31	
686		M0.0 V	8.01	1.19	1.76	1.98	0.57	0.79	0.22	
687		M3.0 V	8.4	1.34	1.91	2.13	0.57	0.79	0.22	
693		M3.5 V	9.35	1.33	1.88	2.16	0.56	0.84	0.28	
694		M3.0 V	8.21	1.29	1.88	2.14	0.59	0.85	0.26	
699		M4.0 V	10.47	1.55	1.96	2.27	0.41	0.72	0.31	
701		M0.0 V	7.84	1.14	1.73	1.99	0.59	0.85	0.26	
721	Vega	A0 V	0.59	cold dust
725 A		M3.0 V	8.74	1.29	1.74	2.05	0.45	0.76	0.31	
725 B		M3.5 V	9.39	1.41	1.93	2.13	0.52	0.72	0.2	16" visible orbit, poss. RV variable (3)
729		M3.5 V	10.29	1.43	1.99	2.28	0.57	0.85	0.29	
745 A		M3.0 V	8.83	1.24	...	2.02	...	0.77	...	
745 B		M2.0 V	8.82	1.25	...	2.01	...	0.76	...	115" visible orbit (3)
752 A		M3.0 V	7.94	...	1.85	2.11	0.26	
752 B	VB 10	M8.0 V	14	2.93	3.61	4.07	0.68	1.14	0.46	74" visible orbit (3)
780		G8 V	3.86	
784		M0.0 V	7.16	1	...	1.84	...	0.84	...	
785		K0 V	5.07	
793		M3.0 V	8.6	1.37	1.97	2.18	0.6	0.8	0.2	
803		M1.5 V	6.75	1.28	1.89	2.19	0.61	0.91	0.3	

TABLE 4.3 (CONTINUED)
NEARBY STAR DATA FOR SPECTROSCOPIC AND PHOTOMETRIC DISTANCE ESTIMATES (1)

Star (GJ)	Alternate Name	Spectral Type	M _I (mag)	I-J (mag)	I-H (mag)	I-K (mag)	J-H (mag)	J-K (mag)	H-K (mag)	Comments
809		M0.0 V	7.34	1.15	...	1.96	...	0.81	...	
820 B		K7.0 V	6.69	29" visible orbit (6)
825		M0.0 V	6.93	
827		F8 V	3.79	
832		M3.0 V	8.01	1.12	...	1.97	...	0.85	...	
845	ε Indi	K5 Ve	5.73	
849		M4.0 V	8.17	1.37	1.98	2.29	0.61	0.92	0.31	
867 B		M3.5 V	9.1	1.44	...	2.29	...	0.85	...	24" visible orbit (3)
873		M3.5 V	9.03	1.44	2	2.25	0.55	0.81	0.26	
876 A		M3.5 V J	9.07	1.5	2.08	2.42	0.59	0.92	0.34	
877		M3.0 V	8.27	1.33	1.87	2.14	0.53	0.81	0.27	
879		K5 Ve	5.84	0.73	7,060" visible orbit (3)
880		M1.5 V	7.37	1.19	1.75	2.03	0.56	0.84	0.28	
881	Fomalhaut	A3 V	1.65	cold dust
884		<K5.0 V	6.68	0.88	...	1.75	...	0.87	...	
887		M1.5 V	7.73	
905		M5.5 V	11.32	1.94	2.57	2.89	0.64	0.95	0.32	
908		M1.0 V	8.08	1.12	1.67	1.91	0.55	0.78	0.24	
1002		M5.5 V	11.79	1.83	2.36	2.71	0.53	0.88	0.35	
1057		M5.0 V	10.92	1.81	2.37	2.75	0.57	0.94	0.38	
1065		M3.0 V	10.15	1.47	...	2.29	...	0.82	...	

TABLE 4.3 (CONTINUED)
NEARBY STAR DATA FOR SPECTROSCOPIC AND PHOTOMETRIC DISTANCE ESTIMATES (1)

Star (GJ)	Alternate Name	Spectral Type	M_I (mag)	I-J (mag)	I-H (mag)	I-K (mag)	J-H (mag)	J-K (mag)	H-K (mag)	Comments
1093		M5.0 V	11.74	2.03	2.64	2.96	0.61	0.93	0.32	
1105		M4.0 V	9.71	1.51	2.11	2.36	0.6	0.86	0.26	
1111		M6.5 V	12.84	2.41	3.02	3.38	0.62	0.97	0.36	
1125		M3.0 V	9.15	1.43	1.95	2.26	0.51	0.83	0.31	
1138		M4.5 V	10.22	1.62	2.12	2.42	0.49	0.79	0.3	
1151		M4.5 V	10.6	1.68	2.22	2.53	0.54	0.85	0.32	
1154		M5.5 V	10.84	1.99	2.59	2.91	0.6	0.92	0.32	
1156		M5.0 V	11.26	1.82	2.46	2.77	0.64	0.95	0.31	
1224		M4.5 V	11.04	1.79	2.35	2.6	0.55	0.81	0.26	
1227		M4.5 V	10.77	1.71	2.3	2.61	0.59	0.9	0.3	
1235		M4.5 V	10.43	1.63	2.21	2.5	0.58	0.86	0.28	
1245 B		M6.0 V	11.98	2	2.54	2.88	0.55	0.89	0.34	8'' visible orbit (7)
1253		M5.0 V	11	1.81	...	2.74	...	0.93	...	
1256		M4.5 V	10.4	1.72	2.28	2.61	0.57	0.89	0.33	
1286		M5.5 V	11.73	1.88	2.52	2.85	0.64	0.97	0.32	
1289		M3.5 V	10.12	1.55	2.21	2.43	0.66	0.88	0.22	
2066		M2.0 V	8.06	1.24	1.82	2.09	0.59	0.86	0.27	
3325	LHS 1731	M3.0 V	9.31	1.33	1.91	2.21	0.58	0.88	0.31	
3378	LHS 1805	M3.5 V	9.59	1.52	2.04	2.35	0.52	0.83	0.31	
3380	LHS 1809	M5.0 V	11.29	1.78	2.36	2.69	0.58	0.91	0.33	
3421	LHS 224	M4.5 V	10.33	1.61	2.06	2.37	0.44	0.76	0.32	

TABLE 4.3 (CONTINUED)
NEARBY STAR DATA FOR SPECTROSCOPIC AND PHOTOMETRIC DISTANCE ESTIMATES (1)

Star (GJ)	Alternate Name	Spectral Type	M _I (mag)	I-J (mag)	I-H (mag)	I-K (mag)	J-H (mag)	J-K (mag)	H-K (mag)	Comments
3517	LHS 2065	M9.0 V	14.89	3.33	4.07	4.6	0.74	1.27	0.53	
3622	LHS 292	M6.5 V	13.05	2.47	3.07	3.4	0.59	0.93	0.34	
3801	LHS 2784	M3.5 V	9.49	1.48	2.06	2.29	0.58	0.81	0.23	
3855	LHS 2930	M6.5 V	13.39	2.52	3.17	3.52	0.65	1	0.35	
3877	LHS 3003	M7.0 V	13.51	2.56	3.22	3.6	0.65	1.04	0.39	
3959	G 180-060	M5.0 V	12.26	1.83	2.42	2.78	0.59	0.96	0.36	
3988	LHS 3262	M5.0 V	10.58	1.7	2.28	2.55	0.57	0.85	0.27	
4247	G 188-038	M3.5 V	9.4	1.52	2.12	2.38	0.6	0.86	0.26	
4274	LHS 3799	M4.5 V	10.68	1.8	2.4	2.72	0.6	0.92	0.32	

NOTE.—“cpm” is “common proper motion” and “poss. RV variable” is “possible radial velocity variable.”

REFERENCES.—(1) T. Henry 2003, private communication; (2) Lippincott 1972; (3) Gliese 1969; (4) Bernstein 1997; (5) Heintz 1982; (6) Josties & Harrington 1984; (7) Gliese 1979

From Table 4.3, the 132 stars later than K4V were used to plot absolute I-magnitude (M_I) against spectral type (Sp), as shown in Figure 4.3. A fourth-order polynomial in spectral type was fitted to the data as follows

$$M_I = -0.002 ST^4 + 0.0174 ST^3 + 0.0704 ST^2 + 0.2301 ST + 7.2549 \quad (4.1)$$

where spectral type is expressed as a decimal value. The Pearson product moment correlation coefficient (r^2) associated with this fit is 0.9151; a value of 1.0 would indicate complete correlation. The error associated with this fit is 0.53 magnitudes.

First, the absolute I-magnitude was calculated for each possible nearby star in the proposed sample for which a spectral type was available using Equation 4.1. Then, the (I-J) color was estimated from Figure 4.2 and

$$M_I = -0.07747661(I - J)^4 + 1.146075(I - J)^3 - 6.065660(I - J)^2 + 16.31289(I - J) - 4.580526 \quad (4.2)$$

(T. Henry 2003, private communication) using the absolute I-magnitude obtained earlier. The error associated with this fit is 0.54 magnitudes. Adding 2MASS J (1.235 μm ; Cohen, Wheaton, & Megeath 2003) to the (I-J) color provided an estimate of the apparent I-magnitude (m_I). At the time of selection, only the second incremental data release of the 2MASS point source catalog was available (Skrutskie *et al.* 1997). For the nearest stars, reddening should not play a significant factor. Therefore, the distance modulus formula

$$m_I - M_I = 5 \log(d_{sp}) - 5 \quad (4.3)$$

can be used to estimate a spectroscopic distance (d_{sp}). Table 4.4 lists the distance estimates obtained in this manner. The formal errors indicate that these distances

TABLE 4.4
COMPARISON OF DISTANCE ESTIMATES FOR POSSIBLE NEARBY STARS

Star	Spectral Type	Distance Estimates (pc)			Parallactic Distances (pc) ^d		Ratios ^a		References	Comment
		Literature ^b	Spectroscopic ^c		Type ^e	L	S			
LP 991-84	...	8 ± 1	...		8.64 ± 0.24	r	1.1	...	1	
LHS 1363	M6.5V	10.1 ± 1.4	9.8 ± 3.1		12.42 ± 0.60	r	1.2	1.3	2	
G 75-35	M4.0V	11.2 ± 0.8	14.6 ± 5.1		11.83 ± 0.54	r	1.1	0.8	3	
2MA 0251-0352	L3	12.1 ± 1.1	1200 ± 1800		12.7 ± 1.2	r	1.0	...	2	poor spectroscopic estimate
LP 888-18	M7.5V	12.1 ± 1.2	11.1 ± 3.3		13.44 ± 0.70	r	1.1	1.2	2	
LP 889-37	...	13.4 ± 1.0	...		16.9 ± 1.6	r	1.3	...	4	
LHS 5094	...	11.0 ± 0.8	...		14.0 ± 1.0	r	1.3	...	4	
2MA 0429-3123	M7.5V	9.7 ± 0.9	8.9 ± 2.7		15.14 ± 0.89	a	1.6	1.7	2	binary, see also Table 4.16
LP 834-32	...	12.0 ± 1.4	...		16.5 ± 1.4	r	1.4	...	4	
LP 655-10	M4.5V	18.7 ± 3.7	15.3 ± 5.4		5, 6	see also Table 4.14
LP 716-10	M5.5V	14.3 ± 1.8	14.3 ± 4.9		3	see also Table 4.14
LP 776-25	...	12.4 ± 1.3	...		14.1 ± 2.2	r	1.1	...	4	
2MA 0517-3349	M8V	14.7 ± 1.2	13.4 ± 3.9		17.1 ± 1.3	a	1.2	1.3	2	
LP 717-36	...	12.9 ± 1.5	...		18.4 ± 1.2	r	1.4	...	4	
LHS 2024	M4V	13.9 ± 1.8	21.9 ± 7.7		7, 8	see also Table 4.14
LHS 6167	M4.5	6.7 ± 0.5	9.1 ± 4.2		9.73 ± 0.28	a	1.5	1.1	9, 4	M4-5 in source
2MA 0921-2104	L2	12.4 ...	120 ± 110		11.48 ± 0.35	r	0.9	...	10	poor spectroscopic estimate
G 161-71	M5Ve	6.2 ± 0.5	7.0 ± 2.4		14.16 ± 0.56	a	2.3	2.0	11, 4	
LP 671-8	M3.5	13.3 ± 1.8	15.3 ± 6.6		9, 4	M3-4 in source
LP 731-76	M4.5	11.6 ± 0.8	13.9 ± 6.4		14.42 ± 0.53	a	1.2	1.0	9, 4	M4-5 in source
BD -10°3166 ^f	K0V	< 200	> 9000		50 ± 29	a	12	poor spectroscopic estimate
LHS 2397a	M8.5V	12 ± 2	12.2 ± 3.5		14.29 ± 0.42	a	1.2	1.2	13, 13, 14	binary

TABLE 4.4 (CONTINUED)
COMPARISON OF DISTANCE ESTIMATES FOR POSSIBLE NEARBY STARS

Star	Spectral Type	Distance Estimates (pc)			Parallactic Distances (pc) ^d			Ratios ^a		References	Comment
		Literature ^b	Spectroscopic ^c		Type ^e	L	S				
2MA 1155-3727	L2	12.6 ...	120 ± 210	15, 10	poor spectroscopic estimate		
LP 734-34	M4.0V	15.4 ± 3.1	15.3 ± 5.4	5, 6	see also Table 4.14		
CE 303	M8V	13.3 ± 1.1	12.0 ± 3.5	2			
LHS 2783	M4V	13.3 ± 1.8	13.4 ± 4.7	19.6 ± 1.2	r	1.5	1.5	8, 4	binary		
LP 739-2	...	13.8 ± 1.0	...	17.3 ± 1.1	r	1.3	...	4			
LHS 2880	M4.5V	9.8 ± 0.7	11.2 ± 4.0	25.8 ± 2.2	a	2.6	2.3	7, 4			
2MA 1507-2000	M7.5V	14.2 ± 1.4	13.0 ± 3.9	22.8 ± 1.7	a	1.6	1.8	2			
LHS 3056	M4V	11.6 ± 1.3	10.5 ± 3.7	19.10 ± 0.71	a	1.6	1.8	7, 4			
2MA 1534-1418	M8V	13.5 ...	10.1 ± 3.1	11.09 ± 0.28	a	0.8	1.1	15, 10			
LP 869-19	...	10 ± 1	...	18.4 ± 1.1	a	1.8	...	1			
LP 869-26	...	9 ± 1	...	13.97 ± 0.68	a	1.6	...	1	possible new binary		
LP 870-65	...	10 ± 2	...	17.9 ± 1.5	a	1.8	...	1			
LP 756-3	M5.5	15 ± 2	8.4 ± 3.8	17.4 ± 1.4	a	1.2	2.1	16, 1	M5-6 in source		
LP 984-92	...	8 ± 1	...	18.9 ± 2.0	a	2.4	...	1			
LP 876-10	...	7.2 ± 0.8	...	7.41 ± 0.19	a	1.0	...	1			
LP 932-83	...	14.1 ± 2.4	...	25.9 ± 4.6	r	1.8	...	8			
2MA 2306-0502	M7.5V	11.3 ± 2.0	11.1 ± 3.3	12.41 ± 0.62	r	1.1	1.1	2, 13			
LP 822-101	...	15 ± 2	...	22.7 ± 4.5	r	1.5	...	1			
2MA 2351-2537	L1	13.2 ...	31 ± 16	10	see also Table 4.14		
LP 704-15	M3V	13.2 ± 1.7	16.7 ± 5.7	7, 8	see also Table 4.14		

TABLE 4.4 (CONTINUED)

COMPARISON OF DISTANCE ESTIMATES FOR POSSIBLE NEARBY STARS

NOTES.—^aRatios are the distance from the trigonometric parallax divided by either the literature distance in the “L” column or by the spectroscopic distance in the “S” column.

^bDistance estimates from literature include photometric and spectroscopic techniques.

^cSpectroscopic distance estimates are from this work as discussed in section 4.2.2.

^dTrigonometric parallaxes are from this work as discussed in section 4.3 with the exception of LHS 2397a.

^eAn “a” in the Type column indicates that the distance is from a preliminary absolute parallax while an “r” indicates that the distance is calculated from a preliminary relative parallax.

^fBD -10°3166 was not part of the sample of possible nearby stars but is included as a possible common proper motion companion to LP 731-76.

REFERENCES.—(1) Reid *et al.* 2003; (2) Cruz *et al.* 2003; (3) Cruz & Reid 2002; (4) Reid, Kilkenny, & Cruz 2002; (5) T. D. Beaulieu 2006, private communication; (6) Scholz, Meusinger, & Jahreiß 2005; (7) Reid, Hawley, & Gizis 1995; (8) Reid & Cruz 2002; (9) Gigoyan, Hambaryan, & Azzopardi 1998; (10) Cruz, K. I. 2003, private communication; (11) Torres *et al.* 2000; (12) Butler *et al.* 2000; (13) Gizis *et al.* 2000; (14) Monet *et al.* 1992; (15) Gizis 2002; (16) Abrahamyan *et al.* 1997

are good to about 30%; using more consistent photometry would eliminate the need for Equation 4.2, which makes a large contribution to the error. Spectroscopic distances could not be estimated for the eighteen stars either with no spectral type or inadequate spectral type information. In addition, the revised distances obtained for the early L dwarfs are unreasonably large in most cases; Table 4.3 provides no examples of such cool objects so the absolute I-magnitudes were extrapolated. Although L dwarf parallaxes could have been located in the literature to improve the derived relationship between absolute I-magnitude and spectra type, an alternative color relationship was explored instead.

2MASS provides a comprehensive source of consistent infrared photometry. Therefore, J and K_s (2.16 μm) should be available for all the possible nearby stars in the proposed sample (Cohen, Wheaton, & Megeath 2003). The 117 stars in Table 4.3 with a (J-K) color were plotted against absolute I-magnitude as shown in Figure 4.4 from which no meaningful relationship was apparent.

Rather than spending additional time reviewing the literature for additional photometry or obtaining further supporting observations, T. Henry, CTIOPI program director, tentatively accepted the potential sample of forty-three stars for inclusion in CTIOPI.

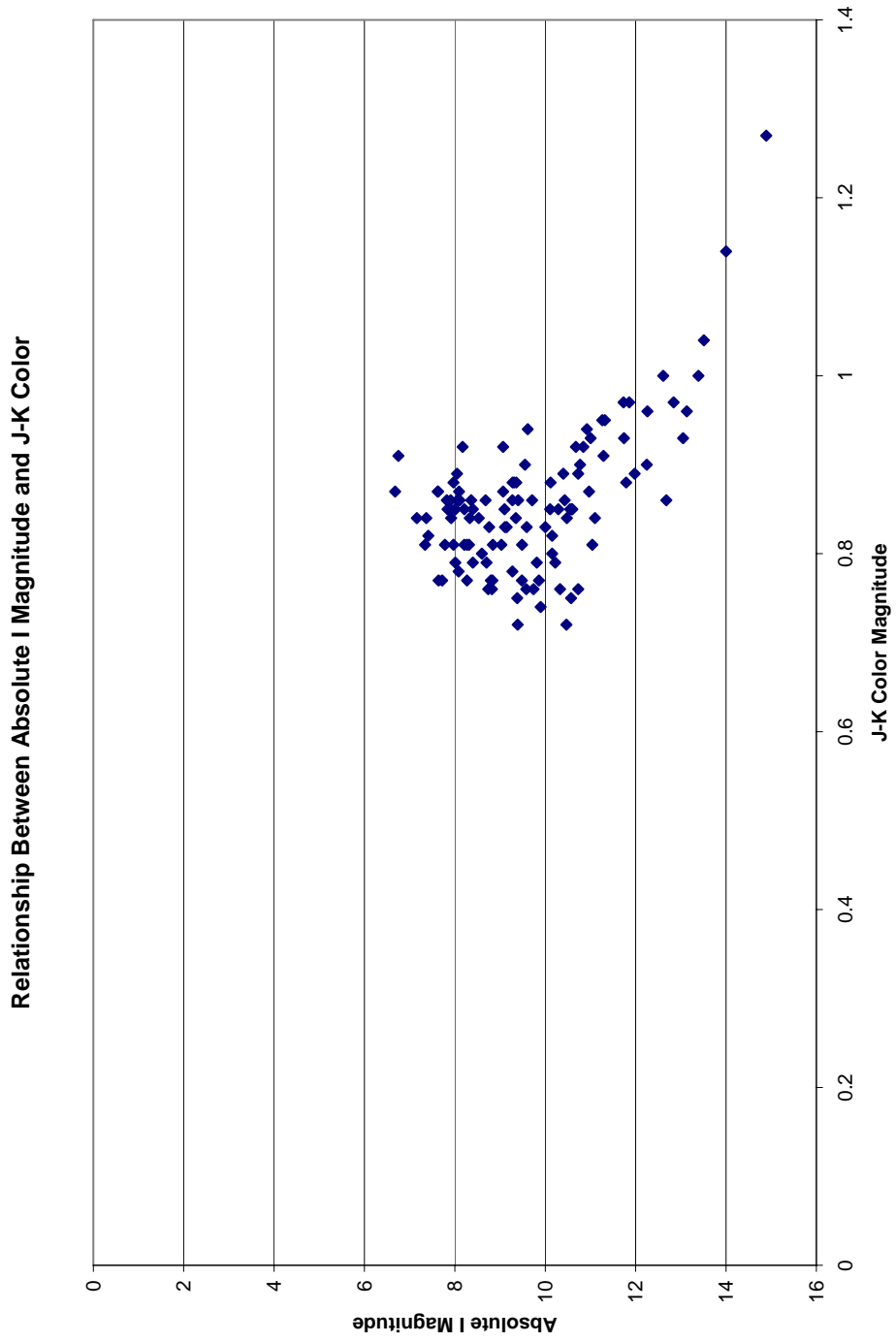


FIG. 4.4.— Absolute I-Magnitude and (J-K) Color for Known Nearby Stars. Plot is based on data in Table 4.3, which was provided by T. Henry (2003, private communication).

4.3 ASTROMETRY

Set-up and observation of the accepted CTIOPI subsample of forty-three stars began in 2003 December. Finding charts for all of the stars were prepared for use at CTIO; copies of most of them are in Appendix A. Since then, programmatic concerns have reduced the subsample to thirty-two stars that continue to be observed as of 2006 November. The number of possible nearby stars observed by CTIOPI with right ascensions between three and four hours and twelve and thirteen hours was becoming congested. To complete parallax and proper motions observations quickly, the observing list should contain no more than fourteen stars per hour of right ascension on a telescope that is available for an average of a week each month (T. Henry 2006, private communication).

CTIOPI stars are observed for a minimum of two years and, then, until the following conditions are met

- Error in relative parallax is no greater than 3 milliseconds of arc (mas)
- At least forty useable images have been processed
- Astrometric observations include at least four seasons, with each season including two or three months of observations at positive or negative parallax factor
- Photometric observations are available in V_C , R_{KC} , and I_{KC} bands.

Meeting these conditions usually requires less than 2.5 years (Jao *et al.* 2005). Although no specific requirements for coverage of the parallactic ellipse are set, the individual

reducing the astrometric data should consider the range of parallax factors represented. Because the conditions above are not yet met for any of the stars in the subsample, final parallaxes and proper motions are not yet possible. However, I undertook preliminary reductions for thirty stars in the subsample at Georgia State University in 2006 May to estimate the eventual parallaxes and proper motions. The observations utilized are summarized in Table 4.5.

The stars in this subsample were observed using the 2048x2048 Telectronix CCD camera on the 0.9-meter telescope, which has a plate scale of 401.2 ± 0.3 mas pixel⁻¹ (Jao *et al.* 2003). The central quarter of the chip is used for a 6.8 minutes of arc² field of view (Jao *et al.* 2005). The CTIOPI observing procedures are based on those established for the SPP. The observations of a possible nearby star are made with a filter selected to balance the brightness of the star of interest with potential reference stars in the field of view (Jao 2004). Bias and dome flat frames are taken each night for use in the preliminary reduction of the observations. The exposure time for each field is selected to maximize the counts in the images of the science star and the potential reference stars without saturating any stellar images. Generally, three to ten observations are made within thirty minutes of the meridian to minimize the effects of DCR (Jao *et al.* 2005).

TABLE 4.5
SUMMARY OF OBSERVATIONS USED TO MEASURE PRELIMINARY PARALLAXES AND PROPER MOTIONS

Star	Filter	Seasons ^a	# Observations ^b		Useable Frames ^c	Baseline (yr)	Reference Stars	Suggested Improvements
			Evening	Morning				
LP 991-84	V	2c+	14	22	30	1.95	7	
LHS 1363	I	2c+	8	19	22	1.87	6	
G 75-35	R	1c+	11	15	22	1.76	9	
2MA 0251-0352	I	2c+	12	7	16	1.94	9	
LP 888-18	I	2c+	6	21	25	1.86	7	better trail plate
LP 889-37	R	2s+	6	10	15	1.85	10	
LHS 5094	V	2c+	6	11	13	1.93	10	
2MA 0429-3123	R	2c+	6	16	22	1.94	11	better photometry and trail plate
LP 834-32	V	1s+	6	5	11	1.04	8	
LP 776-25	V	1c+	6	11	13	1.31	12	
2MA 0517-3349	I	2c+	12	11	22	2.26	10	
LP 717-36	V	3c	21	15	34	1.95	12	
LHS 6167	V	3c	18	22	40	2.27	9	
2MA 0921-2104	I	3c	20	8	28	2.12	9	
G 161-71	V	3c	15	9	24	2.28	9	
LP 731-76	I	2c	30	10	35	1.28	6	better photometry
BD -10°3166 ^d	I	1c+	17	5	15	1.94	5	better photometry
LHS 2783	R	3c	17	21	32	1.28	9	
LP 739-2	I	3c	9	23	29	1.92	6	
LHS 2880	R	3c	11	14	25	1.92	8	
2MA 1507-2000	I	3c	27	16	43	1.92	10	
LHS 3056	V	3s	20	20	36	1.93	6	better photometry
2MA 1534-1418	I	3s	17	21	37	1.93	11	better trail plate

TABLE 4.5 (CONTINUED)
SUMMARY OF OBSERVATIONS USED TO MEASURE PRELIMINARY PARALLAXES AND PROPER MOTIONS

Star	Filter	Seasons ^a	# Observations ^b		Useable Frames ^c	Baseline (yr)	Reference Stars	Suggested Improvements
			Evening	Morning				
LP 869-19	R	3c	26	20	40	1.81	10	better trail plate
LP 869-26	I	3c	37	13	37	1.79	11	
LP 870-65	R	3c	22	5	24	1.80	9	get morning observations
LP 756-3	R	3c	14	11	25	1.79	10	
LP 984-92	R	2c+	6	18	22	1.96	6	
LP 876-10	V	3c+	11	21	31	2.43	7	
LP 932-83	V	2c+	6	17	22	1.68	7	
2MA 2306-0502 ^e	I	2c	6	11	17	0.98	11	better trail plate
LP 822-101	V	2c+	16	19	29	1.68	9	

NOTES.—^aSeasons indicates the number of observing seasons during which the star was observed; each season may contain 2–3 months. A “c” indicates that the observations were continuous during most seasons while an “s” indicates that only scattered observations were available. A plus sign (+) indicates that images were used from “seasons” during which fewer than four observations were available; “seasons” with so few exposures are not included in the count.

^bNumber of Observations indicates the number of morning and evening frames taken for astrometric purposes, some of which may not have been excluded from the reduction due to poor quality.

^cUseable Frames is the total number of frames used in this analysis, including all astrometric observations of adequate quality possibly supplemented by frames taken for other purposes.

^dBD -10°3166 was not part of the sample of possible nearby stars but is included as a possible common proper motion companion to LP 731-76.

^eThe CTIOPI 1.5-meter program recently finalized a parallax for this star using 45 frames over 3.3 years with 18 reference stars (Costa *et al.* 2006)

The preliminary reductions followed the methodology outlined in Jao *et al.* (2005) and described in greater detail in Jao (2004). Five to fifteen reference stars surrounding the star for which the parallax and proper motion are to be measured were selected based on their photometry, shape (ellipticity less than 0.2), and brightness. A small ellipticity throughout the frame indicates that the guiding was adequate during the exposure; a small ellipticity for individual stars helps eliminate close double stars and background galaxies. Source-Extractor (Bertin & Arnouts 1996; hereafter SExtractor) determined the centroids for each star of interest in every frame; this software was designed to produce a list of detected objects from an astronomical image.

The coordinates for the possible nearby star were obtained from 2MASS and adjusted to epoch 2000.0 using published proper motions (Jao 2004), as shown in Table 4.6. When no proper motions were available from literature, 2MASS coordinates were used directly until a preliminary proper motion was calculated based on CTIOPI observations. Then, the preliminary proper motion was used to update the coordinates that were used in turn to re-reduce the region. The coordinates in Table 4.1 are updated in this manner for those stars with preliminary relative parallaxes and proper motions. The coordinates and observation times were used to calculate parallax factors and hour angles.

TABLE 4.6
 PROPER MOTIONS FOR POSSIBLE NEARBY STARS

Star	From Literature		Preliminary Results		Reference	Comment
	Proper Motion ^a (mas yr ⁻¹)	Position Angle (deg.)	Proper Motion (mas yr ⁻¹)	Position Angle (deg.)		
LP 991-84	279 ± 25 ^a	150 ...	258.7 ± 5.8	151.2 ± 2.5	1	
LHS 1363	540 ± 25 ^b	106.4 ...	531.8 ± 5.5	107.5 ± 1.1	2	
G 75-35	377 ± 27 ^c	106.0 ± 4.5 ^c	355.0 ± 8.8	96.5 ± 2.2	3	
2MA 0251-0352	2,185 ± 57.0	149.300 ...	2,153.7 ± 8.6	149.40 ± 0.44	4	initial reduction updated position
LP 888-18	425 ± 25 ^a	175 ...	407.5 ± 5.6	171.9 ± 1.2	1	
LP 889-37	26 ± 25 ^a	195 ...	261.6 ± 8.9	176.7 ± 2.9	1	
LHS 5094	560 ± 100	176.8 ± 5	480.5 ± 9.4	188.2 ± 1.8	2	
2MA 0429-3123	132.7 ± 5.9	40.0 ± 5.1		initial reduction updated position
LP 834-32	205 ± 25 ^a	158 ...	203 ± 11	161.9 ± 5.4	1	
LP 655-43	198 ± 25 ^a	204	1	dropped from CTIOPI
LP 716-10	386 ± 25 ^a	238	1	dropped from CTIOPI
LP 776-25	256 ± 25 ^a	254 ...	243 ± 15	149.1 ± 6.4	1	
2MA 0517-3349	545.6 ± 13.2	125.09 ...	526.1 ± 6.1	125.5 ± 1.3	5	
LP 717-36	186 ± 25 ^a	167 ...	194.5 ± 4.3	168.0 ± 2.1	1	
LHS 2024	660 ± 25 ^b	241.4	2	dropped from CTIOPI
LHS 6167	459 ± 25 ^b	244.3 ...	446.1 ± 2.6	244.20 ± 0.62	2	
2MA 0921-2104	965 ± 16.0	162.600 ...	940.5 ± 2.8	164.1 ± 0.30	4	
G 161-71	347 ± 27 ^c	270.7 ± 4.5 ^c	334.1 ± 2.2	276.10 ± 0.64	3	
LP 671-8	451 ± 27 ^c	199.2 ± 4.5 ^c	3	dropped from CTIOPI

TABLE 4.6 (CONTINUED)
 PROPER MOTIONS FOR POSSIBLE NEARBY STARS

Star	From Literature				Preliminary Results				Reference	Comment
	Proper Motion ^a (mas yr ⁻¹)		Position Angle (deg.)		Proper Motion (mas yr ⁻¹)		Position Angle (deg.)			
LP 991-84	279	± 25 ^a	150	...	258.7 ± 5.8	151.2 ± 2.5	1			
LP 731-76	203	± 25 ^a	250	...	218.1 ± 4.5	244.5 ± 2.2	1	initial reduction updated position		
BD -10°3166 ^d	203	± 25 ^a	250	...	184 ± 19	272 ± 8.6				
LHS 2397a	513.4 ± 7.8	263.8 ± 0.9	6	dropped and then reinstated		
2MA 1155-3727	868 ± 39.0	172.500	4	dropped from CTIOPI		
LP 734-34	420.0 ± 5.5	144.68 ± 0.75	7	dropped from CTIOPI		
LP 615-149	308 ± 27 ^c	271.1 ± 4.5 ^c	3	dropped from CTIOPI		
LHS 5226	500 ± 25 ^b	253.3	2	dropped from CTIOPI		
CE 303	376 ± 2	179 ± 1	8	dropped from CTIOPI		
LHS 2783	510 ± 25 ^b	91.5	518.5 ± 5.4	267.20 ± 0.90	2			
LP 739-2	350 ± 25 ^a	278	339.3 ± 4.2	276.7 ± 1.1	1			
LHS 2880	758 ± 25 ^b	237.1	718.1 ± 4.8	236.90 ± 0.75	2			
2MA 1507-2000	125.8 ± 4.0	124.2 ± 3.5		initial reduction updated position		
LHS 3056	680 ± 100	245.7 ± 5	771.5 ± 2.7	258.50 ± 0.32	2			
2MA 1534-1418	966.5 ± 2.9	251.20 ± 0.32		initial reduction updated position		
LP 869-19	260 ± 25 ^a	163	254.4 ± 4.9	163.1 ± 1.9	1			
LP 869-26	347 ± 25 ^a	118	347.2 ± 5.1	117.1 ± 1.6	1			
LP 870-65	333 ± 25 ^a	165	360.5 ± 5.4	161.8 ± 1.6	1			
LP 756-3	353 ± 25 ^a	99	348.9 ± 5.1	102.0 ± 1.6	1			

TABLE 4.6 (CONTINUED)
 PROPER MOTIONS FOR POSSIBLE NEARBY STARS

Star	From Literature			Preliminary Results			Reference	Comment
	Proper Motion ^a (mas yr ⁻¹)	Position Angle (deg.)		Proper Motion (mas yr ⁻¹)	Position Angle (deg.)			
LP 991-84	279 ± 25 ^a	150	...	258.7 ± 5.8	151.2 ± 2.5		1	
LP 984-92	206 ± 25 ^a	120	...	221.0 ± 6.3	123.0 ± 3.2		1	
LP 876-10	355 ± 25 ^a	120	...	369.5 ± 4.7	117.3 ± 1.4		1	
LP 932-83	289 ± 25 ^a	216	...	303.2 ± 7.9	220.9 ± 3.0		1	
2MA 2306-0502	1,042 ± 25.0	119.700	...	1,035.6 ± 8.1	117.90 ± 0.87		4	
LP 822-101	344 ± 25 ^a	139	...	349.7 ± 1.3	142.5 ± 4.1		1	
2MA 2351-2537	4,203.0 ± 20.9	60.44		5	dropped from CTIOPI
LP 704-15	203 ± 27 ^c	85.5	4.5 ^c		3	dropped from CTIOPI

NOTES.—^aProper motion errors for (1) are estimated from (9).

^bProper motion in (2) is based on (1) and so the error is estimated from (9).

^cProper motion errors for (3) are estimated from (10).

^dBD -10°3166 was not part of the sample of possible nearby stars but is included as a possible common proper motion companion to LP 731-76.

REFERENCES.—(1) *NLTT*; (2) Bakos, Sahu, & Nemeth 2002; (3) Giclas, Burnham, & Thomas 1978; (4) Deacon, Hambly & Cooke 2005; (5) Pokorny *et al.* 2004; (6) Tinney 1996; (7) Salim & Gould 2003; (8) Lodiou *et al.* 2005; (9) Gould & Salim 2003; (10) Giclas 1966

A high-quality frame taken close to the meridian was selected based on the shape and brightness of the stellar images to serve as the “trail plate” (Jao *et al.* 2005). First, the trail plate was rotated to align with *The Guide Star Catalog, Version 2.2* (STScI & OAT 2001). Then, all the other frames were reduced with respect to the rotated trail plate; consequently, careful selection of an appropriate trail plate is essential. If photometry was available for the reference frames during the astrometric reduction, then DCR corrections were made for the parallax star and its reference stars (Jao *et al.* 2005). For those stars without photometry, DCR corrections could not be included in the preliminary reduction. However, photometry will be obtained so that DCR corrections will be included in the calculations of final parallaxes and proper motions.

GaussFit¹³ (Jefferys *et al.* 1987; hereafter GaussFit), a program for astrometric modeling using both least-squares and robust estimation approaches, calculated the preliminary relative parallax and proper motion of each possible nearby star. It used a standard three plate-constant model, with scale, orientation, and origin terms. The small parallactic shifts and proper motions of the reference stars can affect the calculation of the plate constants. GaussFit assumed that both of these motions summed to zero over the reference frame (Jao *et al.* 2005).

After GaussFit calculated the preliminary parallax and proper motion, the quality of the solution was assessed. For many fields, only a few observations at a limited number of epochs were available so large errors in parallax and proper motion

¹³GaussFit is available at <ftp://clyde.as.utexas.edu/pub/gaussfit>

were expected. The errors in these values along with the mean errors of unit weight are reviewed along with a number of factors that can contribute to the quality of the results. The distribution of hour angles and range of seeing at which individual observations were made was considered. Keeping the hour angles as small as possible reduces the DCR effects. However, to obtain sufficient frames for preliminary parallaxes, some set-up and photometry images taken at large hour angles were used. The parallax reduction pipeline rejects frames with seeing worse than 2.5 seconds of arc ("). Although the seeing at CTIO is generally good, it is rarely so good that a lower limit must be specified. The range of parallax factors sampled by the observations is considered. The difference between calculated and measured positions, or residuals, is reviewed in each coordinate for individual observations of the possible nearby star and its reference stars. Figure 4.5 summarizes this information for LP 876-10, the star with the largest preliminary parallax in this subsample. If individual frames or reference stars appear to have a significant negative effect on the overall result, they can be removed and a new preliminary parallax and proper motion calculated. Because of the preliminary nature of the astrometric reductions reported herein, most frames and reference stars were retained. Once all of these factors appear reasonable, the preliminary relative parallax is complete.

If photometry was available for a region, then the correction to absolute was also calculated. Before any parallax is finalized, photometry is obtained. Therefore, the final relative parallaxes will all be corrected to absolute values.

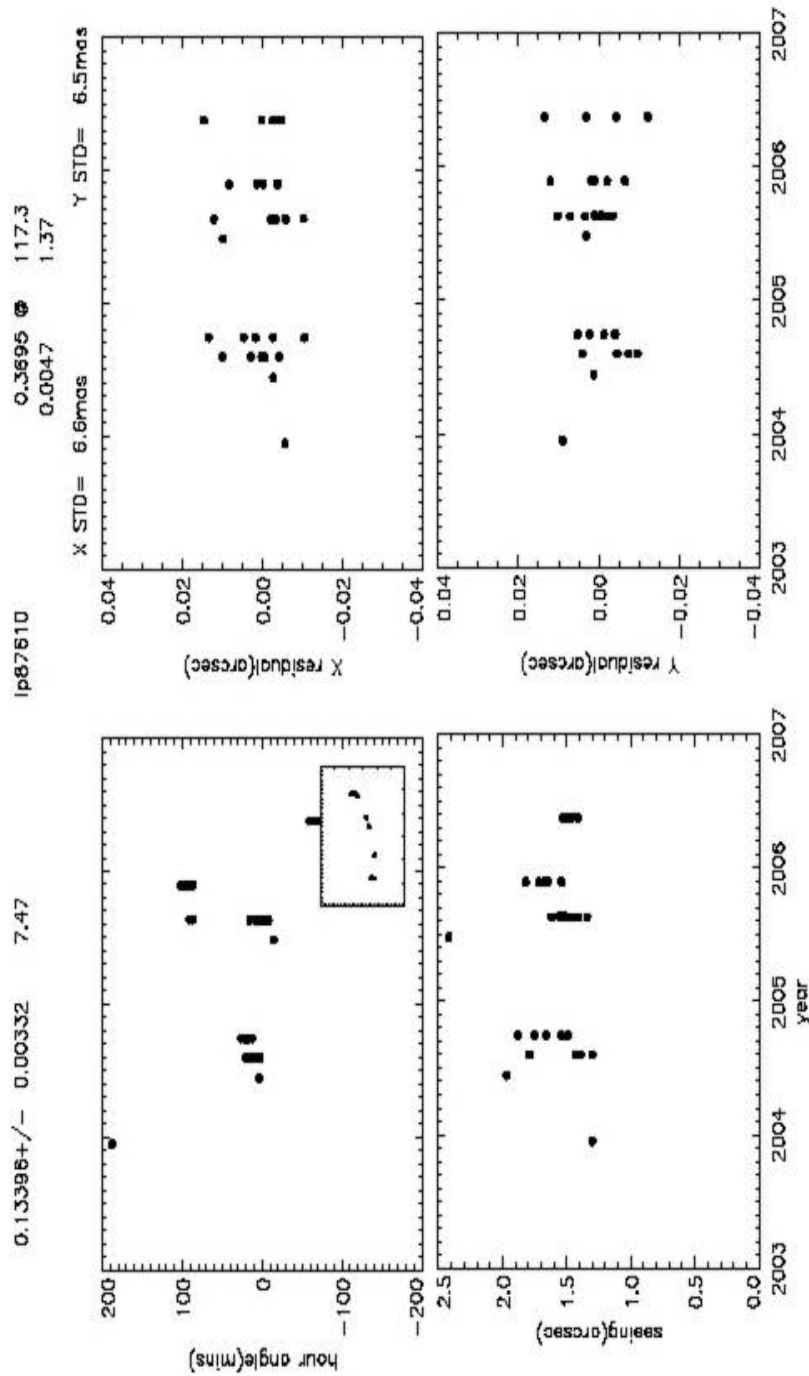


FIG. 4.5.— Preliminary Relative Parallax Reduction for LP 876-010. The upper-left values are parallax with associated error in seconds of arc and corresponding distance in parsecs. The upper-right values are proper motions in seconds of arc per year, followed by the position angle in degrees. The associated errors appear directly below the corresponding value. The upper-left plot shows the hour angle for each observation. The insert box shows the range of parallax factors sampled. The lower-left plot shows the seeing conditions for each observation. The upper and lower plots on the right show the range of residuals in the x- (right ascension) and y- (declination) coordinates respectively. The standard deviations appear above the x-residual plot.

Table 4.7 summarizes the preliminary parallax results for thirty-one stars in the subsample plus BD -10°3166. Additional notes on selected individual stars follow in sections 4.3.1 and 4.3.2 *infra*. For stars with parallaxes (π in seconds of arc), the tangential velocity (v_t) in kilometers second⁻¹ (km s⁻¹) can be calculated using

$$v_t = \frac{4.74\mu}{\pi} \quad (4.4)$$

where μ is the total proper motion in seconds of arc year⁻¹. Table 4.8 lists the tangential velocities calculated for stars in this subsample, including BD -10°3166.

4.3.1 Stars with Preliminary Absolute Parallaxes

Preliminary absolute parallaxes have been measured for fifteen stars in this subsample, plus BD -10°3166, as shown in Table 4.7. Of these sixteen stars, all but two (BD -10°3166 and LHS 2880) have formal distances that place them within the solar neighborhood. Two stars (LHS 6167 and LP 876-10) appear to be within 10 pc. Another six had photometric or spectroscopic distance estimates that placed them within 10 pc of the Sun but the preliminary absolute parallaxes place them at greater distances; all of these are discussed in 4.6.9.

High proper motions are frequently associated with nearby stars. As shown in Table 4.6, all but three of these stars have a preliminary proper motion greater than 200 mas year⁻¹ (yr⁻¹), including four with proper motions greater than 500 mas yr⁻¹. The tangential velocities range from 9.53 to 88.0 km s⁻¹, including three faster than 50 km s⁻¹.

TABLE 4.7
PRELIMINARY PARALLAXES FOR POSSIBLE NEARBY STARS

Star	Baseline (yr)	Relative Parallax (mas)	Correction (mas)	Absolute Parallax (mas)	Standard Error X (mas)	Unit Weight Y (mas)	Comment
LP 991-84	1.95	115.7 ± 3.1	9.8	8.8	
LHS 1363	1.87	80.5 ± 3.7	8.1	5.3	
G 75-35	1.76	84.5 ± 3.7	6.7	5.0	
2MA 0251-0352	1.94	79.0 ± 6.8	15.1	17.4	
LP 888-18	1.86	74.4 ± 3.7	6.5	6.3	
LP 889-37	1.85	59.2 ± 5.2	7.7	5.8	
LHS 5094	1.93	71.2 ± 4.9	2.7	5.6	
2MA 0429-3123	1.94	65.8 ± 3.7	0.230 ± 0.050	66.0 ± 3.7	7.4	6.7	
LP 834-32	1.04	60.5 ± 4.7	3.3	3.6	
LP 776-25	1.31	71.0 ± 9.7	4.0	10.2	
2MA 0517-3349	2.26	57.2 ± 4.0	1.340 ± 0.050	58.6 ± 4.0	9.6	8.1	
LP 717-36	1.95	54.5 ± 3.3	5.2	5.6	
LHS 6167	2.27	101.7 ± 2.8	1.09 ± 0.16	102.8 ± 2.8	5.9	5.8	
2MA 0921-2104	2.12	87.1 ± 2.6	9.5	8.8	
G 161-71	2.28	69.7 ± 2.7	0.880 ± 0.060	70.6 ± 2.7	3.5	4.1	
LP 731-76	1.28	66.8 ± 2.4	2.54 ± 0.55	69.4 ± 2.5	4.4	6.2	
BD -10°3166 ^a	1.94	17.3 ± 7.3	2.63 ± 0.66	19.9 ± 7.3	7.6	10.9	
LHS 2783	1.28	51.1 ± 2.9	6.6	6.8	
LP 739-2	1.92	57.9 ± 3.5	4.4	4.2	

TABLE 4.7 (CONTINUED)
PRELIMINARY PARALLAXES FOR POSSIBLE NEARBY STARS

Star	Baseline (yr)	Relative Parallax (mas)	Correction (mas)	Absolute Parallax (mas)	Standard Error X (mas)	Unit Weight Y (mas)	Comment
LHS 2880	1.92	37.7 ± 3.0	0.960 ± 0.080	38.7 ± 3.0	7.2	12.8	
2MA 1507-2000	1.92	43.1 ± 3.1	0.740 ± 0.090	43.8 ± 3.1	7.9	8.8	
LHS 3056	1.93	51.0 ± 1.9	1.36 ± 0.11	52.4 ± 1.9	3.3	6.2	
2MA 1534-1418	1.93	88.4 ± 2.2	1.75 ± 0.19	90.2 ± 2.2	6.6	5.1	
LP 869-19	1.81	51.9 ± 3.0	2.57 ± 0.16	54.4 ± 3.0	7.9	9.6	
LP 869-26	1.79	69.9 ± 3.3	1.630 ± 0.070	71.6 ± 3.3	6.8	5.0	
LP 870-65	1.80	53.6 ± 4.3	2.36 ± 0.30	55.9 ± 4.3	10.9	5.9	
LP 756-3	1.79	56.1 ± 4.4	1.43 ± 0.12	57.5 ± 4.4	4.3	6.8	
LP 984-92	1.96	51.6 ± 5.1	1.20 ± 0.12	52.8 ± 5.1	4.6	7.1	faint reference stars
LP 876-10	2.43	134.0 ± 3.3	0.96 ± 0.19	134.9 ± 3.3	6.6	6.5	
LP 932-83	1.68	38.6 ± 5.8	9.1	6.6	
2MA 2306-0502 ^b	0.98	80.6 ± 3.9	4.1	5.6	
LP 822-101	1.68	44.1 ± 7.3	12.8	10.7	

NOTES.—^aBD -10°3166 was not part of the sample of possible nearby stars but is included as a possible common proper motion companion to LP 731-76.

^bThe CTIOPI 1.5-meter program measured an absolute parallax of 82.6 ± 2.6 mas (12.11 ± 0.39 pc) over 3.3 years (Costa *et al.* 2006).

TABLE 4.8
PRELIMINARY TANGENTIAL VELOCITIES FOR POSSIBLE NEARBY STARS

Star	Parallax (mas)	Type ^a	Proper Motion (mas yr ⁻¹)	Position Angle (deg)	Tangential Velocity (km s ⁻¹)
LP 991-084	115.7 ± 3.1	r	258.7 ± 5.8	151.2 ± 2.5	10.60 ± 11
LHS 1363	80.5 ± 3.7	r	531.8 ± 5.5	107.5 ± 1.1	31.3 ± 1.3
G 75-35	84.5 ± 3.7	r	355.0 ± 8.8	96.5 ± 2.2	19.91 ± 2.0
2MA 0251-0352	79.0 ± 6.8	r	2153.7 ± 8.6	149.40 ± 0.44	129 ± 2.3
LP 888-18	74.4 ± 3.7	r	407.5 ± 5.6	171.9 ± 1.2	26.0 ± 0.68
LP 889-37	59.2 ± 5.2	r	261.6 ± 8.9	176.7 ± 2.9	20.9 ± 1.5
LHS 5094	71.2 ± 4.9	r	480.5 ± 9.4	188.2 ± 1.8	32.0 ± 2.4
2MA 0429-3123	66.0 ± 3.7	a	132.7 ± 5.9	40.0 ± 5.1	9.53 ± 3.0
LP 834-32	60.5 ± 4.7	r	203 ± 11	161.9 ± 5.4	15.9 ± 1.1
LP 776-25	71.0 ± 9.7	r	243 ± 15	149.1 ± 6.4	16.2 ± 0.58
2MA 0517-3349	58.6 ± 4.0	a	526.1 ± 6.1	125.5 ± 1.3	42.6 ± 1.5
LP 717-36	54.5 ± 3.3	r	194.5 ± 4.3	168.0 ± 2.1	16.9 ± 0.87
LHS 6167	102.8 ± 2.8	a	446.1 ± 2.6	244.20 ± 0.62	20.57 ± 0.61
2MA 0921-2104	87.1 ± 2.6	r	940.5 ± 2.8	164.10 ± 0.30	51.2 ± 17
G 161-71	70.6 ± 2.7	a	334.1 ± 2.2	276.10 ± 0.64	22.43 ± 2.8
LP 731-76	69.4 ± 2.5	a	218.1 ± 4.5	244.5 ± 2.2	14.91 ± 1.7
BD -10°3166 ^b	19.9 ± 7.3	a	184 ± 19	272.5 ± 8.6	44 ± 6.8
LHS 2783	51.1 ± 2.9	r	518.5 ± 5.4	267.20 ± 0.90	48.1 ± 1.0
LP 739-002	57.9 ± 3.5	r	339.3 ± 4.2	276.7 ± 1.1	27.8 ± 2.5
LHS 2880	38.7 ± 3.0	a	718.1 ± 4.8	236.90 ± 0.75	88.0 ± 1.3

TABLE 4.8 (CONTINUED)
PRELIMINARY TANGENTIAL VELOCITIES FOR POSSIBLE NEARBY STARS

Star	Parallax (mas)	Type ^a	Proper Motion (mas yr ⁻¹)	Position Angle (deg)	Tangential Velocity (km s ⁻¹)
2MA 1507-2000	43.8 ± 3.1	a	125.8 ± 4.0	124.2 ± 3.5	13.6 ± 1.3
LHS 3056	52.4 ± 1.9	a	771.5 ± 2.7	258.50 ± 0.32	69.8 ± 1.1
2MA 1534-1418	90.2 ± 2.2	a	966.5 ± 2.9	251.20 ± 0.32	50.8 ± 2.4
LP 869-19	54.4 ± 3.0	a	254.4 ± 4.9	163.1 ± 1.9	22.2 ± 2.2
LP 869-26	71.6 ± 3.3	a	347.2 ± 5.1	117.1 ± 1.6	23.0 ± 2.0
LP 870-65	55.9 ± 4.3	a	360.5 ± 5.4	161.8 ± 1.6	30.5 ± 0.36
LP 756-3	57.5 ± 4.4	a	348.9 ± 5.1	102.0 ± 1.6	28.8 ± 5.7
LP 984-92	52.8 ± 5.1	a	221.0 ± 6.3	123.0 ± 3.2	19.8 ± 3.0
LP 876-10	134.9 ± 3.3	a	369.5 ± 4.7	117.3 ± 1.4	12.98 ± 6.4
LP 932-83	38.6 ± 5.8	r	303.2 ± 7.9	220.9 ± 3.0	37.2 ± 11
2MA 2306-0502 ^c	80.6 ± 3.9	r	1035.6 ± 8.1	117.90 ± 0.87	60.9 ± 1.3
LP 822-101	44.1 ± 7.3	r	350 ± 13	142.5 ± 4.1	37.6 ± 2.0

NOTE.—^aAn “a” in the Type column indicates that the distance is from a preliminary absolute parallax while an “r” indicates that the distance is calculated from a preliminary relative parallax.

^bBD -10°3166 was not part of the sample of possible nearby stars but is included as a possible common proper motion companion to LP 731-76.

Additional comments on six stars, for which absolute parallaxes have been measured, that display interesting characteristics or for which further questions remain follow. Section 4.3.2 discusses six additional stars with relative parallax of that also merit further comment.

4.3.1.1 2MA 0517-3349

2MA 0517-3349 is a high proper motion star. The CTIOPI preliminary proper motion of 526.1 ± 6.1 mas yr⁻¹ in $125.5 \pm 1.3^\circ$ is a little slower than an earlier measurement of 576 mas yr⁻¹ in 126.39° with a possible proper motion error of $7\text{--}29$ mas yr⁻¹ (Phan-Bao *et al.* 2003). At a distance of 17.1 ± 1.3 pc, it has a tangential velocity of 42.6 ± 3.0 km s⁻¹. Two more seasons will probably be needed finalize the parallax and proper motion.

4.3.1.2 LHS 6167

The second nearest star for which an absolute parallax was obtained, LHS 6167, has a preliminary absolute parallax of 102.8 ± 2.8 mas, which corresponds to a distance of 9.73 ± 0.28 pc; it is confirmed as a nearby star and is a possible new member of the 10-pc sample. The photometric distance estimate by Reid, Kilkenny, and Cruz (2002) placed it even closer, 6.7 ± 0.5 pc. Because the ratio of the parallactic to photometric distance is 1.5, this star may be a close binary and is discussed further in 4.6.9. Another season of observations should be sufficient to finalize this parallax.

4.3.1.3 BD -10°3166

BD -10°3166 was not initially a member of the subsample, but a preliminary parallax was calculated because the *New Luyten Two-Tenths Catalogue* (Luyten 1980, *NLTT*) identified it as a common proper motion pair with a member of this subsample,

LP 731-76. The preliminary absolute parallax 19.9 ± 7.3 mas indicates that this star lies well outside the solar neighborhood at a distance of 50 ± 29 pc. The parallax is based on fifteen observations primarily within one season. Consequently, the error is large enough that it may still be a nearby star. Several more seasons of observations and improved photometry are required before a final parallax will be achieved for this star. It is discussed further in 4.6.2.

4.3.1.4 LHS 2880

LHS 2880 has the smallest preliminary parallax, relative or absolute, of any possible nearby star in this subsample. Its preliminary absolute parallax of 38.7 ± 3.0 mas corresponds to a distance of 25.8 ± 2.2 pc, which places it outside the solar neighborhood. However, the associated error is large enough that it may still be a nearby star. The photometric distance estimate by Reid, Kilkenny, and Cruz (2002) places it within 10 pc, 9.8 ± 0.7 pc, while the spectroscopic distance estimate described in 4.2.2 places it at 11.2 ± 4.0 pc. Because of the large discrepancy between the current parallactic and the other distance estimates, the possibility that it is a close binary is discussed in 4.6.9. Two more seasons of observations may be required to finalize this parallax.

4.3.1.5 2MA 1534-1418

2MA 1534-1418 is a new high proper motion star with a preliminary proper motion of 966.5 ± 2.9 mas yr⁻¹ in $251.2 \pm 0.32^\circ$. At a distance of 11.09 ± 0.28 pc, it has a tangential velocity of 50.8 ± 1.3 km s⁻¹. One more season should be sufficient to finalize the parallax and proper motion.

4.3.1.6 LP 876-10

LP 876-10 appears to be the nearest star in the subsample. It displays the largest preliminary parallax, relative or absolute, of any star in this subsample. Its preliminary absolute parallax of 134.9 ± 3.3 mas corresponds to a distance of 7.41 ± 0.19 pc. Thus, it is confirmed as a nearby star and a new member of the 10-pc sample. Another season of observations should be sufficient to finalize this parallax.

4.3.2 Stars with Preliminary Relative Parallaxes

Preliminary relative parallaxes are available for another sixteen stars in this subsample, as shown in Table 4.7. Of these, all but LP 932-83 have formal distances that place them within the solar neighborhood. LP 991-84 appears to be within 10 pc. Another, LHS 1363, had a spectroscopic distance estimate that placed it within 10 pc of the Sun but its preliminary relative parallax places it at a greater distance.

All but one of the possible nearby stars with only preliminary relative parallaxes also could be considered high proper motion stars because their proper motions are greater than 200 mas yr^{-1} . As shown in Table 4.6, five of these stars also have a preliminary proper motion greater than 500 mas yr^{-1} , including two with proper motions greater than $1'' \text{ yr}^{-1}$. The tangential velocities range from 10.60 to 129 km s^{-1} , including two between 50 and 100 km s^{-1} .

4.3.2.1 LP 991-84

LP 991-84 has the second largest preliminary relative parallax, 115.7 ± 3.1 mas, which corresponds to a distance of 8.64 ± 0.24 pc. It is confirmed as a nearby star and a new member of the 10-pc sample. Two more seasons plus photometry are probably necessary in order to finalize this parallax.

4.3.2.2 LHS 1363

The distances for LHS 1363 listed in Table 4.4 range from 9.8 to 12.42 pc. Although the spectroscopic distance estimated in 4.2.2 places LHS 1363 within the 10-pc sample, the preliminary relative parallax of 80.5 ± 3.7 mas indicates otherwise. The parallactic distance falls within the errors of the spectroscopic distance estimate. At least two seasons plus photometry are required to finalize this parallax.

4.3.2.3 2MA 0251-0352

2MA 0251-0352 is interesting because it has the highest preliminary proper motion in this subsample. The CTIOPI preliminary proper motion of $2.1537 \pm 0.0086''$ yr^{-1} in $149.4 \pm 0.44^\circ$ agrees with the measurement of $2.185 \pm 0.057''$ yr^{-1} in 149.300° (Deacon, Hambly, & Cooke 2005). At a distance of 12.7 ± 1.2 pc, it has a tangential velocity of 129 ± 11 km s^{-1} , which is also the highest in this subsample. Three more seasons plus photometry may be required to finalize the parallax and proper motion.

4.3.2.4 2MA 0921-2104

2MA 0921-2104 is another high proper motion star. The CTIOPI preliminary proper motion of 940.5 ± 2.8 mas yr^{-1} in $164.1 \pm 0.30^\circ$ is slightly lower than the measurement of 965 ± 16 mas yr^{-1} in 162.600° last year (Deacon, Hambly, & Cooke 2005). At a distance of 11.48 ± 0.35 pc, it has a tangential velocity of 51.2 ± 1.5 km s^{-1} . Two more seasons plus photometry may be required to finalize the parallax and proper motion.

4.3.2.5 LP 932-83

LP 932-83 has one of the smallest preliminary relative parallaxes, 38.6 ± 5.8 mas, which corresponds to a distance of 25.9 ± 4.6 pc. It is probably not a member of

the solar neighborhood. However, its error is large enough that it may still be a nearby star. Reid and Cruz (2002) estimated that it was only 14.1 ± 2.4 pc away. Because the ratio of the parallactic distance to spectroscopic distance is 1.8, the possibility that it is a close binary is discussed in 4.6.9. In addition, the *LDS Catalogue* (Luyten 1987; hereafter *LDS*) identifies it as a common proper motion pair with LTT 9210; this possibility is discussed further in 4.6.7. Another season of observations plus additional photometry should be sufficient to finalize this parallax.

4.3.2.6 2MA 2306-0502

2MA 2306-0502 is another high proper motion star. At the 0.9-meter telescope, CTIOPI measured a preliminary proper motion of $1.0356 \pm 0.0081'' \text{ yr}^{-1}$ in $117.9 \pm 0.87^\circ$, which is in agreement with both the value of $1.0358 \pm 0.0018'' \text{ yr}^{-1}$ in $117.1 \pm 0.19^\circ$ obtained by the CTIOPI 1.5-meter program (Costa *et al.* 2006) and the measurement of $1.042 \pm 0.025'' \text{ yr}^{-1}$ in 119.700° made by Deacon, Hambly, and Cooke (2005). At a distance of 12.41 ± 0.62 pc, it has a tangential velocity of $60.9 \pm 3.0 \text{ km s}^{-1}$. Three more seasons plus photometry may be required to finalize the parallax and proper motion.

4.3.3 Dropped Stars

During the course of observations, eleven stars in the subsample were dropped from the astrometric program. Of these, LHS 2397a is now being actively observed and is discussed below. Table 4.9 summarizes the observational status of the other stars and their standing as nearby stars is revisited in section 4.5. A rough preliminary parallax was calculated for LP 834-32 using only eleven frames. If the quality of the available frames for LHS 2024, 2MA 2351-2537, and LP 704-15 is adequate, similar rough

parallaxes might be calculated for these regions as well. The resulting distance estimates would be the best indicator of whether to resume observations in the future.

TABLE 4.9
ASTROMETRIC OBSERVATIONS OF DROPPED STARS

Star	# Observations		Started	Comment
	Eve.	Morn.		
LP 655-43	1	0	2003 Dec	
LP 716-10	1	0	2003 Dec	
LHS 2024	5	4	2003 Dec	rough preliminary parallax possible
LP 671-8	0	0		not set-up
2MA 1155-3727	0	0		not set-up
LP 734-34	0	0		not set-up
LP 615-149	0	0		not set-up
LHS 5226	0	0		not set-up
CE 303	0	0		not set-up
2MA 2351-2537	9	3	2004 Aug	rough preliminary parallax possible
LP 704-15	2	5	2003 Dec	rough preliminary parallax possible

NOTE.—Rough preliminary parallax calculated for LP 834-32 used only eleven frames.

LHS 2397a was initially included in this CTIOPI subsample. The SPP observed it previously, but the Siding Spring observations are too sparse for the measurement of a parallax and proper motion. Additional review of the literature revealed an earlier absolute trigonometric parallax of 70 ± 2 mas (Monet *et al.* 1992), which puts it at a distance of 14.3 ± 0.4 pc and establishes it as a proven member of the nearby star sample. In addition, further review of the literature produced a V_{JM} magnitude of 18.3 ± 0.2 (Salim & Gould 2003). Either datum would have excluded this star from this subsample. During a periodic pruning of the CTIOPI observing list, it was dropped without having been set-up because it was too faint for easy observation (T. Henry

2006, private communication). However, Freed, Close, & Siegler (2003) resolved it into two components.

On further consideration, such very low-mass binary within 20 pc is an important system for the RECONS Masses and Stellar Systems with Interferometry (MASSIF) program, which seeks to improve the mass-luminosity relationship at both ends of the main sequence (Henry 2004). From models, the mass of LHS 2397aB, the brown dwarf companion, was estimated to be 0.061–0.069 solar mass units (M_{\odot}) (Freed, Close, & Siegler 2003); currently the lowest dynamically determined mass is $0.074 \pm 0.005 M_{\odot}$ for GJ 1245 (Henry 2004). Therefore, LHS 2397a was re-instated to CTIOPI and observations began in 2005 February. As of 2006 August 16, nineteen evening and twelve morning frames have been collected so a preliminary parallax would be possible. In addition, recent CTIOPI joint photometry indicates that the system has an I_{KC} equal to 14.86 ± 0.02 mag, which is brighter than the I-band selection limit of sixteenth magnitude.

4.4 PHOTOMETRY

Because V_J , R_{KC} , and I_{KC} photometry is used both to correct for DCR and to convert relative parallaxes to absolute ones, all stars on the astrometry observing program are also photometric targets. Final photometry is best with at least three independent observations. As of 2006 July 20, final photometry is available for three stars, as listed in Table 4.10 along with fourteen other stars that have at least one night of photometric observations. The algorithms used for DCR correction and reduction to absolute are not very sensitive to small errors in photometry; therefore a single

observation in each filter will suffice (W.-C. Jao 2004, 2006, private communication).

As of 2006 May 26, photometry was included in the astrometric reductions for sixteen stars.

The stars in this subsample were observed using the same telescope for photometry as astrometry. Nightly bias and dome flat fields were taken for use during the preliminary reduction of the observations. Each star is observed in the available V_J , R_{KC} , and I_{KC} filters on photometric nights with a sufficient exposure time to ensure a signal-to-noise ratio of at least 100 for the possible nearby star without saturating the potential reference stars (Jao *et al.* 2005). Fields of standard stars from the work of Landolt (1992) and Graham (1982) were also observed throughout the night in order to determine the transformation equations; the selected fields contain an average of ten standard stars each. Because many of the CTIOPI stars are fairly red, including this particular subsample, at least one red standard star, with $(V-I)$ greater than 3.7, is also observed. Over the course of a photometric night, four or five standard fields are usually observed two or three times each (Jao *et al.* 2005)

TABLE 4.10
PHOTOMETRY FOR POSSIBLE NEARBY STARS

Star	V_J^a (mag)	R_{KC}^b (mag)	I_{KC}^c (mag)	# ^d	J (mag)	H (mag)	K_S (mag)
LP 991-84		9.209 ± 0.023	8.629 ± 0.034	8.274 ± 0.026
LHS 1363		10.481 ± 0.024	9.858 ± 0.021	9.485 ± 0.020
G75-35		9.199 ± 0.022	8.581 ± 0.061	8.246 ± 0.027
2MA 0251-0352		13.059 ± 0.027	12.254 ± 0.024	11.662 ± 0.019
LP 888-18		11.360 ± 0.022	10.700 ± 0.022	10.264 ± 0.019
LP 889-37		9.775 ± 0.027	9.164 ± 0.025	8.823 ± 0.023
LHS 5094		9.303 ± 0.024	8.718 ± 0.025	8.411 ± 0.019
2MA 0429-3123	17.471 ± 0.026	15.859 ± 0.023	14.052 ± 0.019	1	10.874 ± 0.024	10.211 ± 0.024	9.770 ± 0.022
LP 834-32		8.240 ± 0.023	7.646 ± 0.031	7.406 ± 0.024
LP 655-43		9.730 ± 0.023	9.136 ± 0.023	8.818 ± 0.021
LP 716-10		10.502 ± 0.022	9.965 ± 0.022	9.606 ± 0.019
LP 776-25		7.740 ± 0.021	7.146 ± 0.031	6.891 ± 0.027
2MA 0517-3349	19.833 ± 0.054	17.382 ± 0.014	14.955 ± 0.010	1	12.004 ± 0.022	11.317 ± 0.024	10.832 ± 0.024
LP 717-36		8.454 ± 0.026	7.882 ± 0.033	7.623 ± 0.027
LHS 2024		10.070 ± 0.023	9.489 ± 0.022	9.136 ± 0.021
LHS 6167	13.809 ± 0.019	12.298 ± 0.015	10.394 ± 0.016	1	8.605 ± 0.027	8.074 ± 0.040	7.733 ± 0.017
2MA 0921-2104		12.779 ± 0.024	12.152 ± 0.022	11.690 ± 0.023
G 161-71	13.757 ± 0.013	12.265 ± 0.011	10.360 ± 0.011	2	8.496 ± 0.024	7.919 ± 0.024	7.601 ± 0.018
LP 671-8		8.877 ± 0.023	8.254 ± 0.042	7.970 ± 0.027
LP 731-76	14.431 ± 0.026	13.028 ± 0.022	11.220 ± 0.028	1	9.512 ± 0.023	8.965 ± 0.022	8.640 ± 0.021
BD -10°3166 ^e	10.034 ± 0.026	9.593 ± 0.022	9.186 ± 0.028	1	8.611 ± 0.032	8.300 ± 0.040	8.124 ± 0.026
LHS 2397a	19.44 ± 0.11	17.245 ± 0.024	14.862 ± 0.016	1	11.928 ± 0.021	11.233 ± 0.025	10.735 ± 0.023

TABLE 4.10 (CONTINUED)
PHOTOMETRY FOR POSSIBLE NEARBY STARS

Star	V_J^a (mag)		R_{KC}^b (mag)		I_{KC}^c (mag)		# ^d	J (mag)		H (mag)		K_S (mag)	
2MA 1155-3727	12.811 ± 0.024	12.040 ± 0.026	11.462 ± 0.021
LP 734-34	9.292 ± 0.024	8.684 ± 0.034	8.412 ± 0.027
LP 615-149	8.763 ± 0.030	8.123 ± 0.034	7.852 ± 0.020
LHS 5226	9.516 ± 0.023	8.969 ± 0.022	8.674 ± 0.023
CE 303	11.785 ± 0.022	11.082 ± 0.022	10.669 ± 0.024
LHS 2783	8.971 ± 0.018	8.391 ± 0.047	8.089 ± 0.023
LP 739-2	9.728 ± 0.021	9.174 ± 0.021	8.887 ± 0.020
LHS 2880	13.863 ± 0.014	12.509 ± 0.011	10.779 ± 0.012	2	9.040 ± 0.032	8.453 ± 0.040	8.163 ± 0.029
2MA 1507-2000	18.768 ± 0.068	16.704 ± 0.021	14.283 ± 0.022	1	11.713 ± 0.023	11.045 ± 0.022	10.661 ± 0.021
LHS 3056	12.858 ± 0.019	11.631 ± 0.015	10.048 ± 0.016	1	8.507 ± 0.026	7.862 ± 0.027	7.582 ± 0.020
2MA 1534-1418	19.189 ± 0.052	16.693 ± 0.014	14.153 ± 0.017	2	11.380 ± 0.023	10.732 ± 0.022	10.305 ± 0.023
LP 869-19	13.222 ± 0.014	11.9309 ± 0.0092	10.284 ± 0.011	3	8.692 ± 0.019	8.079 ± 0.038	7.816 ± 0.031
LP 869-26	14.102 ± 0.011	12.6468 ± 0.0083	10.8505 ± 0.0078	3	9.169 ± 0.029	8.571 ± 0.044	8.265 ± 0.027
LP 870-65	13.019 ± 0.015	11.7485 ± 0.0092	10.097 ± 0.012	3	8.559 ± 0.027	8.012 ± 0.049	7.701 ± 0.029
LP 756-3	13.742 ± 0.029	12.484 ± 0.018	10.850 ± 0.022	1	9.349 ± 0.027	8.728 ± 0.034	8.435 ± 0.021
LP 984-92	13.369 ± 0.029	12.049 ± 0.018	10.320 ± 0.022	1	8.681 ± 0.02	8.057 ± 0.034	7.793 ± 0.026
LP 876-10	12.583 ± 0.024	11.291 ± 0.017	9.600 ± 0.020	2	8.075 ± 0.023	7.527 ± 0.055	7.206 ± 0.021
LP 932-83	9.342 ± 0.02	8.780 ± 0.051	8.474 ± 0.021
2MA 2306-0502	11.354 ± 0.022	10.718 ± 0.021	10.296 ± 0.023
LP 822-101	8.877 ± 0.027	8.290 ± 0.059	8.004 ± 0.023
2MA 2351-2537	12.471 ± 0.026	11.725 ± 0.022	11.269 ± 0.026

TABLE 4.10 (CONTINUED)
PHOTOMETRY FOR POSSIBLE NEARBY STARS

Star	V _J ^a (mag)	R _{KC} ^b (mag)	I _{KC} ^c (mag)	# ^d	J (mag)	H (mag)	K _S (mag)
LP 704-15		8.636 ± 0.021	8.074 ± 0.029	7.806 ± 0.031

NOTES.—^acentral wavelength 547.5 nanometers (nm)

^bcentral wavelength 642.5 nm

^ccentral wavelength 807.5 nm

^dNumber in “#” column is the number of observations included.

^eBD -10°3166 was not part of the sample of possible nearby stars but is included as a possible common proper motion companion to LP 731-76.

REFERENCES.—V_J, R_{KC}, and I_{KC} photometry is from this work. J, H, and K_S photometry is from 2MASS.

The CTIOPI photometry pipeline is described by Jao *et al.* (2005, Jao 2004).

Instrumental magnitudes are measured in a 7'' radius around stars of interest: parallax candidates, reference stars, or photometric standard stars. The sky background is obtained from an annulus with inner and outer radii of 20'' and 25'', respectively, around the each star of interest. The Image Reduction and Analysis Facility (Tody 1986, 1993; hereafter IRAF¹⁴) fitparams task performs a least-squares calculation to determine the transformation coefficients ($a_1, a_2, a_3, a_4, b_1, b_2, b_3, b_4, c_1, c_2, c_3, c_4$) that will convert the instrumental magnitudes (m_V, m_R, m_I) of standard stars to those (V, R, I) measured by Landolt (1992) using the following equations

$$\begin{aligned} V &= m_V + a_1 + a_2 AM + a_3(m_V - m_I) + a_4(m_V - m_I)AM \\ R &= m_R + b_1 + b_2 AM + b_3(m_R - m_I) + b_4(m_R - m_I)AM \\ I &= m_I + c_1 + c_2 AM + c_3(m_R - m_I) + c_4(m_R - m_I)AM \end{aligned} \quad (4.5)$$

where AM represents air mass (Jao 2004). Once the transformation coefficients have been established for a particular night, they are applied to the stars of interest in the fields taken of parallax stars.

The formal errors associated with the V_J , R_{KC} , and I_{KC} photometry in Table 4.10 represent a combination of the errors associated with the standard star transformations for a specific night and the photon error of a particular stellar image. The stars with multiple observations indicate a night-to-night variation of 0.031 magnitude in V_J and 0.014 in R_{KC} and I_{KC} . For another RECONS sample observed at CTIO,

¹⁴IRAF is distributed by the National Optical Astronomy Observatories, which are operated by the Association of Universities for Research in Astronomy, Inc., under cooperative agreement with the National Science Foundation.

Henry *et al.* (2004) found larger night-to-night variation in the latter two bands: 0.031 magnitude in V_J , 0.021 in R_{KC} , and 0.020 in I_{KC} . Table 4.11 compares the V_J photometry obtained by CTIOPI with the values available in literature.

Infrared photometry from 2MASS has been included in Table 4.10. The J, H, and K_S errors reported are the total photometric uncertainties. The errors are usually between 0.02–0.03 magnitudes, but range from 0.017 in K_S for LHS 6167 up to 0.061 in H band (1.662 μm ; Cohen, Wheaton, & Megeath 2003) for G 75-35.

With a distance and apparent magnitude, calculating absolute magnitude and estimating stellar mass is possible. Table 4.11 lists the absolute V_J magnitudes obtained in this study. Table 4.12 lists the absolute K_S magnitudes calculated from 2MASS photometry along with mass estimates. To obtain masses, the 2MASS J and K_S photometry was transformed to the California Institute of Technology system defined by Elias *et al.* (1982, hereafter CIT with $K_{\text{CIT}} = 2.2 \mu\text{m}$) using the equations by Carpenter (2006). This transformation is necessary to use the K_{CIT} -band mass-luminosity relationship derived by Delfosse *et al.* (2000), which is appropriate for low mass stars no fainter than 9.5 magnitude.

The recent incorporation of a photometric variability model expands the astrometric and photometric reduction software described in Jao (2004); this model

TABLE 4.11
V-BAND PHOTOMETRY FOR POSSIBLE NEARBY STARS

Star	V_{JM} (mag)		Distance		Type ^b	M_V^a (mag)	References	Comment
	From Literature	From CTIOPI	(pc)					
LP 991-84	14.517 ± 0.007	...	8.64 ± 0.24		r	14.83 ± 0.31	1	
G75-35	13.800 ± 0.002	...	11.83 ± 0.54		r	13.43 ± 0.50	1	
LP 888-18	18.26 ± 0.25	...	13.44 ± 0.70		r	17.62 ± 0.62	2	
LP 889-37	14.52 ± 0.02	...	16.9 ± 1.6		r	13.4 ± 1.0	3	
LHS 5094	14.02 ± 0.02	...	14.0 ± 1.0		r	13.28 ± 0.80	3	
2MA 0429-3123	...	17.471 ± 0.026	15.14 ± 0.89		a	16.57 ± 0.64		binary
LP 834-32	12.38 ± 0.02	...	16.5 ± 1.4		r	11.29 ± 0.89	3	
LP 776-25	11.61 ± 0.02	...	14.1 ± 2.2		r	10.9 ± 1.6	3	
2MA 0517-3349	...	19.833 ± 0.054	17.1 ± 1.3		a	18.67 ± 0.79		
LP 717-36	12.56 ± 0.02	...	18.4 ± 1.2		r	11.24 ± 0.70	3	
LHS 6167	13.76 ± 0.02	13.809 ± 0.019	9.73 ± 0.28		a	13.87 ± 0.32	3	
G 161-71	13.73 ± 0.02	13.757 ± 0.013	14.16 ± 0.56		a	13.00 ± 0.44	3	
LP 731-76	14.39 ± 0.02	14.431 ± 0.026	14.42 ± 0.53		a	13.64 ± 0.41	3	
BD -10°3166 ^c	9.223 ± 0.048	10.034 ± 0.026	50 ± 29		a	6.5 ± 4.2	4, 5	
LHS 2397a	18.26 ± 0.25	19.44 ± 0.11	14.29 ± 0.42		a	18.66 ± 0.35	2, 6	binary
LHS 2783	13.39 ± 0.02	...	19.6 ± 1.2		r	11.93 ± 0.66	3	
LP 739-2	14.41 ± 0.02	...	17.3 ± 1.1		r	13.22 ± 0.70	3	
LHS 2880	13.83 ± 0.02	13.863 ± 0.014	25.8 ± 2.2		a	11.80 ± 0.89	3	
2MA 1507-2000	...	18.768 ± 0.068	22.8 ± 1.7		a	16.98 ± 0.80		
LHS 3056	12.84 ± 0.02	12.858 ± 0.019	19.10 ± 0.71		a	11.45 ± 0.41	3	

TABLE 4.11 (CONTINUED)
V-BAND PHOTOMETRY FOR POSSIBLE NEARBY STARS

Star	V_{JM} (mag)		Distance		Type ^b	M_V^a (mag)	References	Comment
	From Literature	From CTIOPI	(pc)					
2MA 1534-1418	...	19.189 ± 0.052	11.09 ± 0.28		a	18.96 ± 0.29		
LP 869-19	13.21 ± 0.02	13.222 ± 0.014	18.4 ± 1.1		a	11.90 ± 0.63	1	
LP 869-26	14.078 ± 0.016	14.102 ± 0.011	13.97 ± 0.68		a	13.38 ± 0.54	1	new binary
LP 870-65	13.01 ± 0.26	13.019 ± 0.015	17.9 ± 1.5		a	11.76 ± 0.88	1	
LP 756-3	13.762 ± 0.024	13.742 ± 0.029	17.4 ± 1.4		a	12.54 ± 0.88	1	
LP 984-92	13.381 ± 0.026	13.369 ± 0.029	18.9 ± 2.0		a	12.0 ± 1.1	1	
LP 876-10	12.618 ± 0.012	12.583 ± 0.024	7.41 ± 0.19		a	13.23 ± 0.28	1	
LP 932-83	13.93 ± 0.02	...	25.9 ± 4.6		r	11.8 ± 1.7	7	
LP 822-101	13.12 ± 0.00	...	22.7 ± 4.5		r	11.4 ± 1.9	1	

NOTES.—^aAbsolute visual magnitude on Johnson-Morgan system based on CTIOPI V_J photometry when available and on literature values otherwise.

^bAn “a” in the Type column indicates that the distance is from a preliminary absolute parallax while an “r” indicates that the distance is calculated from a preliminary relative parallax.

^cBD -10°3166 was not part of the sample of possible nearby stars but is included as a possible common proper motion companion to LP 731-76.

REFERENCES.—(1) Reid *et al.* 2003; (2) Salim & Gould 2003; (3) Reid, Kilkenney, & Cruz 2002; (4) Høg *et al.* 2000; (5) Hipparcos; (6) Monet *et al.* 1992; (7) Ryan 1992

TABLE 4.12
STELLAR MASSES ESTIMATED FROM INFRARED PHOTOMETRY

Star	K_S 2MASS ^a (mag)	Distance (pc)	Type ^c	M_K 2MASS (mag)	Stellar Masses ^b (M_\odot)	Comment
LP 991-84	8.274 ± 0.026	8.64 ± 0.24	r	8.590 ± 0.064	0.134 ± 0.043	
LHS 1363	9.485 ± 0.020	12.42 ± 0.60	r	9.01 ± 0.10	0.111 ± 0.043	
G75-35	8.246 ± 0.027	11.83 ± 0.54	r	7.880 ± 0.098	0.187 ± 0.043	
2MA 0251-0352	11.662 ± 0.019	12.7 ± 1.2	r	11.15 ± 0.19	...	too faint for M-L relationship
LP 888-18	10.264 ± 0.019	13.44 ± 0.70	r	9.62 ± 0.11	...	too faint for M-L relationship
LP 889-37	8.823 ± 0.023	16.9 ± 1.6	r	7.68 ± 0.19	0.206 ± 0.047	
LHS 5094	8.411 ± 0.019	14.0 ± 1.0	r	7.67 ± 0.15	0.207 ± 0.045	
2MA 0429-3123	9.77 ± 0.022	15.14 ± 0.89	a	8.87 ± 0.12	0.118 ± 0.043	binary
LP 834-32	7.406 ± 0.024	16.5 ± 1.4	r	6.31 ± 0.17	0.397 ± 0.052	
LP 776-25	6.891 ± 0.027	14.1 ± 2.2	r	6.15 ± 0.30	0.427 ± 0.070	
2MA 0517-3349	10.832 ± 0.024	17.1 ± 1.3	a	9.67 ± 0.15	...	too faint for M-L relationship
LP 717-36	7.623 ± 0.027	18.4 ± 1.2	r	6.30 ± 0.13	0.398 ± 0.049	
LHS 6167	7.733 ± 0.017	9.73 ± 0.28	a	7.793 ± 0.062	0.195 ± 0.043	
2MA 0921-2104	11.69 ± 0.023	11.48 ± 0.35	r	11.391 ± 0.068	...	too faint for M-L relationship
G 161-71	7.601 ± 0.018	14.16 ± 0.56	a	6.845 ± 0.085	0.310 ± 0.044	
LP 731-76	8.64 ± 0.021	14.42 ± 0.53	a	7.845 ± 0.080	0.190 ± 0.043	
BD -10°3166 ^d	8.124 ± 0.026	50.2 ± 29.3	a	4.62 ± 0.80	0.74 ± 0.17	
LHS 2397a ^e	10.735 ± 0.023	14.29 ± 0.42	a	9.960 ± 0.066	...	too faint for M-L relationship
LHS 2783	8.089 ± 0.023	19.6 ± 1.2	r	6.63 ± 0.13	0.343 ± 0.047	binary
LP 739-2	8.887 ± 0.020	17.3 ± 1.1	r	7.70 ± 0.13	0.204 ± 0.045	
LHS 2880	8.163 ± 0.029	25.8 ± 2.2	a	6.10 ± 0.17	0.435 ± 0.053	

TABLE 4.12 (CONTINUED)
 STELLAR MASSES ESTIMATED FROM INFRARED PHOTOMETRY

Star	K_S 2MASS ^a (mag)	Distance (pc)	Type ^c	M_K 2MASS (mag)	Stellar Masses ^b (M_\odot)	Comment
2MA 1507-2000	10.661 ± 0.021	22.8 ± 1.7	a	8.87 ± 0.15	0.118 ± 0.043	
LHS 3056	7.582 ± 0.020	19.10 ± 0.71	a	6.177 ± 0.080	0.421 ± 0.038	
2MA 1534-1418	10.305 ± 0.023	11.09 ± 0.28	a	10.080 ± 0.058	...	too faint for M-L relationship
LP 869-19	7.816 ± 0.031	18.4 ± 1.1	a	6.50 ± 0.12	0.365 ± 0.047	
LP 869-26	8.265 ± 0.027	13.97 ± 0.68	a	7.54 ± 0.10	0.221 ± 0.044	possible new binary
LP 870-65	7.701 ± 0.029	17.9 ± 1.5	a	6.44 ± 0.17	0.375 ± 0.051	
LP 756-3	8.435 ± 0.021	17.4 ± 1.4	a	7.23 ± 0.17	0.257 ± 0.047	
LP 984-92	7.793 ± 0.026	18.9 ± 2.0	a	6.41 ± 0.21	0.381 ± 0.056	
LP 876-10	7.206 ± 0.021	7.41 ± 0.19	a	7.856 ± 0.057	0.189 ± 0.043	
LP 932-83	8.474 ± 0.021	25.9 ± 4.6	r	6.41 ± 0.33	0.380 ± 0.071	
2MA 2306-0502	10.296 ± 0.023	12.41 ± 0.62	r	9.83 ± 0.11	...	too faint for M-L relationship
LP 822-101	8.004 ± 0.023	22.7 ± 4.5	r	6.23 ± 0.36	0.412 ± 0.078	

NOTES.—^a K_S photometry is from 2MASS.

^bStellar masses calculated using the K_{CIT} band mass-luminosity relationship from Delfosse *et al.* (2000). K_S (2MASS) was transformed to K_{CIT} using the transformations by Carpenter (2006). Errors are calculated from errors in photometry plus estimated errors associated with mass-luminosity relationship used.

^cAn “a” in the Type column indicates that the distance is from a preliminary absolute parallax while an “r” indicates that the distance is calculated from a preliminary relative parallax.

^dBD -10°3166 was not part of the sample of possible nearby stars but is included as a possible common proper motion companion to LP 731-76.

^eDistance for LHS 2397a is based on trigonometric parallax in Monet *et al.* (1992).

follows the methodology of Honeycutt (1992; Henry *et al.* 2006). Instrumental magnitudes for the parallax star and its reference stars are obtained for each astrometric observation and plotted. After the variability of the stars of interest to this study was evaluated in 2006 May, a problem with the magnitudes derived in this manner has been detected. Flares and significant photometric variation detected by the old software are still valid (W.C. Jao 2006, private communication); however, during the final parallax reduction, the variability of these stars will be re-checked using the revised software.

All M stars are probably variable at the 0.02–0.10 magnitude level over long periods (Bessell 1991). None of the possible nearby stars demonstrated any changes in brightness of 0.1 magnitude or greater. Five of twelve reference stars for LP 717-36 show excursions in magnitude on 2004 September 26 that are probably due to the bright sky background just before dawn. Five of nine reference stars for LP 822-101 show excursions in magnitude on 2004 November 20 that are also probably due to the bright sky background that night; one of its reference stars shows some evidence of flaring (W. C. Jao 2006, private communication).

4.5 SPECTROSCOPY

The initial subsample of forty-three stars included eighteen stars either with no spectral type or at most with spectral type “MVe.” These stars were added to the RECONS spectroscopy program on the 1.5-meter CTIO telescope, which is described by Henry *et al.* (2004). Later, the spectroscopy-observing list was expanded to include a total of forty stars from this sample.

Stars are observed with the Ritchey-Chrétien spectrograph using grating 32 and the Loral 1,200 x 800 pixel charge-coupled device (CCD) detector. This combination provides 0.86-nm resolution from 600 to 950 nm. The resulting spectra were reduced using IRAF for bias subtraction and flat-fielding with either dome or sky flats. The appropriate flats were used to remove fringing. Next, the ALLSTAR program (Henry *et al.* 2002) compared the new spectra to those available in its library of approximately 500 late type stars.

As of 2006 September 30, spectral types were available for thirty-two nearby stars, which are listed in Table 4.13. The expected error in these spectral types is ± 0.5 subclass. For comparison, Table 4.13 also lists the initial spectral types taken from the literature when selecting this subsample.

When provided in the literature, the errors associated with these values were also ± 0.5 subclass. In addition, Scholz, Meusinger, and Jahrei (2005) recently published new spectral types for *NLTT* stars. Lodieu *et al.* (2005) also published new spectral types for red, high-proper motion stars in the southern hemisphere with formal errors of 0.5 subclasses for optical spectra. With the inclusion of these spectral types, all stars in this subsample now have spectral types.

TABLE 4.13
SPECTRAL TYPES FOR POSSIBLE NEARBY STARS

Star	Spectral Types from Literature		RECONS	References	Comment
	Initial	Recent			
LP 991-84	M4.5V	1	
LHS 1363	M6.5V	...	M5.5V	2, 1	
G 75-35	M4.0V	M4.5V	M4.0V	3, 4, 1	
2MA 0251-0352	L3	2	
LP 888-18	M7.5V	M8.0V	M8.0V	2, 12, 1	
LP 889-37	M4.5V	1	
LHS 5094	M4.5V	1	
2MA 0429-3123	M7.5V	...	M6.5V	2, 1	joint, see Table 4.15
LP 834-32	M3.5V	1	
LP 655-43	...	M4.0V	M4.5V	4, 1	
LP 716-10	M5.5V	M5.5V	M5.0V	3, 4, 1	
LP 776-25	...	M3.0V	M3.0V	4, 1	
2MA 0517-3349	M8V	...	M8.0V	2, 1	
LP 717-36	...	M4.0V	M3.5V	4, 1	
LHS 2024	M4V	...	M4.5V	5	
LHS 6167	M4-5	M5.0V	M4.5V	6, 4, 1	
2MA 0921-2104	L2	7	
G 161-71	M5Ve	M5.0V	M5.0V	8, 4, 1	
LP 671-8	M3-4	M4.0V	...	6, 4	
LP 731-76	M4-5	M5.0V	M4.5V	6, 4, 1	
BD -10°3166 ^a	K0V	...	K4.0V	9, 1	
LHS 2397a	M8.5V	...	M8.0V	10, 1	joint, see Table 4.19
2MA 1155-3727	L2	12	
LP 734-34	...	M4.0V	M4.0V	4, 1	
LP 615-149	...	M3.5V	M3.5V	4, 1	
LHS 5226	...	M4.5V	M4.0V	4, 1	
CE 303	M8V	M8.0V	...	2, 12	
LHS 2783	M4V	5	joint, not yet resolved
LP 739-002	...	M4.0V	M4.0V	4, 1	
LHS 2880	M4.5V	5	
2MA 1507-2000	M7.5V	2	
LHS 3056	M4V	5	
2MA 1534-1418	M8V	11	
LP 869-19	...	M4.0V	M4.0V	4, 1	
LP 869-26	...	M5.0V	M4.5V	4, 1	joint, poss. new binary
LP 870-65	...	M4.5V	M4.0V	4, 1	
LP 756-3	M5-6	M4.0V	M4.0V	13, 4, 1	
LP 984-92	M4.5V	1	

TABLE 4.13 (CONTINUED)
SPECTRAL TYPES FOR POSSIBLE NEARBY STARS

Star	Spectral Types			References	Comment
	Initial	Recent	RECONS		
LP 876-10	...	M4.0V	M4.0V	4, 1	
LP 932-83	...	M5.0V	M4.5V	4, 1	
2MA 2306-0502	M7.5V	2	
LP 822-101	...	M3.0V	M3.5V	4, 1	
2MA 2351-2537	L1	M9.0V	M8.5V	7, 12, 1	
LP 704-15	M3V	...	M3.5V	5, 1	

NOTES.—Papers that estimate errors in spectral type give errors of ± 0.5 subclasses. The error in RECONS spectral types is ± 0.5 subclasses.

REFERENCES.—(1) T. D. Beaulieu 2006, private communication; (2) Cruz *et al.* 2003; (3) Cruz & Reid 2002; (4) Scholz, Meusinger, & Jahrei 2005; (5) Reid, Hawley, & Gizis 1995; (6) Gigoyan, Hambaryan, & Azzopardi 1998; (7) K. I. Cruz 2003, private communication; (8) Torres *et al.* 2000; (9) Butler *et al.* 2000; (10) Gizis *et al.* 2000; (11) Gizis 2002; (12) Lodieu *et al.* 2005; (13) Abrahamyan *et al.* 1997

With additional spectral type information now available and final 2MASS photometry, spectroscopic distance estimates may be made or updated for those stars in the subsample dropped from the astrometric program. Table 4.14 provides revised spectroscopic distance estimates calculated in the manner described in 4.2.2 along with recent distance estimates from the literature, where available. The status of each of these possible nearby stars is discussed in more detail below.

TABLE 4.14
REVISED SPECTROSCOPIC DISTANCE ESTIMATES FOR POSSIBLE NEARBY STARS

Star	Spectral Type	Literature ^a Distance (pc)	Spectroscopic ^b Distance (pc)	References	Comment
LP 655-43	M4.5V	18.7 ± 3.7	15.3 ± 5.4	1, 2	
LP 716-10	M5.0V	14.2 ± 2.8	17.7 ± 6.2	1, 2	
LHS 2024	M4.5V	13.9 ± 1.8	17.9 ± 6.3	1, 3	
LP 671-8	M4.0V	12.6 ± 2.5	12.0 ± 4.3	2	
2MA 1155-3727	L2	12.6 ...	120 ± 110	5	poor spectroscopic estimate
LP 734-34	M4.0V	15.4 ± 3.1	15.3 ± 5.4	1, 2	
LP 615-149	M3.5V	15.5 ± 3.1	14.6 ± 5.1	1, 2	
LHS 5226	M4.0V	13.6 ± 2.7	13.0 ± 4.7	1, 2	
CE 303	M8.0V	13.6 ± 1.6	12.1 ± 3.5	6	
2MA 2351-2537	M8.5V	16.0 ± 1.9	15.6 ± 4.5	1	
LP 704-15	M3.5V	13.2 ± 1.7	13.8 ± 4.8	1, 4	

NOTES.—^aDistance estimates from literature include photometric and spectroscopic techniques.

^bSpectroscopic distance estimates are from this work as discussed in section 4.2.2.

REFERENCES.— (1) T. D. Beaulieu 2006, private communication; (2) Scholz, Meusinger, & Jahrei 2005; (3) Reid, Hawley, & Gizis 1995; (4) Reid & Cruz 2002; (5) K. I. Cruz 2003, private communication; (6) Lodieu *et al.* 2005

4.5.1 LP 655-43

The photometric distance estimate by Reid, Kilkenny, and Cruz (2002) for LP 655-43 is 14.7 ± 1.2 pc, which places it just inside the 15-pc limit for the selection of this subsample. Based on it being a M4.5V star (T. D. Beaulieu 2006, private communication), a spectroscopic distance of 15.3 ± 5.4 pc was estimated. It has a V_{JM} magnitude of 14.44 ± 0.02 (Reid, Kilkenny, & Cruz 2002). LP 665-43 is still a possible nearby star; RECONS should eventually consider reinstating it.

4.5.2 LP 716-10

LP 716-10 is another star at the edge of the 15-pc selection limit for this subsample. Cruz and Reid (2002) estimated the distance spectroscopically as 14.3 ± 1.8 pc, just inside the 15-pc selection limit for this subsample. They assigned it a spectral type of M5.5V, which agrees with Scholz, Meusinger, & Jahreiß (2005). The recent RECONS spectral type is slightly earlier, M5.0V (T. D. Beaulieu 2006, private communication), which places it at a greater distance of 17.7 ± 6.2 pc. In addition, LP 716-10 would be difficult to observe with the CTIO 0.9-meter telescope because its $V_{\text{photographic}}$ is only 15.97 ± 0.25 (Salim & Gould 2003). Had this photometry been considered during sample selection, LP 716-10 would not have been included in the subsample.

4.5.3 LHS 2024

The photometric and spectroscopic distance estimates to LHS 2024 vary. Reid and Cruz (2002) estimated the distance to LHS 2024 as 13.9 ± 1.8 pc using spectral indices. Based on a spectral type of M4.5V (T. D. Beaulieu 2006, private communication), a spectroscopic distance of 17.9 ± 6.3 pc was calculated, which would

be outside the 15-pc selection limit. Its V_E magnitude of 15.0 ± 0.01 (Eggen 1987; Ryan 1989) is at the limit of what can be observed easily at the CTIO 0.9-meter telescope.

Therefore, LHS 2024 was dropped after nine observations. LHS 2024 is still a possible nearby star. Depending on the quality of the frames available, a rough preliminary parallax may be obtained from the current observations. Such an estimate would be the best method of determining whether further observations should be considered.

4.5.4 LP 671-8

LP 671-8 appears to be a nearby star based on photometric and spectroscopic estimates. The estimated photometric distance is 13.3 ± 1.8 pc (Reid, Kilkenny, & Cruz 2002). Using a spectral type of M3-4 (Gigoyan, Hambaryan, & Azzopardi 1998), a spectroscopic distance of 15.3 ± 5.3 pc was calculated, but, using the more recent spectral type of M4.0V (Scholz, Meusinger, & Jahrei 2005), a spectroscopic distance of 12.0 ± 4.3 pc is obtained. Reid, Kilkenny, and Cruz (2002) also provide a V_{JC} magnitude of 13.24 ± 0.02 , which indicates LP 671-8 could be comfortably observed by the CTIO 0.9-meter telescope. LP 671-8 should continue to be of interest to RECONS.

4.5.5 2MA 1155-3727

Although 2MA 1155-3727 was initially accepted for parallax determination, it was dropped without being set-up. Cruz (2003, private communication) estimated the distance to 2MA 1155-3727 to be 12.6 pc and identified it as having spectral type L2. The method of spectroscopic distance estimates described in section 4.2.2 does not appear to work well when extrapolated to L dwarfs as shown in Table 4.4. Since this star was dropped from the subsample, Deacon, Hambly, and Cook (2005) identified it as a high proper motion object, moving 870 ± 40 mas yr⁻¹ in 172.5° . 2MA 1155-3727 is

a possible nearby brown dwarf and because so few brown dwarf parallaxes are available, it should remain of interest to RECONS.

4.5.6 LP 734-34

Henry *et al.* (2004) announced improved photometric relationships for RECONS distance estimation; the application of these to LP 734-34 might allow it to be properly prioritized within the larger RECONS program. After initially accepting this object for inclusion within the sample, it was dropped without being set up. Initially, Reid, Kilkenny, and Cruz (2002) estimated the photometric distance as 12.9 ± 1.16 pc. However, spectroscopic distance estimates placed this star just outside of the 15-pc selection limit. If the spectral type is M4.0V (T. D. Beaulieu 2006, private communication), a spectroscopic distance of 15.3 ± 5.4 pc may be estimated. For the same spectral type, Scholz, Meusinger, and Jahrei (2005) calculated a distance of 15.4 ± 3.1 pc. LP 734-34 is still a possible nearby star.

4.5.7 LP 615-149

Initially, LP 615-149 was thought to be at the selection limit of this subsample because of a photometric distance estimate of 15.0 ± 1.7 pc (Reid, Kilkenny, & Cruz 2002). Recently, a distance of 14.6 ± 5.1 pc was estimated based on the RECONS spectral type of M3.5V. However, Scholz, Meusinger, and Jahrei (2005) place it at a distance of 15.5 ± 3.1 pc based on the same spectral type. Although LP 615-149 was initially accepted for parallax determination, it was dropped without being set-up. LP 615-149 is still a possible nearby star. The application of the improved RECONS photometric distance relationships (Henry *et al.* 2004) to LP 615-149 might allow it to be properly prioritized within the larger RECONS program.

4.5.8 LHS 5226

LHS 5226 is apparently within 15 pc, and should remain of interest to RECONS. It was initially accepted for parallax determination, but was dropped without being set-up. Using photometry, Reid, Kilkenny, and Cruz (2002) estimated the distance to LHS 5226 as 12.5 ± 0.9 pc. Spectroscopically, assuming it is a M4.0V type star (T. D. Beaulieu 2006, private communication), the distance would be 13.0 ± 4.7 pc, which is consistent with the photometric estimate.

4.5.9 CE 303

Cruz *et al.* (2003) estimated the spectroscopic distance to CE 303 as 13.3 ± 1.1 pc and assigned it a spectral type of M8V. From that spectral type, a distance of 12.0 ± 3.5 pc was estimated in section 4.2.2. Lodieu *et al.* (2005) also identified CE 303 as an M8.0V star at a distance of 13.6 ± 1.6 pc and with a proper motion of 376 ± 2 mas yr⁻¹ in $179 \pm 1^\circ$. CE 303 continues to be a possible nearby star and should continue to be of interest to RECONS.

4.5.10 2MA 2351-2537

2MA 2351-2537 is an interesting object. K. I. Cruz (2003, private communication) estimated the distance to 2MA 2351-2537 as 13.2 pc and identified it as having spectral type L1. The method of spectroscopic distance estimates described in section 4.2.2 does not appear to work well when extrapolated to L dwarfs as shown in Table 4.4. Now that it is thought to have a spectral type of M8.5V (T. D. Beaulieu 2006, private communication), a revised spectroscopic distance estimate of 15.6 ± 4.5 pc is obtained, which is just beyond the selection limit of this subsample. Pokorny, Jones, and Hambly (2003) identified it as a high proper motion object, moving at 420 ± 30 mas

yr^{-1} in 60.44° . 2MA 2351-2537 was initially accepted for parallax determination but was dropped after twelve observations. 2MA 2351-2537 is still a possible nearby star or brown dwarf. Depending on the quality of the frames available, a rough preliminary parallax may be obtained from the current observations. Such an estimate would be the best method of determining whether further observations should be considered.

4.5.11 LP 704-15

The distance to LP 704-15 is estimated to be 13.2 ± 1.7 pc using spectral indices (Reid & Cruz 2002) which is consistent with a spectroscopic distance of 13.8 ± 4.8 pc obtained from the recent RECONS spectral type of M3.5V (T. D. Beaulieu 2006, private communication). Thus, it is slightly inside the study volume. LP 704-15 was initially accepted for parallax determination but was dropped after seven observations. LP 704-15 is still a possible nearby star. These frames might permit a rough preliminary parallax to be obtained and help determine whether further observations should be made. An additional consideration is the presence of LP 704-14, a possible common proper motion companion, in these frames as discussed in 4.6.8.

4.6 MULTIPLICITY

About 67% of systems containing solar-type stars appear to be multiples (Duquennoy & Mayor 1991), while the fraction of M dwarfs, like the majority of the stars in this subsample, that are the primary component of a multiple system appears to be closer to 32–42% (Henry & McCarthy 1990; Fischer & Marcy 1992). For the later types, M8.0-L0.5, Close *et al.* (2003) find that 15% have companions of similar or lower mass. In earlier work, Worley (1977) found that 38% of nearby systems and 22% of systems with an M dwarf primary were non-single. This subsample could be

expected to include as many as eighteen binaries. As shown in Table 4.1 and discussed below, three close binaries and four common proper motion pairs had been previously identified.

In addition, CTIOPI resolved one new binary, LP 869-26, into two components and identified eleven stars that are at least 1.5 times more distant than their photometric or spectroscopic distances would indicate. If all of these identifications are confirmed, then the stars of this subsample are associated with eighteen binaries plus one triple star system, which would be within expectations. However, even the previously identified binaries could use additional observations to confirm and strengthen the assertion that they are physically related. Moreover, the apparently single stars discussed herein may eventually be resolved into additional components or have more distant companions identified.

4.6.1 2MA 0429-3123AB

Close (2003; Siegler *et al.* 2005) resolved 2MA 0429-9123 as a close, very low mass binary using the adaptive optics system on the Very Large Telescope (VLT). The stellar components are separated by 531 ± 2 mas with a 50_{-11}^{+12} year orbit; Table 4.15 lists additional physical characteristics. Although they argue that the probability of a chance alignment of 2MA 0429-3123 with a background L dwarf is negligible, they provide no proper motion for 2MA 0429-3123B. The photometric and spectroscopic distance estimates in Table 4.16 indicate the star is slightly closer than the distance calculated by preliminary absolute parallax. Such discrepancies can be evidence of a binary star; however, the two photometric estimates considered the nature of the double

star. The individual components are not resolved in any of the CTIOPI observations through 2005 November 22. Additional observations of the individual objects are necessary to determine whether 2MA 0429-3123 is a binary or merely an optical double.

TABLE 4.15
CHARACTERISTICS OF 2MA 0429-3123AB

Characteristic	2MA 0429-3123A	2MA 0429-3123B	Reference	Comment
Spectral Type	M7.5 ± 1.5	L1.0 ± 1.5	1	photometric
I_{KC} (mag)	14.052 ± 0.019	...	2	1 joint observation
K_S (mag)	10.14 ± 0.03	11.12 ± 0.07	1	
Mass (M_{\odot})	0.073–0.104	0.061–0.085	1	from models

REFERENCES.—(1) Siegler *et al.* 2005; (2) this work, section 4.4

TABLE 4.16
DISTANCE ESTIMATES FOR 2MA 0429-3123AB

Technique	Distance (pc)	Distance Ratio	Ref.	Comment
Absolute Parallax	15.14 ± 0.89	...	1	preliminary
Spectroscopic	9.7 ± 0.9	1.6	2	
Photometric (prob.)	11.1 ...	1.4	3	separates components
Spectroscopic	8.9 ± 2.7	1.7	4	joint
Photometric	11 ± 2	1.4	5	resolved binary components

NOTE.—Distance ratio is the preliminary absolute parallax divided by the distance estimate from the corresponding technique.

REFERENCES.—(1) this work, section 4.3; (2) Cruz *et al.* 2003; (3) Close 2003; (4) this work, section 4.2.2; (5) Siegler *et al.* 2005

4.6.2 LP 731-76 and BD -10°3166

The *NLTT* identifies LP 731-76 as a common proper motion companion to BD -10°3166, which has gained significant attention as the host of an extrasolar planet (Butler *et al.* 2000). Luyten described it as having a separation of 180 mas and an orbital period of 219 days. Together, these stars are known as LDS 4041. More recent measurements listed in Table 4.17 do not appear to support the common proper motion

identification. I. N. Reid (2004, private communication) also indicated that a comparison of Palomar Optical Sky Survey images with 2MASS images did not support the pairing and Scholz, Meusinger, and Jahreiß (2005) call it a “dubious common proper motion” pairing.

Photometric and spectroscopic distance estimates place these stars at significantly different distances, as shown in Table 4.18. The estimates for LP 731-76 range from 11 to 16 pc while those for BD -10°3166 fall between 34 and 68 pc. The distance estimates from the SuperCosmos Sky Survey (Hambly *et al.* 2001; hereafter SSS) scans of photographic plates overlap but the CTIOPI photometric distances differ by more than three times their errors (Raghavan *et al.* 2006).

The preliminary relative and absolute parallaxes support the theory that LP 731-76 and BD -10°3166 are too far apart to be related physically, as also shown in Table 4.7 and Table 4.18. The distance measurements do not overlap within the range of formal errors. However, they do overlap when the ranges are extended to twice the formal errors; the probability of such an occurrence is 14% (Beers 1957). The error associated with the preliminary relative parallax of BD -10°3166 is especially large, 7.3 mas

TABLE 4.17
PROPER MOTIONS FOR LP 731-76 AND BD -10°3166

Source	Proper Motion (mas yr ⁻¹)				Position Angle of Proper Motion (degrees)				Comment
	LP 731-76		BD -10°3166		LP 731-76		BD -10°3166		
NLTT	203	...	203	...	250	...	250	...	identified as common proper motion pair
SSS	202	± 10	189	± 10	242	...	252	...	common proper motion within errors
UCAC2	245	± 1	187	± 2	245	± 1	268.1	± 0.4	proper motions appear different
CTIOPI	218.1	± 4.5	184	± 19	244.5	± 2.2	272.5	± 8.6	proper motions appear different, large errors

REFERENCES.—SSS proper motions are from Raghavan *et al.* 2006 and Hambly *et al.* 2001. CTIOPI values are preliminary proper motions from this work. UCAC2 is Zacharias *et al.* 2004.

TABLE 4.18
DISTANCE ESTIMATES FOR LP 731-76 AND BD -10°3166

Method	Distance Estimates (pc)				References	Comment
	LP 731-76		BD -10°3166			
Photometric	11.6	± 0.8			1	motivated initial selection
Spectroscopic, based on M4.5	13.9	± 4.9			2	too early for estimate (BD)
Spectroscopic, based on M5.0	11.0	± 2.2			3	
Photometric			64		3	
Photometric, SSS—digitized photographic plates	16.4	± 10.1	33.8	± 8.8	4	
Photometric, RECONS—CCD observations	12.5	± 2.0	66.8	± 10.0	4	
Photometric, Ryan and Hipparcos			68		4, 5, 6	
Photometric and spectroscopic (M4-5V and K0V)	13		67		7	
Preliminary relative parallax	14.34	± 0.58	57	± 42	8	large parallax errors (BD)
Preliminary absolute parallax	14.42	± 0.53	50	± 29	8	large parallax errors (BD)

NOTE.—(9) describes the distance to BD -10°3166 as “considerably less than 200 pc.”

REFERENCES.—(1) Reid, Kilkenny, & Cruz 2002; (2) section 4.2.2 of this work; (3) Scholz, Meusinger, & Jahrei 2005; (4) Raghavan *et al.* 2006; (5) Ryan 1992; (6) Hipparcos; (7) Mugrauer *et al.* 2006; (8) section 4.3 of this work; (9) Butler *et al.* 2000

compared to the 4.7-mas average for the preliminary parallaxes in this study or the 3-mas threshold for final parallaxes. Only two stars in this subsample, LP 822-101 and LP 776-25, have larger errors. The quality of the parallax measured for BD -10°3166 is also discussed in 4.3.1.3. The final trigonometric parallaxes for these stars from CTIOPI should resolve the issue and will probably uphold the growing consensus that these two stars are physically unrelated.

4.6.3 LHS 2397aAB

Freed, Close, and Siegler (2003) resolved LHS 2397a into a binary using the Hokupa'a adaptive optics system on the Gemini North telescope. They estimate this very low mass binary to have an orbital period of 22 years (Siegler *et al.* 2005) based on a separation of about 227.72 ± 0.3 mas (Freed, Close, & Siegler 2003); other physical characteristics of the stars are listed in Table 4.19. Although they argue that the probability of a chance alignment of LHS 2397a, a high proper motion star, with a background L dwarf is negligible, the agreement between the available proper motions is not great. Basri and Reiners (2006) failed to detect any variation in its radial velocity. The individual components are not resolved in any of the CTIOPI observations through 2006 May 15. Additional observations could provide better data for determining whether these two objects are physically related.

TABLE 4.19
CHARACTERISTICS OF LHS 2397aAB

Characteristic	LHS 2397aA	LHS 2397aB	Ref.	Comment
Spectral Type	M8.0V \pm 1	...	1	joint
Spectral Type	M8 \pm 1	L7.5 \pm 1	2	photometric
I_{KC} (mag)	14.862 \pm 0.016	...	3	1 joint observation
I_{Cousins} (mag)	15.07 \pm 0.03	19.49 \pm 0.17	2	
K_{S} (mag)	10.80 \pm 0.03	13.57 \pm 0.10	2	
Mass (M_{\odot})	0.089–0.094	0.068–0.069	2	from models
μ (mas yr ⁻¹) ^a	513.4 \pm 7.8	555.1 \pm 8.2	4, 2	poor agreement
μ (mas yr ⁻¹) ^a	515 \pm 10 ^b	...	5	
μ Position Angle (°) ^c	263.8 \pm 0.9	259.6 \pm 0.9	4, 2	
μ Position Angle (°) ^c	261 \pm 5 ^b	...	5	

NOTE.— ^aProper motion measurements for LHS 2397a are used for LHS 2397aA.

^bError estimated from (6).

^cPosition angle of proper motion measurements for LHS 2397a are used for LHS 2397aA.

REFERENCES.—(1) T. D. Beaulieu 2006, private communication; (2) Freed, Close, & Siegler 2003; (3) this work, section 4.4; (4) Tinney 1996; (5) Luyten 1979; (6) Bakos, Sahu, & Nemeth 2002

4.6.4 LHS 2783AB

Eggen (1993) identified LHS 2783 as a binary member of the Hyades supercluster. He identified all stars within 20 pc of the Sun and with proper motions greater than 500 mas yr⁻¹ as potential members of the Hyades supercluster. He, then, separated single members from binary members based on their total velocity; binary members, like LHS 2783, had total velocities between 30 and 40 km s⁻¹. The two components of this hypothetical binary have not been resolved. Treating LHS 2783 as a single star, he calculated an I-band distance modulus of 0.60 magnitudes, which corresponds to a distance of approximately 13.2 pc similar to the literature and spectroscopic distances listed in Table 4.4. When he took its binary nature into

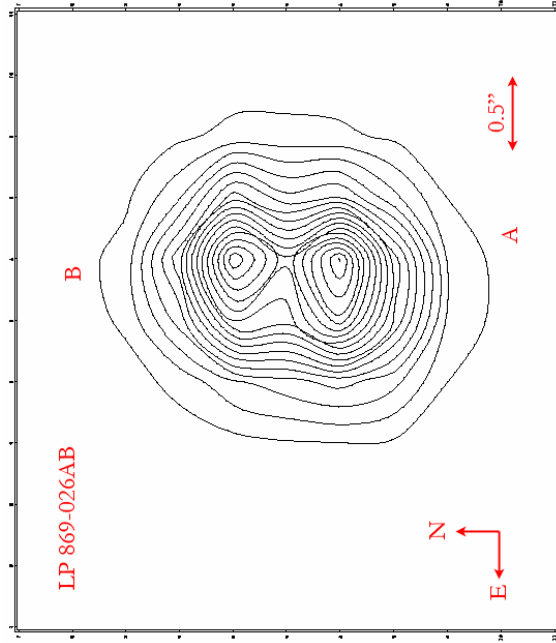
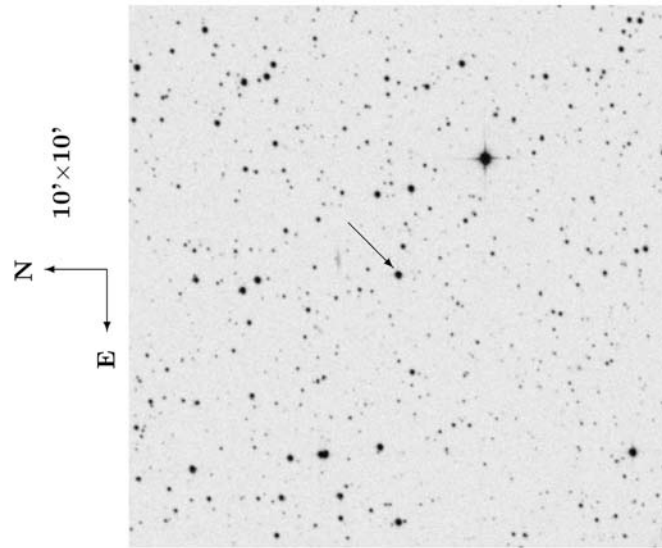
consideration, he obtained a distance modulus of 1.07 magnitudes, which corresponds to a distance of 16.37 pc. The latter is closer to the distance of 19.6 ± 1.2 pc from the preliminary relative parallax by CTIOPI. Although the discrepancy between the photometric and spectroscopic distances provides some support for the binary nature of this star, the current CTIOPI observations of LHS 2783 are unlikely to confirm Eggen's assertion.

4.6.5 LP 869-26AB

LP 869-26 was resolved as a binary star in 2006 May by CTIOPI as shown in Figure 4.6; a finding chart is also available in Appendix A. A review of the individual images and observer's notes indicated that it might be a binary because the point-spread function of this star did not match those of the reference stars. The second component appears to be at a distance of 730 ± 31 mas and $356.85 \pm 0.13^\circ$ east of north.

Earlier photometric and spectroscopic distance estimates placed LP 869-26 near the boundary of the 10-pc sample: 9 ± 1 pc, photometric (Reid *et al.* 2003); 10.7 pc, photometric (Jahreiß 2005); and 9 ± 2 pc, spectroscopic (Scholz, Meusinger, & Jahreiß 2005). Our preliminary absolute parallax indicates a slightly greater distance of 13.97 ± 0.68 ; part of the discrepancy may be due to unrecognized joint photometry of this pair. LP 869-26AB is clearly resolved in only a single frame at this time. Therefore, the possibility that LP 869-26B may be a faint background star cannot be eliminated. Additional observations are necessary to determine the nature of this new star and its relationship to LP 869-26A.

19:44:53.7 -23:37:59



LP869-026

FIG. 4.6.— LP 869-026AB Finding Chart and Contours. (Finding Chart DSS2 Red Image © Anglo-Australian Observatory Board. Contours CTIOPI astrometry image taken on 2006 May 11). These contours are extracted from a 10-second exposure with 0.8" seeing through the R_{KC} filter using the IRAF imexamine task. The B component appears to be at a distance of 730 ± 31 mas and $356.85 \pm 0.13^\circ$ east of north. Annotations by R. J. Paterson, J. L. Bartlett, & J. L. Bartlett.

4.6.6 LP 984-92 and LP 984-91

The *NLTT* identifies LP 984-92 as a common proper motion companion to LP 984-91 with a 36'' separation and a 133-day orbit. LP 984-91 also has a M4.5 companion, LHS 3524 (Song, Bessell, & Zuckerman 2002). The proper motions listed in Table 4.20 do not agree within the range of their formal errors. In addition, the CTIOPI preliminary relative parallax for LP 984-92 does not overlap with the Hipparcos absolute parallax for LP 984-91 within the range of formal errors (ESA 1997; hereafter Hipparcos). However, they do overlap when the ranges are extended to twice the formal errors; the probability of such an occurrence is 14% (Beers 1957). The error associated with the preliminary relative parallax of LP 984-92 is above the average for this work, 5.1 mas versus 4.7-mas average, and the error of the Hipparcos parallax for LP 984-01 is greater than 3 mas, the maximum error allowed in a final CTIOPI parallax. If the images of LP 984-91 are not saturated in the LP 984-92 observations, a new parallax for LP 984-91 could be measured using the same frames. Even if the final CTIOPI parallaxes for these stars show that they are not physically related, improved distance measurements for these members of the solar neighborhood will enhance the nearby star census.

TABLE 4.20
CHARACTERISTICS OF LP 984-92 AND LP 984-91

Characteristic	LP 984-92	LP 984-91 ^a	Ref.	Comment
Spectral Type	...	M4.0 ± 0.5 ^b	1	Pre-MS
V _{JM} (mag)	13.369 ± 0.029	11.70 ...	2, 3	1 CTIOPI obs.
NLTT μ (mas yr ⁻¹)	206 ± 25 ^c	206 ± 25 ^c	4	identified cpm
UCAC2 μ (mas yr ⁻¹)	203 ± 14	249.2 ± 2.4	5	
CTIOPI μ (mas yr ⁻¹)	221.0 ± 6.3	...	6	preliminary
NLTT μ Position Angle (°)	120 ...	120 ...	4	identified cpm.
UCAC2 μ Position Angle (°)	126.6 ± 3.9	118.50 ± 0.52	5	
CTIOPI μ Position Angle (°)	123.0 ± 3.2	...	6	preliminary
Absolute Parallax (mas)	...	42.35 ± 3.37	3	
Relative Parallax (mas)	51.6 ± 5.1	...	6	preliminary

NOTE.— ^aLP 984-91 is a pre-main sequence (pre-MS) binary with a M4.5 companion, LHS 3524 (1).

^bError is estimated from (7).

^cError is estimated from (8).

REFERENCES.—(1) Song, Bessell, & Zuckerman 2002; (2) this work, section 4.4; (3) Hipparcos; (4) NLTT; (5) Zacharias *et al.* 2004; (6) this work, section 4.3; (7) Reid, Hawley, & Gizis 1995; (8) Gould & Salim 2003;

4.6.7 LP 932-83 and LTT 9210

LP 932-83 is the common proper motion companion of LTT 9210, which together are identified as LDS 4999. According to the *LDS*, their separation is 217.0". As shown in Table 4.21, the proper motions are very close to being the same within the errors. However, within the range of formal errors, our preliminary relative parallax for LP 932-83 does not overlap with the absolute parallax of LTT 9210 from Hipparcos. The distances do overlap when the ranges are extended to twice the formal errors; the probability of such an occurrence is 14% (Beers 1957). The error associated with the preliminary relative parallax of LP 932-83 is above the average for this work, 5.8 mas versus 4.7-mas average. The quality of the parallax is also discussed in 4.3.2.5 and the

possibility that LP 932-83 is also a close binary is mentioned in 4.6.9. The final trigonometric parallaxes for LP 932-83 from CTIOPI should resolve its relationship with LTT 9210 and will probably indicate that two stars are physically unrelated.

TABLE 4.21
CHARACTERISTICS OF LP 932-83 AND LTT 9210

Characteristic	LP 932-83	LTT 9210	Ref.	Comment
Spectral Type	M5.0V \pm 0.5	K7V ...	1, 2	
V_{JM} (mag)	13.93 \pm 0.02	10.7 \pm 0.1	3, 4	
<i>LDS</i> μ (mas yr ⁻¹)	289	289	5	identified c.p.m.
<i>UCAC2</i> μ (mas yr ⁻¹)	302 \pm 12	293.7 \pm 1.3	6	
CTIOPI μ (mas yr ⁻¹)	303.2 \pm 7.9		7	preliminary
<i>LDS</i> μ Position Angle (°)	216	216	5	identified c.p.m.
<i>UCAC2</i> μ Position Angle (°)	213.1 \pm 2.3	215.87 \pm 0.25	6	
CTIOPI μ Position Angle (°)	220.9 \pm 3.0		7	preliminary
Absolute Parallax (mas)		23.03 \pm 2.04	8	
Relative Parallax (mas)	38.6 \pm 5.8		7	preliminary

REFERENCES.—(1) Scholz, Meusinger, & Jahrei 2005; (2) Uppgren *et al.* 1972; (3) Ryan 1992; (4) Hg *et al.* 2000; (5) *LDS*; (6) Zacharias *et al.* 2004; (7) this work, section 4.3; (8) Hipparcos

4.6.8 LP 704-15 and LP 704-14

The *NLTT* identifies LP 704-14 as a common proper motion companion to LP 704-15 with a separation of 20'' and a 294-day orbit. As shown in Table 4.22, Salim and Gould (2003) measured essentially identical proper motions for the pair. Reid, Hawley, and Gizis (1995) calculated spectroscopic distances for these two objects that overlap within the errors. If a rough preliminary parallax is measured for LP 705-15 as discussed in 4.5.11, a similar measurement could be made for LP 705-14 as well to determine whether they are physically related.

TABLE 4.22
CHARACTERISTICS OF LP 704-15 AND LP 704-14

Characteristic	LP 704-15	LP 704-14	Ref.	Comment
Spectral Type	M3V	M4V	1	
Spectral Type	M3.5V		2	
V_{JM} (mag)	12.93 ± 0.02	12.98 ± 0.02	3	
$NLTT \mu$ (mas yr ⁻¹)	193	193	4	identified c.p.m.
Updated μ (mas yr ⁻¹)	210 ± 6	210 ± 6	5	good agreement
$NLTT \mu$ Position Angle (°)	84	84	4	identified c.p.m.
Updated μ Position Angle (°)	83 ± 2	83 ± 2	5	good agreement
Spectroscopic distance	20 ± 6	13 ± 4	1	same within errors

REFERENCES.—(1) Reid, Hawley, Gizis 1995; (2) T. D. Beaulieu 2006, private communication; (3) Weis 1991; (4) *NLTT*; (5) Salim & Gould 2003

4.6.9 Distance Discrepancies

The joint photometry of an unresolved binary will appear brighter than it would if its individual components were considered separately. The resulting photometric or spectroscopic distances will underestimate the actual distance to the star. For instance, a pair whose magnitudes differ by 0.75 magnitudes will appear about 18% closer than if only the flux from a single component was considered. The comparison of trigonometric parallax distance with that obtained from either photometric or spectroscopic techniques may signify the presence of an unknown companion. Several of the possible close binaries discussed above have such discrepancies in their distance measurements: 2MA 0429-3123, LHS 2397a, LHS 2783, and LP 869-26. The ratios of their parallactic distances to other distance measurements are 1.2–1.7, as listed in Table 4.4. Other stars in this study have parallactic distances at least 1.5 times one of their other distance measurements: LHS 6167, G 161-71, LHS 2880, 2MA 1507-2000, LHS 3056, LP 869-19, LP 870-65, LP 756-3, LP 984-92, LP 932-83, and LP 822-101. Future

observations may resolve these latter eleven stars into binaries or future improvements in the photometric and spectroscopic distance relationships may reduce the current discrepancies that appear in Table 4.4.

4.7 DISCUSSION

This chapter contributes to the nearby star census by presenting preliminary parallaxes and proper motions for thirty-two possible nearby stars, which may be finalized in the next three observing seasons. In addition, new preliminary V_J , R_{KC} , and I_{KC} photometry for seventeen possible nearby stars and new spectroscopy for thirty-two possible nearby stars is also provided. Figure 4.7 plots the relationship between spectral type and 2MASS J-K_s color for the stars in this subsample plus 116 nearby stars listed in Table 4.3 for which this data was available; the three L dwarfs included do not yet have RECONS spectral types. This subsample of possible nearby stars appears consistent with the previously known nearby main sequence stars with no significant outliers. Figure 4.8 is a 2MASS-based infrared color-magnitude diagram for the possible nearby stars in this sample with preliminary parallaxes. The plot of absolute J magnitude versus J-K_s color shows the expected lower main sequence.

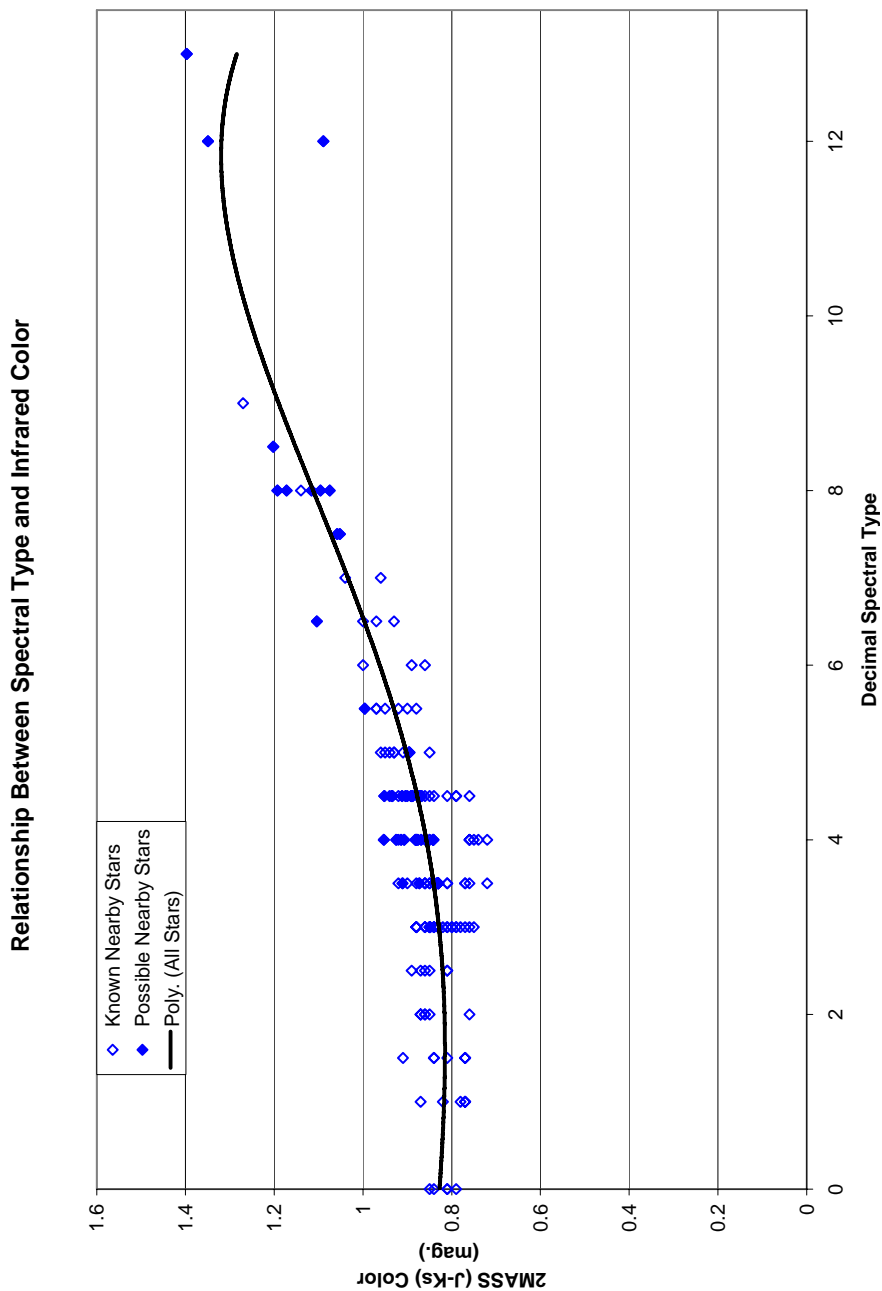


FIG. 4.7.— Infrared Color versus Spectral Type of Known and Possible Nearby Stars. Plot is based on data in Table 4.3 (open diamonds), which was provided by T. Henry (2003, private communication), and values for stars in this subsample (filled diamonds). The trend line is fourth-order polynomial fit to all the stars similar to those discussed in section 4.2.2.

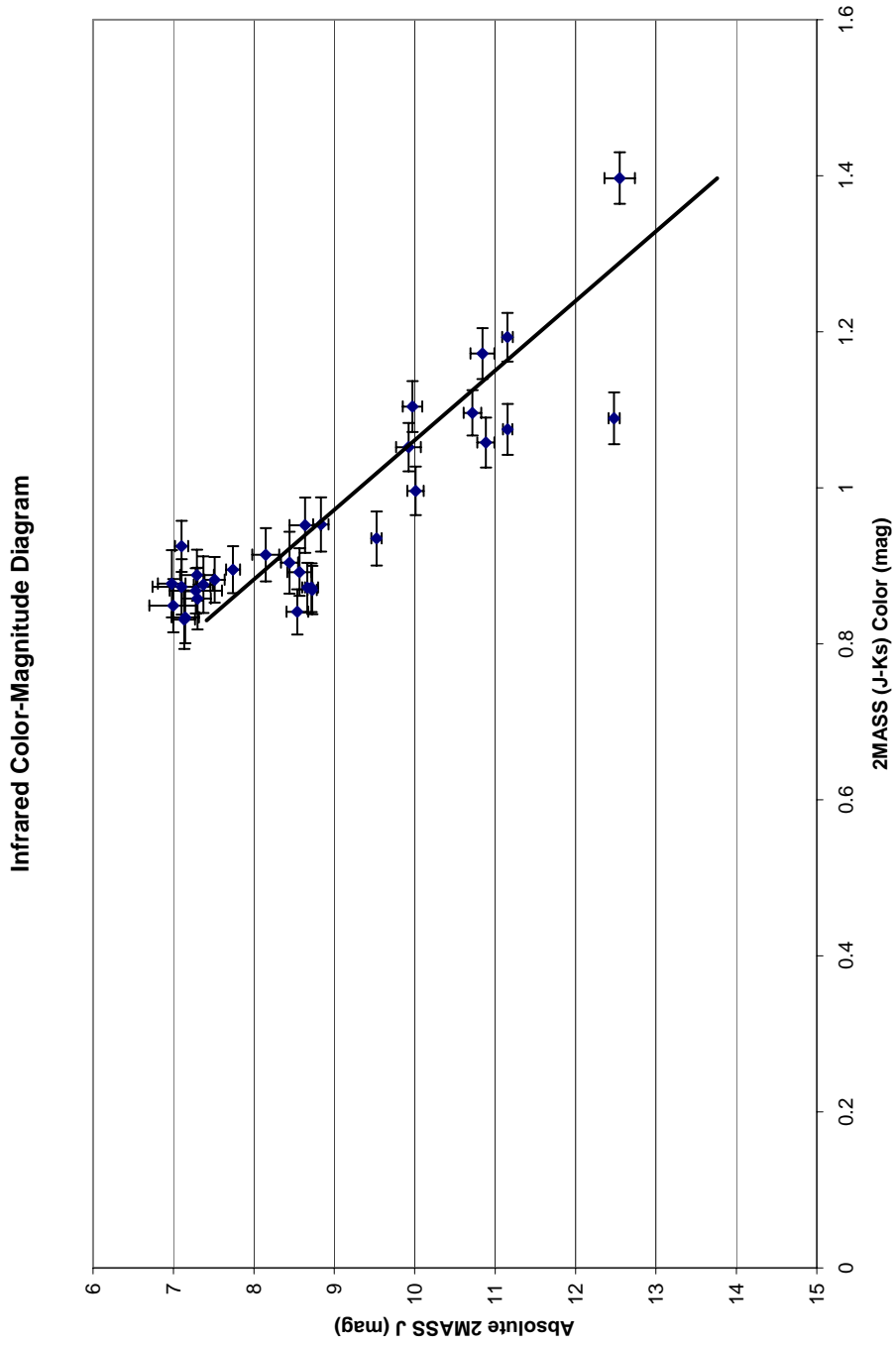


FIG. 4.8.— Infrared Color-Magnitude Diagram for Possible Nearby Stars. Plot is based on preliminary parallaxes from this work and 2MASS photometry.

Twenty-eight stars are confirmed as lying within 25 pc of the Sun, including three that appear to be new members of the 10-pc sample. The errors associated with the measurements of three more stars leave their status in doubt. One star, LP 869-26, was resolved into two stars; additional observations will provide more information about the relationship between the components of this possible new binary. All but three of the stars with preliminary proper motions have proper motions greater than 200 mas yr⁻¹, including nine stars with proper motions between 500 mas yr⁻¹ and 1'' yr⁻¹ and two with proper motions greater than 1'' yr⁻¹. The spectral types range from M3.0V through L3 and include objects as faint as 19.83 magnitudes in V_J. When completed this CTIOPI subsample will have contributed to our knowledge of the solar neighborhood and slightly reduced the number of missing systems within 10 pc.

When added to what we already know about the stars within the solar neighborhood, this study will enable enhanced approximations of the stellar luminosity function, the mass-luminosity relationship, stellar velocity distribution, and the stellar multiplicity fraction. The improvements in our knowledge of these functions will advance our understanding of stellar populations, stellar evolution, and star formation history and contribute to a better larger picture of galactic structure.

Chapter 5 Continuing The Solar Neighborhood Census: Infrared Parallax Program At Fan Mountain Observatory

5.1 INTRODUCTION

Even in the well-surveyed northern hemisphere, only 1,153 stellar systems are identified as being within 25 parsecs (pc) out of an expected 2,750 systems (Henry *et al.* 2002). The known systems incorporate the bright nearby stars filled in by the Hipparcos Space Astrometry Mission (ESA 1997, hereafter Hipparcos). The Hipparcos catalog includes stars as faint as 12.4 magnitude in V-band ($V_{\text{Johnson-Morgan}}=550$ nm according to Johnson and Morgan 1951, 1953). However, it is significantly incomplete for stars fainter than 9 magnitude (Perryman *et al.* 1997); the 12.4 magnitude corresponds to an M5V star at approximately 10.5 pc, the 9 magnitude to a distance of about 2.2 pc (Drilling & Landolt 2000). Most of the missing systems must therefore consist of intrinsically faint stars and brown dwarfs; such cool objects will have their peak emission at wavelengths of 0.9 micrometers (μm) and longer (Drilling & Landolt 2000). As demonstrated in Chapter 4, infrared surveys, such as the Two Micron All Sky Survey (Skrutskie *et al.* 2006, hereafter 2MASS) and the Deep Near Infrared Survey of the Southern Sky (Epchtein *et al.* 1999, hereafter DENIS) are fertile sources of potential nearby stars.

These infrared surveys are also significant sources of brown dwarfs, which cool continuously because they lack sufficient mass to sustain nuclear fusion. Trigonometric parallaxes to these substellar objects would allow accurate determination of their luminosities. According to Chabrier and Baraffe (2000), most brown dwarf radii should be similar to that of Jupiter. Therefore, better luminosities would also improve

temperature estimates. Gelino, Kirkpatrick, and Burgasser (2004) list 581 likely L and T dwarfs of which only 75 have parallax measurements.¹⁵ As discussed in Chapter 4, the Cerro Tololo Inter-American Observatory Parallax Investigation (CTIOPI) includes some southern L dwarfs. However, all brown dwarfs within the reach of ground-based astrometry should have their distances measured, regardless of whether they lie within the immediate solar neighborhood.

From 2000 until 2006, the United States Naval Observatory (USNO) operated an infrared parallax program in Flagstaff, Arizona, using the 61-inch (1.55-meter) reflector and an astrometric, infrared detector known as ASTROCAM. In response to the need for brown dwarf parallax measurements, Vrba *et al.* published preliminary infrared parallaxes for 40 L and T dwarf in 2004; at the time, another two years of observations was anticipated in order to finalize them. Unfortunately, a Dewar explosion during a nearby forest fire in June 2006 destroyed ASTROCAM. The program will be suspended for at least a year and perhaps longer (F. Vrba 2006, private communication). Even when the USNO program was operating, a desire for an additional infrared parallax program to increase the number of brown dwarfs with such determinations was clear.

The University of Virginia (UVa) had long been a leader in the measurement of parallaxes with programs at Leander McCormick Observatory, Fan Mountain Observatory, and Siding Spring Observatory. However, the last of these,

¹⁵DwarfArchive.org maintains a list of late type stars at <http://spider.ipac.caltech.edu/staff/davy/ARCHIVE/> Counts reported herein were accurate as of 2006 October 16.

the UVa Southern Parallax Program at Siding Spring Observatory in Australia, discontinued observations in July 2002. Once the Virginia Astronomical Instrumentation Laboratory (VAIL) began development of an infrared camera for use at Fan Mountain Observatory, this study of the feasibility of a new parallax program was instigated. In addition, M. Skrutskie (2005, private communication) obtained 15 percent (%) of the time on the Fred Lawrence Whipple Observatory 1.3-meter telescope, which is now the Peters Automated Infrared Imaging Telescope (PAIRITEL) on Mount Hopkins in exchange for remounting the former 2MASS camera there. This allocation provides another possible opportunity for infrared astrometry at UVa.

5.2 FAN MOUNTAIN 31-INCH TELESCOPE

UVa operates Fan Mountain Observatory at a dark site approximately 19 miles (30 kilometers) south of Charlottesville, Virginia, in Covesville. Tinsley Laboratories built the 31-inch (0.8-meter) astrometric reflector in the 1960's for use with a photographic plate spectrograph and photomultipliers. In 2004, VAIL, led by Skrutskie, refurbished the telescope and outfitted it with a new infrared camera, FanCam.

VAIL designed and developed the infrared camera (Kanneganti *et al.*, in preparation). Its initial science goals include variability studies of young stars, measurements of fundamental properties for low mass stars and brown dwarfs, observations of asteroids, and follow-up of carbon stars identified by 2MASS (VAIL 2005¹⁶). It saw first light in December 2004. The telescope has a focal plane scale of 16.92 seconds of arc (") millimeter (mm^{-1}) and a field-of-view 39.4 minutes of arc (')

¹⁶An on-line version of an informational poster that VAIL displayed locally is available <http://www.astro.virginia.edu/research/instrumentation/images/poster-20050406.jpg>

across (UVa 2006).¹⁷ When mounted on this telescope, FanCam has a 27.56'' mm⁻¹ scale and an 8.7' field-of-view (VAIL 2006).¹⁸ Table 5.1 describes the telescope and camera further, and Table 5.2 details some of the available filters.¹⁹ Figure 5.1 is a mechanical drawing illustrating some of the features of FanCam.

TABLE 5.1
CHARACTERISTICS OF THE FAN MOUNTAIN REFLECTOR AND CAMERA

Parameter		Description
Objective Size	(meters)	0.8
	(inches)	31
Optics		Classical Cassegrain
Telescope Focal Ratio		f/15.484
Telescope Effective Focal Length	(meters)	12.192
	(inches)	480.0
Telescope Focal Plane Scale	('' mm ⁻¹)	16.92
Focal Plane Array		Rockwell Hawaii-I HgCdTe
Focal Plane Array Description		thick, back-illuminated, coated
FanCam Field of View	(°)	8.7
Detector Size	(pixels)	1,024 x 1,024
Detector Pixel Size	(μm)	18.5
FanCam resolution	('' pixel ⁻¹)	0.5098
Detector Gain	(e ⁻ DN ⁻¹)	4.6
Detector Read Noise	(e ⁻ rms)	17
Optimal Detector Temperature	(K)	77

REFERENCES.—UVa 2006; VAIL 2006; Kanneganti *et al.* in preparation, S. Kanneganti 2006, private communication

¹⁷Telescope specifications maintained by UVa are available at
<http://www.astro.virginia.edu/research/observatories/31inch/31-specs.php>

¹⁸Instrument specifications maintained by VAIL are available at
http://www.astro.virginia.edu/research/instrumentation/firc_specs.php

¹⁹VAIL lists filter specifications on-line at
<http://www.astro.virginia.edu/research/observatories/FMOfilters.php#31inch> and
http://www.astro.virginia.edu/research/instrumentation/firc_specs.php

TABLE 5.2
CHARACTERISTICS OF SELECTED FILTERS

Filter ^a (2MASS Prototype)	Passband ^b (μm)	Central Wavelength (μm)	Limiting Magnitude ^c
J	1.105 – 1.395	1.250	19.0
H	1.515 – 1.817	1.666	18.0
K _S	2.045 – 2.335	2.190	17.0

NOTES.— ^aAdditional filters currently include K, Y, H₂, Br- γ , FE-II, Pa- β , and two polarizers. Future plans include the installation of a low-resolution prism plus medium- and high-resolution grisms.

^bPassbands were measured at room temperature by manufacturer.

^cLimiting magnitude is based on a 10- σ detection after 10 minutes of on-source observation.

REFERENCES.— Passbands are from VAIL 2006 and S. Kanneganti 2006, private communication. Limiting magnitudes are from Kanneganti *et al.*, in preparation.

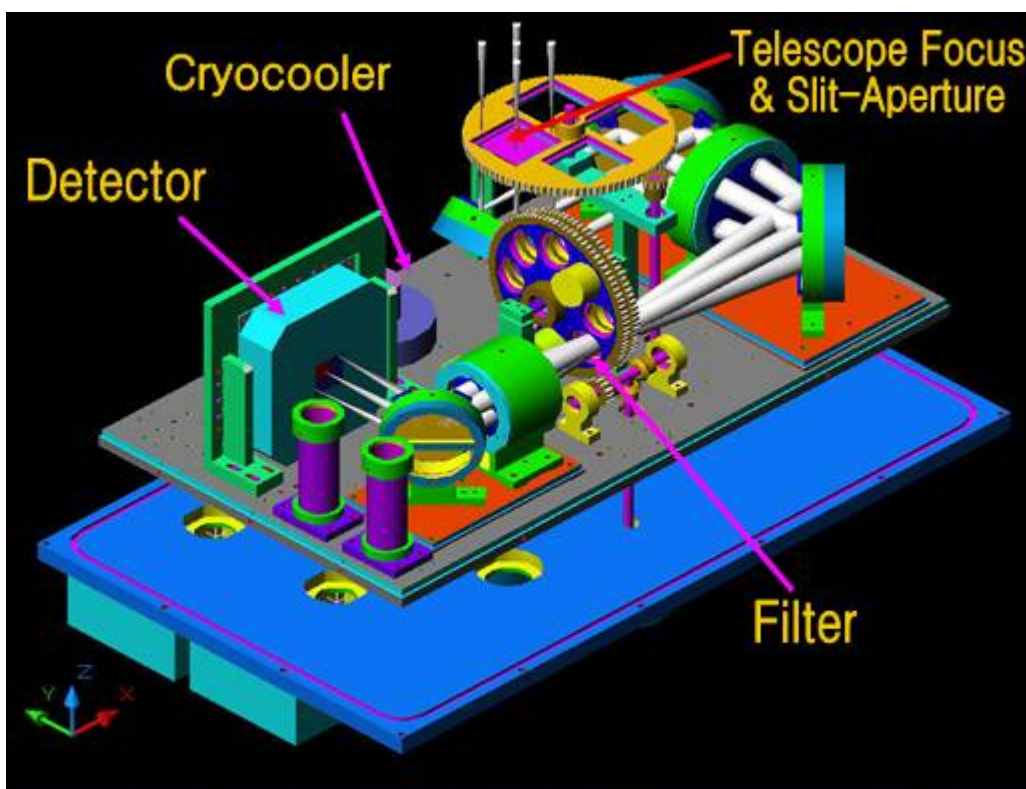


FIG. 5.1. — FanCam Mechanical Drawing. Image source: VAIL.

Plans for FanCam and the 31-inch reflector include the development of an autoguider. However, the telescope currently tracks the sky reliably for at least

30 seconds. Longer exposures are possible, but image motion will occasionally render an exposure useless. To observe objects of 17th magnitude or fainter, multiple short exposures are combined. For astrometric accuracy, the individual frames in the stacked exposure might need to be aligned within a fraction of a pixel. Appropriate plate constants may be able to account for large shifts or rotations but time-constraints prevented testing this technique. Therefore, observations for this study were limited to single exposures of 30 seconds or fewer.

The nightly pointing calibration of FanCam and the 31-inch reflector uses a known bright star positioned so that it is visible in the finder but does not impinge on the detector. This offset protects the sensitive focal plane array (FPA) in FanCam. However, it also introduces a small but uncertain offset between coordinates displayed by the telescope control system and the center of the field that the telescope is observing. This discrepancy can increase the difficulty of setting up and observing faint objects not visible in the finder.

5.3 ASTROMETRIC CALIBRATION REGION

Ideally, the astrometric quality testing and calibration of FanCam would have included the measurement of preliminary parallaxes and proper motions for several stars that have high-quality parallaxes observed at other facilities. However, selected stars from the *Catalogue of Stars with Proper Motions Exceeding 0.5" Annually* (Luyten 1979) were either too bright for 2-second exposures or too faint to be identified reliably with the current telescope pointing. Several early L dwarfs with spectroscopic

distance estimates (K. I. Cruz 2004, private communication) were too faint to observe using single 30-second exposures or too faint to be identified reliably.

During Fall 2005, FanCam was removed from the telescope to re-weld and refinish the vacuum seal surfaces (Kanneganti *et al.*, in preparation). While it was being serviced, a decision was made to use open clusters as astrometric calibration regions because several had been previously observed as part of other projects. NGC 2169 and NGC 2420 were selected as the best candidates based on the quality and quantity of frames available. Although many exposures were available, a significant number were taken at large hour angle and without careful positioning to ensure a consistent group of stars was visible. After FanCam was re-installed in November 2005, additional observations of these fields were made with the specific intention of using them as astrometric calibration regions.

Astrometric calibration probably should also consider all of the proposed filters, which for FanCam would include J, H, and K_S as described in Table 5.2. However, due to the limited observing time available during Fall 2005 and Spring 2006, only the frames taken with the J filter were included in this study. J-band has the advantage of reduced sky brightness compared to the other bands; it is the filter most likely to be used for a parallax program with FanCam. The USNO infrared parallax program observed L dwarfs in H band and T dwarfs in J band with similar precision in each filter.

During the reduction of the astrometric calibration regions, the selection of images was further narrowed to observations of NGC 2420 on three nights. Table 5.3

provides additional information about this cluster. Table 5.4 lists the frames selected.

Table 5.5 lists the twenty stars selected within this region for evaluation, which are also identified in Figure 5.2.

In a separate analysis, S. Kanneganti (2005, private communication) compared ninety stars from NGC 2420 frames with 2MASS images and determined that 51% of the FanCam stellar images were within 50 milliseconds of arc (mas), or 1.8 μm , of the 2MASS positions. However, for stars with K_s (2.159 μm according to Cohen, Wheaton, & Megeath 2003) magnitudes between 9 and 14, 2MASS positions are internally repeatable to within 40 to 50 mas and show residuals of 70 to 80 mas (Cutri 2005) when compared with the *USNO CCD Astrograph Catalog* (Zacharias *et al.* 2000, hereafter UCAC).

TABLE 5.3
PROPERTIES OF NGC 2420 FROM LITERATURE

Parameter	Value	Reference
Position (2000.0)	07 38 23 +21 34 24	1
Classification	Open Cluster	
Distance (pc)	2742	2
Proper Motion (mas yr^{-1})	4.3 \pm 0.3	3
Position Angle of Proper Motion (degrees)	198 \pm 5	3
Radial Velocity (km/s)	67 \pm 8	4
Age (years)	2.00 $\times 10^9$	2
Metallicity ([Fe/H])	-0.38 \pm 0.07	4

REFERENCES.—(1) Xin & Deng 2005; (2) Tadross *et al.* 2002; (3) Loktin & Beshenov 2003; (4) Friel *et al.* 2002;

TABLE 5.4
 CATALOG OF NGC 2420 FRAMES USED FOR ASTROMETRIC CALIBRATION

Observation Date	Frame	EST Time ^a (hh:mm)	Hour Angle ^b (minutes)	Exposure (seconds)	Seeing ^c (")	Shape ^d	Inadequate Stars ^e	Original Purpose ^f
2005-JAN-09	234	00:36	2E	2	2.0	skewed	1, 2, 3	Saturn
2005-JAN-09	235	00:36	2E	2	1.8	skewed	1, 2, 3	Saturn
2005-JAN-09	236	00:37	1E	2	1.5	slightly skewed	1, 2, 3	Saturn
2005-JAN-09	237	00:37	1E	2	1.8	oval	1, 2, 3	Saturn
2005-JAN-09	238	00:37	1E	2	2.0	roundish	1, 2, 3	Saturn
2005-JAN-09	239	00:37	1E	2	2.0	oval	2, 3	Saturn
2005-JAN-09	240	00:37	1E	2	2.0	skewed	2, 3	Saturn
2005-JAN-09	241	00:38	0	2	2.3	skewed	2, 3	Saturn
2005-JAN-09	242	00:38	0W	5	2.0	roundish	2, 3	Saturn
2005-JAN-09	243	00:38	0W	5	2.0	roundish	2, 3, 10	Saturn
2005-JAN-09	244	00:39	1W	5	2.0	round	2, 3	Saturn
2005-JAN-09	245	00:39	1W	5	2.0	roundish	1, 2, 3	Saturn
2005-JAN-09	246	00:39	1W	5	1.8	skewed	1, 2, 3	Saturn
2005-JAN-09	247	00:39	1W	5	1.8	fairly round	1, 2, 3	Saturn
2005-JAN-09	248	00:40	2W	5	2.0	skewed	1, 2, 3	Saturn
2005-JAN-09	249	00:40	2W	5	2.3	slightly oval	1, 2, 3	Saturn
2005-JAN-09	250	00:40	2W	5	2.3	slightly oval	1, 2, 3	Saturn
2005-JAN-09	251	00:41	3W	5	1.8	slightly oval	1, 2, 3	Saturn
2005-FEB-19	283	00:45	169W	5	1.5	skewed	1, 2, 3	Saturn
2005-FEB-19	284	00:47	171W	5	2.0	skewed	1, 3	Saturn
2005-FEB-19	285	00:48	172W	5	2.0	skewed	1	Saturn
2005-FEB-19	286	00:48	172W	5	2.0	skewed	1	Saturn

TABLE 5.4 (CONTINUED)
 CATALOG OF NGC 2420 FRAMES USED FOR ASTROMETRIC CALIBRATION

Observation Date	Frame	EST Time ^a (hh:mm)	Hour Angle ^b (minutes)	Exposure (seconds)	Seeing ^c (")	Shape ^d	Inadequate Stars ^e	Original Purpose ^f
2005-FEB-19	287	00:49	173W	5	1.9	skewed	1	Saturn
2005-FEB-19	288	00:49	173W	5	1.9	skewed	1	Saturn
2005-FEB-19	289	00:49	173W	5	2.0	skewed	1	Saturn
2005-FEB-19	290	00:49	173W	5	2.1	skewed	1, 3	Saturn
2005-FEB-19	291	00:49	173W	5	2.6	skewed	1, 2, 3	Saturn
2005-FEB-19	292	00:49	173W	5	1.9	skewed	1, 2, 3	Saturn
2005-NOV-19	403	03:46	13E	10	1.5	round	7	astrometry
2005-NOV-19	404	03:46	13E	10	1.8	round	7	astrometry
2005-NOV-19	405	03:46	13E	10	2.0	round	7, 17	astrometry
2005-NOV-19	406	03:47	12E	10	2.0	round	7, 10, 17	astrometry
2005-NOV-19	407	03:47	12E	10	1.8	roundish	7, 10	astrometry
2005-NOV-19	408	03:47	12E	10	1.8	slightly oval	7,	astrometry
2005-NOV-19	409	03:47	12E	10	1.8	round	7, 12,	astrometry
2005-NOV-19	410	03:48	11E	10	1.8	round	7	astrometry
2005-NOV-19	411	03:48	11E	10	1.0	skewed	1, 3, 7	astrometry
2005-NOV-19	412	03:48	11E	10	1.8	round	1, 7	astrometry
2005-NOV-19	423	03:53	6E	20	1.8	oval	1, 2, 3, 7, 12, 15	astrometry
2005-NOV-19	424	03:54	5E	20	1.8	round	1, 2, 3, 7, 12, 15	astrometry
2005-NOV-19	425	03:54	5E	20	2.2	round	1, 2, 3, 7, 12, 15, 17	astrometry
2005-NOV-19	426	03:55	4E	20	2.0	round	1, 3, 7, 12, 15, 17	astrometry
2005-NOV-19	427	03:55	4E	20	1.8	round	1, 3, 7, 12, 15	astrometry

TABLE 5.4 (CONTINUED)
 CATALOG OF NGC 2420 FRAMES USED FOR ASTROMETRIC CALIBRATION

Observation Date	Frame	EST Time ^a (hh:mm)	Hour Angle ^b (minutes)	Exposure (seconds)	Seeing ^c (")	Shape ^d	Inadequate Stars ^e	Original Purpose ^f
2005-NOV-19	428	03:55	4E	20	1.8	round	1, 7, 10, 12, 15	astrometry
2005-NOV-19	429	03:56	3E	20	1.8	skewed	1, 7, 12, 15	astrometry
2005-NOV-19	430	03:56	3E	20	1.8	round	1, 7, 12, 15	astrometry
2005-NOV-19	431	03:57	2E	20	1.5	round	1, 7, 12, 15	astrometry
2005-NOV-19	432	03:57	2E	20	1.5	slightly oval	1, 7, 12, 13, 15	astrometry
2005-NOV-19	443	04:05	6W	30	2.0	round	1, 2, 3, 7, 12, 15, 17	astrometry
2005-NOV-19	444	04:06	7W	30	2.6	oval	1, 2, 3, 7, 12, 15, 17	astrometry
2005-NOV-19	445	04:06	7W	30	1.8	slightly skewed	1, 3, 7, 12, 15	astrometry
2005-NOV-19	446	04:07	8W	30	2.0	round	1, 3, 7, 12, 15, 17	astrometry
2005-NOV-19	447	04:07	8W	30	1.5	round	1, 3, 7, 12, 13, 15	astrometry
2005-NOV-19	448	04:08	9W	30	1.8	fairly round	1, 2, 3, 7, 12, 15	astrometry
2005-NOV-19	449	04:08	9W	30	2.2	skewed	1, 2, 3, 7, 12, 15	astrometry
2005-NOV-19	450	04:09	10W	30	1.8	mostly round	1, 2, 3, 7, 12, 13, 15	astrometry
2005-NOV-19	451	04:10	11W	30	1.8	round	1, 2, 3, 7, 12, 15	astrometry
2005-NOV-19	452	04:10	11W	30	2.0	round	1, 2, 3, 7, 12, 13, 15 17	astrometry
2005-NOV-19	535	04:50	51W	10	1.3	round	7	sensitivity
2005-NOV-19	536	04:50	51W	10	1.5	round	7	sensitivity
2005-NOV-19	537	04:50	51W	10	1.5	round	7	sensitivity
2005-NOV-19	538	04:51	52W	10	0.9	round	7, 12, 15	sensitivity
2005-NOV-19	539	04:51	52W	10	1.2	round	7, 15	sensitivity
2005-NOV-19	540	04:51	52W	10	1.0	round	7, 12, 15	sensitivity

TABLE 5.4 (CONTINUED)
 CATALOG OF NGC 2420 FRAMES USED FOR ASTROMETRIC CALIBRATION

Observation Date	Frame	EST Time ^a (hh:mm)	Hour Angle ^b (minutes)	Exposure (seconds)	Seeing ^c (")	Shape ^d	Inadequate Stars ^e	Original Purpose ^f
2005-NOV-19	541	04:51	52W	10	1.0	round	7	sensitivity
2005-NOV-19	542	04:52	53W	10	1.2	round	7, 12	sensitivity
2005-NOV-19	543	04:52	53W	10	1.0	round	7, 15	sensitivity
2005-NOV-19	544	04:52	53W	10	1.8	round	7	sensitivity

NOTES.—^aEastern Standard Time (EST) of observations based on timestamp associated with digital file containing raw frame.

^bHour angle in minutes indicates how far east (E) or west (W) of the meridian NGC 2420 was midway through each exposure.

^cSeeing is estimated from the full-width at half-maximum (FWHM) of evaluation star 20 in each image.

^dShape is described based on the contours and overall appearance of evaluation star 20 in each image.

^eInadequate stars were dropped from individual frames for several reasons: missing, too close to an edge, saturated, or extremely misshapen.

^fMost frames used herein were not taken specifically for astrometric calibration (astrometry). The January and February frames were used for calibration during observations of the moons of Saturn. The frames taken late on November 19 were used to determine the limiting magnitudes of FanCam (C. Park 2006, private communication).

TABLE 5.5
ASTROMETRIC EVALUATION STARS SELECTED IN NGC 2420

Evaluation Star	2MASS Designation ^a	J (mag)	H (mag)	K _s (mag)	USNO-B1.0 Designation	NGC 2420 ID ^b
1	07380627+2136542	10.781 ± 0.021	10.198 ± 0.019	10.125 ± 0.018	1116-0164806	41
2	07381549+2138015	10.903 ± 0.021	10.405 ± 0.023	10.305 ± 0.018	1116-0164869	76
3	07382696+2138244	10.590 ± 0.021	10.057 ± 0.022	9.982 ± 0.018	1116-0164970	174
4	07382208+2136432	10.806 ± 0.022	10.277 ± 0.024	10.192 ± 0.020	1116-0164929	119
5	07382195+2135508	10.840 ± 0.024	10.350 ± 0.026	10.210 ± 0.020	1115-0161842	
6	07382687+2135460	11.987 ± 0.022	11.904 ± 0.022	11.861 ± 0.020	1115-0161940	172
7 ^c	07381507+2134589	8.572 ± 0.021	7.854 ± 0.016	7.687 ± 0.027	1115-0161730	
8	07382148+2135050	11.345 ± 0.022	10.805 ± 0.024	10.707 ± 0.018	1115-0161830	
9	07382984+2134509	11.107 ± 0.022	10.592 ± 0.022	10.475 ± 0.017	1115-0161983	192
10	07383760+2134119	10.848 ± 0.022	10.358 ± 0.024	10.234 ± 0.020	1115-0162073	236
11	07382936+2134309	12.049 ± 0.028	12.038 ± 0.030	11.946 ± 0.023	1115-0161978	190
12	07382166+2133514	9.5430 ± 0.024	8.954 ± 0.023	8.799 ± 0.018	1115-0161834	115
13	07382696+2133313	10.182 ± 0.022	9.772 ± 0.022	9.662 ± 0.017	1115-0161945	173
14	07382724+2133166	11.792 ± 0.022	11.331 ± 0.022	11.216 ± 0.018	1115-0161953	176
15	07382418+2132540	9.388 ± 0.021	8.721 ± 0.018	8.572 ± 0.018	1115-0161886	140
16	07381822+2132062	10.882 ± 0.022	10.413 ± 0.024	10.272 ± 0.018	1115-0161775	91
17	07382406+2132148	10.758 ± 0.029	10.279 ± 0.031	10.180 ± 0.026	1115-0161881	
18	07382935+2132375	11.784 ± 0.021	11.265 ± 0.022	11.183 ± 0.020	1115-0161977	
19	07382114+2131418	10.988 ± 0.022	10.524 ± 0.024	10.413 ± 0.017	1115-0161826	111
20 ^d	07382285+2134069	12.021 ± 0.021	11.490 ± 0.022	11.427 ± 0.017	1115-0161858	

NOTES.—^a2MASS designations are based on right ascension and declination (J2000) and have the form hhmmss.ss+ddmmss.s.

^bNGC 2420 identification follows the numbering in Cannon & Lloyd (1970).

^cAstrometric evaluation star 7 is also TYC 1373-01207-1 (Høg *et al.* 2000).

^dastroc and MPRP treated astrometric evaluation star 20 as the expected parallax star. The grading of frames is based on the quality of the image of this star.

REFERENCES.—Photometry is from 2MASS. USNO-B1.0 is Monet *et al.* (2003).

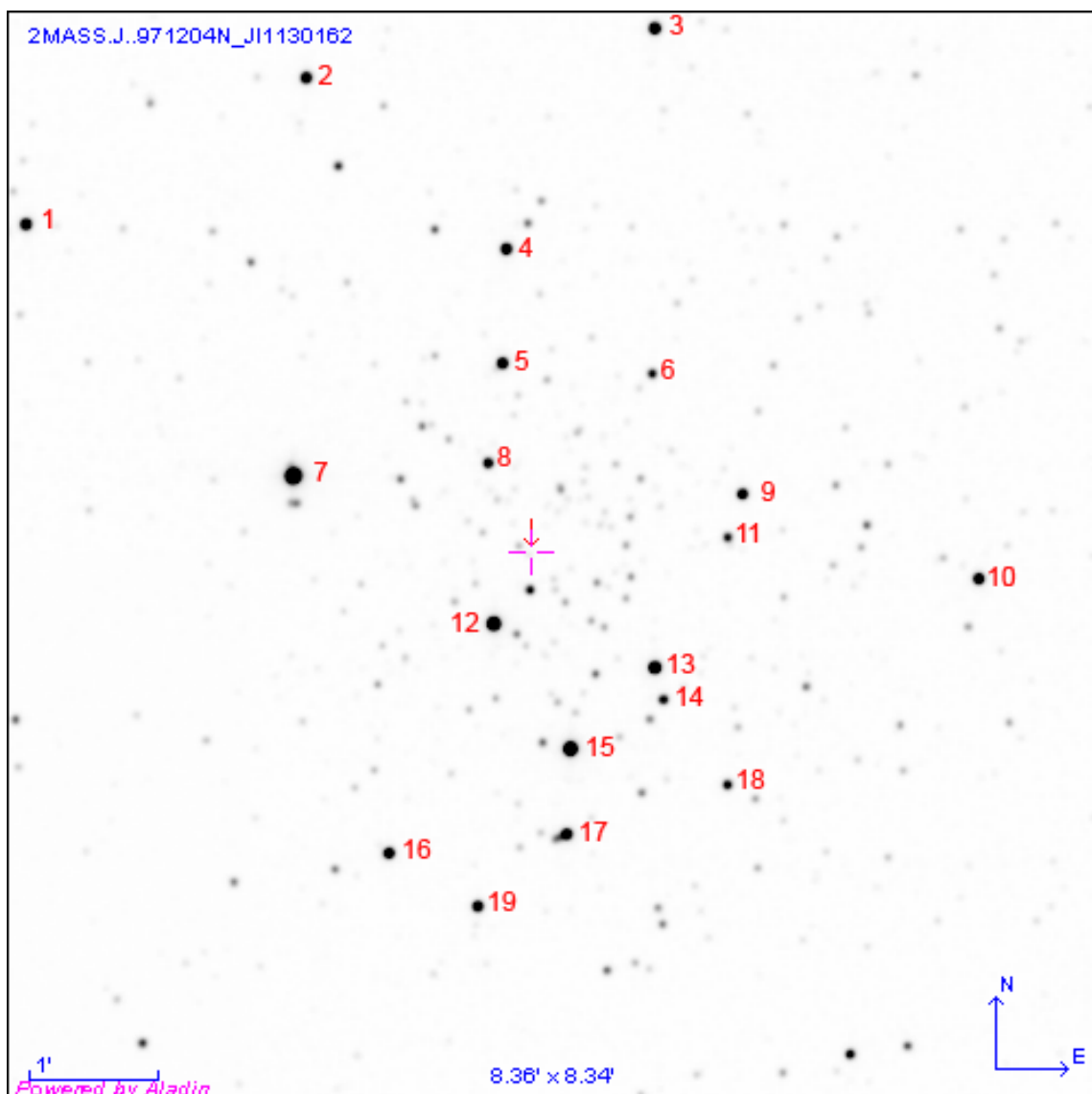


FIG. 5.2. — NGC 2420 with Astrometric Evaluation Stars Identified. Image Source: 2MASS J-band image taken 1997 April 17 via Aladin with annotations by J. L. Bartlett & J. L. Bartlett.

5.4 OBSERVATIONS AND ANALYSIS

Sixty-eight exposures of NGC 2420 taken with FanCam in January, February, and November 2005 using the J filter form the basis of this study. Exposure times ranged from 2 to 30 seconds. FanCam does not use a shutter. The custom imaging

software, *astrix* (A. Smith 2004, private communication), read out the FPA at the beginning and end of each exposure; *voodoo* (Leach & Low 2000; M. Nelson 2006, private communication) has now replaced *astrix*. The difference between those two read-outs was stored as the image in Flexible Image Transport System (FITS) format. No identifying or explanatory header information was included; observation times were later obtained from the computer time-stamp associated with the raw frames. Observations were made in batches. The telescope was moved slightly while each image was being read-out to provide manual dithering.

In November, a series of identical length exposures were also made close to the astrometric calibration field for use in estimating the sky background. Previously, the science images themselves were used to estimate the sky background.

When the sky was clear near sunset or sunrise, sky flats and dark exposures were also obtained for calibration purposes. Otherwise, the most recent sky flats and dark exposures were used for calibration.

The raw images (flats, darks, science images, and sky background images) were downloaded from the imaging computer in the 31-inch telescope control room or from a compact disc-read only memory (CD-ROM) produced on that machine. Then, rows 511 and 512 in all frames were replaced with pixels from rows 1,023 and 1,024 shifted by one column to the left using an Image Reduction and Analysis Facility (IRAF) routine (Tody 1986, 1993; hereafter IRAF²⁰) developed by C. Park (2005 & 2006, private communication); these rows are displaced during the read-out as shown in Figure 5.3 on

the following page. The current recommended reduction procedure is to treat these rows as bad pixels rather attempt to fix them (C. Park 2006, private communication). Next, all of the images were trimmed to eliminate bad columns and rows caused by misalignment of the camera with the focal plane aperture. VAIL has decided to leave these dark regions as they are for the time being (C. Park 2006, private communication).

Another IRAF routine developed by C. Park (2005 & 2006, private communication) was used to flatten images in batches of identical regions through identical filters with identical exposure times. This routine combined the flats, darks, and sky background frames into single representative images. The sky background frames had the same exposure length as the science frames that they would be used to flatten. The representative dark image was subtracted from the representative sky flat to produce a master flat. The representative sky image was subtracted from each science image. Then, the sky-subtracted science images were divided by the master flat image. Finally, previously identified bad pixels were fixed.

²⁰IRAF is distributed by the National Optical Astronomy Observatories, which are operated by the Association of Universities for Research in Astronomy, Inc., under cooperative agreement with the National Science Foundation.

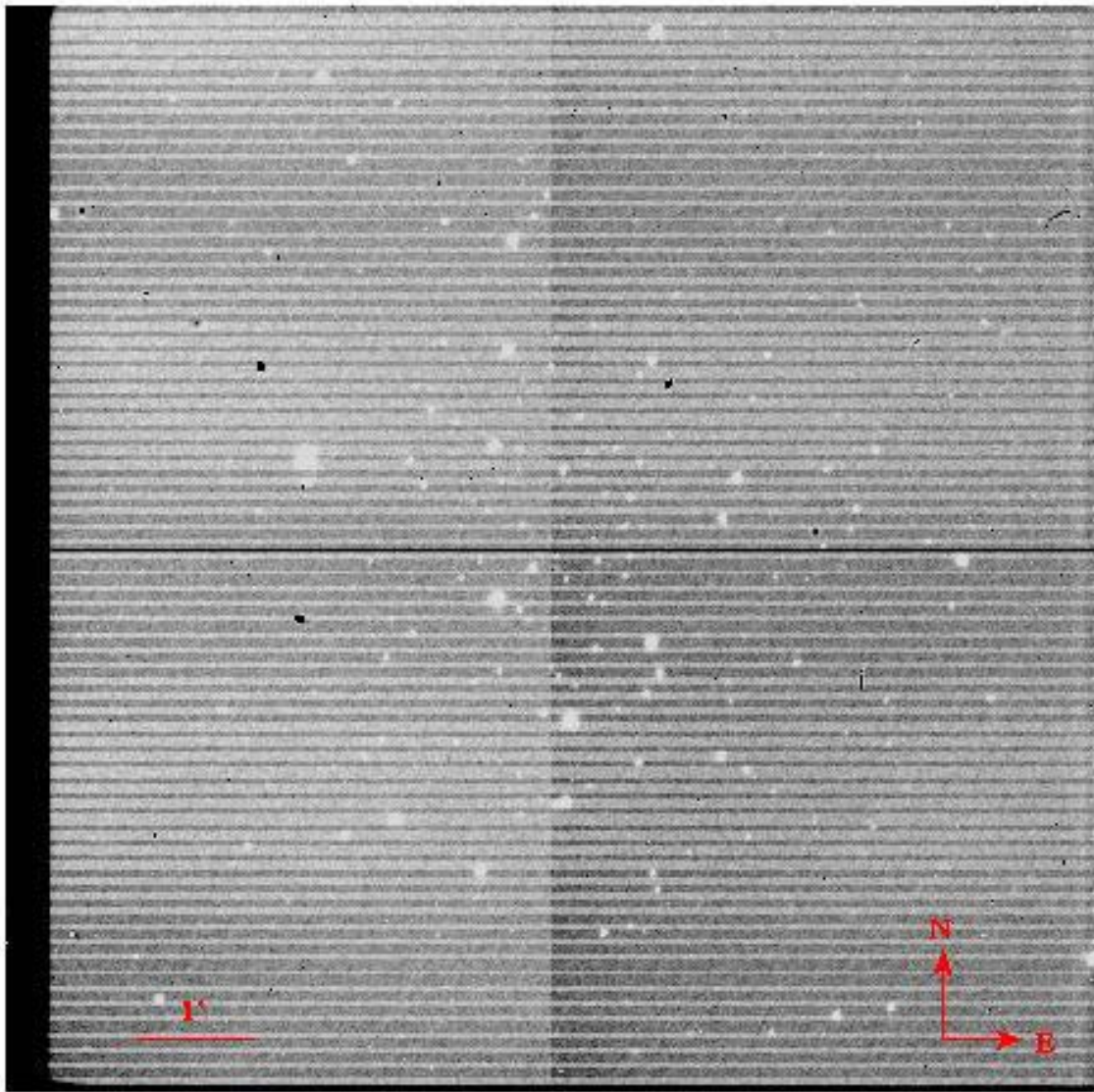


FIG. 5.3.—NGC 2420, Raw J-Band Frame 285 Taken 2005 February 19. In the middle of the frame, bad rows 511 and 512 can be seen. Misalignment of the detector and vacuum window caused the dark region along bottom and left side of the frame. Image Source: VAIL, O. Fox, & C. Park with annotations by J. L. Bartlett & J. L. Bartlett.

After this processing, the intensity of some pixels was negative, which is non-physical. Therefore, an appropriate constant was added to each pixel in a particular

image to bring the minimum value above zero. After this flattening procedure, the quality of the images was improved but visible structure remained in a number of images, as shown in Figure 5.4. However, samples of the sky background indicate this variation is significantly less than 1%. Furthermore, this type of artifact is rarely seen in FanCam images (C. Park 2006, private communication).

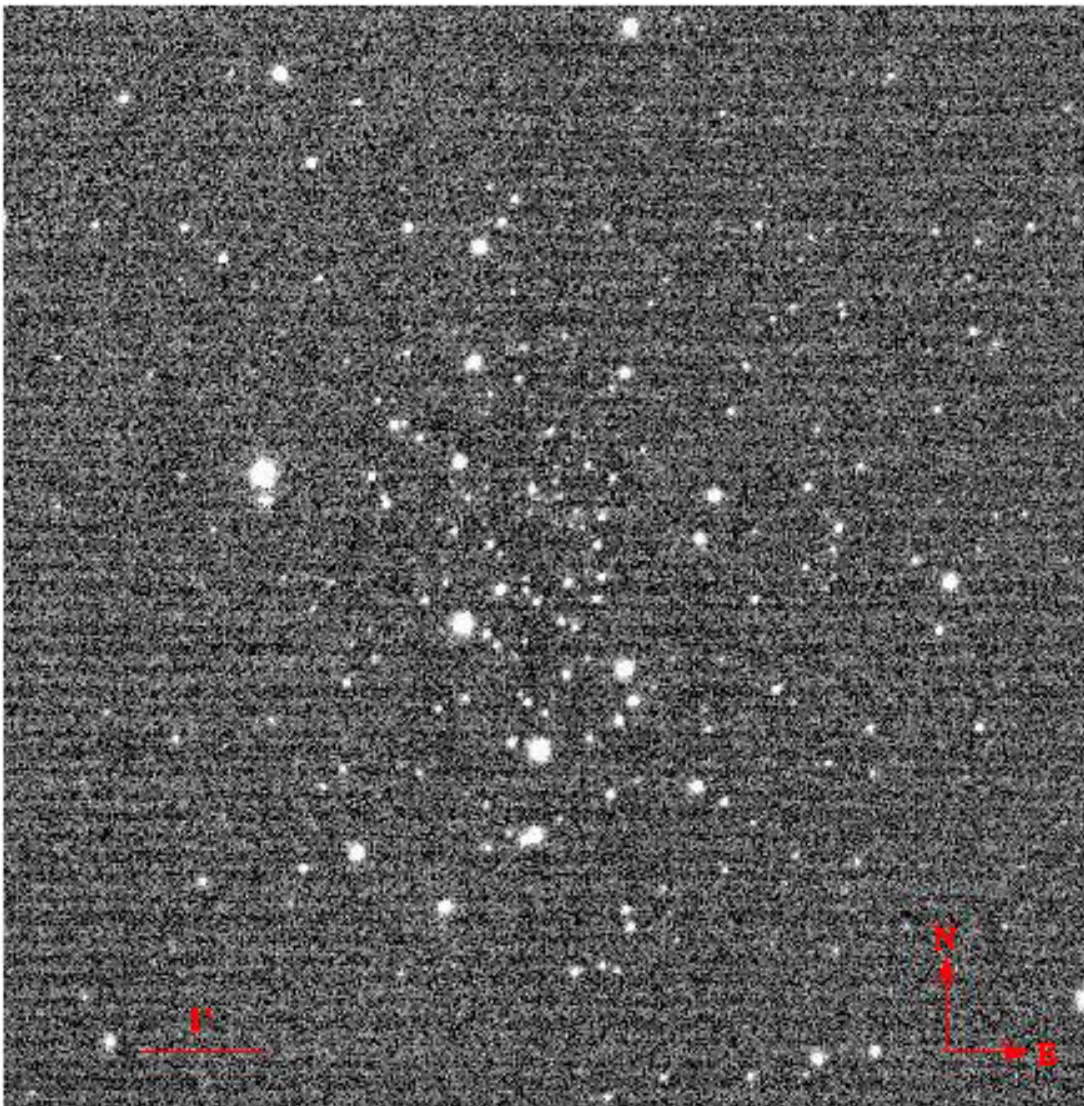


FIG. 5.4. — NGC 2420, Flattened J-Band Frame 285 Taken 2005 February 19. Some structure remains in the image after processing as described in section 5.4. Image Source: VAIL, O. Fox, & C. Park with processing by J. L. Bartlett & C. Park and annotations by J. L. Bartlett & J. L. Bartlett.

The flattened images were rotated so that north was to the top and east was to the left. The astrometric evaluation stars were checked individually for saturation and distortion. Then, Starlink conversion routines produced copies of the images in the format used by Figaro Version 2 (DST) for further processing using Figaro.

Begam, Ianna, and Patterson (2006, in preparation; hereafter BIP) describe the Figaro-based image reduction pipeline developed for the UVa Southern Parallax Program. Following these procedures, the images were cataloged and graded. The *astcor* routine extracted the position of each astrometric evaluation star. In frames where large constants had been added to ensure all pixels contained positive intensities, the constants had to be subtracted again in order for *astcor* to run properly.

Once positions for individual stars were measured, several combinations of images were considered: all images, individual nights, January and November images with moderate hour angles, and February and November images with large hour angles. Parallax input files (*pif*'s) were constructed for each case treating the central star, astrometric evaluation star 20, as the "parallax" star. For individual nights and for the February and November combination, the image with the best quality overall along with the image taken immediately after it were averaged to serve as the "trail plate." For the other combinations, four January images taken close to the meridian were averaged as the trail plate. Averaging several images increases the coordinate precision associated with the trail plate. The January trail plate lacked four astrometric evaluation stars so those stars were dropped from further analysis.

The McCormick Parallax Reduction Program (sager; hereafter MPRP) reduced the positions of the astrometric evaluation stars in each additional image to the selected trail plate. MPRP calculated a three plate-constant model to describe the mean positions of the astrometric evaluation stars

$$\begin{aligned}\varepsilon &= ax + by + c \\ \eta &= dx + ey + f\end{aligned}\tag{5.2}$$

where (x, y) are the coordinates of the astrometric evaluation stars in the system of their own image; (ε, η) are the coordinates of the astrometric evaluation star in the system of the trail plate; $a, b, c, d, e,$ and f are the plate constants that account for scale, orientation, and origin.

The mean error in a single observation of unit weight, estimated herein using the standard deviation of the plate adjustment model for each frame, is a measure of repeatability of positions. Table 5.6 lists the averages for each batch of frames considered; the x - and y -coordinates, which correspond to right ascension and declination, are considered separately. The errors range from 0.57 to 2.02 μm . The early November frames that were taken specifically as astrometric calibration frames have the smallest errors in x and y . The batches taken at large hour angles (February, November late, and both combined) have larger errors in y than x . The January frames taken within five minutes of the meridian have the largest errors, with its x -coordinate slightly worse than the y .

The precision for all frames considered is about $\pm 1.3 \mu\text{m}$, which is only slightly better than the single-position precision of $\pm 1.5 \mu\text{m}$ achieved for photographic plates. Charge-coupled device (CCD) images at the visible wavelengths should be repeatable

to nearly one-fiftieth (0.02) of a pixel (Monet *et al.* 1992), which translates to about $0.054 \mu\text{m}$ for FanCam. None of the batches evaluated approached this level of precision. The average mean error of unit weight for the Southern Parallax Program CCD Cousins V, R, and I (effective wavelengths 551.28, 654.82, and 816.10 nanometers, respectively) observations discussed in Chapter 3 is $0.41 \pm 0.11 \mu\text{m}$. The November images made within 15 minutes of the meridian come closest to this CCD program. However, photographic plates were the detector of choice for parallax programs throughout most of the twentieth century. Therefore, a parallax program should be possible using FanCam as well.

In comparison, USNO preliminary astrometric testing using cluster fields obtained mean errors of unit weight for a single observation of $\pm 7 \text{ mas}$ in J-band using a camera, IRCAM, that was not optimized for astrometry (Vrba *et al.* 2004). Their IRCAM results are better than approximately $\pm 40 \text{ mas}$ for FanCam frames overall or $\pm 19 \text{ mas}$ for the November frames taken within 15 minutes of the meridian. Encouraged by their IRCAM results, the USNO developed an infrared detector specifically for astrometry, ASTROCAM, with $27\text{-}\mu\text{m}$ pixels and a pixel resolution of $365.4 \text{ mas pixel}^{-1}$. Vrba *et al.* (2004) report preliminary parallaxes from ASTROCAM with average mean errors of unit weight of $15.5 \pm 4.9 \text{ mas}$, or $1.15 \pm 0.36 \mu\text{m}$, and $17.9 \pm 4.9 \text{ mas}$, or $1.32 \pm 0.36 \mu\text{m}$, in x and y respectively; these results are within the range achieved by FanCam. Better ASTROCAM results were achieved by using dithered triplets and by limiting the reference frame to the four brightest stars. Additional improvements in ASTROCAM precision were anticipated with the calculation of

parallaxes; the final solutions would include proper motions of the reference stars, differential color refraction (DCR), and the exclusion of frames with poor seeing.

5.5 DISCUSSION

The positions measured for the astrometric evaluation stars selected in NGC 2420 are similar in quality to those obtained for photographic plates but not as good as results achieved using CCD's in the visual and near-infrared bands. Therefore, the measurement of parallaxes using FanCam is possible. However, additional testing would be worthwhile before committing substantial amounts of observing time to a new infrared parallax program. Such testing should include the evaluation of possible higher-order plate constants, the analysis of stacked images, the assessment of the other proposed filters, and the measurement of an actual parallax. Astrometric improvements could be obtained by

- Increasing the number of exposures used, which should not be difficult using exposures shorter than 30 seconds
- Refining the initial image reduction process to obtain flatter images, which is expected as part of the continuing software development
- Optimizing the parallax reduction pipeline for use with infrared images and with the new hardware
- Installing the planned autoguider
- Modeling the atmospheric refraction so that DCR corrections may be included as necessary; although the effect should be small in the infrared, DCR corrections may improve measurements made at large hour angle

- Establishing appropriate astrometric observing procedures, including guidelines for grading frames

The results achieved with FanCam also indicate that a similar investigation of PAIRITEL may also be worthwhile. While PAIRITEL would have more limited time for astrometry, it is capable of detecting fainter objects than the smaller FanCam. With the probable loss of the USNO infrared parallax program, a need exists for another such program in the northern hemisphere. FanCam has an opportunity to meet this need.

Chapter 6 The Solar Neighborhood: Future Development

6.1 INTRODUCTION

The census of the solar neighborhood will command the efforts of astronomers for some time to come. Progress on the 5- and 10-parsec (pc) samples only exposes the incompleteness of the 20- and 25-pc samples. Finishing the innermost volume will allow additional effort to be put into the next shell. Technological improvements increase our access to the dimmest stars and substellar objects and enable us to expand the solar neighborhood. Each advance in our census flows outward and enhances many branches of astronomy. Despite great progress in determining the fundamental properties of nearby stars and measuring their distances through trigonometric parallaxes, this work has demonstrated that the census remains incomplete. Work on the defining solar neighborhood will continue well into this century.

6.2 BARNARD'S STAR

Although only a slight chance remains that the planets described by van de Kamp (1963b, 1982) orbit Barnard's Star (McCarthy *et al.* 2007, in preparation), this work has contributed to our knowledge of the position and motion of the second closest stellar system to our own. However, the absolute parallax resulting from this study suffers from a large and highly uncertain correction to absolute ($5.6 \text{ mas} \pm 6.7 \text{ mas}$), which is significantly larger than the corrections used by the United States Naval Observatory (Harrington *et al.* 1993) and Benedict *et al.* (1999). Therefore, the value of this final measurement from the Leander McCormick Observatory would benefit from additional data. Spectra were recently obtained for the reference stars using the 40-inch

reflector at Fan Mountain Observatory. Spectroscopic distances based on these spectra may improve the distances obtained using broad-band photometry and reduce the size and uncertainty in the correction to absolute.

Of historical interest, a time-series analysis, similar to that discussed in Chapter 2, could be applied to the measurements of Barnard's Star obtained by van de Kamp at Sproul Observatory (1982). For his final analysis, van de Kamp measured nearly 20,000 exposures on 4,580 plates taken on 1,200 nights between 1938 and 1981. This collection of Barnard's Star images is unique and is unlikely to be matched. If Sproul Observatory still has the measurements made with the Grant two-coordinate measuring machine (van de Kamp 1977a) and is willing to make those available, a time-series analysis would be relatively straight-forward. Such an effort could provide further insight into van de Kamp's work and the continuing debate on whether he could have detected the planets he described (1982).

6.3 SOUTHERN PARALLAX PROGRAM

The Southern Parallax Program (SPP) observed about ninety stars between 1987 and 2002, including those described in Chapter 3. Begam, Ianna, and Patterson are preparing the final parallaxes and proper motions for publication. Additional photometry is planned to improve the differential color refraction (DCR) corrections and to reduce the relative measurements to absolute ones.

Of the thirteen SPP stars tested for low mass companions, LHS 288 remains an intriguing possibility. Further monitoring of LHS 288, such as currently undertaken by the Research Consortium on Nearby Stars (RECONS) or possibly using the Hubble

Space Telescope (HST), could clarify whether the apparent signal is spurious or the product of a planet. The Cerro Tololo Inter-American Observatory (CTIO) Parallax Investigation (CTIOPI) recently published a parallax for LHS 288 (Henry *et al.* 2006); the residuals from that measurement could also be subjected to a time-series analysis to see whether similar periods emerge from that data set.

When selecting stars from the SPP for time-series analysis, we selected those with small errors in their relative parallaxes, which should be accompanied by small residuals. A perturbation due to a companion should stand out from the noise in those residuals. However, the small errors may be an indication that no orbital component is present. An alternative approach would have used larger errors to identify host candidates. The corresponding large residuals may be evidence of presence of an orbital component. On the other hand, the large error may merely reflect noisy or sparse data. Another selection from the ninety SPP stars using the second approach could be more fruitful and might also produce candidates for further monitoring. In addition, a comparison of the results of the two searches could provide guidance for future selections from other programs.

6.4 CTIOPI

The preliminary results from the CTIOPI subsample described in Chapter 4 are encouraging. When complete, this work will probably contribute twenty-nine stars to the solar neighborhood including three new members of the 10-pc sample. When the final parallaxes and proper motions are calculated, distances should also be obtained for the members of identified common proper motion pairs that were not determined during

this preliminary analysis. The dropped stars should be reconsidered for inclusion. In addition, when resources permit the expansion of CTIOPI again, the lists of possible nearby stars from which this subsample was drawn still contain more than two hundred candidates. Many of these CTIOPI stars will be potential targets for the Space Interferometry Mission (SIM).

As demonstrated in Chapters 2 and 3, once final parallaxes and proper motions are established, the resulting residuals can be tested for any periodic motion indicative of the presence of a low-mass companion. Therefore, a time-series analysis using the Lomb-Scargle method (Press *et al.* 1992) is a reasonable extension of a modern parallax program. Eventually, such an analysis should be carried out for selected stars in this CTIOPI subsample to determine whether any of these host planets. The detection or non-detection of such planets would provide additional insight into the frequency of planets around low mass stars.

6.5 FAN MOUNTAIN OBSERVATORY

The initial astrometric evaluation of the new infrared camera on the refurbished 31-inch reflector at Fan Mountain Observatory (Kanneganti *et al.* 2007, in preparation) indicates that the currently attainable precision is adequate to measure parallaxes. Chapter 5 suggests some improvements to the current hardware, software, and procedures that might improve the results achieved.

The determination of parallaxes and proper motions requires a multi-year commitment of observing time; CTIOPI measurements typically require four seasons of observations spread over 2.5 years (Jao *et al.* 2005). Before the University of Virginia

(UVa) commits to an infrared parallax program, some additional astrometric testing might be appropriate, including evaluation of possible higher-order plate constants, the analysis of stacked images, the assessment of the other proposed filters, and the measurement of an actual parallax. Other factors, such as weather patterns and light pollution at the site, will also play a role in the final decision. Another consideration is whether a sufficient number of the brown dwarf candidates visible from Charlottesville are bright enough to be observed using FanCam. Should such a program go forward, it could make a significant contribution both to the nearby star census and to our knowledge of brown dwarfs generally.

6.6 DISCUSSION

Additional projects grow naturally from the work described herein, each of which would contribute to our knowledge of the nearest stars. Similarly, detecting and characterizing new members of the solar neighborhood will continue to put forward fresh questions about the solar neighborhood and the Milky Way Galaxy of which it is part. While each of these undertakings brings us closer to completing the 25-pc census, identifying the nearly 4,100 missing stellar systems within the current limits of the solar neighborhood is an ambitious mission. However, large-scale surveys, such as the recently dedicated Panoramic Survey Telescope and Rapid Response System (Pan-STARRS)²¹ and planned Large Synoptic Survey Telescope (LSST)²², should produce

²¹The University of Hawai'i maintains a website describing their new telescope at <http://pan-starrs.ifa.hawaii.edu/public/>

²²The LSST Corporation maintains a website detailing their proposed telescope at http://www.lsst.org/lsst_home.shtml

immense quantities of astrometric data. Extracting information pertinent to the solar neighborhood will employ new techniques along with the traditional tools.

As we continue to develop our knowledge of the stars within the solar neighborhood, we will derive an appropriate sense of place within both our Milky Way Galaxy and the larger Universe. Someday, we hope to know thoroughly these stars that lie so close to our own Sun. For a limited volume, we may be able to claim that we can tell the number of the stars and call them by their names.

Acknowledgements

This work would not have been possible without the knowledgeable guidance of my adviser, P. Ianna, who is a national treasure of astrometry. Not only was he willing to take on a non-traditional graduate student but he continued with this project long after his retirement. I am forever grateful for his guidance and encouragement.

My family supported this work through their individual efforts, through their emotional support of me, and through their financial generosity. My grandfather, G. Dormann, gave me a telescope when I was in grade school because he believed I would be an astronomer. My parents created me and encouraged me in every way. Without the technical support of my father, the original J. L. Bartlett, this document would not have come to fruition. My husband, K. Riggleman, agreed to help me study fuzzy dots and has kept that promise for six years of married life. I also appreciate the teasing and good-natured questioning of this project by my mother and my brother. My in-laws have been remarkably tolerant of the demands this work placed on family life. I love each of you very much.

R. Rood encouraged me to pursue astronomy when I visited the University of Virginia (UVa) as a junior high school student. Then, he supported my application to enter UVa as a part-time graduate student. Finally, he evaluated this work. I am grateful for his faith in me.

When P. Ianna was unavailable, R. J. Patterson and L. Fredrick tried to answer my questions. Their knowledge of astrometry and the parallax programs at Leander

McCormick Observatory and Siding Spring Observatory contributed to the planet searches described therein. R. J. Patterson also undertook to teach me photometry.

M. Begam, who developed the data reduction pipeline for the Southern Parallax Program (SPP), made the initial calculations of parallaxes and proper motions on which the work in Chapter 3 is based. He generously provided assistance throughout the analysis of these stellar motions and during the adaption of the SPP data reduction pipeline for use with 31-inch (0.8-meter) Fan Mountain Observatory (FMO) telescope. In addition, he patiently taught me to observe with the 26.25-inch Leander McCormick Observatory telescope.

T. Henry generously accepted the subsample described in Chapter 4 for inclusion in the Cerro Tololo Inter-American Observatory (CTIO) Parallax Investigation (CTIOPI). The RECONS Team, especially T. Henry, W.-C. Jao, J. Subasavage, T. Beaulieu, and J. Winters, obtained essential observations and supplied indispensable data reduction assistance. CTIOPI would not be possible without the excellent support provided by the CTIO staff, including A. Miranda, E. Cosgrove, and A. Gomez. I look forward to continuing to work with them on this project. CTIOPI was a National Optical Astronomy Observatory (NOAO) Survey Program and continues as part of the Small and Moderate Aperture Telescope Research System (SMARTS) Consortium.

M. Skrutskie was generous in making observing time on and archival observations from the 31-inch FMO telescope available. C. Park and S. Kanneganti were most helpful throughout the observations, data reduction, and analysis. I hope that

their efforts will lead to a revitalization of Fan Mountain Observatory, including astrometric work.

Not only did D. M. Whittle and W. T. Joyner serve on my dissertation committee, but they provided invaluable personal encouragement and support throughout this work. D. M. Whittle ensured that I navigated all the necessary preliminary requirements and helped shape the final document. W. T. Joyner ensured that I survived my first full-year teaching at Hampden-Sydney College.

G. F. Benedict graciously agreed to serve on my dissertation committee. Before that he also gave impetus to this work when he assured me that the early periodograms for Barnard's Star looked just like his.

C. Summers generously assisted with the identification and location of essential research materials. The Astronomy Library is fortunate to have her.

V. Bossong, B. Johnson, and J. Harding kept the Astronomy Department running throughout the time of this project. Their administrative support was essential in so many ways that most of us are not aware. C. Wienstein, K. Xiluri, and H. Powell provided the computing resources and support necessary to all of the functions of the Astronomy Department. We should all say thank you to these critical support people more often than we do.

This research made use of

- National Aeronautics and Space Administration's (NASA's) Astrophysics Data System (ADS);
- Vizier (Ochsenbein, Bauer, & Marcout 2000);

- Set of Identifications, Measurements, and Bibliography for Astronomical Data (SIMBAD) database, operated at Centre de Données astronomiques de Strasbourg (CDS), Strasbourg, France;
- data products from 2MASS, which is a joint project of the University of Massachusetts and the Infrared Processing and Analysis Center/California Institute of Technology (CIT), funded by the NASA and the National Science Foundation (NSF);
- Aladin;
- WEBDA database, operated at the Institute for Astronomy of the University of Vienna; and
- M, L, and T dwarf compendium housed at DwarfArchives.org and maintained by C. Gelino, D. Kirkpatrick, and A. Burgasser.

I also acknowledge the data analysis facilities provided by the Starlink Project, which is run by the Council for the Central Laboratory of the Research Councils (CCLRC) on behalf of the Particle Physics and Astronomy Research Council (PPARC).

This research made use of Second Generation Digital Sky Survey images (McLean *et al.* 2000; hereafter DSS2) and first epoch Digital Sky Survey images (DSS) that were obtained by the Anglo-Australian Observatory (AAO) with the United Kingdom (UK) Schmidt Telescope. The Space Telescope Science Institute (STScI) digitized and compressed images under United States (US) Government grant NAG W-2166. The AAO Board retains the copyright to the DSS2 images. The UK Science and

Engineering Research Council/PPARC (SERC/PPARC), and the Anglo-Australian Telescope Board jointly hold the copyright to the DSS images. The UK Schmidt Telescope was operated by the Royal Observatory Edinburgh (ROE) with funding from the UK SERC (later UK PPARC), until 1988 June, and thereafter by the AAO. In addition, the authoress acknowledges the use of NASA's *SkyView* (McGlynn, Scollick, & White 1996²³) facility located at NASA Goddard Space Flight Center.

This research also uses photographic data obtained using Oschin Schmidt Telescope on Palomar Mountain. The Palomar Observatory Sky Survey was funded by the National Geographic Society. The Oschin Schmidt Telescope is operated by the CIT and Palomar Observatory, who hold the copyright to these images. The plates were processed into the present compressed digital format with their permission. The DSS was produced at the STScI under US Government grant NAG W-2166.

The research was funded by

- NSF grants AST 98-20711 and AST 05-07711;
- Space Interferometry Mission (SIM);
- Georgia State University;
- Litton Marine Systems, Incorporated;
- Governor's Fellowship of the University of Virginia (UVa);
- Hampden-Sydney College; and
- F. H. Levinson Fund of the Peninsula Community Foundation.

First and last, I praise God for creating the stars and me.

²³*SkyView* may be accessed at <http://skyview.gsfc.nasa.gov>

References

- Abrahamyan, H. V., Gigoyan, K. S., Hambaryan, V. V., & Azzopardi, M. 1997, *Astrophys.*, 40, 131
- Alden, H. L. & van de Kamp, P. 1927, *Publ. Leander McCormick Obs.*, 4, 301
- Aristotle. c328 BC, *On the Heavens I and II*, trans. S. Leggatt (Warminster, Wiltshire: Aris & Phillips, Ltd., 1995)
- Baade, W. 1944, *Astrophys. J.*, 100, 137
- Backman, D., Henry, T., Okimura, T., Mariani, P., Blackwell, J., & Jue, S. 2000, *Bull. AAS*, 32, 1596 (Nstars Database)
- Bakos, G. A., Sahu, K. C., & Nemeth, P. 2002, *Astrophys. J. Suppl. Ser.*, 141, 187
- Barnard, E. E. 1916, *Astron. J.*, 29, 181
- Barning, F. J. M. 1963, *Bull. Astron. Inst. Ned.*, 1, 22
- Bartlett, J. L. & Ianna, P. A. 2001, *Bull. AAS*, 33, 891
- Bartlett, J. L., Ianna, P. A., & Begam, M. C. 2002, *Bull. AAS*, 34, 658
- Basri, G. & Reiners, A. 2006, *Astron. J.*, 132, 663
- Beardsley, W. R., Wagman, N. E., Erskine, E., Hubbell, E., & Gatewood, G. 1973, *Astron. J.*, 78, 95
- Beers, Y. 1957, *Introduction to the Theory of Error*, (2nd ed., Reading, MA: Addison-Wesley Publ. Company, Inc.)
- Benedict, G. F. *et al.* 1999, *Astron. J.*, 118, 1086
- _____ . 2002, *Astrophys. J.*, 581, L115
- Bergeron, P., Leggett, S. K., & Ruiz, M. T. 2001, *Astrophys. J. Suppl. Ser.*, 133, 413

- Bernstein, H.-H. 1997, in ESA SP-402, *HIPPARCOS '97*, ed. B. Battrock, M. A. C. Perryman, & P. L. Bernacca (Noordwijk: ESA), 705
- Bertin, E. & Arnouts, S. 1996, *Astron. Astrophys. Suppl. Ser.*, 117, 393 (SExtractor)
- Bessel, F. W. 1838, *Mon. Not. RAS*, 4, 152
- Bessell, M. S. 1976, *Publ. ASP*, 88, 557
- _____ . 1979, *Publ. ASP*, 91, 589
- _____ . 1990, *Astron. Astrophys. Suppl. Ser.*, 83, 357
- _____ . 1991, *Astron. J.*, 101, 662
- _____ . 1995, *Publ. ASP*, 107, 672
- Bessell, M. S. & Brett, J. M. 1988, *Publ. ASP*, 100, 1134
- Bessell, M. S. & Stringfellow, G. S. 1993, *Annu. Rev. Astron. Astrophys.*, 31, 433
- Bessell, M. S. & Weis, E. W. 1987, *Publ. ASP*, 99, 642
- Beutler, F. J. 1970, *IEEE Trans.*, IT-16, 147
- Bidelman, W. P. 1985, *Astrophys. J. Suppl. Ser.*, 59, 197
- Black, D. C. & Scargle, J. D. 1982, *Astrophys. J.*, 263, 854
- Bonnarel *et al.* 2000, *Astron. Astrophys. Suppl. Ser.*, 143, 33 (Aladin)
- Burrows, A., Hubbard, W. B., Luine, J. I., & Liebert, J. 2001, *Rev. Mod. Phys.*, 73, 719
- Butler, R. P., Vogt, S. S., Marcy, G. W., Fischer, D. A., Henry, G. W., & Apps, K.
2000, *Astrophys. J.*, 545, 504
- Butler, R. P., Vogt, S. S., Marcy, G. W., Fischer, D. A., Wright, J. T., Henry, G. W.,
Laughlin, G., & Lissauer, J. J. 2004, *Astrophys. J.*, 617, 580
- Campbell, B., Walker, G. and Yang, S. 1988, *Astrophys. J.*, 331, 902

- Cannon, R. D. & Lloyd, C. 1970, *Mon. Not. R. Astron. Soc.*, 150, 279
- Carpenter, J. 2006, in *Explanatory Supplement to the 2MASS All Sky Data Release*, R. M Cutri *et al.* (Pasadena, CA: Infrared Processing and Analysis Center)
http://www.ipac.caltech.edu/2mass/releases/allsky/doc/sec6_4b.html
- Castelaz, M. W., Persinger, T., Stein, J. W., Prosser, J., & Powell, H. D. 1991, *Astron. J.*, 102, 2103
- Caillault, J. P. & Patterson, J. 1990, *Astron. J.*, 100, 825
- Chabrier, G. & Baraffe, I. 2000, *Annu. Rev. Astron. Astrophys.*, 38, 337
- Close, L. M. 2003 in Cruz, K. L., Reid, I. N., Liebert, J., Kirkpatrick, J. D., & Lowrance, P. J. 2003, *Astron. J.*, 126, 2421
- Cohen, M., Wheaton, W. A., & Megeath, S. T. 2003, *Astron. J.*, 126, 1090
- Costa, E., Méndez, R. A., Jao, W.-C., Henry, T. J., Subasavage, J. P., Brown, M. A., Ianna, P. A., & Bartlett, J. L. 2005, *Astron. J.*, 130, 337
- Costa, E., Méndez, R. A., Jao, W.-C., Henry, T. J., Subasavage, J. P., & Ianna, P. A. 2006, *Astron. J.*, 132, 1234
- Cousins, A. W. J. 1976, *Mon. Not. Astron. Soc. S. Afr.*, 25, 70
 _____ . 1980a, *Mon. Not. Astron. Soc. S. Afr.*, 39, 22
 _____ . 1980b, *S. Afr. Astron. Obs. Circ.*, 1, 66
 _____ . 1984, *S. Afr. Astron. Obs. Circ.*, 8, 69
- Cruz, K. I. & Reid, I. N. 2002, *Astron. J.*, 123, 2828
- Cruz, K. L., Reid, I. N., Liebert, J., Kirkpatrick, J. D., & Lowrance, P. J. 2003, *Astron. J.*, 126, 2421

- Cutri, R. M. 2005, in *Explanatory Supplement to the 2MASS All Sky Data Release*, R. M. Cutri *et al.* (Pasadena, CA: Infrared Processing and Analysis Center)
http://www.ipac.caltech.edu/2mass/releases/allsky/doc/sec2_2.html#pscstrprop
- Dawson, P. C. & De Robertis, M. M. 2004, *Astron. J.*, 127, 2009
- Deacon, N. R., Hambly, N. C., & Cooke, J. A. 2005, *Astron. Astrophys.*, 435, 363
- Delfosse, X., Forveille, T., Ségransan, D., Beuzit, J.-L., Udry, S., Perrier, C., & Mayor, M. 2000, *Astron. Astrophys.*, 364, 217
- Drilling, J. S. & Landolt, A. U. 2000 in *Allen's Astrophysical Quantities*, ed. A. N. Cox (4th ed.; New York: Springer-Verlag)
- Ducourant, C., Dauphole, B., Rapaport, M., Colin, J., & Geffert, M. 1998, *Astron. Astrophys.*, 333, 882
- Duquenooy, A. & Mayor, M. 1991, *Astron. Astrophys.*, 248, 485
- Eggen, O. J. 1969, *Astrophys. J. Suppl. Ser.*, 19, 57
_____. 1987, *Astron. J.*, 93, 379
_____. 1993, *Astron. J.*, 106, 1885
- Elias, J. H., Frogel, J. A., Matthews, K., & Neugebauer, G. 1982, *Astron. J.*, 87, 1029
- Endl, M., Cochran, W. D., Tull, R. G., & MacQueen, P. 2003, *Astron. J.*, 126, 3099
- Endl, M., Kürster, M., Els, S., Hatzes, A. P., Cochran, W. D., Dennerl, K., Döbereiner, S. 2002, *Astron. Astrophys.*, 392, 671
- Epchtein, N. *et al.* 1999, *Astron. Astrophys.*, 349, 631 (DENIS)
- ESA. 1997, *The Hipparcos and Tycho Catalogues*, (ESA SP-1200) (Noordwijk, Netherlands: ESA Publications Division) (Hipparcos)

- Farihi, J., Becklin, E. E., & Zuckerman, B. 2005, *Astrophys. J. Suppl. Ser.*, 161, 394
- Fischer, D. A. & Marcy, G. W. 1992, *Astrophys. J.*, 396, 178
- Fischer, D. A., Marcy, G. W., Butler, R. P., Vogt, S. S., Frink, S., & Apps, K. 2001, *Astrophys. J.*, 551, 1107
- Frebel, A. *et al.* 2005, *Nat.*, 434, 871
- Fredrick, L W. & Ianna, P. A. 1985, *Bull. AAS*, 17, 551
- Freed, M., Close, L. M., & Siegler, N. 2003, *Astrophys. J.*, 584, 453
- Friel, E. D., Janes, K. A., Tavaréz, M., Scott, J., Katsanis, R., Lotz, J., Hong, L., & Miller, N. 2002, *Astron. J.*, 124, 2693
- Gatewood, G. 1972, "An Astrometric Study of Barnard's Star," Ph.D. diss., University of Pittsburg
- Gatewood, G. 1973, *Astron. J.*, 78, 777
- Gatewood, G. 1995, *Astrophys. Space Sci.*, 223, 91
- Gatewood, G. & Eichhorn, H. 1973, *Astron. J.*, 78, 769
- Gelino, C. R., Kirkpatrick, J. D., & Burgasser, A. J. 2004, *Bull. AAS*, 36, 1354
- Giclas, H. L. 1966, *Vistas Astron.*, 8, 23
- Giclas, H. L., Burnham, Jr., R., & Thomas, N. G. 1978, *Lowell Obs. Bull.*, 8, 89
- Gigoyan, K. S., Hambaryan, V. V., & Azzopardi, M. 1998, *Astrophys.*, 41, 356
- Gizis, J. E. 1997, *Astron. J.*, 113, 806
- Gizis, J. E. 2002, *Astrophys. J.*, 575, 484
- Gizis, J. E., Monet, D. G., Reid, I. N., Kirkpatrick, J. D., Liebert, J., & Williams, R. J. 2000, *Astron. J.*, 120, 1085

- Gizis, J. E., Reid, I. N., Knapp, G. R., Liebert, J., Kirkpatrick, J. D., Koerner, D. W.,
 Burgasser, A. J. 2003, *Astron. J.*, 125, 3302
- Gliese, W. 1957, *Mitt. Ser. A Astron. Rechen-Inst. Heidelb.*, 8, 1
- Gliese, W. 1969, *Veröff. Astron. Rechen-Inst. Heidelb.*, 22, 1
- Gliese, W. & Jahreiß, H. 1979, *Astron. Astrophys. Suppl. Ser.*, 38, 423
- _____. 1991, on *The Astronomical Data Center CD-ROM: Selected
 Astronomical Catalogs*, Vol. I; ed. L. E. Brodzmann & S. E. Gesser (Greenbelt,
 MD: NASA/Astronomical Data Center) [http://vizier.cfa.harvard.edu/viz-
 bin/VizieR?-source=V/70A](http://vizier.cfa.harvard.edu/viz-bin/VizieR?-source=V/70A)
- Gould, A. & Salim, S. 2003, *Astrophys. J.*, 582, 1001
- Graham, J. A. 1982, *Publ. ASP*, 94, 244
- Grossenbacher, R., Mesrobian, W. S., & Upgren, A. R. 1968, *Astron. J.*, 73, 744
- Guinan, E. F. & Ianna, P. A. 1983, *Astron. J.*, 88, 126
- Hambly, N. C. *et al.* 2001, *Mon. Not. RAS*, 326, 1279 (SSS)
- Harrington, R. S. & Harrington, B. J. 1987, *Mercur*, 16, 77
- Harrington, R. S. *et al.* 1993, *Astron. J.*, 105, 1571
- Hawley, S. L., Gizis, J. E., & Reid, I. N. 1996, *Astron. J.*, 112, 2799
- Heintz, W. D. 1982, *Obs.*, 102, 42
- _____. 1988 in Marcy, G. W. & Benitz, K. J. 1989, *Astrophys. J.*, 344, 441
- Henderson, T. 1839, *Mem. RAS*, 11, 61

- Henry, T. J. 2004 in *Spectroscopically and Spatially Resolving the Components of the Close Binary Stars*, ed. R. W. Hidlitch, H. Hensberge, & K. Pavlovski (San Francisco: ASP)
- Henry, T. J., Backman, D. E., Blackwell, J., & Okimura, T. 2000, *Bull. AAS*, 32, 1596
- Henry, T. J., Franz, O. G., Wasserman, L. H., Benedict, G. F., Shelus, P. J., Ianna, P. A., Kirkpatrick, J. D., & McCarthy, D. W., Jr. 1999, *Astrophys. J.*, 512, 864
- Henry, T. J., Ianna, P. A., Kirkpatrick, J. D., & Jahreiß, H. 1997, *Astron. J.*, 114, 388
- Henry, T. J., Jao, W.-C., Subasavage, J. P., Beaulieu, T. D., Ianna, P. A., Costa, E., Mendez, R. A. 2006, *Astron. J.*, 132, 2360, in press
- Henry, T. J. & McCarthy, Jr., D. W. 1990, *Astrophys. J.*, 350, 334
- Henry, T. J. & McCarthy, Jr., D. W. 1993, *Astrophys. J.*, 106, 773
- Henry, T. J., Subasavage, J. P., Brown, M. A., Beaulieu, T. D., Jao, W.-C., & Hambly, N.C. 2004, *Astron. J.*, 128, 2460
- Henry, T., Walkowicz, L. M., Barto, T. C., & Golimowski, D. 2002, *Astron. J.*, 123, 2002
- Hershey, J. L. 1973, *Astron. J.*, 78, 421
- Hertzsprung, E. 1907, *Z. Wiss. Photogr., Photophysik Photochemie*, 5, 86
- _____ . 1911, *Publ. Astrophys. Obs. Potsdam*, 63, 1
- _____ . 1922, *Bull. Astron. Inst. NL*, 1, 21
- Hinz, J. L., McCarthy, Jr., D. W., Simons, D. A., Henry, T. J., Kirkpatrick, J. D., McGuire, P. C. 2002, *Astron. J.*, 123, 2027
- Høg, E. *et al.* 2000, *Astron. Astrophys.*, 355, L27 (Tycho)

- Holtzman, J. A., Burrows, C. J., Casertano, S., Hester, J. J., Tauger, J. T., Watson, A. M., & Worthey, G. 1995, *Publ. ASP*, 107, 1065
- Honeycutt, R. K. 1992, *Publ. ASP*, 104, 435
- Houk, N. & Swift, C. 1999, *Michigan Catalogue of Two-Dimensional Spectral Types for the HD stars*, Vol. 5 (Ann Arbor, MI: University of Michigan)
- Hunter, A. & Martin, E. G. 1956, *Vistas Astron.*, 2, 1023
- Ianna, P.A. 1995, *Astrophys. Space Sci.*, 223, 136
- Ianna, P. A. 1997 in Henry, T. J., Ianna, P. A., Kirkpatrick, J. D., & Jahreiß, H. 1997, *Astron. J.*, 114, 388
- Ianna, P. A. & Bessell, M. S. 1986, *Publ. ASP*, 98, 658
- Jahreiß, H. 2005, in Scholz, R.-D., Meusinger, H., & Jahreiß, H. 2005, *Astron. Astrophys.*, 442, 211
- Jao, W.-C. 2004, "Discovery and Characterization of the Highest Proper Motion Stars," Ph.D. diss., Georgia State University
- Jao, W.-C., Henry, T. J., Subasavage, J. P., Bean, J. L., Costa, E., Ianna, P. A., Méndez, R. A. 2003, *Astron. J.*, 125, 332
- Jao, W.-C., Henry, T. J., Subasavage, J. P., Brown, M. A., Ianna, P. A., Bartlett, J. L., Costa, E., & Méndez, R. A. 2005, *Astron. J.*, 129, 1954
- Jefferys, W. H., Fitzpatrick, M. J., & McArthur, B. E. 1987, *Celest. Mech.*, 41, 39 (GaussFit)
- Johnson, H. L. & Morgan, W. W. 1951, *Astrophys. J.*, 114, 522 (Johnson-Morgan)
- _____ . 1953, *Astrophys. J.*, 117, 313 (Johnson-Morgan)

- Joshi, K. J. & Rasio, F. A. 1997, *Astrophys. J.*, 479, 948
- Josties, F. J. & Harrington, R. S. 1984, *Astrophys. J. Suppl. Ser.*, 54, 103
- Kirkpatrick, J. D., Henry, T. J., & McCarthy, Jr., D. W. 1991, *Astrophys. J. Suppl. Ser.*, 77, 417
- Kitchin, C. R. 1998, *Astrophysical Techniques*, (3rd ed., Philadelphia: Inst. Phys. Publishing)
- Kodak. 1989, *Kodak Scientific Imaging Catalog*, (Rochester, NY: Eastman Kodak Company)
- Kuiper, G. P. 1942, *Astrophys. J.*, 95, 201
- Kürster, M. *et al.* 2003, *Astron. Astrophys.*, 403, 1077
- Landolt, A. U. 1992, *Astron. J.*, 104, 340
- Leach, B. & Low, F. 2000, in *Proc. SPIE 4008, Optical and IR Telescope Instrumentation and Detectors*, ed. M. Iye & A. F. Moorwood (Bellingham, WA: SPIE), 337
- Leggett, S. K. 1992, *Astrophys. J. Suppl. Ser.*, 82, 351
- Leinert, C., Henry, T., Glindemann, A., McCarthy, Jr., D. W. 1997, *Astron. Astrophys.*, 325, 159
- Lippincott, S. L. 1972, *Astron. J.*, 77, 165
- _____. 1978, *Space Sci. Rev.*, 22, 153
- Lodieu, N., Scholz, R.-D., McCaughrean, M. J., Ibata, R., Irwin, M., & Zinnecker, H. 2005, *Astron. Astrophys.*, 440, 1061
- Loktin, A. V. & Beshenov, G. V. 2003, *Astron. Rep.*, 47, 6

- Lomb, N. R. 1976, *Astrophys. Space Sci.*, 38, 447
- Lutz, T. E. & Kelker, D. H. 1973, *Publ. ASP*, 8, 573
- Luyten, W. J. 1979, *A Catalogue of Stars with Proper Motions Exceeding 0.5"*
Annually (2nd ed.; Minneapolis: University of Minnesota) (*LHS*)
- _____. 1980, *New Luyten Two-Tenths Catalogue*, Vol. 3 & 4, (Minneapolis:
 University of Minnesota) (*NLTT*)
- _____. 1987, *LDS Catalogue: Doubles with Common Proper Motion*, ed. J.-L.
 Halbwachs & F. Ochsenbein (Strasbourg, FR: Centre de Données astronomiques de
 Strasbourg) <http://vizier.u-strasbg.fr/viz-bin/VizieR?-source=I/130>
- Marcy, G. W. & Benitz, K. J. 1989, *Astrophys. J.*, 344, 441
- Marcy, G., Butler, R. P., Fischer, D., Vogt, S., Wright, J. T., Tinney, C. G., & Jones, H.
 R. A. 2005, *Prog. Theor. Phys. Suppl.*, 158, 24
- Marcy, G., Butler, R., Fischer, D., Laughlin, G., Vogt, S., Henry, G., & Pourbaix, D.
 2002, *Astrophys. J.*, 581, 1375
- McCarthy, C., Butler, P., Fisher, D., Marcy, G., & Vogt, S. 2004, in *Search for Other
 Worlds*, ed. S. Holt & D. Deming (Melville, NY: Am. Inst. Phys.)
- McCaughrean, M. J., Close, L. M., Scholz, R.-D., Lenzen, R., Biller, B., Brandner, W.,
 Hartung, M., & Lodieu, N. 2004, *Astron. Astrophys.*, 413, 1029
- McCook, G. P. & Sion, E. M. 2003, *A Catalogue of Spectroscopically Identified White
 Dwarfs*, (Ver. 2003 Jun; Strasbourg, France: Centre de Données astronomiques de
 Strasbourg) <http://vizier.cfa.harvard.edu/viz-bin/VizieR?-source=III/235>

- McGlynn, T., Scollick, K., & White, N., 1996 in IAU Symp. 179, *New Horizons from Multi-Wavelength Sky Surveys*, ed. B. J. McLean *et al.* (Boston: Kluwer Academic Publishers), 465
- McLean, B. J., Greene, G. R., Lattanzi, M. G., & Pirenne, B. 2000, in ASP Conf. Proc. 216, *Astronomical Data Analysis Software and Systems IX*, ed. N. Manset, C. Veillet, & D. Crabtree (San Francisco: ASP), 145
- Méndez, R. A. & van Altena, W. F. 1998, *Astron. Astrophys.*, 330, 910
- Menzies, J. W., Cousins, A. W. J., Banfield, R. M., & Laing, J. D. 1989, *S. Afr. Astron. Obs. Circ.*, 13, 1
- Menzies, J. W., Marang, F., Laing, J. D., Coulson, I. M., & Engelbrecht, C. A. 1991, *Mon. Not. RAS*, 248, 642
- Mitchell, S. A. *et al.* 1921, *Publ. Leander McCormick Obs.*, 3, 1
- Mitchell, S. A. *et al.* 1940, *The Trigonometric Parallaxes of Six Hundred and Fifty Stars*, *Publ. McCormick Obs.* Vol. 8 (Ann Arbor, MI: Edwards Brothers, Inc.)
- Monet, D. G., Dahn, C. C., Vrba, F. J., Harris, H. C., Pier, J. R., Luginbuhl, C. B., & Ables, H. D. 1992, *Astron. J.*, 103, 638
- Monet, D. G. *et al.* 2003, *Astron. J.*, 125, 984 (USNO-B1.0)
- Mugrauer, M., Neuhäuser, R., Mazeh, T., Guenther, E., Fernández, M., Broeg, C. 2006, *Astron. Nachr.*, 327, 321
- Narayanan, V. K. & Gould, A. 1999, *Astrophys. J.*, 523, 328

- NASA & JPL. 2005, *SIM PlanetQuest: A Mission for Astrophysics and Planet-Finding*, ed. C. Edberg, M. Shao, & C. Beichman (Pasadena, CA: JPL)
http://planetquest.jpl.nasa.gov/documents/WhitePaper05ver18_final.pdf
- Neece, G. D. 1984, *Astrophys. J.*, 277, 738
- Nelson, R. 2001, *Lecture Notes Phys.*, 577, 35
- Newcomb, S. 1904, *The Stars* (New York: G. P. Putnam's Sons)
- Nidever, D. L., Marcy, G. W., Butler, R. P., Fischer, D. A., & Vogt, S. S. 2002, *Astrophys. J. Suppl. Ser.*, 141, 503
- Ochsenbein, F., Bauer, P., & Marcout, J., 2000, *Astron. Astrophys. Suppl. Ser.*, 143, 221
 (Vizier)
- Oppenheimer, B. R., Golimowski, D. A., Kulkarni, S. R., Matthews, K., Nakajima, T., Creech-Eakman, M., Durrance, S. T. 2001, *Astron. J.*, 121, 2189
- Patterson, R. J., Ianna, P. A., & Begam, M. C. 1998, *Astron. J.*, 115, 1648
- Perryman, M. A. C. *et al.* 1997, *Astron. Astrophys.*, 323, L49
 _____ . 1998, *Astron. Astrophys.*, 331, 81
- Phan-Bao, N. *et al.* 2003, *Astron. Astrophys.*, 401, 959
- Pokorny, R. S, Jones, H. R. A., & Hambly, N. C. 2003, *Astron. Astrophys.*, 397, 575
- Pokorny, R. S, Jones, H. R. A., Hambly, N. C., & Pinfield, D. J. 2004, *Astron. Astrophys.*, 421, 763
- Press, William H. & Rybicki, George B. 1989, *Astrophys. J.*, 338, 227

- Press, W. H., Teukolsky, S. A., Vetterling, W. T., & Flannery, B. P. 1996, *Numerical Recipes in FORTRAN 77: The Art of Scientific Computing*, Vol. 1 (2d ed., New York: Cambridge Univ. Press)
- Pritchard, C. 1887, *Mon. Not. RAS*, 47, 87
- _____. 1888, *Mon. Not. RAS*, 49, 2
- Quirrenbach, A. *et al.* 2004, in *New Frontiers in Stellar Interferometry*, ed. W. A. Traub (Bellingham, WA: SPIE)
- Ragahavan, D., Henry, T. J., Mason, B. D., Subasavage, J. P., Jao, W.-C., Beaulieu, T. D., & Hambly, N. C. 2006, *Astrophys. J.*, 646, 523
- Ranyard, A. C. 1887, *Obs.*, 10, 167
- Reid, I. N & Cruz, K. L. 2002, *Astrophys. J.*, 123, 2806
- Reid, I. N. & Gizis, J. E. 1997, *Astron. J.*, 113, 2246
- Reid, I. N., Gizis, J. E., & Hawley, S. L. 2002, *Astron. J.*, 124, 2721
- Reid, I. N., Hawley, S. L., & Gizis, J. E. 1995, *Astron. J.*, 110, 1838
- Reid, I. N., Kilkenny, D., & Cruz, K. L. 2002, *Astron. J.*, 123, 2822
- Reid, I. N. *et al.* 1999, *Astrophys. J.*, 521, 613
- _____. 2003, *Astron. J.*, 126, 3007
- Rivera, E. *et al.* 2005, *Astrophys. J.*, 634, 625
- Rodgers, A. W. & Eggen, O. J. 1974, *Publ. ASP*, 86, 742
- Russell, H. N. 1913, *Obs.*, 36, 324
- Ryan, S. G. 1989, *Astron. J.*, 98, 1693
- _____. 1992, *Astron. J.*, 104, 1144

- Salim, S. & Gould, A. 2003, *Astrophys. J.*, 582, 1011
- Scargle, J. 1982, *Astrophys. J.*, 263, 835
- Schlegel, D. J., Finkbeiner, D. P., & Davis, M. 1998, *Astrophys. J.*, 500, 525
- Schlesinger, F. 1910, *Astrophys. J.*, 32, 372
- Schlesinger, F., Palmer, M., & Pond, A. 1924, *General Catalogue of Stellar Parallaxes*
(New Haven, CT: Yale Univ.)
- Schneider, D. P., Gunn, J. E., Hosessel, J. G. 1983, *Astrophys. J.*, 264, 337
- Scholz, R.-D., McCaughrean, M. J., Lodieu, N., & Kuhlbrodt, B. 2003, *Astron. Astrophys.*, 398, L29
- Scholz, R.-D., Meusinger, H., & Jahrei, H. 2005, *Astron. Astrophys.*, 442, 211
- Schroeder, D. J. *et al.* 2000, *Astron. J.*, 119, 906
- Schott North America. 2006, *Optics for Devices: Glass Filter Catalog*, (Duryea, PA: Schott North America) http://www.us.schott.com/optics_devices
- Siegler, N., Close, L. M., Cruz, K. L., Martn, E. L., & Reid, I. N. 2005, *Astrophys. J.*, 621, 1023
- Skrutskie, M. F. 2003, in *Explanatory Supplement to the 2MASS All Sky Data Release*, R. M Cutri *et al.* (Pasadena, CA: Infrared Processing and Analysis Center) http://www.ipac.caltech.edu/2mass/releases/allsky/doc/sec3_1b.html
- Skrutskie, M. F., Forrest, W. J., & Shure, M. 1989, *Astron. J.*, 98, 1409
- Skrutskie, M. F. *et al.* 2006, *Astron. J.*, 131, 1163 (2MASS)
- Skrutskie, M. F. *et al.* 1997, in *The Impact of Large Scale Near-IR Sky Surveys*, eds. F. Garzon *et al.*, 25. (Dordrecht, Netherlands: Kluwer Academic Publishing Company)

- Smith, Jr., H. 2003, *Mon. Not. RAS*, 338, 891
- Soderblom, D. R., Nelan, E., Benedict, G. F., McArthur, B., Ramirez, I., Spiesman, W., & Jones, B. F. 2005, *Astron. J.*, 129, 1616
- Soederhjelm, S. 1999, *Astron. Astrophys.*, 341, 121
- Song, I., Bessell, M. S., & Zuckerman, B. 2002, *Astrophys. J.*, 581, L43
- Sozzetti, A. 2005, *Publ. ASP*, 117, 836
- Stone, R. C. 1996, *Publ. ASP*, 108, 1051
- STScI & OAT. 2001, *The Guide Star Catalogue*, (Ver. 2.2; Baltimore, MD: STScI)
<http://vizier.u-strasbg.fr/viz-bin/VizieR?-source=I/271>
- Tadross, A. L., Werner, P., Osman, A., & Marie, M. 2002, *New Astron.*, 7, 553
- Thorsett, S. E., Arzoumanian, Z., & Taylor, J. H. 1993, *Astrophys. J.*, 412, L33
- Tinney, C. G. 1996, *Mon. Not. RAS*, 281, 644
- Tody, D. 1986, in *Instrumentation in Astronomy VI*, ed. D. L. Crawford (Bellingham, WA: SPIE), 733
- Tody, D. 1993, in *ASP Conf. Ser. 52, Astronomical Data Analysis Software and Systems II*, eds. R. J. Hanisch, R. J. V. Brissenden, & J. Barnes (Provo, UT: ASP), 173
- Tokunaga, A. T. 2000 in *Allen's Astrophysical Quantities*, ed. A. N. Cox (4th ed.; New York: Springer-Verlag)
- Torres, C. A. O., da Silva, L., Quast, G. R., de la Reza, R., & Jilinski, E. 2000, *Astron. J.*, 120, 1410
- Uppgren, A. R., Grossenbacher, R., Penhallow, W. S., MacConnell, D. J., & Frye, R. L. 1972, *Astron. J.*, 77, 486
- van Altena, W. F. 1974, *Astron. J.*, 79, 826

- van Altena *et al.* 1997, *Astrophys. J.*, 486, L123
- van Altena, W. F., Lee, J. T., & Hoffleit, E. D. 1995, *The General Catalogue of Trigonometric Stellar Parallaxes* (4th ed., New Haven: Yale Univ. Obs.) (YPC)
- van Altena, W. F., Lee, J. T., Hanson, R. B., & Lutz, T. E. 1988, in *Calibration of Stellar Ages*, ed. A. G. D. Philip (Schenectady, NY: L. Davis Press), 175
- Van Buren, D., Brundage, M., Ressler, M. Terebey, S. 1998, *Astron. J.*, 116, 1992
- van de Kamp, P. 1930, *Popular Astron.*, 38, 17
- _____ . 1935, *Astron. J.*, 44, 74
- _____ . 1940, *Popular Astron.*, 48, 297
- _____ . 1945, *Publ. ASP*, 57, 34
- _____ . 1953, *Publ. ASP*, 65, 73
- _____ . 1963a, *Astron. J.*, 68, 296
- _____ . 1963b, *Astron. J.*, 68, 515
- _____ . 1969a, *Astron. J.*, 74, 238
- _____ . 1969b, *Astron. J.*, 74, 757
- _____ . 1969c, *Publ. ASP*, 81, 5
- _____ . 1975, *Astron. J.*, 80, 658
- _____ . 1977a, *Vistas Astron.*, 20, 501
- _____ . 1977b, *Vistas Astron.*, 21, 289
- _____ . 1981, *Stellar Paths* (Dordrecht, Holland: D. Reidel, Publ. Company)
- _____ . 1982, *Vistas Astron.*, 26, 141
- _____ . 1986, *Space Sci. Rev.*, 43, 211

- van Maanen, A. 1933, *Publ. ASP*, 45, 247
- von Struve, F. G. W. 1840, *Astron. Nachr.*, 17, 178
- Vrba, F. J. *et al.* 2004, *Astron. J.*, 127, 2948
- Vyssotsky, A. N. & van de Kamp, P. 1937, *Publ. Leander McCormick Obs.*, 7, 1
- Vyssotsky, A. N. & Williams, Emma T. R. 1948a, *Publ. Leander McCormick Obs.*, 10, 33
- Vyssotsky, A. N. & Williams, Emma T. R. 1948b, *Publ. Leander McCormick Obs.*, 10, 41
- Weis, E. W. 1993, *Astron. J.*, 105, 1962
- Winglee, R. M., Dulk, G. A., & Bastian, T. S. 1986, *Astrophys. J.*, 209, L59
- Wolszczan, A. & Frail, D. A. 1992, *Natur.*, 355, 145
- Woolley, R., Epps, E., Penston, M. J., & Pocock, S. B. 1970, *R. Obs. Ann.*, 5, 5
- Worley, C. E. 1977, *Rev. Mex. Astron. Astrophys.*, 3, 57
- York, D. G. *et al.* 2000, *Astron. J.*, 120, 1579 (SDSS)
- Xin, Y. & Deng, L. 2005, *Astrophys. J.*, 619, 824
- Zacharias, N., Urban, S. E., Zacharias, M. I., Wycoff, G. L., Hall, D. M., Germain, M. E., Holdenried, E. R., & Winter, L. 2004, *Astron. J.*, 127, 3043 (UCAC2)
- Zacharias, N. *et al.* 2000, *Astron. J.*, 120, 2131 (UCAC)

Appendix A.

Finding Charts for Possible Nearby Stars

Finding charts for all possible nearby stars in the subsample discussed in Chapter 4 were prepared for CTIOPI use. For many of the stars from the Luyten-Palomar Survey (LP), finding charts are not easily available in the literature and those are presented here. For the other stars, references are provided to sources of available charts.

1. FINDING CHARTS FOR LUYTEN HALF SECOND STARS

LHS1363	LHS 5226
LHS5094	LHS 2880
LHS 2024	LHS 3056
LHS 6167	LHS 2783
LHS 2397a	

Finding charts are available in Luyten, W. J. & Albers, H. 1979, *An Atlas of Identification Charts for LHS Stars* (Minneapolis: University of Minnesota)

2. FINDING CHARTS FOR TWO MICRON ALL SKY SURVEY STARS

2MA 0251-0352 (02511490-0352459)
2MA 0429-3123 (04291842-3123568)
2MA 0517-3349 (05173766-3349027)
2MA 0921-2104 (09211410-2104446)
2MA 1155-3727 (11553952-3727350)
2MA 1507-2000 (15072779-2000431)

2MA 1534-1418 (15345704-1418486)

2MA 2306-0502 (23062928-0502285)

2MA 2351-2537 (23515044-2537367)

Finding charts may be prepared from the on-line version of the Two Micron All Sky Survey All-Sky Data Release (Skrutskie, M. F. *et al.* 2006, "The Two Micron All Sky Survey (2MASS)," *Astron. J.*, 131, 1163 (2MASS))

<http://www.ipac.caltech.edu/2mass/releases/allsky/>.

3. FINDING CHARTS FOR "GICLAS" STARS

G 75-35

G 161-71

Finding charts for these two stars are available in

Giclas, H. L., Burnham, R., & Thomas, N. G. 1961, "Lowell proper motions III," *Lowell Obs. Bull.*, 5, 61 for G 75-35

Giclas, H. L., Burnham, R., & Thomas, N. G. 1961, "Lowell proper motions VI," *Lowell Obs. Bull.*, 6, 135 for G 161-71

4. FINDING CHARTS FOR CALÁN-EUROPEAN SOUTHERN OBSERVATORY PROPER MOTION STARS

CE 303

A finding chart is for this star is available in

Ruiz, M. T., Wischnjewsky, M. Rojo, P. M., & Gonzalez, L. E. 2001, "Calán-ESO Proper-Motion Catalog," *Astrophys. J. Suppl. Ser.*, 133, 119

5. FINDING CHARTS FOR LUYTEN-PALOMAR SURVEY STARS

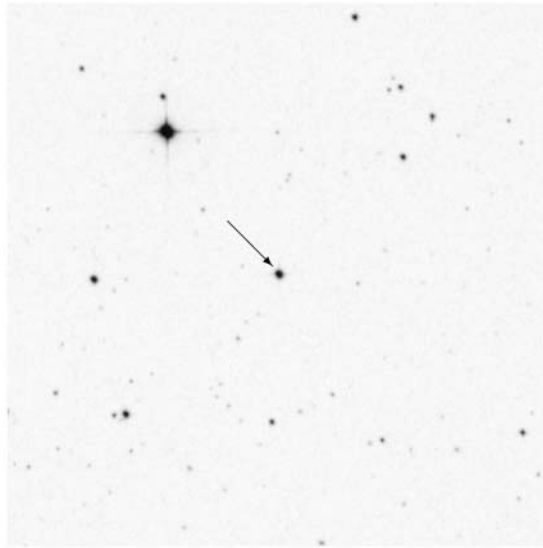
On the following pages, there are finding charts for these twenty-two stars from the Luyten-Palomar Survey:

LP 991-84 (Figure A-1)	LP 615-149 (Figure A-12)
LP 888-18 (Figure A-2)	LP 739-2 (Figure A-13)
LP 889-37 (Figure A-3)	LP 869-19 (Figure A-14)
LP 834-32 (Figure A-4)	LP 869-26 (Figure A-15)
LP 655-43 (Figure A-5)	LP 870-65 (Figure A-16)
LP 716-10 (Figure A-6)	LP 756-3 (Figure A-17)
LP 776-25 (Figure A-7)	LP 984-92 (Figure A-18)
LP 717-36 (Figure A-8)	LP 876-10 (Figure A-19)
LP 671-8 (Figure A-9)	LP 932-83 (Figure A-20)
LP 731-76 (Figure A-10)	LP 822-101 (Figure A-21)
LP 734-34 (Figure A-11)	LP 704-15 (Figure A-22)

Figures A-1 through 24 are finding charts for these stars based on red Second Generation Digital Sky Survey (McLean, B. J., Greene, G. R., Lattanzi, M. G., & Pirene, B. 2000, in ASP Conf. Proc. 216, *Astronomical Data Analysis Software and Systems IX*, ed. N. Manset, C. Veillet, & D. Crabtree (San Francisco: ASP), 145) provided by *SkyView* (McGlynn, T., Scollick, K., & White, N., 1996 in IAU Symp. 179, *New Horizons from Multi-Wavelength Sky Surveys*, ed. B. J. McLean *et al.* (Boston: Kluwer Academic Publishers), 465).

01:39:21.7 - 39:36:08

N
E
10'×10'

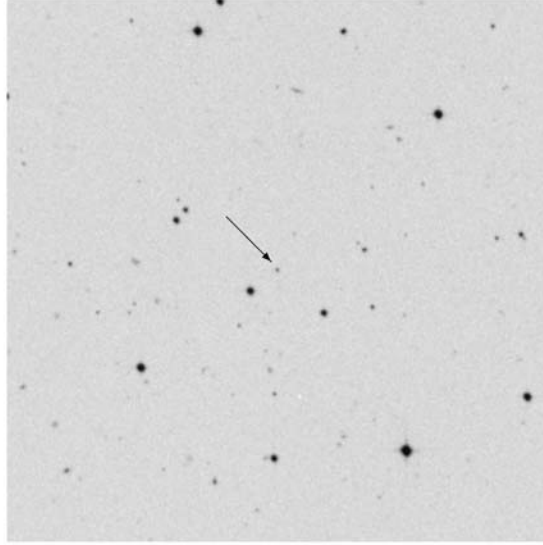


LP991-084

FIG. A-1.—LP 991-084 Finding Chart. Annotations by R. J. Patterson, J. L. Bartlett, & J. L. Bartlett. Image © Anglo-Australian Observatory Board.

03:31:30.2 - 30:42:38

N
E
10'×10'

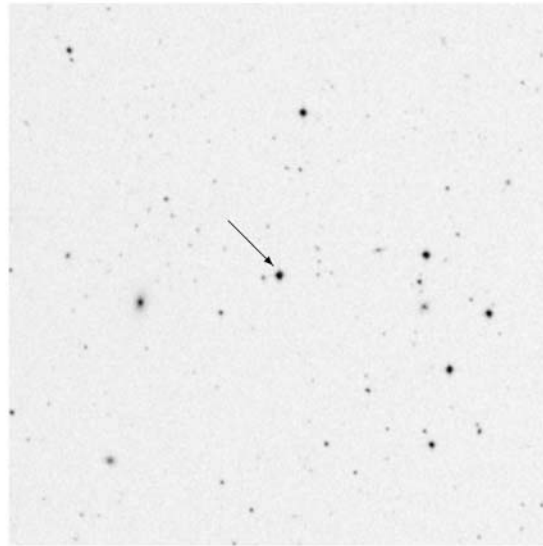


LP888-018

FIG. A-2.—LP 888-018 Finding Chart. Annotations by R. J. Patterson, J. L. Bartlett, & J. L. Bartlett. Image © Anglo-Australian Observatory Board.

04:08:55.5 - 31:28:53

N
E
10' × 10'

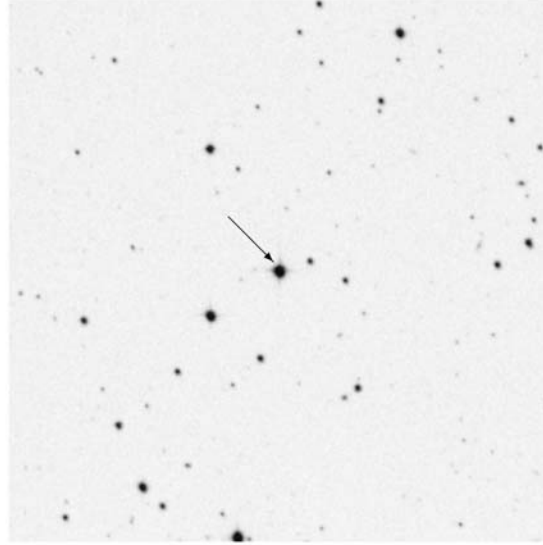


LP889-037

FIG. A-3.— LP 889-037 Finding Chart. Annotations by R. J. Patterson, J. L. Bartlett, & J. L. Bartlett. Image © Anglo-Australian Observatory Board.

04:35:36.1 - 25:27:34

N
E
10' × 10'

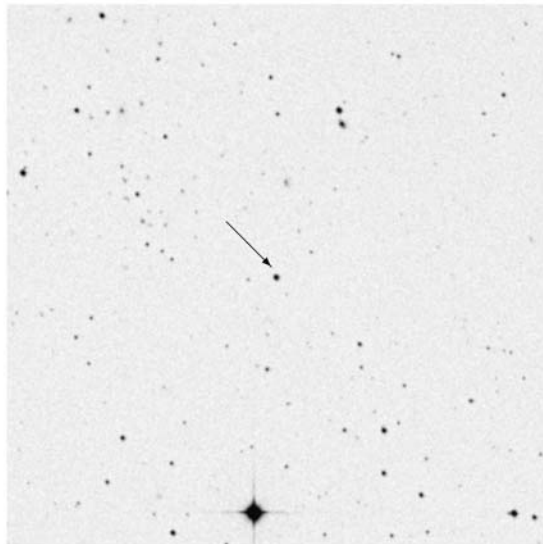


LP834-032

FIG. A-4.— LP 834-032 Finding Chart. Annotations by R. J. Patterson, J. L. Bartlett, & J. L. Bartlett. Image © Anglo-Australian Observatory Board.

04:52:04.01 - 10:58:21.87

N
10' × 10'
E

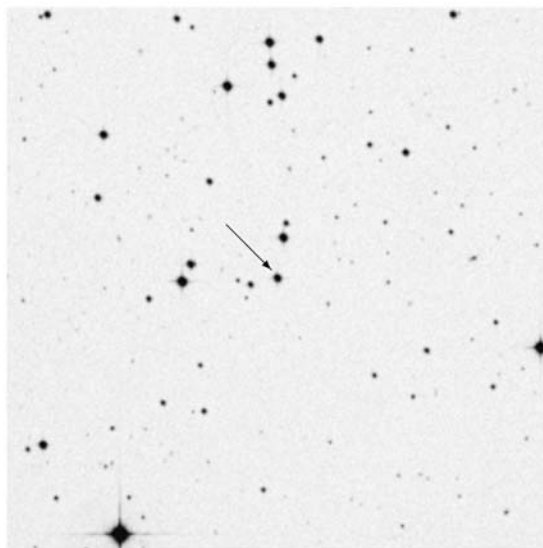


LP716-010

FIG. A-6.—LP 716-010 Finding Chart.
Annotations by R. J. Paterson, J. L. Bartlett,
& J. L. Bartlett. Image © Anglo-Australian
Observatory Board.

04:38:02.5 - 05:56:13

N
10' × 10'
E

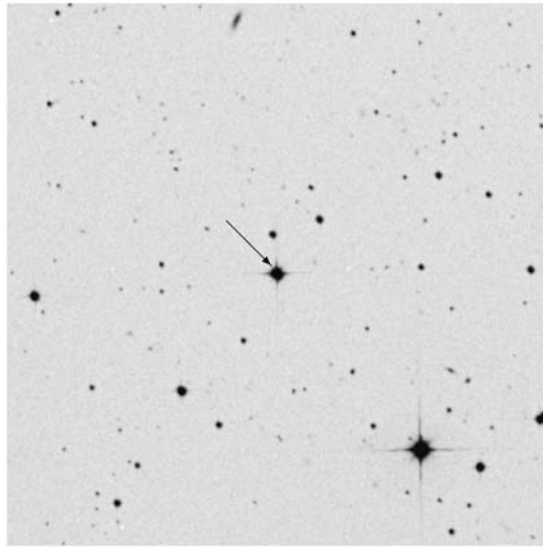


LP655-043

FIG. A-5.—LP 655-043 Finding Chart.
Annotations by R. J. Paterson, J. L. Bartlett,
& J. L. Bartlett. Image © Anglo-Australian
Observatory Board.

04:52:24.4 -16:49:21

N
E
10'×10'

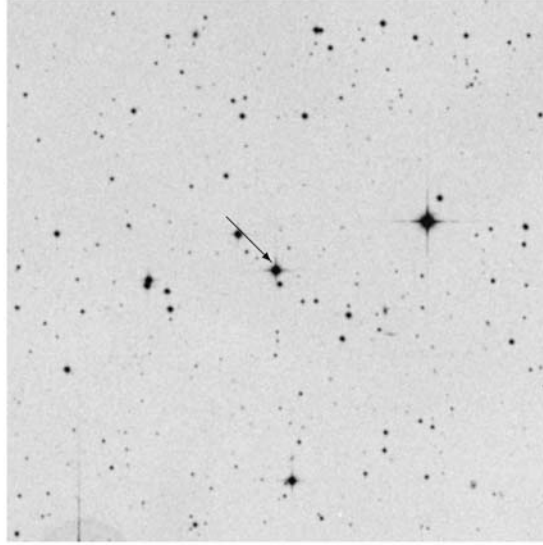


LP776-025

FIG. A-7.—LP 776-025 Finding Chart. Annotations by R. J. Patterson, J. L. Bartlett, & J. L. Bartlett. Image © Anglo-Australian Observatory Board.

05:25:41.6 -09:09:12

N
E
10'×10'

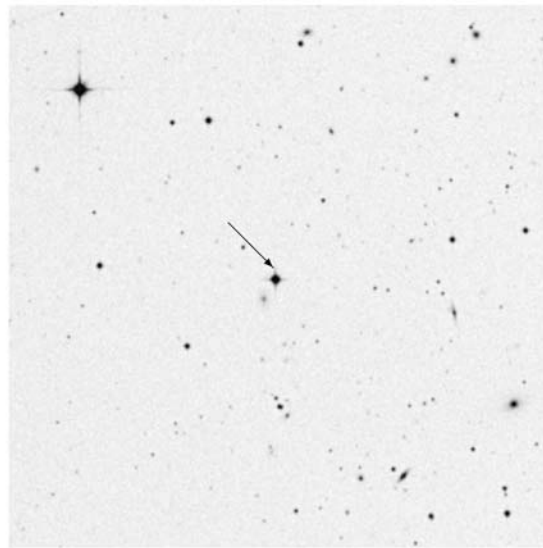


LP717-036

FIG. A-8.—LP 717-036 Finding Chart. Annotations by R. J. Patterson, J. L. Bartlett, & J. L. Bartlett. Image © Anglo-Australian Observatory Board.

10:54:41.9 -07:18:32

N
E
10'×10'

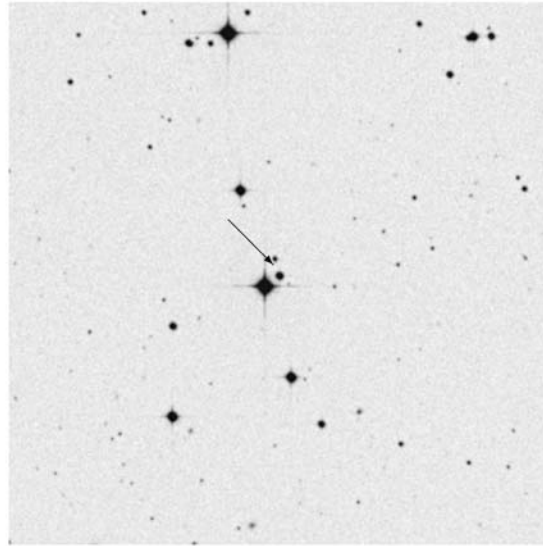


LP671-008

FIG. A-9—LP 671-008 Finding Chart. Annotations by R. J. Patterson, J. L. Bartlett, & J. L. Bartlett. Image © Anglo-Australian Observatory Board.

10:58:27.9 -10:46:30

N
E
10'×10'

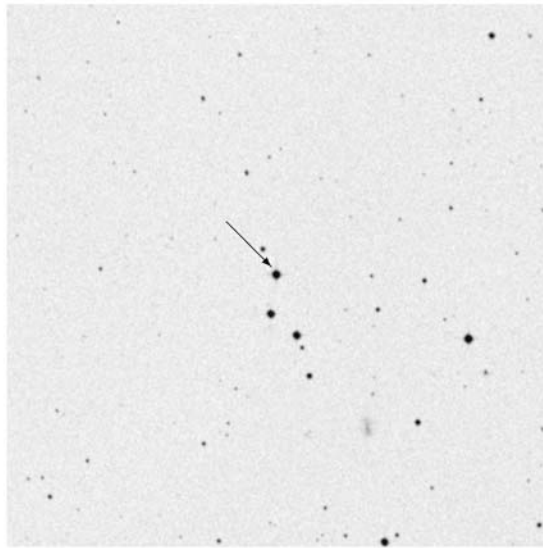


LP731-076

FIG. A-10.—LP 731-076 Finding Chart. BD-10°3166 is the very bright star immediately to the northeast of LP 731-076; they are a possible common proper motion pair. Annotations by R. J. Patterson, J. L. Bartlett, & J. L. Bartlett. Image © Anglo-Australian Observatory Board.

12:10:28.3 -13:10:23

N
10'×10'
E

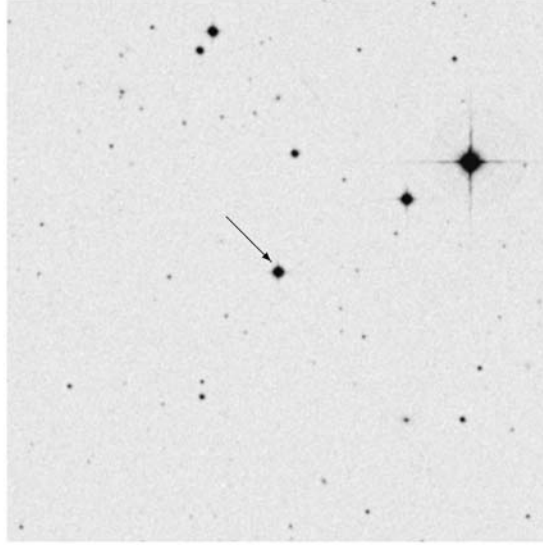


LP734-034

FIG. A-11 — LP 734-034 Finding Chart.
Annotations by R. J. Patterson, J. L. Bartlett,
& J. L. Bartlett. Image © Anglo-Australian
Observatory Board.

12:27:44.7 -03:15:00

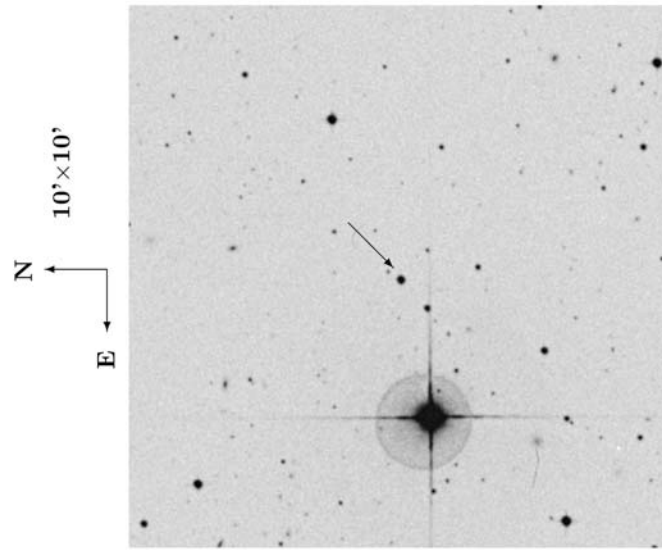
N
10'×10'
E



LP615-149

FIG. A-12.— LP 615-149 Finding Chart.
Annotations by R. J. Patterson, J. L. Bartlett,
& J. L. Bartlett. Image © Anglo-Australian
Observatory Board.

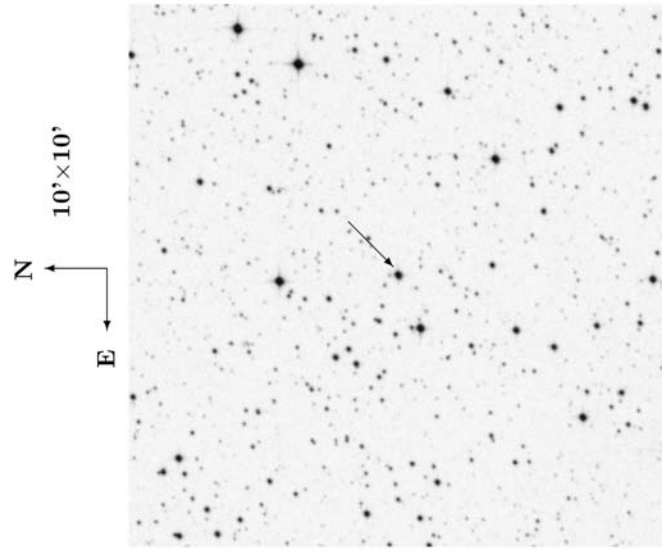
13:58:16.1 - 12:02:58



LP739-002

FIG. A-13 — LP 739-002 Finding Chart.
Annotations by R. J. Patterson, J. L. Bartlett,
& J. L. Bartlett. Image © Anglo-Australian
Observatory Board.

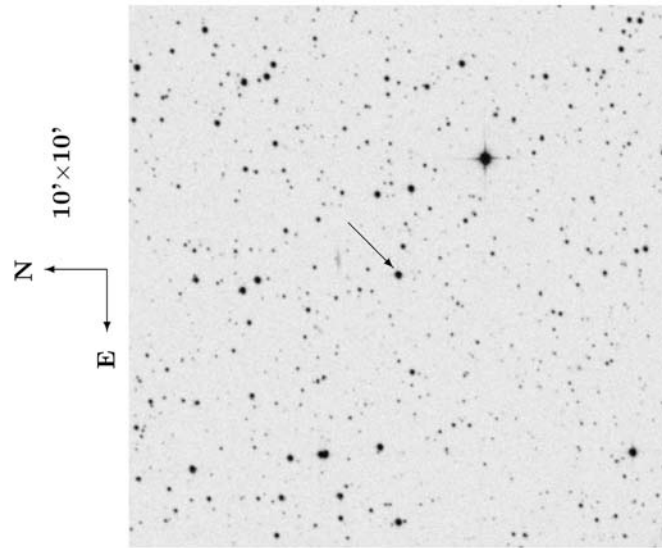
19:42:00.6 - 21:04:05



LP869-019

FIG. A-14.— LP 869-019 Finding Chart.
Annotations by R. J. Patterson, J. L. Bartlett,
& J. L. Bartlett. Image © Anglo-Australian
Observatory Board.

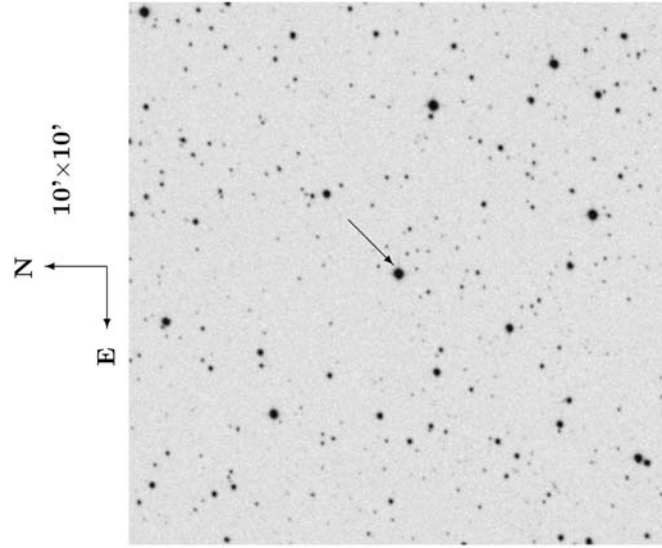
19:44:53.7 -23:37:59



LP869-026

FIG. A-15.—LP 869-026 Finding Chart. CTIOP1 resolved LP 869-026 into two components as shown in Figure 4.6. Annotations by R. J. Patterson, J. L. Bartlett, & J. L. Bartlett. Image © Anglo-Australian Observatory Board.

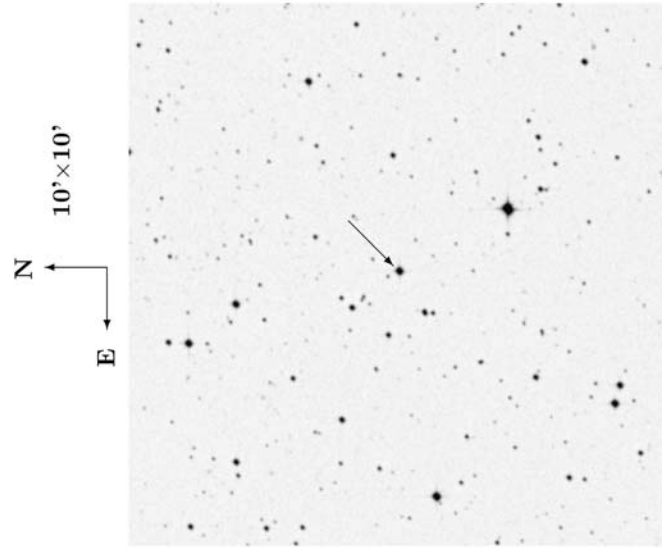
20:04:30.7 -23:42:01



LP870-065

FIG. A-16.—LP 870-065 Finding Chart. Annotations by R. J. Patterson, J. L. Bartlett, & J. L. Bartlett. Image © Anglo-Australian Observatory Board.

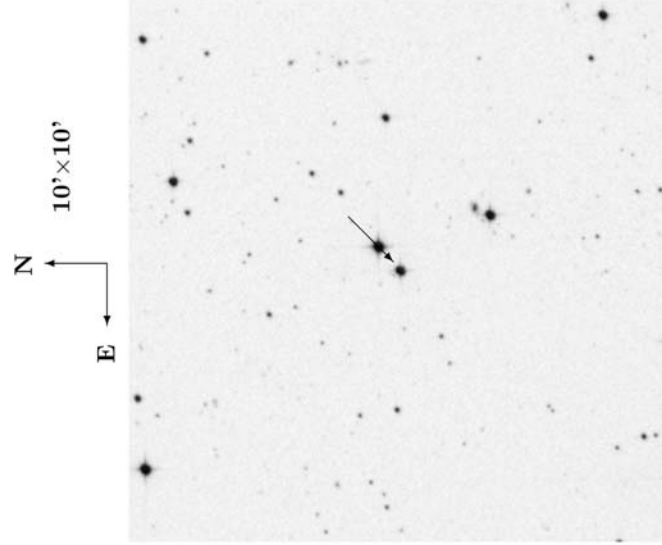
20:46:43.6 -11:48:13



LP756-003

FIG. A-17.— LP 756-003 Finding Chart. Annotations by R. J. Patterson, J. L. Bartlett, & J. L. Bartlett. Image © Anglo-Australian Observatory Board.

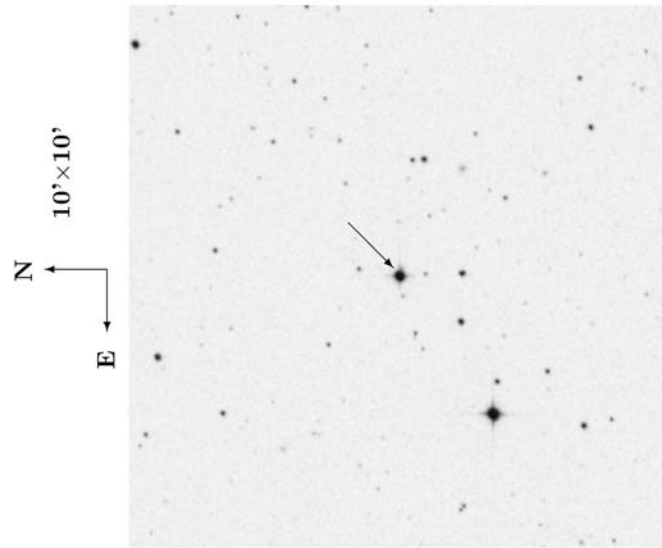
22:45:00.0 -33:15:25



LP984-092

FIG. A-18 — LP 984-092 Finding Chart. LP 984-091 is the brighter star to the northwest of LP 984-092; they are a possible common proper motion pair. Annotations by R. J. Patterson, J. L. Bartlett, & J. L. Bartlett. Image © Anglo-Australian Observatory Board.

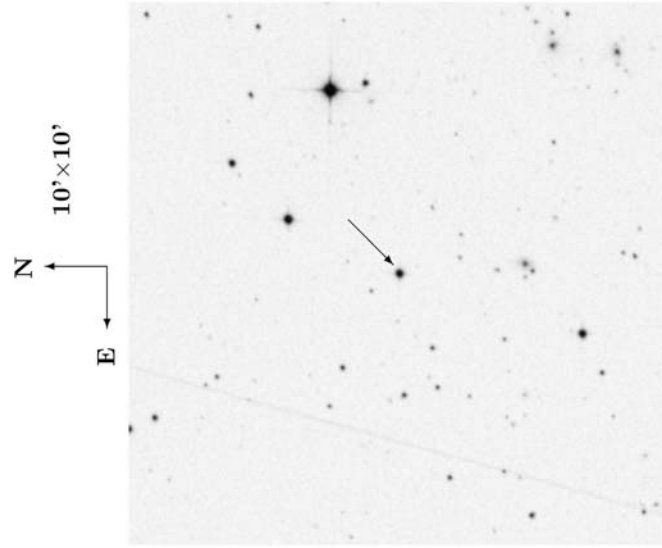
22:48:04.4 -24:22:07



LP876-010

FIG. A-19.— LP 876-010 Finding Chart. Annotations by R. J. Patterson, J. L. Bartlett, & J. L. Bartlett. Image © Anglo-Australian Observatory Board.

22:49:08.4 -28:51:19

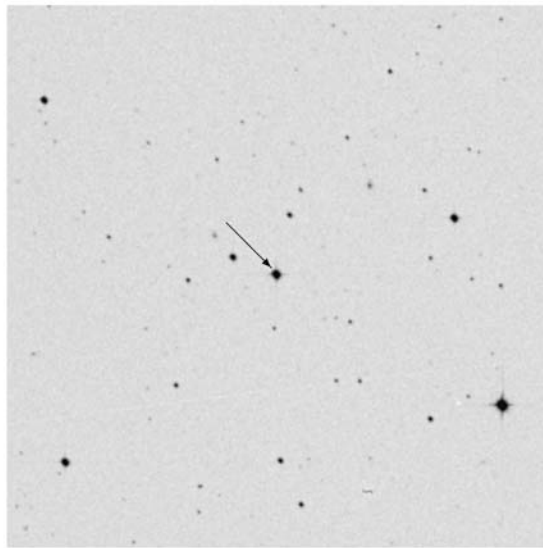


LP932-083

FIG. A-20 — LP 932-083 Finding Chart. LTT 9210 is the very bright star to the northwest of LP 932-083; they are a possible common proper motion pair. Annotations by R. J. Patterson, J. L. Bartlett, & J. L. Bartlett. Image © Anglo-Australian Observatory Board.

23:31:25.0 -16:15:57

N
E
10'×10'

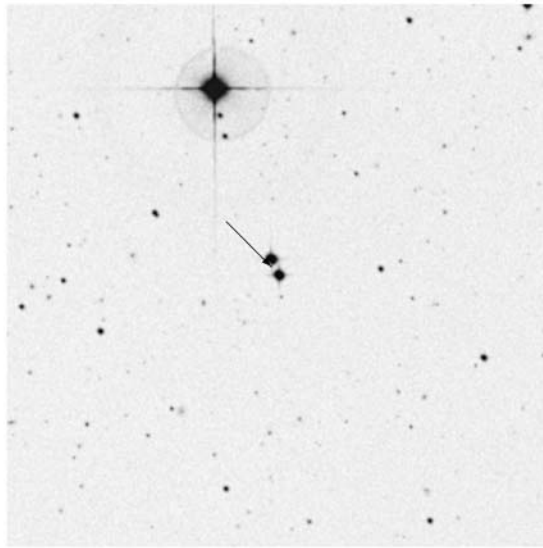


LP822-101

FIG. A-21— LP 822-101 Finding Chart. Annotations by R. J. Patterson, J. L. Bartlett, & J. L. Bartlett. Image © Anglo-Australian Observatory Board.

23:57:20.5 -12:58:48

N
E
10'×10'



LP704-015

FIG. A-22 — LP 704-015 Finding Chart. LP 704-016 is the star of comparable brightness just to the northwest of LP 704-015; they are a potential common proper motion pair. Annotations by R. J. Patterson, J. L. Bartlett, & J. L. Bartlett. Image © Anglo-Australian Observatory Board.